BIOLOGICAL RESEARCH CENTRE
HUNGARIAN ACADEMY OF SCIENCES, SZEGED
INSTITUTE OF BIOPHYSICS

AND

DOCTORAL SCHOOL OF THEORETICAL MEDICINE
UNIVERSITY OF SZEGED

TARGETING THE BLOOD-BRAIN BARRIER WITH SOLID AND VESICULAR NANOPARTICLES DECORATED WITH LIGANDS OF SOLUTE CARRIERS

Ph.D. Thesis

Mária Mészáros

Supervisors:

Mária A. Deli, M.D., Ph.D., D.Sc.

Szilvia Veszelka, Ph.D.

SZEGED

2019

CONTENTS

PUBLICATIONS RELATED TO THE SUBJECT OF THE THESIS

I. Veszelka S, **Mészáros M**, Kiss L, Kóta Z, Páli T, Hoyk Z, Bozsó Z, Fülöp L, Tóth A, Rákhely G, Deli MA.
Biotin and glutathione targeting of solid nanoparticles to cross human brain endothelial cells.
Current Pharmaceutical Design. 2017 Jul 27; 23:4198-4205.
IF: 2.86, Q1

II. Veszelka S, Tóth A, Walter FR, Tóth AE, Gróf I, **Mészáros M,** Bocsik A, Hellinger É, Vastag M, Rákhely G, Deli MA.
Comparison of a rat primary cell-based blood-brain barrier model with epithelial and brain endothelial cell lines: gene expression and drug transport.
Frontiers in Molecular Neuroscience. 2018 May 22; 11:166.
IF: 3.902, Q1

III. **Mészáros M,** Porkoláb G, Kiss L, Pilbat AM, Kóta Z, Kupihár Z, Kéri A, Galbács G, Siklós L, Tóth A, Fülöp L, Csete M, Sipos Á, Hülper P, Sipos P, Páli T, Rákhely G, Szabó-Révész P, Deli MA, Veszelka S.
Niosomes decorated with dual ligands targeting brain endothelial transporters increase cargo penetration across the blood-brain barrier.
European Journal of Pharmaceutical Sciences. 2018 Oct 15; 123:228-240.
IF: 3.466, Q1

OTHER PUBLICATION

I. Sántha P, Veszelka S, Hoyk Z, **Mészáros M**, Walter FR, Tóth AE, Kiss L, Kincses A, Oláh Z, Seprényi G, Rákhely G, Dér A, Pákáski M, Kálmán J, Kittel Á, Deli MA.
Restraint stress-induced morphological changes at the blood-brain barrier in adult rats.
Frontiers in Molecular Neuroscience. 2016 Jan 14; 8:88.
IF: 5.08, Q1

ABBREVIATIONS

A	dodecanoyl-alanine
ASCT	alanine/serine/cysteine (neutral amino acid) transporter (SLC1A)
BBB	blood-brain barrier
CNS	central nervous system
EBA	Evans blue-labeled bovine serum albumin
GLUT	glucose transporter (SLC2A family)
GP	N-dodecyl-β-D-glucopyranose
GSH	pegylated-glutathione
hCMEC/D3	human cerebral microvascular endothelial cell line
LAT-1	large amino acid transporter-1
MTT	3-(4,5-dimethylthiazol-2-yl)-2,5-diphenyltetrazolium bromide
N	non-targeted niosome
N-A	alanine-targeted niosome
N-A-GP	alanine-glucopyranose dual-targeted niosome
N-A-GSH	alanine-glutathione dual-targeted niosome
N-GP	glucopyranose-targeted niosome
N-GP-GSH	glucopyranose-glutathione dual-targeted niosome
N-GSH	glutathione-targeted niosome
NP	nanoparticle
P_{app}	apparent permeability coefficient
PB	phosphate buffer
PBS	phosphate buffer solution
PEG	polyethylene glycol
RBEC	rat brain endothelial cell
SLC	solute carrier
SMVT	sodium-dependent multivitamin transporter (SLC5A6)
SNAT	sodium-coupled neutral amino acid transporter (SLC38A family)
SNP	solid nanoparticle
SNP-B	biotin-targeted solid nanoparticle
SNP-B-GSH	biotinylated glutathione-targeted solid nanoparticle
TfR	transferrin receptor
TJ	tight junction
TMA-DPH	1-(4-trimethylammoniumphenyl)-6-phenyl-1,3,5-hexatriene

1. INTRODUCTION

1.1. Structure and function of the blood-brain barrier

A highly controlled brain microenviroment is crucial for the maintenance of neuronal function. The blood-brain barrier (BBB), the most important barrier of the central nervous system (CNS), plays an essential role in separating the brain tissue from the systemic circulation (Abbott, 2002; Abbott et al., 2010). In higher organisms the BBB is the tightest barrier in the vascular system formed by brain capillary endothelium (Haseloff et al., 2015). Brain capillary endothelial cells are connected by tight junctions (TJs), which represent the morphological basis of the BBB (Fig. 1). TJs are integral multiprotein complexes, which tightly close paracellular gaps and are connected to the actin cytoskeleton by linker or adaptor molecules (Haseloff et al., 2015). In addition to this gate function, TJs in the lateral plasmamembrane of endothelial cells act as a fence, segregating membrane components including lipid rafts and transport proteins to the luminal (blood side) and abluminal (brain side) surface of the cells, thus creating cellular polarity (Abbott et al., 2010).

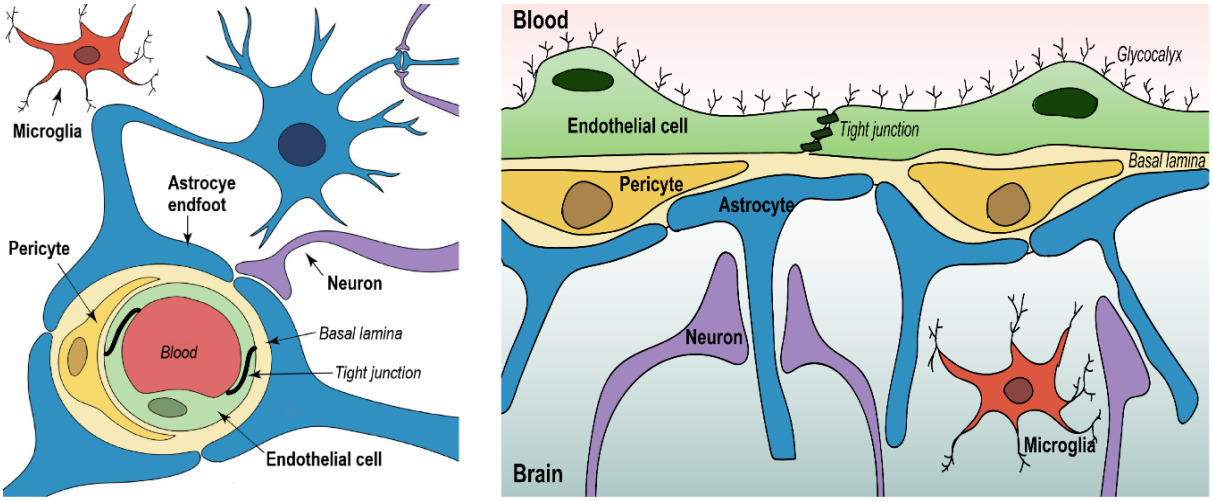

Figure 1. *The cell associations of the neurovascular unit. Cross-section of a brain capillary, connections of endothelial cells, pericytes, astroytes and microglia (based on Fig. 2. Abbott et al., 2010).*

The luminal surface of brain capillary endothelial cells is covered by a negatively charged layer, called glycocalyx (Vorbrodt, 1989), which is composed of proteoglycans, sulfated mucopolysaccharides, sulfated and sialic acid-containing glycoproteins and glycolipids (Hervé et al., 2008). Negatively charged lipid head groups in the plasma membrane also contribute to this protective layer of brain endothelial cells which participate in the regulation of the brain

entry of charged drug molecules (Ribeiro et al., 2012). The brain capillary endothelial cells tightly interact with pericytes and astrocyte endfeet and share with them a common basal lamina (Fig. 1). These three main cell types of the BBB form a functional unit with neurons, microglia and perivascular macrophages, known as the neurovascular unit (Neuwelt et al., 2011; Deli, 2011).

The unique anatomical structure of the BBB contributes to its specific functions. The BBB protects the CNS from toxic agents, pathogenic microorganisms and other insults from the systemic circulation (Abbott et al., 2010). The free exchange of cells and solutes between the blood and brain are restricted due to the lack of fenestrae in the capillaries of CNS, the tight interendothelial junctions, low level of pinocytotic activity and negatively charged luminal surface of brain endothelial cells (Deli, 2011). Only small lipophilic molecules (molecular weight < 400 Da), e.g. alcohol, nicotine, heroin, and blood gases, like O_2 and CO_2 can enter the brain via transcellular lipid-mediated free diffusion (Fig. 2, pathway 1; Pardridge, 2015a). The TJs strictly regulate the passive paracellular transport of molecules: crossing the BBB is inhibited for hydrophilic molecules containing more than seven hydrogen bonds (Pardridge, 2012). Therefore, most proteins, peptides and polysaccharides are not able to penetrate across the BBB. The glycocalyx constitutes an electrostatic barrier against anionic molecules (Lockman et al., 2004; Ribeiro et al., 2012). The negative electrostatic charge of luminal endothelial surface can interact with positively charged plasma proteins and partially allow their entry into the CNS with adsorptive mediated transcytosis (Fig. 2, pathway 3). This pathway is downregulated in physiological conditions, but it can be upregulated in pathologies (Hervé et al., 2008). The transport of biomolecules into or out of the brain and the communication between the periphery and the CNS are also regulated by the BBB. Receptor-mediated transcytosis and nutrient transporters (solute carriers, SLCs), two BBB specific pathways, provide the brain with nutrients, vitamins, minerals and metabolic precursors (Fig. 2; pathways 5 and 6, respectively; Campos-Bedolla et al., 2014). The active efflux transporters protect the brain against xenobiotics and regulate the levels of neurotransmitters and metabolites (Deli, 2011, César-Razquin et al., 2015).

Around 40 members of the SLC family were identified in brain capillaries (Morris et al., 2017). SLCs are membrane-coupled proteins, which maintain saturable, bi-directional transport of nutrients. SLCs can act as facilitated transporters, or ion-coupled transporters or exchangers, and their functions are independent from ATP hydrolysis (Campos-Bedolla et al., 2014). Glucose, the main energy source of the CNS can be delivered from blood into brain by

facilitated glucose transporters (GLUTs, SLC2A) and sodium/glucose co-transporters (SGLTs, SLC5A). GLUT1/SLC2A1 is the predominant glucose carrier in the brain, which maintains bidirectional, gradient dependent transport for hexoses (César-Razquin et al., 2015). Amino acids, monocarboxylic acids, nucleosides and vitamins are also carried by members of the SLC family to the brain. Peptides and proteins, like transferrin, insulin, leptin, ghrelin, or low density lipoprotein can reach the brain via receptor mediated transcytosis. These molecules can cross the BBB in three main steps: receptor mediated endocytosis, vesicular transcytosis across the thin cytoplasm and exocytosis (Campos-Bedolla et al., 2014). This transport pathway is energy dependent and can be bidirectional, e.g. in the case of transferrin.

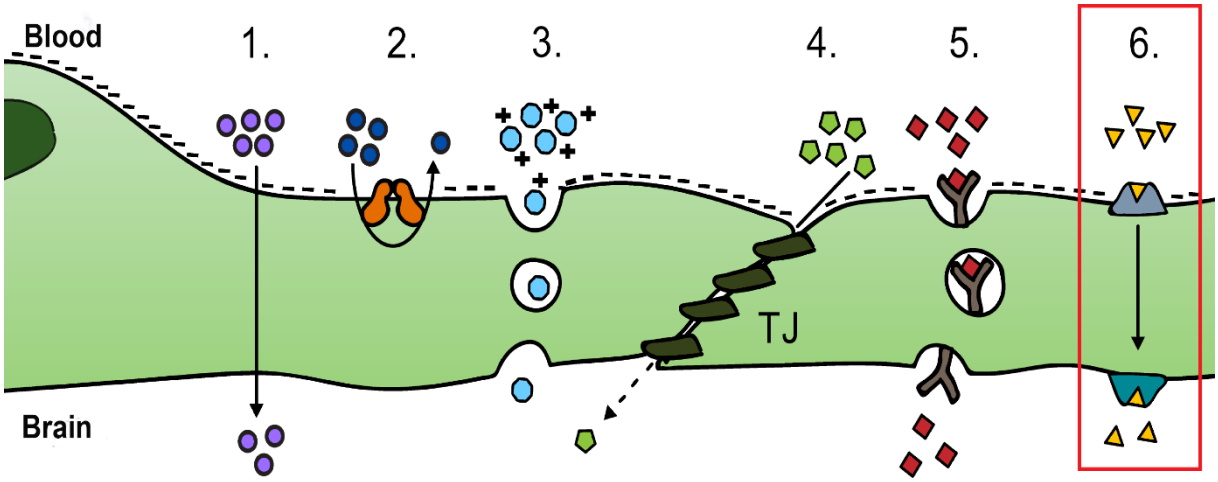

Figure 2. *Schematic drawing of transport pathways across the BBB. (1) lipid-mediated free diffusion, (2) active efflux transport, (3) adsorptive-mediated transcytosis, (4) inhibited paracellular diffusion, (5) receptor-mediated transcytosis, (6) solute carriers (based on Fig. 2. Campos-Bedolla et al., 2014).*

Active efflux proteins are responsible for detoxification and protection of the brain. Several efflux transporters are members of the ATP-binding cassette or ABC transporter family. P-glycoprotein (ABCB1), breast cancer resistance-associated protein (BCRP/ABCG2), and multidrug resistance proteins (MRPs, ABCC subfamily) restrict drug penetration into the brain in an energy dependent manner (Fig. 2, pathway 2; Ohtsuki and Terasaki, 2007; Uchida et al., 2011).

1.2. Drug delivery strategies across the blood-brain barrier

The BBB restricts not only the influx of toxic compounds but also the entry of potential neuropharmaceuticals, especially biopharmacons, like nucleic acids, peptide or protein drugs into the CNS (Pardridge, 2015b). Therefore, the pharmaceutical treatment of most CNS

disorders, like stroke, brain tumors and neurodegenerative diseases including Alzheimer's and Parkinson's diseases, is difficult (Wohlfart et al., 2012). Contrary to the assumption that small molecule drugs can cross the BBB, only a small fraction of them is able to enter the brain parenchyma (Pardridge, 2012; Pardridge, 2015b). Several clinical trials ended with failure because of the low penetration of biologic drugs across the BBB (Pardridge, 2016). To solve this problem different strategies have emerged to increase drug delivery to the CNS, which can be classified into three major groups, namely (i) circumvention of the BBB, (ii) modification of BBB functions, (iii) modification of drug molecules (Table 1; Deli, 2011).

Table 1. *Major strategies to increase drug delivery to the CNS.*

Strategies for drug delivery to CNS		
BBB circumvention	***Modifications of BBB functions***	***Modification of drug molecules***
Direct delivery	TJ modulation	Modificatations of physico-chemical properties
Nasal pathway	Efflux pump inhibition	BBB targeted delivery platforms (eg. nanoparticles)

Invasive drug delivery strategies, like direct intraventricular or intrathecal drug administration are successful in circumventing the BBB, however limitations, such as potential infectious risks must be considered. The non-invasive, alternative nasal pathway for transporting molecules to the brain also has some drawbacks: only a low amount of molecules can be transported to the brain and their distribution is limited to some brain areas, as it was shown earlier by our research group (Horvát et al., 2009; Sipos et al., 2010). Modifications of BBB functions to transiently increase brain endothelial permeability by small molecules (Hülper et al., 2013; Walter et al., 2015), or by peptides acting on interendothelial TJs (Bocsik et al., 2016, 2019) were also studied by our research team. However, problems regarding safety, reversibility, and potential systemic and cerebral side-effects need to be solved before making a decision on their applicability (Deli, 2011). The inhibition of BBB efflux transporters can increase CNS drug delivery even in human subjects, however they are still not used clinically due to toxic side effects (Bauer et al., 2018). There are several methods in medicinal chemistry to change the physico-chemical properties of molecules and thereby enhance their brain delivery. These techniques aim to increase the lipid solubility or the cationic charge of molecules (Banks, 2016). High lipid solubility can augment the transport of a given drug across

the BBB, but it can also enhance its uptake in peripheral tissues and sequestration in the capillary bed, resulting in decreased drug concentration in the blood and in the CNS (Banks, 2009). Therefore, new approaches are needed to improve brain drug delivery. Nanosized drug carriers, or nanoparticles (NPs), are in the focus of research efforts to develop successful drug delivery systems for the CNS (Begley, 2004; Veszelka et al., 2015).

1.3. Nanoparticles used for research on drug delivery to the central nervous system

Nanomedicine research is a rapidly expanding field of nanotechnology. NPs are colloidal systems, in the range of 1-1000 nm, which consist of macromolecular components or metals to carry drugs or bioactive materials (Kreuter, 2014). NPs can deliver therapeutic or imaging agents; if they carry both at the same time, they are called theranostics (Saraiva et al., 2016). The molecule targeting and releasing potential of NPs can be modified by changing their physico-chemical properties (Zhou et al., 2018). The requirements of NPs for CNS drug delivery are their biodegrability and non toxic characteristics, their relatively easy synthesis and their controlled loading or coupling with hydrophilic or hydrophobic drugs (Begley, 2004; Kreuter, 2014). Both solid nanoparticles (SNPs) and vesicular NPs, the two main types of nanoparticles (Fig. 3), are investigated as carriers to cross the BBB.

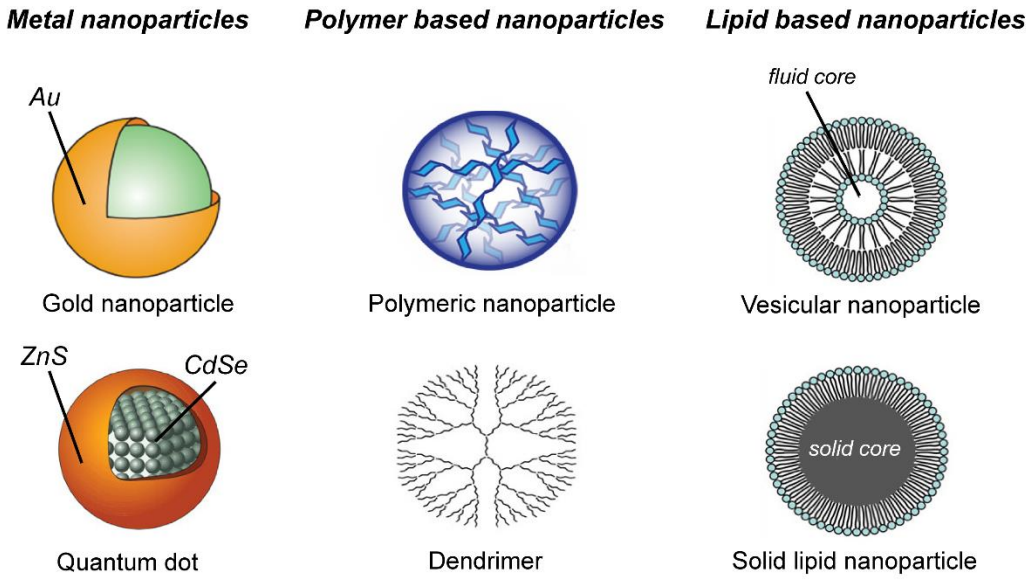

Figure 3. *Major nanoparticle types applied for drug delivery research*

Metal nanoparticles are applied in several fields of nanomedicine such as imaging, therapy and theranostics. The most documented metal NPs for CNS delivery include gold and iron oxides (Mc Carthy et al., 2015). Gold NPs are colloidal particles usually with a size of less

than 10 nm. Their optoelectronic properties and low toxicity make them important tools in nanobiotechnology (Yeh et al., 2012). The surface of gold NPs can be conjugated with antibodies or oligonucleotides in order to sense biomolecules. Drugs with various properties can interact with their surface either in non-covalent or covalent manner. They have been tested for many applications, especially for the diagnosis and therapy of experimental tumors (Yeh et al., 2012).

The iron oxide NPs due to their superparamagnetic properties enable both tracing by magnetic resonance imaging, and drug targeting to selected tissues or areas by applying magnetic fields (Ito et al., 2005). Application of iron nanoparticles is difficult, because they can easily aggregate and lose their function. Polymer coating on the surface of magnetic NPs can prevent their aggregation (Ito et al., 2005). The conjugation of iron oxide NPs with cell penetrating peptides can increase their cellular uptake (Mc Carthy et al., 2015).

Quantum dots are colloidal semi-conductor nanocrystals (< 50 nm), an important class of fluorescent labels for biological, biomedical and bio-sensing applications (Probst et al., 2013). Quantum dots have excellent fluorescent properties including high brightness, photostability, broad absorption spectra, and a tunable, narrow emission spectrum (Mc Carthy et al., 2015). Quantum dots can be useful research tools to follow in real-time the cellular uptake of NPs and their biodistribution in biological systems. They have also potentially useful therapeutic functionalities such as photothermal therapy and magnetofection (Probst et al., 2013). However, drug delivery with quantum dots is controversial due to the toxic heavy metal (Cd, As or Pb) components (Fig. 3) in the core and/or shell of NPs (Libralato et al., 2017; Probst et al., 2013).

Polymeric NPs for drug delivery (Fig. 3) are prepared from various biopolymers: poly(lactic-co-glycolic acid) or PLGA, poly(lactic acid) or PLA, poly-ε-caprolactone or PCL, chitosan, gelatin, poly-butilcynaoacrylates or PBCA, and some other biodegradable polymers (Mc Carthy et al., 2015). These materials form a core polymer matrix where the drugs can be incorporated and used for CNS delivery (Kreuter, 2014). Drugs in polymeric NPs are protected from enzymatic degradation due to their structure (Mc Carthy et al., 2015). Chitosan polymeric and human albumin NPs, which are biodegradable and non-toxic, were shown to cross the BBB and enter the brain in animal studies (Kreuter, 2014). Depending on the method of preparation polymer NPs possess a wide variety of structures, including branched, tree form polymers, called dendrimers (Fig. 3). The hydrophilic branched chains of dendrimers increase their drug

entrapping ability (Masserini et al., 2013). Dendrimers can be functionalized and have also been tested for CNS drug delivery in preclinical studies (Patel, 2014).

Polystyrene is an extensively used polymer, a plastic suitable for preparation of NPs. Polystyrene NPs are non-toxic, cheap, commercially available carriers prepared in a uniform shape and narrow size distribution with a size range of 50 to 300 nm (Loos et al., 2014). They form stable colloids in biological fluids, they can incorporate fluorescent dyes and their surface can be easily functionalized, therefore they are good experimental tools to study biomedical applications such as drug delivery (Loos et al., 2014; Libralato et al., 2017). Fluorescent polystyrene NPs were selected as model nanocarriers in our first study due to these properties.

Solid lipid NPs (Fig. 3) are made of triglycerides, fatty acids and waxes. They have a typical spherical shape and a solid hydrophobic lipid core (Craparo et al., 2011). This type of lipid based NP provides biocompatible carriers (120-200 nm), because organic solvents, which can be toxic for living cells, are not used during their preparation (Gastaldi et al., 2014). The melted lipids are mixed with the therapeutic drugs and dispersed in hydrophilic surfactants with microemulsification, which makes them extremely stable (Blasi et al., 2007). They can encapsulate mainly hydrophobic drugs, which limits their use (Masserini, 2013).

Vesicular lipid-based systems, especially liposomes, are the most widely investigated drug delivery platforms (Fig. 3). Like the plasma membrane of cells, liposomes consist of one or more phospholipid bilayers, which are composed of sphingomyelin, phosphatidylcholine or glycerophospholipids (Craparo et al., 2011; Mc Carthy et al., 2015). Liposomes can be classified as small unilamellar liposomes (< 100 nm), large unilamellar vesicles (> 100 nm) and multilamellar particles with many concentric lipid lamellae in the μm range. Cholesterol is a crucial component of liposomes, because it decreases the permeability of the bilayer, but at the same time it can increase their stability in a dose dependent manner (Masserini, 2013). Hydrophilic drugs can be encapsulated into the aqueous core of liposomes as cargo (Fig. 3), while lipophilic drugs can be inserted into the phospholipid bilayer (Sercombe et al., 2015). Liposomes have already been investigated in preclinical studies for treating brain tumors (Raucher et al., 2018), Alzheimer's disease (Ross et al., 2018), stroke or cerebral ischemia (Vieira and Gamarra, 2016).

Non-ionic surfactant based vesicular nanocarriers, known as niosomes, offer an alternative platform for vesicular drug delivery. Their main components could be alkyl ethers like Brij®, or alkyl esters such as sorbitan fatty acid esters (Span®) or polyoxyethylene sorbitan

fatty acid esters (Tween®) (Abdelkader et al., 2014; Bartelds et al., 2018). Niosomes are uni- or multilamellar vesicles with a neutral surface. Their structure is similar to that of liposomes, but they are more stable and their preparation is cheeper. Niosomes are also able to accumulate both water and lipid soluble drugs and control their release (Bartelds et al., 2018), and have several favorable properties such as good biocompatibility, biodegradability, non-immunogenicity and stability (Abdelkader et al., 2014). Another advantage of non-ionic surfactant based nanocarriers is that they increase the penetration of drugs across biological barriers and reduce their toxic side effects due to the encapsulation process (Masserini, 2013). Initially niosomes were used in the 1970s by the cosmetics industry, but since then they have been increasingly investigated in CNS drug delivery research (Moghassemi and Hadjizadeh, 2014; Bartelds et al., 2018; Gharbavi et al., 2018). For our second study we have chosen niosomes as a versatile carrier system which is less prone to oxidation and more stable than liposomes.

1.4. Properties of nanoparticles to influence drug delivery across the blood-brain barrier

The efficacy of nanoparticles in drug delivery across the BBB is determined by the size, shape, materials, surface charge and functionalization of NPs (Kevadiya et al., 2018). Several investigations showed that small nanoparticles (10–50 nm) can better accumulate in the brain tissue compared to nanoparticles larger than 200 nm in size (Mc Carthy et al., 2015). The average diameter of nanocarriers tested succesfully in animal models of CNS diseases was between 50-100 nm (Saraiva et al., 2016). For BBB targeting, the selected nanocarriers need to be stable for a long time in the systemic circulation, therefore their high chemical and biological stability, low toxicity and immunogenicity are crucial features (Kreuter, 2014).

In the circulating blood many classes of proteins, including opsonins, can attach to the surface of NPs and form a layer called ”corona”. These proteins trigger the removing of NPs from the blood with the help of the reticuloendothelial system, or they induce immune reactions (Masserini, 2013). Polysorbates or polyethylene glycol (PEG) coating on the surface of the carriers can ensure a prolonged circulation time due to protecting NPs from entrapping in the reticuloendothelial system of liver and spleen (Masserini et al., 2013; Mc Carthy et al., 2015). The surface charge of NPs is also a very important factor in brain drug delivery, because the highly positively charged surface could have direct toxic effects on brain endothelial cells. Therefore, NPs should have moderately (−1 to −15 mV) or highly (−15 to −45 mV) negative zeta potentials for successful brain targeting (Saraiva et al., 2016). Well-designed NPs are

protected from efflux transporters and enzymatic degradation, and offer self-regulated drug release (Mc Carthy et al., 2015; Veszelka et al. 2015).

The most important factor influencing biodistribution of nanocarriers, therefore, drug delivery efficacy is surface functionalization (Kevadiya et al., 2018). Molecules used for such purpose include surfactants, polymers, lipids, dendrimers, biomolecules and macromolecules. Many studies use cell-penetrating peptides, like penetratin or Tat (trans-activated transcription peptide of HIV-1 virus) to functionalize NPs (Masserini, 2013, Mc Carthy et al., 2015), however, they do not provide specific targeting to brain.

1.5. Transport pathways for blood-brain barrier specific nanoparticle targeting

Drug encapsulation in NPs alone is not enough for successful delivery of drugs to the CNS (Wohlfart et al., 2012). In order to elevate the permeability of nanocarriers across the BBB specific targeting is needed (Kreuter, 2014). Various essential influx transport systems are expressed on the cerebral endothelium playing a physiological role in nutrient delivery (Campos-Bedolla et al., 2014). These influx transport systems, such as receptor mediated endocytosis, adsorptive mediated endocytosis and carrier mediated transport systems (Abbott, 2013) can be potentially exploited to shuttle nanocarriers to the brain (Kreuter, 2014; Mc Carthy et al., 2015).

Targeting molecules to deliver fusion peptides or NPs to the brain could be antibodies, ligands or peptides interacting with BBB specific receptors (Pardridge, 2015a; Pardridge, 2017; Kevadiya et al., 2018). The transferrin receptor (TfR) is one of the most studied BBB receptor for targeted delivery of drug-loaded NPs to the CNS (Johnsen and Moos, 2016). TfRs are expressed on brain endothelial cells and participate in iron transport. In drug delivery studies mostly liposomes conjugated with anti-TfR antibodies or transferrin were tested. Despite the potential applicability of TfRs there are conflicting reports on sufficient transcytosis of NPs across the BBB using this receptor mediated system (Johnsen and Moos, 2016). A fusion protein, valanafusp alpha, in which the immunoglobulin G domain targets the BBB human insulin receptor to enable transport of the coupled α-L-iduronidase lysosomal enzyme into the brain has been tested in clinical studies and offers a pharmacological approach to the stabilization of cognitive function in mucopolysaccharidosis type I patients (Giugliani et al., 2018).

Another possible route for cationized proteins to enter the brain is the adsorptive mediated endocytosis, which is based on the interaction of the molecules with the negatively charged

membrane surface of brain endothelial cells (Hervé et al., 2008). As an example, the transfer of bovine serum albumin loaded into cationic lipid coated NPs increased 27-fold across a BBB culture model (Fenart et al., 1999).

Glutathione is also used as a targeting ligands of NPs to cross the BBB. This tripeptide with antioxidant properties has a central role in the detoxification of intracellular metabolites (Kannan et al., 2000). Active glutathione transport was described across the BBB, but the putative transporter(s) is unknown (Gaillard, 2016). Nevertheless, glutathione, as a targeting ligand, increased drug delivery to brain by NPs in several studies (Birngruber et al., 2014; Lindqvist et al., 2016). The group of Gaillard demonstrated the efficacy of glutathione targeted liposomal doxorubicin in a mouse glioma model (Gaillard et al., 2014) and these NPs were also investigated in clinical trials (Gaillard, 2016).

1.6. Solute carriers and blood-brain barrier specific nanoparticle targeting

SLC transporters are actively investigated as drug targets and the number of drug candidates developed for these carriers and reaching clinical trials increases steadily (Rask-Andersen et al., 2013). However, this pathway is not fully exploited for drug delivery (César-Razquin et al., 2015), and for targeted NPs in particular. In contrast to NPs targeted with antibodies or peptides for CNS drug delivery, there are only few papers describing NPs labeled with ligands of nutrient transporters present at the BBB.

Among the SLCs, the expression level of glucose transporter GLUT1 (SLC2A1) is the highest at the BBB, but other members of the SLC2A family are also present (Enerson and Drewes, 2006; Campos-Bedolla et al., 2014). Glucose analogs have a potential to be efficient and selective targeting ligands for both solid and vesicular nanocarriers to cross the BBB. Gold NPs covalently labeled with glucose, a ligand of hexose transporters, transferred better than unlabeled NPs across monolayers of a brain endothelial cell line (Gromnicova et al., 2013). Glucose analog-targeted vesicular NPs were used successfully to deliver vasoactive intestinal peptide to brain in mice (Dufes et al., 2004).

The number and expression level of SLCs transporting amino acids across the BBB are also high (Enerson and Drewes, 2006; Shawahna et al., 2011). They not only provide nutrients but contribute to drug delivery (Begley, 2004). The most well known drug to treat Parkinson's disease, L-DOPA, enters the brain via the the large amino acid transporter-1 (LAT1/SLC7A5) transporter (Pardridge, 2015b). Phenylalanine, a ligand of LAT1, was used as a targeting molecule of solid lipid NPs to increase the transfer of the anti-HIV agent efavirenz across the

BBB both in cell culture and in drug penetration studies in rats (Vyas et al., 2015). Neutral amino acids, like alanine, serine and cysteine, are transported by carriers belonging to the sodium-coupled neutral amino acid transporter families (SNAT/SLC38A and ASCT/SLC1A; Campos-Bedolla et al., 2014), but alanine has not been described as a BBB specific targeting ligand of NPs.

SLCs also provide the brain with vitamins for its proper functioning (Campos-Bedolla et al., 2014). The sodium-dependent multivitamin transporter (SMVT/SLC5A6) is responsible for the transport of biotin (vitamin B7) across the BBB (Campos-Bedolla et al., 2014; Uchida et al., 2015). Biotin has long been used for ligation techniques, imaging and diagnostics based on the strong interaction between biotin and avidin. Biotin-avidin technology has a potential to be applied for targeted drug therapy of tumors (Lesch et al., 2010). However, biotin has not yet been tested as a potential targeting ligand of NPs to cross brain endothelial cells.

2. AIMS

Effective CNS drug targeting with NPs is an unsolved problem. Our main purpose was to design nanocarrier systems for elevating the penetration of cargo molecules across the BBB. Since SLCs are highly and specifically expressed at the BBB, our hypothesis was that NPs with SLC ligands, especially dual ligand combinations will increase the brain endothelial uptake and permeability of the cargo across the BBB. Therefore the major aims of our experiments were:

(I) To verify the gene expression levels of selected SLCs in isolated brain microvessels and *in vitro* BBB models

(II) To test biotin and glutathione as targeting ligands for polystyrene SNPs on a culture BBB model

(III) To prepare and characterize non-ionic surfactant based vesicular NPs loaded with large biomolecule serum albumin as a cargo and targeted with single or dual combination of SLC ligands and glutathione

(IV) To investigate niosomes on cellular viability, uptake and permeability of cargo using a BBB culture model

(V) To reveal the possible mechanisms of the cellular uptake process and the role of the brain endothelial surface charge

(VI) To examine the brain penetration of fluorescent cargo encapsulated in single- and dual SLC ligand-targeted niosomes by optical imaging *in vivo*

3. MATERIALS AND METHODS

3.1. Animals

Animal studies were performed following the regulations of the 1998. XXVIII. Hungarian law and the EU Directive 2010/63/EU about animal protection and welfare. Approval for animal studies was obtained from the local animal health authority, the Governmental Office for Csongrád County, Directorate of Food Chain Safety and Animal Health (Permit numbers: XVI./03835/001/2006, XVI./834/2012). For the *in vivo* experiments ten week old male CD1-Foxn1nu nude mice (Charles River Laboratories, Wilmington, MA, USA) were used. For the microvessel and in vitro primary cell isolations, brain tissues were obtained from 3-month-old (microvessels) 3-week-old (brain endothelial cells and pericytes) or newborn (glial cells) outbred Wistar rats (Harlan Laboratories, United Kingdom) of both sexes. Animals were fed on standard rodent chow and water ad libitum and kept under a 12h light/dark cycle in the conventional animal house of the Biological Research Centre. During the experiments, all efforts were made to minimize animal suffering and pain.

3.2. Materials

All reagents were purchased from Sigma-Aldrich Kft. Hungary (part of Merck Life Science), except for those specifically mentioned.

3.3. Cell cultures

The human cerebral microvascular endothelial cell line hCMEC/D3 (Weksler et al., 2013), a human *in vitro* BBB model (Helms et al., 2016) was grown in MCDB 131 medium (PAN-Biotech, Germany) supplemented with FBS (5%), GlutaMAX (100×, Life Technologies, USA), Chemically Defined Lipid Concentrate (100×, Life Technologies, USA), ascorbic acid (10 μg/mL), hydrocortisone (550 nM), heparin (100 μg/mL), bovine basic fibroblast growth factor (1 ng/mL, Roche, Switzerland), insulin (2.5 μg/mL), transferrin (2.5 μg/mL), sodium selenite (2.5 ng/mL) and gentamycin (50 μg/mL). hCMEC/D3 cells (passage number ≤ 35) were cultured for 3-5 days until full confluency and received 10 mM lithium chloride (Merck, USA) 24 h before experiments to induce BBB properties (Liebner et al., 2008; Weksler et al., 2013).

Isolation of primary rat brain endothelial cells (RBECs), pericytes, astroglia and the construction of the in vitro BBB triple co-culture model were performed according to the method described in our previous studies (Veszelka et al., 2007; Nakagawa et al., 2009; Walter

et al., 2015). RBECs were cultured in DMEM/F12 (Dulbecco's modified Eagle medium supplement with nutrient mixture F-12; Gibco, LifeTechnologies, Carlsbad, CA, USA), 15% plasma-derived bovine serum (PDS, First Link, Wolverhampton, UK), 100 µg/mL heparin, medium supplement with 5 µg/mL insulin, 5 µg/mL transferrin, 5 ng/mL sodium selenite (ITS; PAN-Biotech, Germany), 1 ng/mL basic fibroblast growth factor (bFGF, Roche, Basel, Switzerland) and 50 µg/mL gentamycin. During the first three days of culture the medium of RBECs contained 3 µg/mL puromycin to eliminate P-glycoprotein negative, contaminating cell types (Perrière et al., 2005). For the permeability studies a triple co-culture BBB model was used (Nakagawa et al., 2009). For this model, in addition to brain endothelial cells, primary rat brain pericytes were isolated using the same method as for brain endothelial cells, except that pericytes were plated onto uncoated culture dishes and did not receive puromycin. Primary cultures of rat glial cells were prepared from one-day-old Wistar rats and passaged (8.5×10^4 cells/well) to 12 well plates (Corning, Costar, New York, NY, USA) coated with collagen type IV (100 µg/mL in sterile distilled water). Rat glial cells were cultured for two weeks before using them for the co-culture model (Veszelka et al., 2007). Pericytes and glial cells were cultured in DMEM/F12 supplemented with 10% fetal bovine serum (FBS; PAN-Biotech, Germany) and 50 µg/mL gentamycin. To prepare the co-culture model, pericytes at P2 were passaged (1.5×10^4 cells/well) to the collagen coated bottom side of tissue culture inserts (Transwell, polycarbonate membrane, 3 µm pore size, Corning Costar, USA) and brain endothelial cells were seeded (7.5×10^4 cells/insert) to the upper side of the Matrigel (growth factors reduced; Corning Costar, USA) coated membranes. Then the inserts containing brain endothelial cells and pericytes on the two sides of the membrane were placed to 12 well plates in which glial cells were grown at the bottom (Fig. 4). Both the upper and lower fluid compartments of this system received endothelial culture medium supplemented with hydrocortisone (550 nM) and the three types of cells were cultured together for four days before permeability experiments (Nakagawa et al., 2009; Walter et al., 2015).

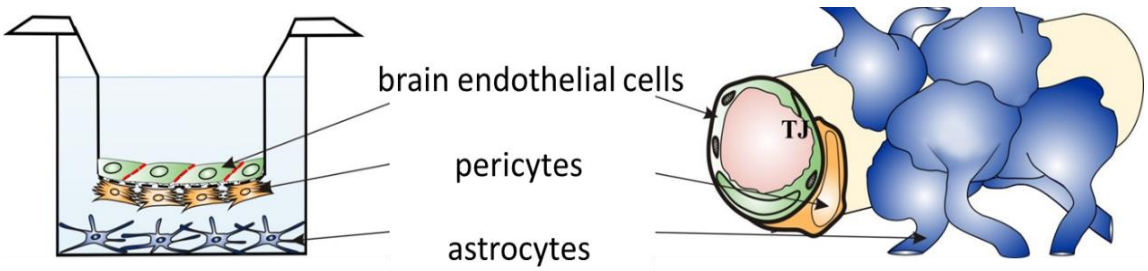

Figure 4. *Schematic drawing of BBB co-culture model.*

3.4. Gene expression study of solute carriers

3.4.1. RNA isolation and quality control

RNA was isolated from rat brain microvessels, hCMEC/D3 cells and RBECs co-cultured with glia and pericytes. The microvessel isolation was based on methods described in previous studies (Veszelka et al., 2007, Dauchy et al., 2008). The RBECs in the BBB model were co-cultured for 4 days and hCMEC/D3 were grown for 5 days in 10 cm dishes. After reaching confluency the cells were scraped, collected and cell pellets were used for total RNA isolation using RNAqueous-4PCR Kit (Ambion, Life Technologies, USA) with DNase1 (RNase-free) treatment according to the manufacturer's instructions. The concentrations and purity of the DNase-treated RNA samples were assessed by a NanoDrop ND-1000 spectrophotometer (NanoDrop Technologies, USA). The integrities of the isolated RNAs were characterized using Bioanalyzer 2100 (Agilent Technologies, USA). The RNA integrity numbers (RIN) were between 9.2 and 10 in the case of all studied RNA samples.

3.4.2. Quantitative real-time polimerase chain reaction and data analysis

In all cases, cDNA synthesis was performed on 1 μg total RNA samples by High Capacity cDNA Reverse Transcription Kit (Life Technologies, USA) using random hexanucleotide primers and MultiScribe Reverse Transcriptase in the presence of RNase inhibitor according to the manufacturer's protocols. The expression of the genes of transporters for glucose (*GLUT1/SLC2A1, GLUT3/SLC2A3, GLUT5/SLC2A5*), the genes of transporters for alanine (sodium-coupled neutral amino acid transporters *SNAT1/SLC38A1, SNAT2/SLC38A2, SNAT3/SLC38A3, SNAT5/SLC38A5*; neutral amino acid transporters *ASCT1/SLC1A4, ASCT2/SLC1A5*) and the genes of transporters for biotin (sodium-dependent multivitamin transporter *SMVT/SLC5A6*) were analyzed by quantitative PCR using TaqMan Low Density Array 384-well microfluidic cards preloaded with TaqMan Gene Expression Assays (Life Technologies, USA). Quantitative real-time PCRs (qPCR) were performed by ABI TaqMan Universal Master Mix (Life Technologies, USA) using the ABI Prism 7900 system (Applied Biosystems, Life Technologies, USA). Data were analyzed using the ABI SDS 2.0 software (Applied Biosystems, Life Technologies, USA). In all samples the expression of genes was normalized to 18S rRNA, which was used as an endogenous control ($\Delta C_t = C_{tgene} - C_{t18S\ rRNA}$). Expression values of studied genes were determined based on the normalized expression of genes calculated with $2^{-\Delta Ct}$ formula which were correlated to the lowest normalized expression measured by the applied qPCR method. For quantification of relative expression level of genes

of interest, the normalized expression data were analyzed using the comparative $\Delta\Delta C_t$ method (Livak and Schmittgen, 2001; Tóth et al., 2014).

3.5. Experiments with targeted solid nanoparticles

3.5.1. Synthesis of the targeting ligand for solid nanoparticles

Biotinyl-6-aminohexanoyl-lysyl-glutathione, as targeting ligand was synthesed for SNPs. The N-terminal amino group of glutathione is positively charged at physiological pH. Acylation of this amino group with biotin would diminish this positive charge. To avoid the change of the overall charge of the molecule a lysine residue was built into the peptide. A 6-aminohexanoic acid spacer was also incorporated between the lysyl-glutathione and the biotin. Biotinyl-6-Ahx-Lys-γGlu-Cys-Gly-OH peptide was synthesized on Fmoc-Gly-Wang resin in 0.25 mmolar scale. Fmoc group was removed by treating the resin with 20% piperidine in DMF first for 5 min then with a new portion of the above mentioned solution for 20 min. All Fmoc protected amino acids and biotin were coupled as follows: 1 mM of the amino acid was activated with DCC/HOBt (1 mM each) in DMF/DCM (1:1, v/v). The coupling time was 2 h. The reaction was monitored with qualitative ninhydrin test. If the test was positive, the coupling was repeated using HATU/DIEA activation of the amino acid. The peptide was cleaved from the resin by treating the peptide-resin with a mixture containing TFA (90 v/v%), TIS (2 v/v%), DTT (4 m/v%) and water (4 v/v%) for 15 min at 0 ºC and for 1 h 45 min at room temperature. The peptide was then precipitated with cold diethyl ether, filtered, washed with diethyl ether, dissolved and lyophilized. The product was analyzed and purified by HPLC. Analytical analysis was done on a Hewlett-Packard Agilent 1100 Series HPLC apparatus using a Luna C18 column (100 Å, 5 µm, 250×4.60 mm; Phenomenex, USA). Preparative chromatography was done on a Shimadzu HPLC apparatus equipped with a Luna C18 column (100 Å, 15 µm, 250×21.2 mm; Phenomenex, USA). As eluent A and eluent B 0.1 % TFA in d.d. water (Solvent A) and 80% ACN, 0.1% TFA in distilled water (Solvent B) was used, respectively.

3.5.2. Functionalization of solid nanoparticles

Neutravidin labeled 40 nm polystyrene red fluorescent nanoparticles (TransFluoSpheres Fluorescent Microspheres, T8860, Thermo Fisher Scientific Inc., USA) were used for the study. The 100 µl nanoparticle suspension bearing 8.23 nM neutravidin functionality, the density of polystyrene was 1.055 g/cm^3 in buffer (50 mM sodium phosphate, 50 mM NaCl, 0.02% Tween 20, 5 mM azide, pH 7.5). To label the nanoparticles 100 µL of suspension was incubated with 30 µL distilled water containing 3-fold molar excess of biotin or biotinylatedglutathione for 2 h

at room temperature. The different groups of nanoparticles were prepared from different batches of TransFluoSpheres. The control, non-labeled solid nanoparticles (SNP) and the derivatized biotin-labeled (SNP-B) and biotinylated glutathione-labeled (SNP-B-GSH) nanoparticles were stored at 4 ºC until the experiments.

3.5.3 Characterization of solid nanoparticles

The nanoparticles were characterized for particle size and zeta potential using dynamic light scattering (Malvern Zetasizer Nano ZS, Worcestershire, UK). Before measurements, the SNPs were diluted and the final concentrations were 0.15 mg/mL in phosphate buffered saline (PBS; KCl 2.7 mM, KH_2PO_4 1.5 mM, NaCl 136 mM, $Na_2HPO_4 \times 2\ H_2O$ 6.5 mM, pH 7.4). The mean particle size and mean zeta potential values were calculated from three measurements per sample. The morphology of nanoparticles was visualized by scanning electron microscopy (SEM; JEOL, JSM-7100F-LV, Akishima, Japan). Before SEM observation, a droplet of nanoparticles was diluted to 10^5 and 1 μL of the solution was pipetted onto a clean mica surface and then air-dried. After sputtering 8 nm gold on the sample, the nanoparticles were imaged in high vacuum mode at 5 kV.

3.5.4. Cell viability measurement: MTT assay

To test the viability and metabolic activity of brain endothelial cells after treatment with SNPs cellular reduction of the yellow 3-(4,5-dimethylthiazol-2-yl)-2,5-diphenyltetrazolium bromide (MTT) dye to formazan crystals was used (Kiss et al., 2013). Confluent cultures of hCMEC/D3 in 96-well plates (Orange Scientific, Belgium) were treated with SNPs diluted in culture medium in the concentration range of 0.01–1 mg/mL for 24 h. Triton X-100 detergent (1 mg/mL) was used as a reference substance to determine the 100% cellular toxicity. After treatment MTT solution (0.5 mg/mL) was added to the wells for 3 h at 37°C. Formazan produced by living cells was dissolved in dimethyl sulfoxide. Absorbance was detected by a multiwell plate reader at 570 nm (Fluostar Optima, BMG Labtechnologies, Germany). Cell viability and metabolic activity are reflected by the MTT dye conversion and was calculated as the percentage of dye reduction by culture medium treated (control) cells.

3.5.5. Measurement of the uptake of solid nanoparticles in human brain endothelial cells

The hCMEC/D3 cells were seeded to 24-well plates (Corning Costar, USA) at the density of 2×10^4 cells/well. After 3 days the confluent monolayers were incubated with 150 μg/mL SNP, SNP-B, SNP-B-GSH for 4 or 8 h at 37 ºC in a CO_2 incubator. After incubation the cells

were washed three times with ice cold PBS and lysed in 500 µL/well Triton X-100 detergent (10 mg/mL). To quantify the uptake of SNPs the fluorescence of cell lysates was measured with a spectrofluorometer (Fluorolog 3, HORIBA Jobin Yvon, Japan) at 488 nm excitation and 605 nm emission wavelengths.

To visualize the cellular uptake of the fluorescent particles brain endothelial cells were grown on collagen coated glass cover slips (VWR, USA) and treated with 150 µg/mL SNP, SNP -B or SNP-B-GSH for 24 h. Cells were fixed with 4% paraformaldehyde in PBS for 30 min, washed three times with PBS then cell nuclei were stained with bis-benzimide (Hoechst dye 33342) for 10 min. Samples were mounted with Fluoromount-G (Southern Biotech, USA), and examined with a confocal laser scanning microscope (Olympus Fluoview FV1000).

3.5.6. Permeabilty of solid nanoparticles across human brain endothelial cell monolayers

For permeability studies hCMEC/D3 cells were seeded onto collagen coated 12-well tissue culture inserts (Transwell clear, polyester membrane, 0.4 µm pore size, Corning Costar, USA; 4×10^4 cells/insert) and cultured for 5 days. Culture medium was changed every second day. The integrity of the monolayers was checked by Evans blue-labeled bovine serum albumin (EBA, 67 kDa; 0.167 mg/mL EB, 10 mg/mL BSA) permeability marker molecule. The cells were treated with 150 µg/mL SNP, SNP-B or SNP-B-GSH diluted in culture medium in the upper compartments (0.5 mL) for 8 h. After incubation samples were collected from the lower compartments (1.5 mL) and measured with a Fluorolog 3 spectrofluorometer at 488 nm excitation and 605 nm emission wavelengths for the SNPs and with Fluostar Optima at 584 nm excitation and 680 nm emission wavelengths for EBA. The apparent permeability coefficients (P_{app}, cm/s) were calculated as described previously (Bocsik et al., 2015) by the following equation:

$$P_{\text{app}}(\text{cm/s}) = \frac{\Delta[C]_A \times V_A}{A \times [C]_D \times \Delta t}$$

Briefly, P_{app} was calculated from the concentration difference of the nanoparticles in the lower or acceptor compartment ($\Delta[C]_A$) after 4 h and $[C]_D$ is the concentration in the donor (upper) compartments at 0 h, and V_A is the volume of the acceptor compartment (1.5 mL), and A is the surface area available for permeability (1.1 cm^2).

3.6. Experiments with targeted vesicular nanoparticles

3.6.1. Synthesis of targeted ligands for niosomes

For the synthesis of DSPE-PEG-glutathione, 13.5 mg glutathione (0.044 mM) was reacted with 100 mg DSPE-PEG-maleimide (0.035 mM) (N-[(3-maleimide-1-oxopropyl) aminopropyl polyethyleneglycol-carbamyl] distearoylphosphatidyl-ethanolamine, or Sunbright® DSPE-020MA; NOF Europe, Belgium) in 0.1 M ammonium acetate for a day under nitrogen. The product was lyophilized three times to remove ammonium acetate.

Dodecanoyl-alanine was prepared according to the literature method (Liu et al., 2014). Briefly, 100 ml NaOH (1 M) and 1.34 g (0.015 mol) L-alanine were added into a one-neck flask. After the system was cooled to 0 ºC, 3.31 ml (0.014 mol) dodecanoyl-chloride was added dropwise to the mixture and maintained for 5 h at 0 ºC. Then 16 ml hydrochloric acid (12 M) was added to the reaction and the white precipitate was filtrated. Finally the product was washed three times with deionized water and dried at 45 ºC for 24 h.

3.6.2. Preparation of targeted niosomes loaded with albumin

Non-ionic surfactants, Span 60 (sorbitane-monostearate) and Solulan C24 (cholesteryl-poly-24-oyxyethylene-ether, Chemron Co. USA) were dissolved with cholesterol in hot 1:2 mixtures of chloroform and ethanol in a round-bottom flask (Fig. 5). N-dodecyl-β-D-glucopyranose (GP, 9% (w/w) of total lipid), dodecanoyl-alanine (A, 5% (w/w) of total lipids) or pegylated-GSH (GSH, 5% (w/w) of total lipids) were added to prepare targeted niosomes (N-GP, N-A, N-GSH) (Dufes et al., 2004; Gaillard et al., 2014). For dual-targeted NPs (N-A-GP, N-A-GSH, N-GP-GSH) the content of ligands was 4-4 % (w/w) of the total lipids. The removal of organic solvents by vacuum pump yielded a thin lipid film layer (Fig. 5).

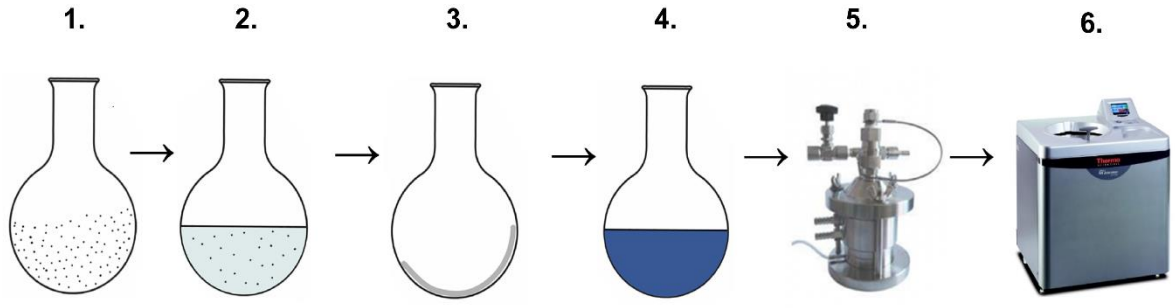

Figure 5. *Preparation steps of niosomes: (1-2) dissolving non-ionic surfactants, cholesterol and transporter ligands in ethanol and chloroform, (3) lipid film formation by evaporation of solvents, (4) hydratation of dried lipid film with the solution containing cargo molecules followed by sonication, (5) high pressure extrusion, (6) ultracentrifugation.*

The dry lipid film was hydrated with PBS containing EBA. The mixture was heated at 40 °C in a water bath and sonicated for 25 min. The suspension was forced through a polycarbonate filter (Whatman filter, 13 mm, 100 nm pore size) by lipid extrusion technique (high pressure thermobarrel extruder, Lipex Biomembranes Inc., USA) to yield vesicles. The non-entrapped cargo was removed by ultracentrifugation (123,249 *g*, 6 h, 4 °C), the pelleted niosomes were resuspended in PBS or phenol red free DMEM/F12 medium and stored at 4 °C.

3.6.3. Preparation of targeted niosomes loaded with lanthanum and lanthanum measurement

For transmission electron microscopy experiments niosomes with the electron dense lanthanum nitrate hexahydrate (433 Da), as a cargo, were prepared by hydrating the lipid film with PBS containing 5 mg/mL lanthanum. The lanthanum content of the particles was determined by a quadrupole Agilent 7700× inductively coupled plasma mass spectrometer (ICP-MS). The sample introduction system consisted of an Agilent I-AS auto sampler and a Micro Mist pneumatic nebulizer in a Peltier-cooled Scott-type spray chamber. The sample uptake rate was 400 μL/min. The ICP plasma and interface parameters were set up as follows: RF forward power: 1550 W, plasma gas flow rate: 15.0 L/min, carrier gas flow rate: 1.05 L/min, sampling depth: 10.0 mm. Ultra trace quality HNO_3 acid was used for the acid dissolution of the samples at 180 °C. The digestion time was 1 h. Signal tuning was performed by Agilent (No. G1820-60410) solutions, whereas calibration was done using solutions prepared from an IV-ICPMS-71A multielement stock standard (Inorganic Ventures, USA). The 99.996% purity argon gas used was purchased from Messer Hungarogáz (Hungary). Data processing was performed within the Agilent Mass Hunter software (Agilent Technologies, USA).

3.6.4. Characterization of niosomes

3.6.4.1. Measurement of size, charge and encapsulation efficiency

The NPs were characterized for particle size and zeta potential using dynamic light scattering (Zetasizer Nano ZS, Malvern Pananalytical, UK). Before measurements the niosome samples were diluted in PBS to a final concentration of 200 μg/mL. The means of particle size and zeta potential data were calculated from the average of three measurements per sample. To examine the stability of particles the physico-chemical properties of niosome samples have been followed for 6 month. To determine the amount of encapsulated dye in the NPs, EBA was released from the niosomes with 50% (v/v) ethanol and measured by a Fluorolog 3 spectrofluorometer at 584 nm excitation and 663 nm emission wavelengths. The fluorescence

values were extrapolated to concentrations from a standard calibration curve (r^2=0.9985). The encapsulation efficiency % (EE%) was calculated by the following equation (Geldenhuys et al., 2015):

$$\text{EE\%} = \frac{\text{Amount of EBA in the NP sample}}{\text{Amount of EBA in the hydrating buffer}} \times 100$$

3.6.4.2. Transmission electron microscopy

Aliquots of the niosome samples (10 µl) were placed on formvar carbon 400-mesh copper grids (Electron Microscopy Sciences, USA). Images were taken on a JEOL JEM-1400 transmission electron microscope (JEOL Ltd., Japan) operating at 120 kV. Images were captured routinely at magnifications of 20 000×, 25 000× and 30 000×, and analyzed with a SightX Viewer Software (EM-15300SXV Image Edit Software, JEOL Ltd., Japan).

3.6.4.3. Atomic force microscopy

A two-beam interference lithography arrangement was applied to generate sub-micrometer periodic intensity modulation in the laser beam irradiating the samples (Csete et al., 2007). The fourth harmonic of a Nd:YAG laser (λ_{FH} = 266 nm, t = 10 ns, f = 10 Hz) was diffracted impinged on a reflective grating (PUV 1200, Spectrogon), and the first order diffracted beams were recombined at the sample surface. The samples were silicone wafer substrates spin-coated by polycarbonate, which were treated by s-polarized beams, to produce linear gratings as described earlier (Csete et al., 2007).

The laser treated surfaces were scanned by atomic force microscopy (AFM) operating in digital pulsed force mode (DPFM, Witec GmbH, Germany). The advantage of this scanning mode is the possibility to map the micromechanical properties of the surface with high resolution. We applied standard PFM tips (NSC 18/NoA1, 2.5 N/m) and collected pictures about the topography and adhesion, which revealed that the adhesion is stronger in the valleys of the linear grating, thus facilitating the deposition of particles.

To examine niosomes the samples with laser-grated surfaces were completely immersed in fresh PBS solutions containing niosomes. Incubation of the samples in the solutions lasted for 1 h at 37 °C, then all samples were washed three times in sterile distilled water on a horizontal shaker and finally allowed to dry overnight at room temperature. An AFM (XE-100,

Park Systems Corp., South Korea) operating in tapping-mode was applied to detect the attached nanoparticles using tapping-mode NT-MDT tips (NSG11, 5.5 N/m, 150 kHz, NT-MDT).

3.6.5. Cell viability assay

Kinetics of RBECs reaction to niosome treatment were monitored by impedance measurement (RTCA-SP instrument; ACEA Biosciences, USA). Impedance measurement is label-free, real time, noninvasive, and correlates linearly with the adherence and growth of cells. After background measurements, cells were seeded at a density of 6×10^3 cells/well in collagen coated 96-well plates with integrated gold electrodes (E-plate 96, ACEA Biosciences). Cells were cultured for 5-7 days in CO_2 incubator at 37 ºC and monitored for 4 h. Triton X-100 detergent (10 mg/mL) was used as a reference compound inducing cell toxicity. Cell index was defined as R_n-R_b at each time point of measurement, where R_n is the cell-electrode impedance of the well when it contains cells and R_b is the background impedance of the well with the medium alone. Cell index values reflect cell number and viability (Kiss et al. 2013; Bocsik et al., 2016).

3.6.6. Measurement of the cellular uptake of niosomes

The RBECs were cultured in 24 well plates (Corning Costar, USA) at the density of 3×10^4 cells/well. The confluent monlayers were incubated with 10 mg/mL niosome solutions (N, N-GP, N-A, N-GSH, N-A-GP, N-GP-GSH, N-A-GSH) in culture medium for 4 h. The uptake of single or dual-targeted niosomes in RBECs was tested at 4 ºC and 37 ºC. To elucidate the uptake mechanisms of targeted niosomes cells were co-treated with metabolic inhibitor sodium azide (1 mg/mL) or pretreated with endocytosis inhibitors, filipin (15 min, 6 μM) and cytochalasin D (1 h, 20 μM) in culture medium. To study the role of the surface charge in cellular uptake of NPs the surface glycocalyx of RBECs was digested with neuraminidase (1 U/mL, 1h pretreatment), or the cells were pretreated with a cationic lipid 1-(4-trimethylammoniumphenyl)-6-phenyl-1,3,5-hexatriene (TMA-DPH; Molecular Probes, Life Technologies, USA) at 54 μM concentration for 30 min before the uptake experiment. After incubation with niosomes RBECs were washed three times with ice cold PBS supplemented with 1% BSA and once with acid stripping buffer (glycine 50 mM, NaCl 100 mM, pH 3) to remove cell surface associated niosomes. Finally cells were lysed in PBS with Triton X-100 detergent (10 mg/mL) and the fluorescent signal was detected with a Fluorolog 3 spectrofluorometer at 584 nm excitation and 663 nm emission wavelengths.

3.6.7. Visualization of the cellular uptake of niosomes

To visualize the uptake of the fluorescent particles RBECs were grown on glass bottom Petri dishes (Corning Costar, USA) coated with Matrigel and treated with 10 mg/mL niosomes for 4 h. To stain cell nuclei *bis*-benzimide (Hoechst dye 33342; 1 μg/mL, 10 min) was used. After incubation living cells were washed three times with Ringer-Hepes buffer (150 mM NaCl, 5.2 mM KCl, 2.2 mM $CaCl_2$, 0.2 mM $MgCl_2$, 5 mM D-glucose, 6 mM $NaHCO_3$ 10 mM Hepes, pH 7.4) supplemented with 1% PDS and examined with a confocal laser scanning microscope (Olympus Fluoview FV1000).

The cellular uptake of targeted NPs was also examined by transmission electron microscopy. RBECs were grown on culture inserts and treated with non-targeted (N) or dual-targeted (N-A-GSH) niosomes (10 mg/mL) containing lanthanum cargo for 4 h at 37 ºC. Control cells were treated 0.2 μg/mL lanthanum, the same concentration as entrapped in the niosomes. After incubation, RBECs were briefly rinsed in 0.1 M phosphate buffer (PB), then fixed in 4% paraformaldehyde + 2.5 % glutaraldehyde dissolved in 0.1 M PB at 4 ºC for 30 min. After rinsing in 0.1 M PB the inserts were removed from the tissue culture plates and transferred into 50 mL centrifuge tubes containing 0.1 M PB and kept at 4 ºC overnight. Cells on the membranes were postfixed in 1% aqueous OsO_4 for 1 h at room temperature, washed in tri-distilled water for 10 min and processed in a graded series of ethanol (50%, 70%, 90%, 96%, 100%, 100%) for 10 min in each solution. Then, 4-5 mm small pieces of the membranes with cells were embedded in Durcupan. Semithin (0.5 μm) sections were cut from the blocks on a Reichert OM-U2 ultramicrotome, which were stained to localize the cell layers on the membranes. Next, ultrathin section (60 nm) were cut on a Leica Ultracut S ultramicrotome, mounted either on formvar coated single slot or uncoated 300 mesh copper grids, and stained with 2% uranyl acetate for 15 min. Sections were examined in a JEOL JEM 1400 Plus electron microscope operated at 100 kV accelerating voltage. Digital images were taken with a Matataki 8 MPix CCD camera at 16-bit gray scale color depth and saved in uncompressed TIFF format.

3.6.8. Permeabilty of niosomes across a blood-brain barrier co-culture model

The tightness of the triple co-culture BBB model was verified by measurement of transendothelial electric resistance (TEER) using an EVOM voltohmmeter (World Precision Instruments, USA) combined with STX-2 electrodes. When high TEER values (539 ± 71 $\Omega \times cm^2$) were obtained, the model was used for experiments. Cells were treated in the upper, donor compartment (0.5 mL) with single or dual-targeted niosomes (10 mg/mL) diluted in

phenol red free DMEM/F12 supplemented with 1% PDS and 1% ITS for 4 h. After incubation samples were collected from the lower, acceptor compartments (1.5 mL) and measured with a Fluorolog 3 spectrofluorometer at 584 nm excitation and 663 nm emission wavelengths. The P_{app} values of the EBA cargo were calculated as described previously (Bocsik et al., 2016) and as shown in the section 3.5.6.

3.6.9. Measurement of plasma membrane fluidity

RBECs grown in culture dishes were treated with N and N-A-GSH samples (10 mg/mL) diluted in culture medium for 4 h at 37°C in a CO_2 incubator. The cells were washed twice with PBS, collected by trypsinization, and resuspended in Ringer-Hepes buffer. The density of cells was set by absorbance measurement to OD_{360}=0.1 (Hewlett Packard 8452A Diode Array Spectrophotometer, USA). Cells were labeled with 0.2 μM TMA-DPH for 5 min. Fluorescence anisotropy was measured on a T-format fluorescence spectrometer (Quanta Master QM-1, Photon Technology International, USA). Excitation and emission wavelengths were 360 and 430 nm, respectively (5 nm and 6 nm slits). Cells were kept at 37°C under stirring conditions. Anisotropy data were acquired in every second for 5 min, then benzyl alcohol (50 mM; Merck, Germany), a strong membrane fluidizer, was added and data were acquired for another 5 min. The average of 50 anisotropy measurements in the last 1 min of each treatments was calculated and compared (Kiss et al., 2014; Lénárt et al., 2015).

3.6.10. *In vivo* imaging of targeted niosomes

Ten-week old male CD1-Foxn1nu nude mice (Winkelmann, Germany) were used for *in vivo* imaging. Animals were kept under conventional controlled conditions (22°C, 55% humidity, day-night rhythm) and had free access to a standard diet (ssniff Spezialdiäten GmbH, Germany) and tap water. A time domain *in vivo* small animal fluorescence imager Optix™ (ART, Canada; Keren et al., 2008; Kumar et al., 2008) was used to monitor the brain penetration of the EBA cargo of niosomes in real-time and over several time points in the same animal. Animals were placed in prone position on the table of the imager. Anesthesia was maintained during the fluorescence detection by offering an oxygen-isoflurane gas mix via a small mask. EBA encapsulated in different niosomes (N, N-A, N-GP, N-A-GP) were injected intravenously (100 μl, tail vein). Fluorescence measurement to visualize the EBA was performed repeatedly after niosome injection at defined time points up to 24 h (0, 10 and 30 min, 3, 6 and 24 h). The animals were returned to their cage and provided access to food and water between the longer measurement points. Head-detector distance was equal in all measurements. The red fluorescent

signal of EBA was detected over the whole body of living anesthetized mice in 0.5 mm steps. For fluorescence detection, a time-correlated single-photon counting system (TCSPC-130) was used. Intensity units were normalized for the same excitation power and excitation time per raster point (integration time).

3.7. Statistical Analysis

Data are presented as means ± SEM or SD. Values were compared using unpaired *t*-test, one-way or two-way analyses of variances (ANOVA) following Dunnett or Bonferroni multiple comparison posttests (GraphPadPrism 5.0; GraphPad Software, USA). Changes were considered statistically significant at $P < 0.05$. All experiments were repeated at least two times and the number of parallel samples was 4-10.

4. RESULTS

4.1. Expression of selected solute carrier genes coding nutrient transporters

We verified the expression of genes for SLC transporters carrying glucose, alanine and biotin in freshly isolated rat brain microvessels, RBECs from triple cultured BBB model and in hCMEC/D3 cells (Fig. 6). Among the carriers of glucose, the expression level of the gene *GLUT1*, coding the predominant glucose transporter at the BBB, was the highest in all tested groups. The expression level of *Glut1* was followed by *Glut5* and *Glut3* in rat brain microvessels. In RBECs the relative transcript levels for *Glut1* and *Glut3* were also high, while that of *Glut5* was very low. In the case of hCMEC/D3, the expression of *GLUT5* level was the lowest similarly to the RBEC. Among the tested neutral amino acid transporters the mRNA level of *SNAT2* was the highest in all models. The expression levels of *SMVT* gene were similar in the BBB model and hCMEC/D3 cells. From the tested ten genes only in three cases, for *GLUT5*, *SNAT1* and *SNAT5* were transcript levels lower in the BBB model than in brain microvessels and/or hCMEC/D3 cells (Fig. 6).

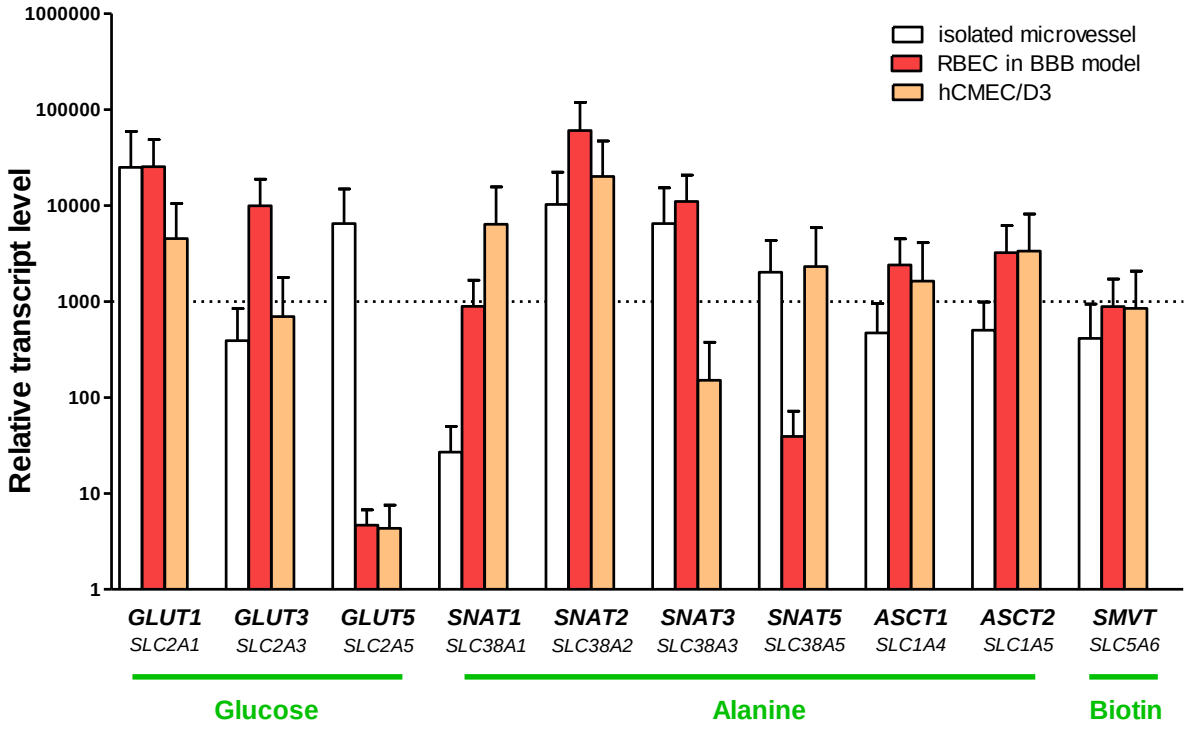

Figure 6. *Expression of genes encoding solute carriers for glucose, alanine and biotin in isolated rat brain microvessels, primary rat brain endothelial cells co-cultured with rat pericytes and astrocytes, and hCMEC/D3 human brain endothelial cell line.*

4.2. Results with solid nanoparticles

4.2.1. Characterization of the non-targeted and targeted solid nanoparticles

The commercially available solid fluorescent particles (SNP, nominal size 40 nm) were already functionalized with neutravidin. These neutravidin-coated particles were labeled with biotin and glutathione targeting ligands (Fig. 7).

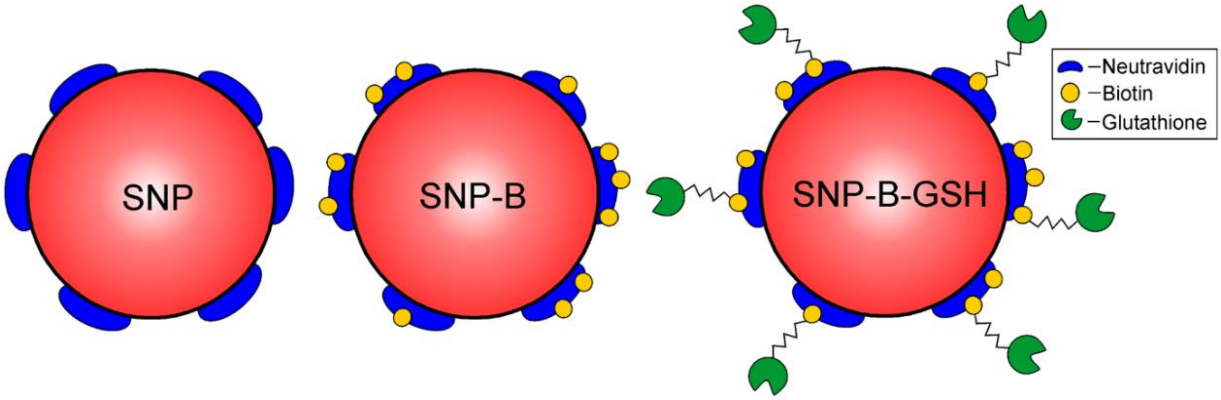

Figure 7*. Schematic drawing of non-targeted (SNP), biotin- (SNP-B) and glutathione-labeled (SNP-B-GSH) solid nanoparticles.*

Table 2 summarizes the main physico-chemical characteristics of the non-targeted and targeted SNPs. The neutravidin labeling enlarged the diameter of SNPs. The biotin and glutathione ligands further increased their size. All SNPs had low polydispersity index, indicating a relatively narrow size distribution. The average zeta potential for both targeted particles was very similar. The charge of the non-labeled SNP was less negative.

Table 2. *Characterization of non-targeted solid nanoparticles (SNP); biotin-targeted solid nanoparticles (SNP-B); glutathione-targeted solid nanoparticles (SNP-B-GSH). Values presented are means ± SD.*

Nanoparticle	Size (nm)	Polydispersity index	Zeta potential (mV)
SNP	93 ± 0.59	0.131 ± 0.02	−14 ± 0.87
SNP-B	118.1 ± 2.9	0.251 ± 0.001	−23.1 ± 0.62
SNP-B-GSH	120.5 ± 2.86	0.261 ± 0.01	−23.8 ± 1.33

The morphology of the nanoparticles was observed by SEM and is shown on Fig. 8. The particles had mostly spherical shapes, but some SNPs were elongated. The size of the SNPs were all in the same range, and corresponds well to data measured by dynamic light scattering. No aggregation was visible.

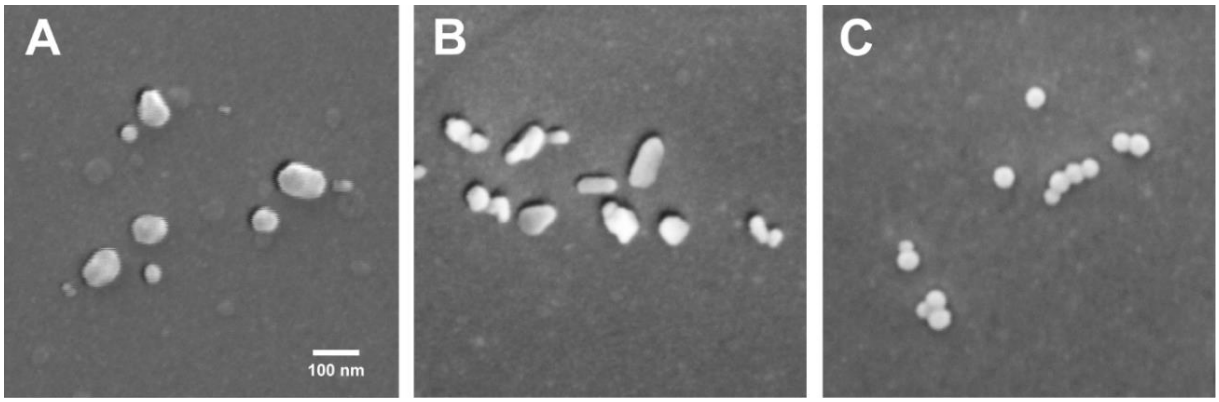

Figure 8. *Scanning electron microscopy images of non-targeted (A), biotin-targeted (B), and glutathione-targeted (C) solid nanoparticles. Bar: 100 nm*

4.2.2. Effect of solid nanoparticles on the cell viability of brain endothelial cells

Incubation of the human brain endothelial cell monolayers with SNP and SNP-B in the 10-1000 µg/mL concentration range for 24 h had no effect on cell viability assessed by MTT dye conversion test (Fig. 9). As a comparison, the reference substance Triton X-100 detergent decreased the cell viability below 10% of the control values. SNP-B-GSH (30-100 µg/mL) increased the metabolic activity of cells, while the highest concentration (1000 µg/mL) caused a reduction in viability (Fig. 9). For further experiments we selected the 150 µg/mL concentration for all three SNPs, which can be considered as non-toxic.

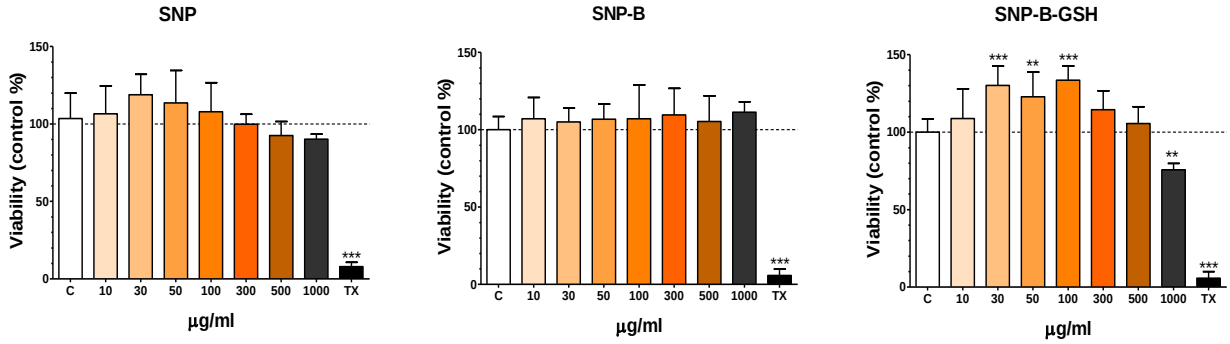

Figure 9. *The effect of non-targeted (SNP), biotin-targeted (SNP-B), and glutathione-targeted (SNP-B-GSH) solid nanoparticles on the viability of brain endothelial cells (24 h). Values presented are means ± SEM. Statistical analysis: one-way ANOVA followed by Dunnett's posttest, ** P < 0.01; *** P < 0.001 compared to control. n = 4-8. X-axis: log-10 scale.*

4.2.3. Uptake of non-targeted and targeted solid nanoparticles in brain endothelial cells

The uptake of SNPs in brain endothelial cells was tested at two time points (Fig. 10). In the design of our study we determined the time points for the uptake experiments based on the results of Gaillard et al. obtained on nanoparticles labeled with GSH, our reference ligand (Gaillard et al., 2012; Gaillard et al., 2014; Rip et al., 2014) To be able to compare our data to these previous observations we selected 4 and 8 h incubations. After 4 h of incubation no significant difference between the uptakes of the three SNPs in cells could be measured, although an increasing trend was seen in case of targeted SNPs. After 8 h incubation the uptake of all tested nanoparticles was significantly higher compared to the 4 h group. Importantly, the uptake of the biotin- and glutathione-targeted SNPs was significantly increased; it was two times higher than the uptake of the non-targeted particle (Fig. 10).

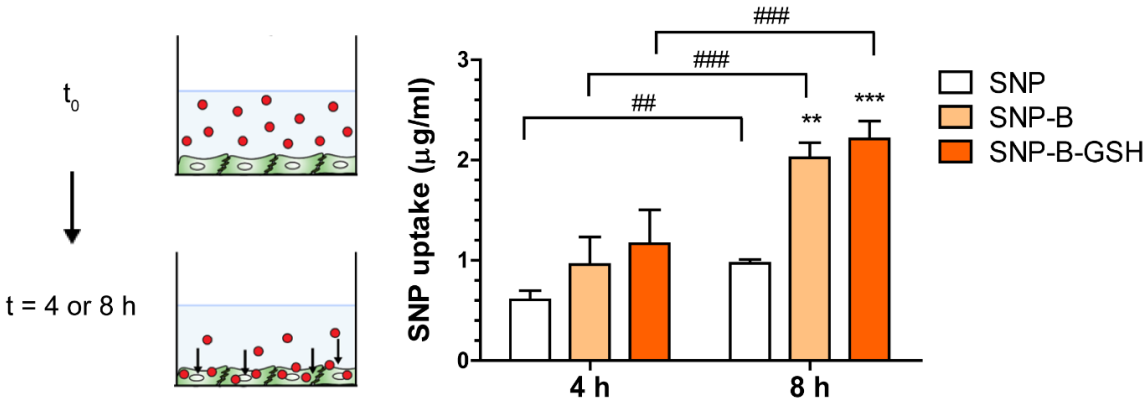

Figure 10. *The uptake of non-targeted (SNP), biotin-labeled (SNP-B) and glutathione-labeled (SNP-B-GSH) solid nanoparticles in brain endothelial cells after 4 or 8 h incubation. The concentration of SNPs is 150 µg/mL in each group. Values presented are means ± SEM. Statistical analysis: two-way ANOVA followed by Bonferroni posttest, where **P < 0.01; ***P < 0.001, compared to SNP treated group, ##P < 0.01; ###P < 0.001, compared to the 4 h incubation group; n = 4–6.*

The uptake of the fluorescent nanoparticles could be visualized in hCMEC/D3 cells by confocal microscopy (Fig. 11). Red fluorescent dots can be seen in the cytoplasm of the cells treated with SNPs. More fluorescent particles were seen in cells incubated with the biotin or glutathione-labeled SNPs indicating better uptake of these nanoparticles as compared to the non-targeted SNPs.

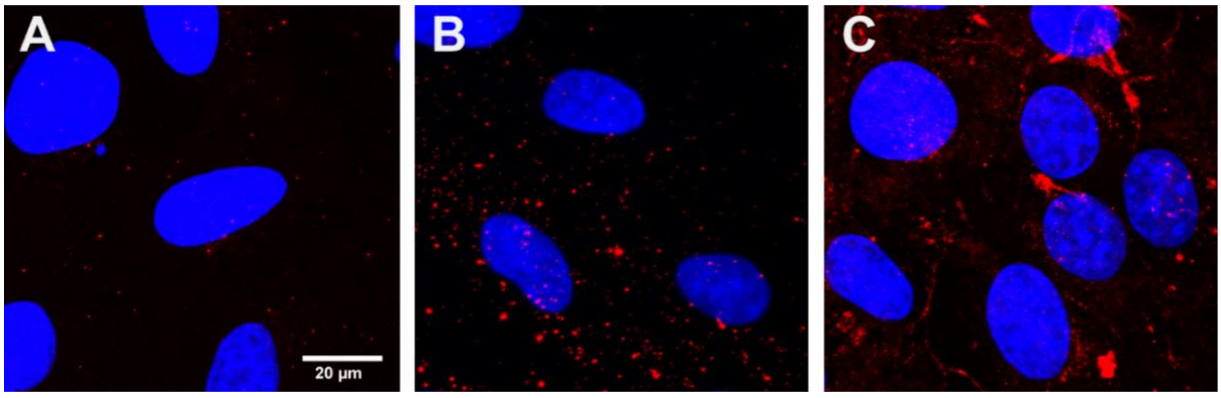

Figure 11. *Confocal microscopy images of cultured human brain endothelial cells incubated with non-labeled (A), biotin-labeled (B), and glutathione-labeled (C) solid nanoparticles (red) for 8 h at 37 ºC. The concentration of SNPs is 150 µg/mL in each group. Cell nuclei were stained with bis-benzimide (blue). Bar: 20 µm.*

4.2.4. Penetration of solid nanoparticles across brain endothelial monolayers

The permeability of hCMEC/D3 monolayers for the marker Evans blue-albumin complex was $1.6 \pm 0.3 \times 10^{-6}$ cm/s, which was in the same range as in our previous study (Walter et al., 2016) and reflects a suitable barrier for testing SNPs. All SNPs crossed the brain endothelial layers in the permeability tests but at different extent (Fig. 12). After 8 h incubation the P_{app} of biotin targeted SNP was 2.8 fold higher than that of the non-targeted SNP. The penetration of the GSH targeted nanoparticles was the highest, a significant, 5.8 fold increase was measured as compared to the unlabeled SNP group.

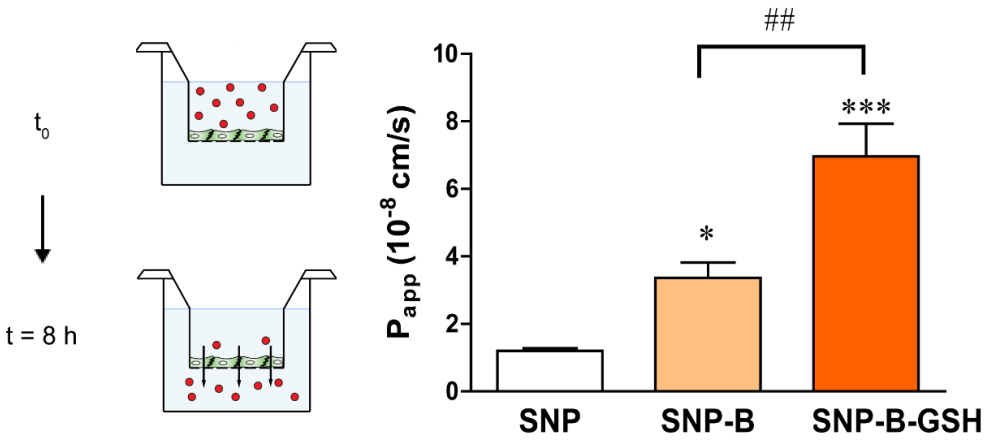

Figure 12*. Permeability assay for targeted and non-targeted SNPs (150 µg/mL, 8 h) across hCMEC/D3 cell monolayers. Values presented are means ± SEM. Statistical analysis: one-way ANOVA followed by Bonferroni posttest. *P < 0.05, ***P < 0.001, compared to non-labeled SNP treated group; ##P < 0.01, compared to biotin-labeled SNP treated group, n = 6.*

4.2. Results with niosomes

4.2.1. Characterization of non-targeted and targeted niosomes

Seven types of niosomes (non-targeted, N), single ligand targeted (N-GP, N-A, N-GSH), and dual-ligand targeted (N-A-GSH, N-A-GP, N-GP-GSH) were prepared with fluorescent EBA cargo (Fig. 11).

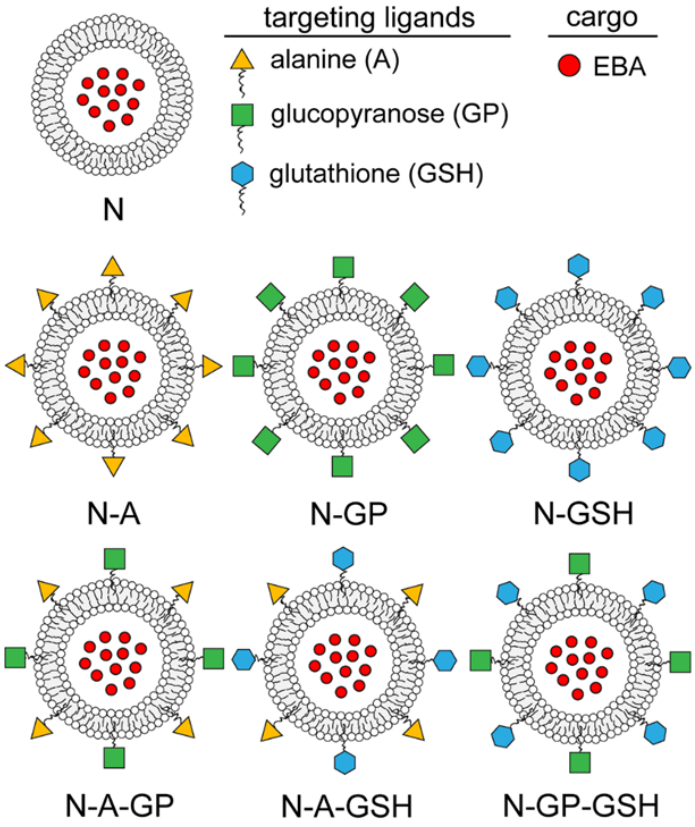

Figure 13*. Schematic drawing of non-targeted (N), single ligand targeted (N-A: alanine, N-GP: glucopyranose, N-GSH: glutathione) and dual-targeted niosomes (N-A-GP: glucose-alanine, N-A-GSH: alanine-glutathione, N-GP-GSH: glucose-glutathione). EBA: Evans blue-albumin complex.*

The main physico-chemical properties of the niosome groups are summarized in Table 2. The average diameter of the niosomes varied between 92 and 107 nm. All groups had low polydispersity index, indicating a relatively narrow size distribution. The zeta potentials of niosomes were between −3 and −4 mV, except those decorated with GSH ligand (N-GSH, N-A-GSH, N-GP-GSH), which had a more negative surface charge, around −7mV. The encapsulation efficiency of the cargo EBA was in the range of 4.6–10.4%. The amount of the encapsulated large hydrophilic biomolecule EBA was between 0.5 and 1.1 mg/100 mg nanoparticle total weight (Table 3).

Table 3. *Characterization of the non-targeted and targeted niosomes. Values presented are means ± SD.*

Niosomes	Size (nm)	Polydispersity index	Zeta potential (mV)	Encapsulation efficiency (%)	Encapsulated BSA (mg/mL)
N	106 ± 10	0.18 ± 0.04	–3.41 ± 0.50	8.47 ± 3.24	0.85 ±0.33
N-A	92 ± 40	0.18 ± 0.01	–4.36 ± 0.60	7.54 ± 3.57	0.75 ± 0.36
N-GP	98 ± 14	0.20 ± 0.04	–4.19 ± 0.29	4.90 ± 0.52	0.49 ± 0.05
N-GSH	107 ± 11	0.17 ± 0.02	–7.39 ± 0.77	10.43 ± 6.17	1.04 ± 0.62
N-A-GSH	103 ± 50	0.18 ± 0.01	–7.14 ± 1.15	6.14 ± 2.60	0.61 ± 0.26
N-A-GP	94 ± 10	0.17 ± 0.01	–3.83 ± 1.03	10.87 ± 0.53	1.09 ± 0.05
N-GP-GSH	101 ± 80	0.17 ± 0.01	–6.40 ± 1.27	4.66 ± 2.53	0.47 ± 0.25

The morphology of the NPs was spherical as observed by transmission electron microscopy (Fig. 14A) and atomic force microscopy (Fig. 14B). No aggregation was visible.

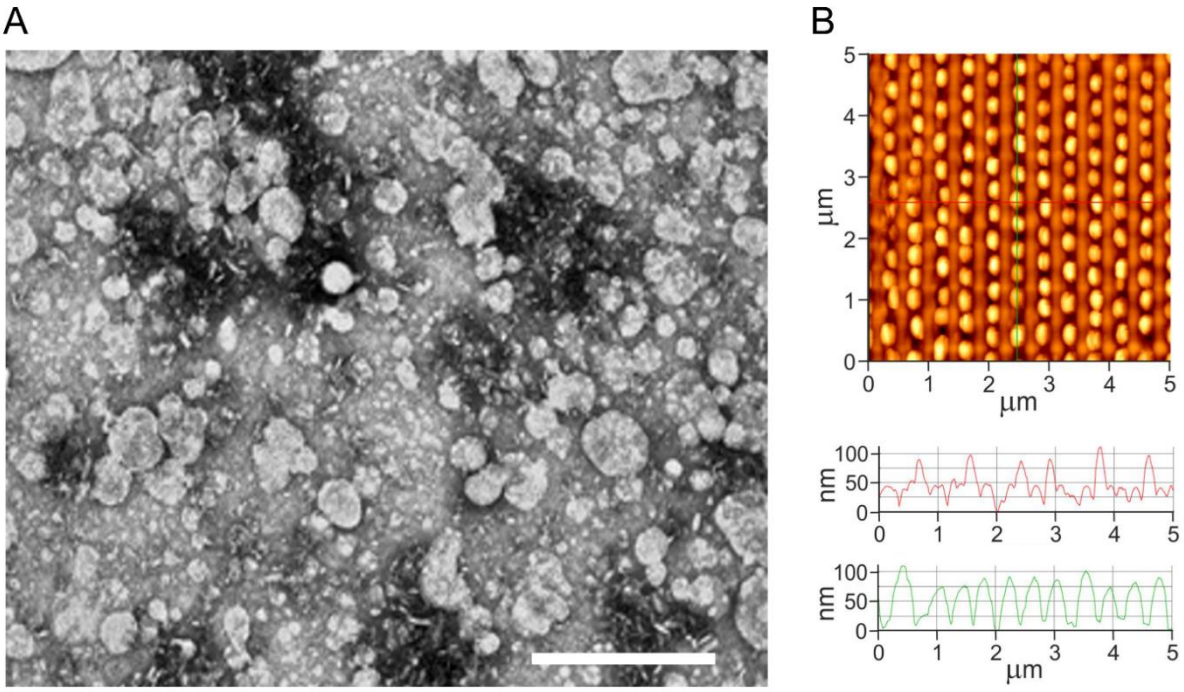

Figure 14. *(A) Transmission electron microscopy image of niosomes, bar: 500 nm. (B) Atomic force microscopy image of niosomes.*

The stability of non-targeted niosome loaded with EBA was followed for six months. The size of niosomes changed from 92.8 ± 1.8 nm to 119.5 ± 1.9 nm during this period. At 6 months the polydispersity index was 0.30 ± 0.003 indicating monodispersity, and the zeta potential (−4.03 ± 0.49 mV vs. −3.67 ± 0.09 mV) and the encapsulation efficiency (11.5% vs. 9.21%) have changed minimally (Table 4.). Based on these data the niosome preparation can be considered as stable regarding size, encapsulated cargo and aggregation for at least 6 months.

Table 4. *Stability of non-targeted EBA loaded niosomes. Values presented are means ± SD*

Time	Size (nm)	Polydispersity index	Zeta potential (mV)	Encapsulation efficiency (%)
0 week	92.8 ± 1.8	0.18 ± 0.02	–4.03 ±0.49	11.50
1 week	97.5±0.3	0.19 ± 0.01	-	-
4 weeks	102.6± 1.0	0.20 ± 0.02	-	-
6 weeks	104.6± 1.1	0.20 ± 0.01	-	-
8 weeks	107.7 ± 0.7	0.20 ± 0.004	-	-
10 weeks	109.1 ± 1.3	0.20 ± 0.02	-	-
6 month	119.5 ± 1.9	0.30 ± 0.003	–3.67 ±0.09	9.21

4.2.2. Effect of niosomes on brain endothelial cell viability

Incubation of RBECs with non-targeted or targeted niosomes in the 0.3–10 mg/mL concentration range for 4h did not decrease the impedance of cell layers reflecting good cell viability (Fig. 15). For further experiments we selected the 10 mg/mL concentration, which can be considered as a safe concentration for all niosome groups.

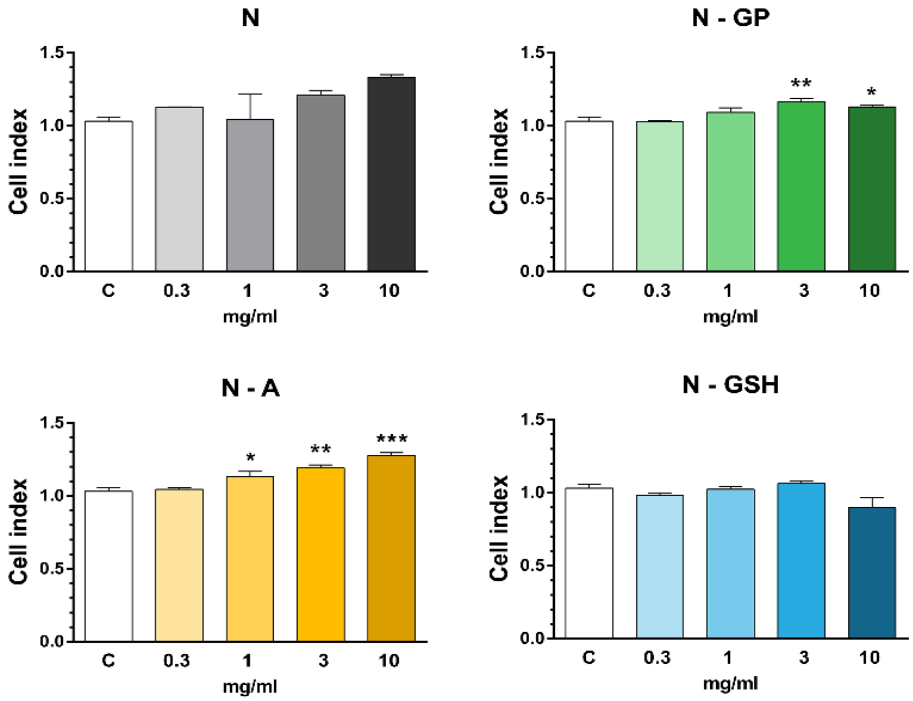

Figure 15. *The effect of non-targeted (N), alanine-targeted (N-A), glucopyranose-targeted (N-GP) and glutathione-targeted (N-GSH) niosomes on the viability of RBECs (4 h). Values presented are means ± SEM. Statistical analysis: ANOVA followed by Dunnett's posttest, *P < 0.05, **P < 0.01, ***P < 0.001, compared to control group, n=8. C: medium treated control group.*

4.2.3. Uptake of the cargo of single and dual-targeted niosomes in RBECs

The uptake of the large hydrophilic free EBA was very low in brain endothelial cells, only 1.5% of the EBA uptake in cells treated with non-targeted niosome (N) containing the cargo (Fig.16).

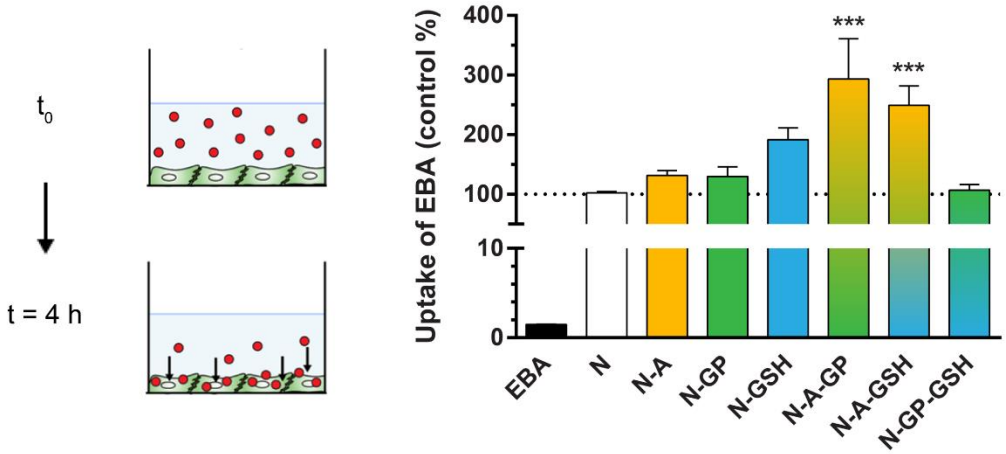

Figure 16. *The uptake of non-targeted (N), single- (N-A, N-GP, N-GSH) and dual-targeted (N-A-GP, N-A-GSH, N-GP-GSH) niosomes in brain endothelial cells (4 h). Values presented are means ± SEM. Statistical analysis: ANOVA followed by Dunnett's posttest, where ***P < 0.001, compared to non-targeted N group; n=10.*

As compared to non-targeted niosomes, the uptake of EBA in RBECs treated with nanovesicles decorated with alanine, glucopyranose or glutathione was higher (N-A: 131%, N-GP: 130%, N-GSH: 191%). The presence of dual-ligands statistically significantly increased the cellular concentration of EBA in brain endothelial cells in the case of N-A-GP (293%) and N-A-GSH groups (249%), but not in the N-GP-GSH group (Fig.16).

4.2.4. Penetration of the cargo by targeted niosomes across BBB co-culture model

The permeability of the BBB model for EBA was also very low (0.13×10^{-6} cm/s) reflecting a tight barrier (Fig. 17). This P_{app} value for EBA is in accordance with our previous results (Walter et al., 2015). The encapsulation of EBA in non-targeted niosomes (N) increased the permeability of the cargo through brain endothelial cells (0.28×10^{-6} cm/s). Labeling the particles with single ligands resulted in further increase in the penetration of EBA across the BBB model (N-A: 1.18×10^{-6} cm/s; N-GP: 1.01×10^{-6} cm/ s; N-GSH: 1.29×10^{-6} cm/s). The amount of EBA cargo that crossed brain endothelial cells was increased 17-fold in case of the N-A-GSH group (2.26×10^{-6} cm/s) and 14-fold in the N-A-GP group (1.83×10^{-6} cm/s) as compared to the EBA group (Fig. 17). The combination of GP-GSH ligands was not efficient to elevate EBA penetration across the BBB model. Based on the results, the N-A, N-GSH and N-A-GSH groups were selected for further in vitro experiments.

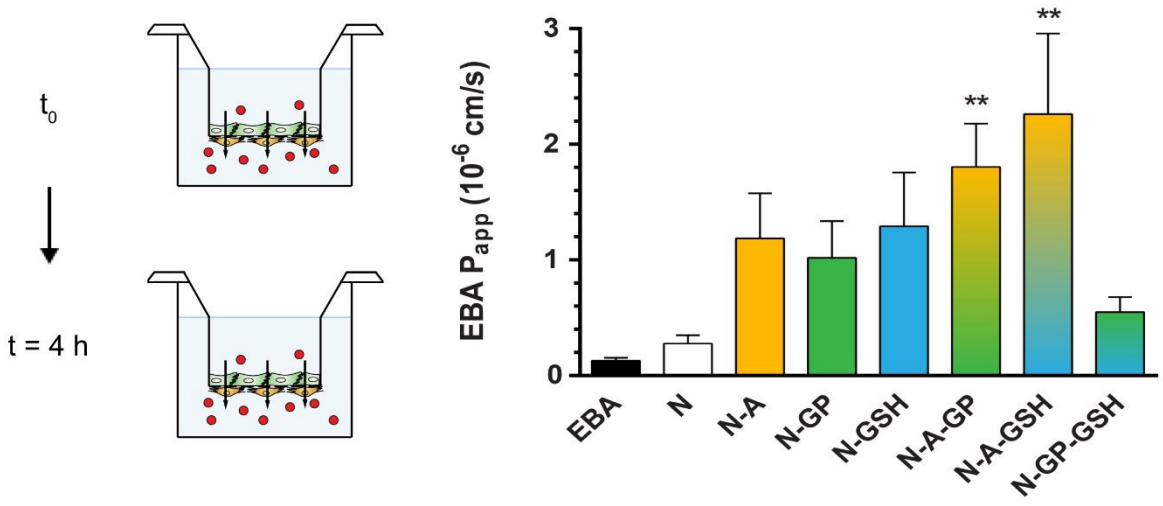

Figure 17. *Permeability of albumin cargo across the BBB culture model after treatment with different niosomes (10 mg/mL, 4h). Values presented are means ± SEM. Statistical analysis: ANOVA, Dunnett's posttest. **P < 0.01, compared to non-targeted N group; n=10.*

4.2.5. Cellular uptake: visualization

Since our model cargo EBA gives a red fluorescent signal (Uyama et al., 1988), the uptake of free EBA and EBA encapsulated in nanovesicles (N, N-A-GSH) was visualized in RBECs by confocal microscopy (Fig. 18A). Red fluorescence was detected in cells treated with dual-targeted N-A-GSH niosomes indicating uptake of the cargo. Less fluorescent signal was seen in the non-targeted vesicle (N) group, while the cellular entry of free dye (EBA) was barely detectable. For transmission electron microscopy the cells were treated with free lanthanum (LA), lanthanum entrapped in non-targeted niosomes (N), and vesicles labeled with dual-ligands containing lanthanum (N-A-GSH) (Fig. 18B). The particles were non toxic (data not shown) and their physico-chemical properties were similar (N: 110 nm, −2.25 mV; N-A-GSH: 115 nm, −5.08 mV). The concentration of lanthanum was equal in each groups. More dark precipitates and structures can be seen in cells treated with N-A-GSH compared to the non-targeted nanoparticle and free lanthanum groups.

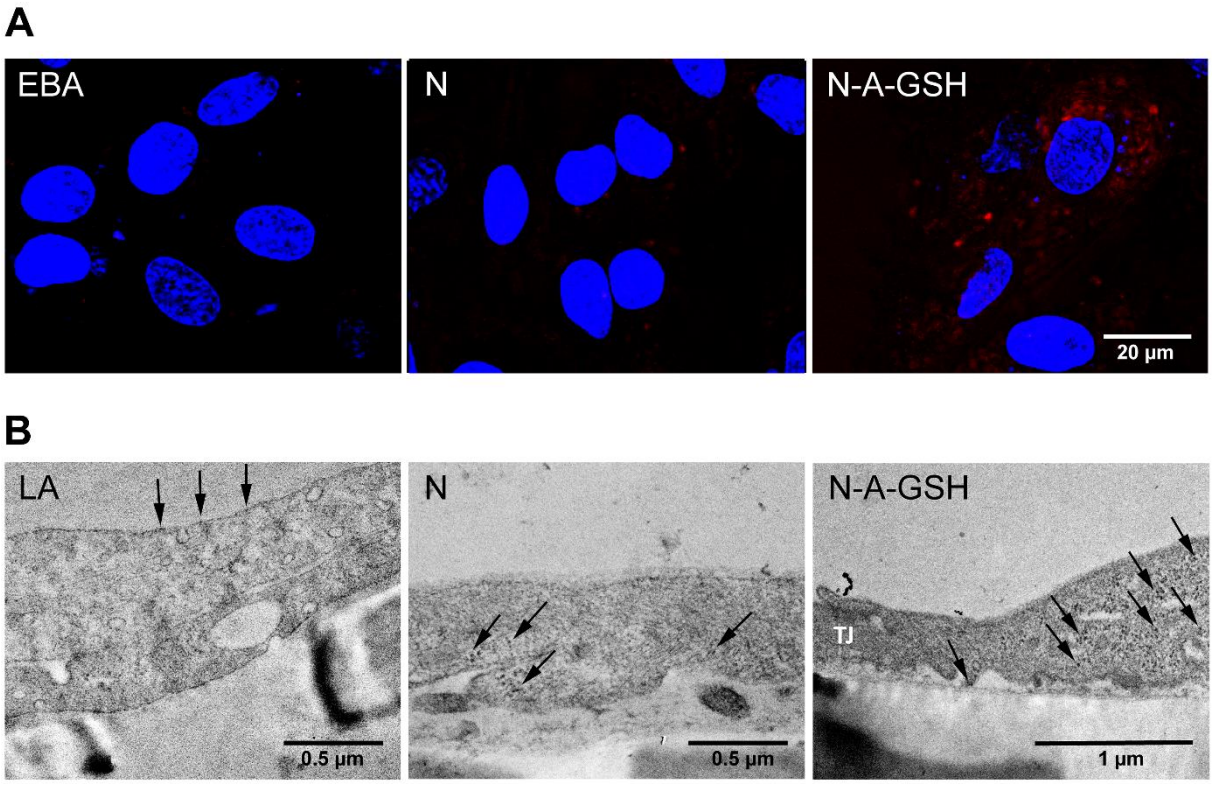

Figure 18. *(A) Confocal microscopy images of cultured brain endothelial cells incubated with unencapsulated cargo (EBA, showing red fluorescence), non-targeted (N) or alanine-glutathione-targeted (N-A-GSH) niosomes for 4h at 37°C. Cell nuclei were stained with bis-benzimide (blue). Bar: 20 µm. (B) Transmission electron microscopy images of the uptake of free lanthanum (LA) and lanthanum encapsulated in non-targeted (N) or alanine-glutathione-targeted (N-A-GSH) niosomes in brain endothelial cells after 4h incubation. Bar: 0.5 and 1 µm. TJ: tight junction. Black arrows: lanthanum.*

4.2.6. Cellular uptake: temperature dependence and metabolic inhibition

To test the temperature dependence of the cellular uptake of nanovesicle encapsulated EBA, cells were treated with selected niosomes (N, N-A, N-GSH, N-A-GSH) at both 4 °C and 37 °C (Fig. 19). At 37 °C the EBA uptake was significantly higher in all targeted nanovesicle groups (N-A: 119%, N-GSH: 150%, N-A-GSH: 308%) compared to the non-targeted group (N: 100%). Decreased EBA uptake was seen in RBECs at 4 °C (N-A: 36%, N-GSH: 55%, N-A-GSH: 17%) as compared to the non-targeted group at 37 °C. Treatment of the cells with metabolic inhibitor sodium azide resulted in lower uptake of the cargo (N-A: 88%, N-GSH: 113%, N-A-GSH: 81%) compared to data measured at 37 °C in the same treatment groups (Fig. 19).

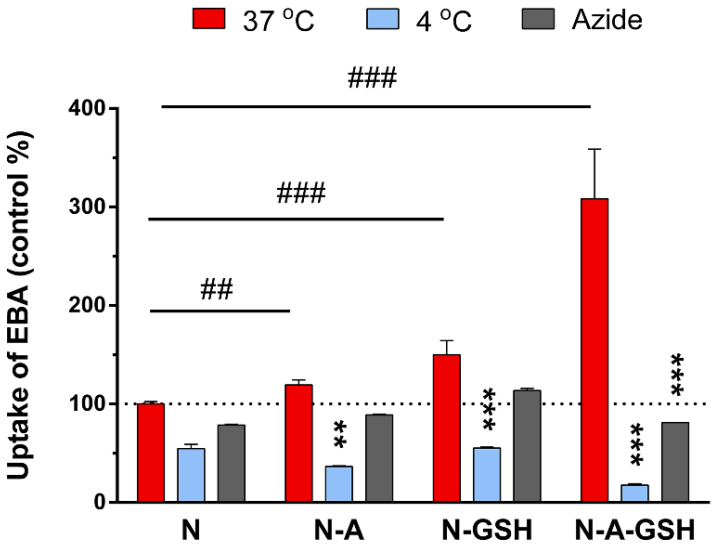

Figure 19. *The effect of temperature and metabolic inhibitor sodium azide (0.1%) on the uptake of EBA cargo in brain endothelial cells after 4h incubation with non-targeted (N), alanine-targeted (N-A), glutathione-targeted (N-GSH) and alanine-glutathione-targeted (N-A-GSH) niosomes. Values presented are means ± SEM. Statistical analysis: two-way ANOVA, Bonferroni posttest. *P < 0.5; **P < 0.01; ***P < 0.001, compared to first column of each groups, ###P < 0.001, compared to N treated group; n=4–6.*

4.2.7. Cellular uptake: inhibition of endocytosis

Two inhibitors of endocytosis (Ivanov, 2008) were used to further elucidate the mechanism of cellular uptake of EBA after treating the cells with dual-targeted N-A-GSH particles (Fig. 20). Filipin, which inhibits lipid raft/caveolae-mediated endocytosis (Fig. 20B), slightly, but statistically significantly decreased the uptake of cargo in RBECs (94% of the control group, Fig. 20A). Cytochalasin-D, a common inhibitor of endocytosis by blocking F-actin

depolymerization (Fig. 20B), also induced a partial, but significant inhibition of EBA uptake (80% as compared to the control group, Fig. 20A).

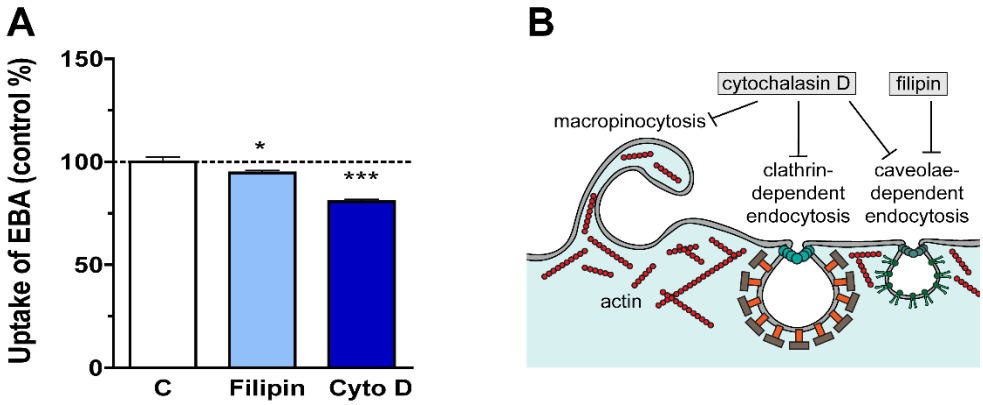

Figure 20. *(A) Inhibition of the uptake of EBA cargo with filipin (6 μM) or cytochalasin D (20 μM) in rat brain endothelial cells after 4 h incubation with alanine-glutathione dual-targeted niosomes (N-A-GSH). Values presented are means ± SEM. Statistical analysis: ANOVA followed by Dunnett's posttest. *P < 0.5; ***P < 0.001, compared to the control group; n=6. (B) Schematic drawing of the effect of cytochalasin D and filipin.*

4.2.8. Cellular uptake: modification of cell surface charge

We modified the surface charge of cultured brain endothelial cells by digestion of the surface glycocalyx with neuraminidase enzyme (Singh et al., 2007) and treatment with a cationic lipid, TMA-DPH (Ribeiro et al., 2012). Surface charge alterations in RBECs did not affect the cellular uptake of EBA after treatment with non-targeted NPs as compared to the control, untreated group (Fig. 21A).

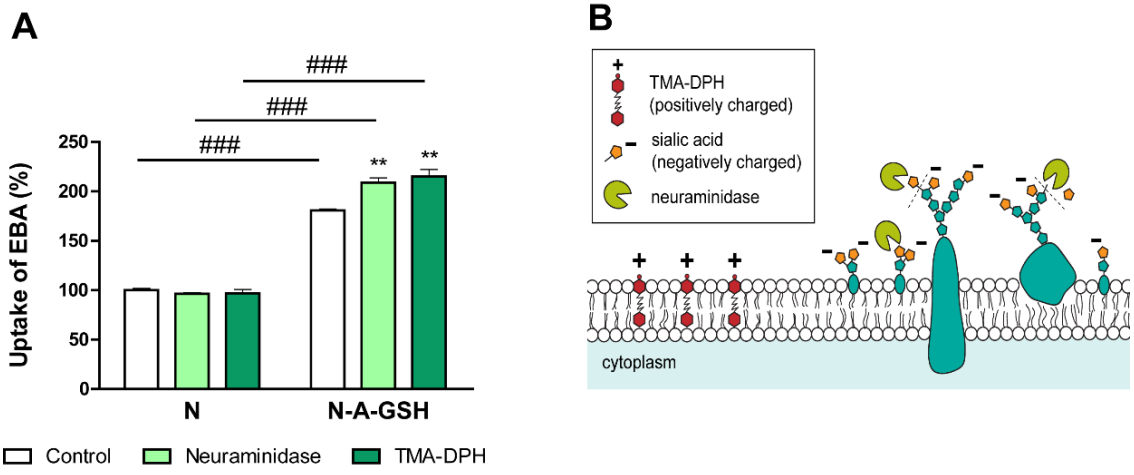

Figure 21. *(A) The effect of neuraminidase (1 U/mL) and TMA-DPH (54 μM) on the uptake of EBA cargo in brain endothelial cells incubated with non-targeted (N) and alanine-glutathione dual-targeted niosomes (N-A-GSH). Statistical analysis: two-way ANOVA, Bonferroni posttest. **P < 0.01 compared to first column of each groups; ###P < 0.001, compared to N treated groups; n=6. (B) Schematic drawing on the effect of TMA-DPH and neuraminidase on the surface charge of RBEC.*

In contrast, both modifications increased significantly the uptake of EBA in brain endothelial cells after incubation with N-A-GSH niosomes (Fig. 21A). The uptake of EBA was increased by 16%, after treatment of RBECs with neuraminidase and by 19% after incubation with TMA-DPH, as compared to untreated cells in the N-A-GSH nanoparticle group.

4.2.9. Interaction of nanovesicles with brain endothelial cells: plasma membrane fluidity

The membrane fluidity of brain endothelial cells, determined by fluorescence anisotropy (Kiss et al., 2014), was significantly decreased after 4h treatment with N and N-A-GSH nanovesicles (Fig. 22A) indicating increased cell membrane fluidity and a fusion process (Fig. 22B). The membrane fluidizer benzyl alcohol (30 mM) quickly and greatly reduced the TMA-DPH fluorescence anisotropy after 3 min compared to the control and niosome treated groups indicating maximal plasma membrane fluidity.

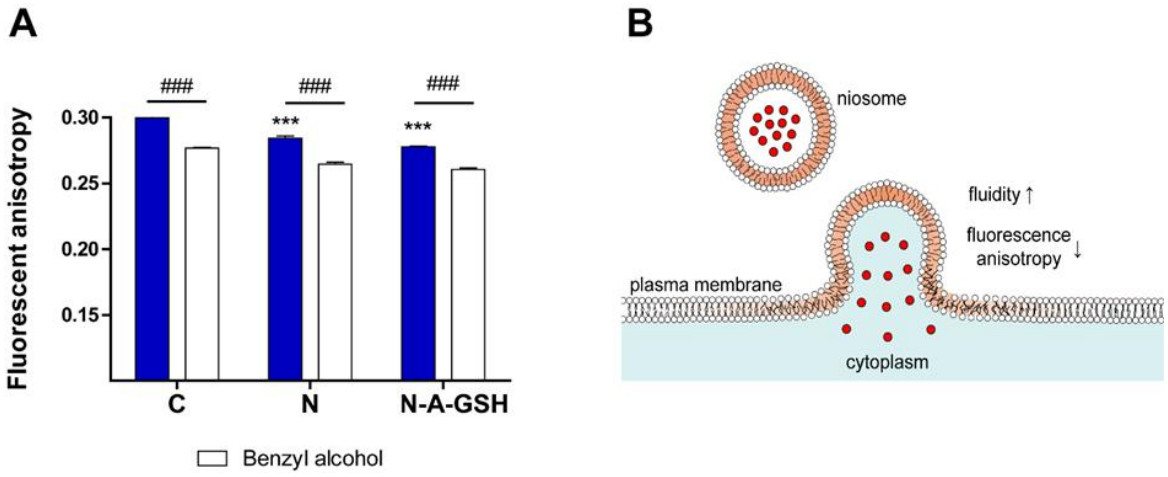

Figure 22. *(A) The effect of non-targeted (N) and alanine-glutathione dual-targeted niosomes (N-A-GSH), and benzyl alcohol (30 mM) on plasma membrane fluidity measured by fluorescence anisotropy of living brain endothelial cell suspensions. Values presented are means ± SEM. Statistical analysis: two-way ANOVA, Bonferroni posttest. ***P < 0.001, all groups were compared to non-treated control (C); ###P < 0.001, compared to first column of each groups, n=3. (B) Schematic drawing on the fusion of a niosome with cellular plasma membrane.*

4.2.10. Imaging of EBA cargo in mice after intravenous injection of targeted niosomes

The brain penetration of the red fluorescent EBA was measured by *in vivo* imaging in nude mice. Free EBA and EBA encapsulated in targeted and non-targeted niosomes were injected intravenously. The biodistribution of non-targeted and targeted niosome in mice was different. Increased fluorescent intensity was seen in the liver and eyes of mice 6 h after the injection of non-targeted NPs, while in mice which received N-GP increased signal was visible in the brain (Fig. 22A). In mice which were injected with free EBA there was no significant elevation in the signal intentsity in the brain area during the experiment (Fig. 22B). Encapsulation of EBA in non-targeted niosomes resulted in enhanced brain fluorescent intensity. The fluorescent signal in the brain area was further increased in the single ligand targeted N-A and N-GP groups, while in the dual-ligand targeted N-A-GP group it was the highest, as compared to all groups at all time points (Fig. 22B). The differences between targeted, dual-ligand targeted and non-targeted niosomes were still visible at 24 h.

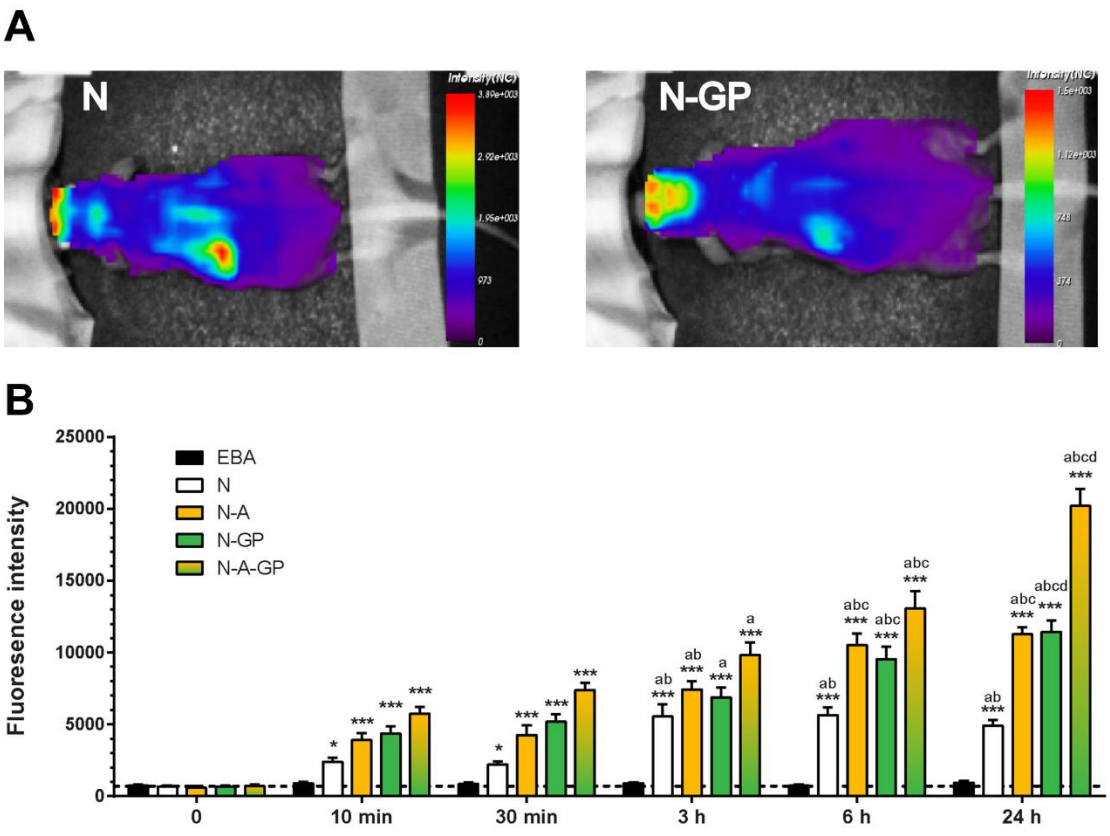

Figure 22. *(A) In vivo optical imaging of nude mice 6 h after tail vein injection of non-targeted (N) and glucose targeted (N-GP) niosomes containing EBA. (B) Fluorescent intensity of EBA in the brain regions of mice after injection of free EBA or EBA encapsulated in non-targeted (N), single- (N-A, N-GP) or dual-targeted (N-A-GP) niosomes measured by optical imaging. Values presented are means ± SD. Statistical analysis: two-way ANOVA, Bonferroni posttest.* P < 0.5; **P < 0.01; ***P < 0.001, as compared to the EBA-treated group within each time point; a: as compared to the 10 min, b: as compared to the 30 min, c: as compared to the 3h, d: as compared to the 6 h time points within each group, n=3–4.*

5. DISCUSSION

5.1. Nanoparticle targeting with ligands of BBB specific transporters

Although nanocarrier systems for treatment of CNS disorders represent a rapidly expanding research field (Loureiro et al., 2015; Saraiva et al., 2016; Kevadiya et al., 2018) there are still no targeted NPs used in human therapy to deliver therapeutics to the brain in a controlled, effective and non-invasive manner. The key problem of effective targeting of NPs to the brain is the proper functionalization of these carriers to cross the BBB (Wohlfart et al., 2012; Kreuter, 2014). NPs accumulate in several organs, including liver, spleen, and kidney, and only specific BBB targeting can increase the ratio of nanocarriers penetrating the CNS (Saraiva et al., 2016; Kevadiya et al., 2018). To ensure this relative brain specificity it is important to functionalize NPs with targeting molecules which bind the physiological transporters of the BBB and trigger active and specific transport mechanisms to cross the BBB (Masserini, 2013).

Among the BBB specific physiological transport pathways, the receptor mediated transcytosis is the most widely researched area for CNS targeting of NPs (Kreuter, 2014; Saraiva et al., 2016). There are two major possibilities to label NPs to exploit this transport route: either to coat NPs with molecules that bind plasma proteins, which are ligands of BBB receptors, or to use molecules that directly bind to BBB receptors (Kreuter, 2013; Kevadiya et al., 2018). For the first possibility a good example is the use of polysorbate 80 as a coating on polymer NPs, which by binding apolipoproteins AI and E, ligands of lipoprotein and scavenger receptors of brain endothelial cells, facilitates the brain entry process (Reimold et al., 2008; Kreuter, 2013; Kreuter, 2014).

The second option is to decorate the surface of the NPs with binding partners – peptides, proteins or antibodies – of BBB receptors, such as receptors for insulin or transferrin (Zhou et al., 2018). Insulin receptors are expressed at high levels on the luminal side of brain endothelial cells, and brain accumulation of insulin targeted gold NPs was greater as compared to non-targeted NPs in mice (Shilo et al., 2014). Human serum albumin NPs covalently coupled with insulin or transferrin increased the brain entry of their loperamide cargo, a ligand of P-glycoprotein efflux pump not crossing the BBB under physiological conditions (Ulbrich et al., 2009; Ulbrich et al., 2011). Targeting the TfR elevates the BBB uptake and permeability of encapsulated drugs in liposomal drug delivery systems in *in vitro* and *in vivo* studies (Johnsen and Moos, 2016).

As compared to other BBB transporters, SLCs are underresearched as molecular targets of CNS drug delivery systems, although they are essential in transporting nutrients and drugs across the BBB (Rask-Andersen et al., 2013; Campos-Bedolla et al., 2014). In our study, we selected different ligands of endogenous nutrient transporters expressed in the brain endothelium to target solid and vesicular NPs.

5.2. Solid nanoparticles targeted with solute carrier ligands

5.2.1. Biotin, a solute carrier ligand, as a potential drug targeting molecule

Biotin is one of the ligands of SMVT, which is a highly expressed carrier at the human BBB and in the hCMEC/D3 brain endothelial cell line (Tóth et al., 2014; Uchida et al 2015). We have verified the expression of SMVT transporter in isolated rat brain microvessels, in RBECs from our triple co-culture BBB model and in hCMEC/D3 cell line (Fig. 6). Due to the high expression levels of *SMVT* gene both in the BBB model and hCMEC/D3 cells we identified biotin as a potential BBB targeting ligand of NPs.

Biotin is a cofactor for several carboxylase enzymes and a cell growth promoter. It cannot be synthesized endogenously in the brain, therefore it is supplied from the blood across the BBB. The biotin concentration in the brain is about 50-fold higher than that in the plasma (Spector and Johanson, 2007). Biotin technology based on the exceptionally strong binding between biotin and avidin has long been used in immunohistochemistry and molecular biology. Recently, biotin-avidin technology has been applied for drug targeting to tumors (Lesch et al., 2010). NPs are often biotinylated to easily detect them with streptavidin-FITC in tissue slices (Merodio et al., 2000). Biotinylation of drugs is also used to bind them to avidin-functionalized particles (Neves et al., 2015). However, none of the studies used biotin as a ligand for BBB targeting.

In our study polystyrene SNPs were chosen for functionalization due to their favorable physico-chemical properties such as size and imaging possibilities. Polystyrene NPs are frequently used as model nanocarriers: the uptake of polystyrene NPs functionalized with anti-intercellular adhesion molecule (ICAM) antibody was studied in a rat brain endothelial cell line (Kolhar et al., 2013), while the uptake and permeability of green and red fluorescent non-targeted polystyrene NPs with variable size and surface charge were tested on a mouse cerebral endothelial cell line (Guarnieri et al., 2014).

We prepared and characterized biotin- and biotinylated glutathione-labeled SNPs from neutravidin-coated commercially available red fluorescent polystyrene particles (Fig. 7). In accordance with literature data on biotinylated albumin NPs (Merodio et al 2000), labeling with biotin and biotinylated glutathione resulted in an increase of particle size. The average size and surface charge of the targeted SNPs were similar, as measured by dynamic light scattering (Table 2). The heterogeneity seen by scanning electron microscopy may be related to the different batches of SNPs used for labeling (Fig. 8). The relationship between the size of NPs and their cellular uptake and biodistribution is widely investigated. In general, particles with a size below 100 nm can be taken up by all cells via endocytosis and are considered as high risk NPs in light of nanotoxicology, especially if they are non-biodegradable (Müller et al., 2011). These small NPs are nonspecifically taken up by the liver, lungs and kidneys. This is the reason why the size of most NPs developed for possible therapeutic application is in the range of 100-200 nm. The glutathione targeted NPs studied by Gaillard and his colleagues were also in this range, namely 108 nm (Rip et al., 2014) and 95 nm (Gaillard et al., 2014) NPs were used. The size of SNPs tested in our study fell also in this range. The entry of NPs larger than 200 nm to brain tissue is less than that of smaller NPs (Mc Carthy et al., 2015). In agreement with *in vivo* findings NPs with 400 nm size did not cross a BBB culture model (Hanada et al., 2014).

5.2.2. Uptake and permeability of targeted solid nanoparticles

We are the first to demonstrate that biotin-labeling increases the uptake and transfer of SNPs in brain endothelial cells as compared to unlabeled particles (Fig.10 and 11). This finding is in agreement with the active transport of biotin at the BBB *in vivo* (Spector and Mock, 1984) and in hCMEC/D3 brain endothelial cell cultures (Uchida et al., 2015). An experimental study indicated that biotinylated NPs were able to enter the brain (Merodio et al., 2000) and this targeting concept may work *in vivo,* too. Intravenously administered biotinylated albumin NPs could be detected in several brain regions of rats with experimental autoimmune encephalomyelitis using post mortem streptavidin-FITC labeling (Merodio et al., 2000). However, this observation may provide indirect support only, because the aim of this study was the visualization of albumin NPs in the CNS, and no data are available in control rats or with unlabeled albumin NPs.

We showed a high uptake for the biotinylated glutathione-labeled SNPs in brain endothelial cells (Fig. 10 and 11). Gaillard et al. proved in several studies the increased uptake of glutathione-labeled pegylated liposomes in rat and human brain endothelial cells (Rip et al.,

2014; Gaillard et al., 2014). We found that the transfer of glutathione-labeled SNPs across the *in vitro* BBB model was the highest among the tested particles and several fold higher than that of the non-targeted ones (Fig. 12). Our results are in concordance with *in vivo* data on enhanced brain penetration of drugs and biopharmacons, including doxorubicin, a cytostatic drug, methylprednisolone, an antiinflammatory agent, DAMGO, an opioid peptide, and an anti-amyloid antibody, using glutathione-labeled vesicular NPs. Glutathione as a targeting ligand of NPs increased the brain delivery of doxorubicin (543 Da) cargo in rats (Birngruber et al., 2014), and these targeted NPs inhibited tumor growth and increased survival in a mouse model of glioblastoma multiforme (Gaillard et al., 2014). Brain uptake of methylprednisolone (374 Da) was elevated by glutathione targeting (Gaillard et al., 2012), and improved therapeutic efficacy was described for GSH-pegylated liposomal methylprednisolone in experimental autoimmune encephalomyelitis in rats (Gaillard et al., 2012), in mice (Lee et al., 2014), and in ocular inflammation in rats (Reijerkerk et al., 2014). Increased brain delivery was demonstrated for the opioid pentapeptide DAMGO (513 Da) using GSH-pegylated liposomes in rats (Lindqvist et al., 2016). Enhanced GSH-pegylated liposomal brain delivery of a llama single domain anti-amyloid antibody fragment (15 kDa) was observed in a mouse model for Alzheimer's disease (Rotman et al., 2015), indicating that the platform may also be used for CNS delivery of biopharmacons.

5.2.3. Possible mechanisms of targeted solid nanoparticle transfer

Targeted NPs may use several transport routes at the BBB (Rempe et al., 2014). Solid NPs were described to cross brain endothelial cells by receptor- or adsorption-mediated transcytosis (Müller et al., 2011, Rempe et al., 2014). The higher transfer of SNP-B and SNP-B-GSH particles may be related to transcytosis due to the binding of targeting ligands to the surface of brain endothelial cells. In the case of biotin targeted SNPs, we hypothesize that the targeting ligand helps nanocarrier binding to the surface of brain endothelial cells, which triggers transcytosis across brain endothelial monolayers. For the clinical-stage GSH drug delivery platform, although the BBB receptor/transporter is unknown, a specific liposomal endocytosis pathway indicative of receptor-mediated transcytosis is suggested as a mechanism of BBB crossing (Gaillard et al., 2012). Further experiments are needed to explore the exact mechanism.

5.3. Vesicular nanoparticles targeted with single and dual ligands of solute carriers

5.3.1. Niosomes as potential vesicular delivery systems across the BBB

Niosomes are comparable to liposomes in terms of stability and permeability for drug-size molecules (Abdelkader et al., 2014; Bartelds et al., 2018). In addition, niosomes can be easily stored and handled, and their components are cheap and not sensitive to oxidation. In this study we prepared many types of BBB targeted niosomes with uniform size (average diameter: ~100 nm), narrow size distribution (polydispersity index < 0.2), and with spherical shape (Fig. 13 and 14, Table 3). Spherical nanocarriers in this size range are widely used in animal models to investigate CNS drug delivery (Saraiva et al., 2016). Like liposomes, niosomes are suitable for the encapsulation of both water and lipid soluble molecules (Abdelkader et al., 2014). Fluorescent EBA, our model cargo was successfully encapsulated in the hydrophilic core of niosomes. Due to the high molecular mass of EBA (67 kDa) the encapsulation efficiency varied in the range of 4.6–10.4%. Prior to our study, vasoctive intestinal peptide, a 3.3 kDa hormone, was the largest cargo encapsulated in niosomes and targeted successfully to brain in mice (Dufes et al., 2004). The molecular mass of our cargo, serum albumin, is 20 times bigger, suggesting that niosomes are able to deliver large biomolecules.

The stability of the niosomes has been followed for six months. The size, polydispersity index and cargo encapsulation efficiency of the niosomes changed minimally during half a year, indicating that they are easy to store (Table 4). In contrast to liposomes which are already used in pharmacotherapy, niosomes have not been reported to date in clinical studies, only preclinical data are available regarding their application. In our study we assessed the efficacy of BBB targeted niosomes as a delivery system.

5.3.2. Functionalization of niosomes by solute carrier ligands for BBB targeting

Niosomes were decorated with glucose, alanine and glutathione ligands and their dual combinations to elevate their BBB targeting specificity (Fig. 13). The surface charge of glucose and alanine targeted niosomes was less negative (−3 and −4 mV), than that of the glutathione labeled ones (N-GSH, N-A-GSH, N-GP-GSH), which was around −7 mV. Niosomes show low toxicity due to their non-ionic components and good biodegradability (Abdelkader et al., 2014) as it was observed in our viability study as well. The effect of targeted niosomes on cellular viability was followed real time and no change was detected after 4h (Fig. 15).

The brain is the most glucose consuming organ, and hexose transporters, especially GLUT-1, are highly expressed at the BBB (Campos-Bedolla et al., 2014). We confirmed that several glucose transporters were expressed in rat brain microvessels and BBB culture models and *GLUT1* showed the highest mRNA expression in all groups (Fig. 6). N-dodecyl-β-D-glucopyranose was selected as a non-metabolizable glucose analog for niosome decoration. Using culture models of the BBB, a 30% increase in the uptake and a three-fold elevation in the permeability of the EBA cargo with N-GP was found, as compared to non-targeted niosomes, but these changes were not statistically significant (Fig. 16 and 17).

In mice the brain fluorescence of EBA significantly increased at 10 min and a several fold elevation was observed until 24 h after tail vein injection of N-GP (Fig. 22B). Our *in vivo* results are in agreement with the findings of Dufes et al., who described that niosomes targeted with N-palmitoylglucosamine ligand enhanced the brain entry of the cargo vasoactive intestinal peptide in mice (Dufes et al., 2004). Small gold NPs covalently coated with β2-mercaptoethoxy-glucose entered and crossed cultured human brain endothelial cells better than non-brain endothelial cells (Gromnicova et al., 2013). NPs, including liposomes, micelles and solid polymeric NPs derivatized with different glucose analogs improve the delivery of encapsulated drugs or fluorescent dyes to the brain by targeting GLUTs, as reviewed by Patching (2017), indicating the potential applicability of these SLCs.

The small neutral amino acid alanine, which is transported by several SLCs at the BBB (Campos-Bedolla et al., 2014), was selected as the other targeting ligand of the tested niosomes. The mRNAs of the sodium coupled neutral amino acid carriers were highly represented in brain microvessels and BBB culture models (Fig. 6). To our best knowledge, this is the first report indicating that NPs decorated with alanine as a targeting ligand elevate the uptake of the cargo in cultured brain endothelial cells (Fig. 16) and its brain entry in mice (Fig. 22B).

Niosomes were also functionalized with glutathione as a reference targeting ligand. Labeling of niosomes with GSH-PEG significantly increased the uptake of EBA in brain endothelial cells (Fig. 16) and elevated four-fold the EBA permeability across the BBB culture model as compared to untargeted NPs (Fig. 17). These findings are in concordance with our data on the uptake and permeability of SNP-B-GSH, and show that GSH targeting can rise the transfer of NPs across brain endothelial cells. The GSH-PEGylated liposomal drug delivery system was effective also in rodent models for brain delivery of different drug cargos, like

doxorubicin (Gaillard et al., 2014) or ribavirin (Maussang et al., 2016), indicating the *in vivo* applicability of GSH.

5.3.3. Targeting of BBB transporters by dual labeling of nanoparticles

In concordance with our hypothesis, dual labeling of niosomes with ligands of BBB transporters (N-A-GP and N-A-GSH) elevated the cargo uptake into and penetration across the BBB model as compared to both single ligand targeted or non-targeted NPs (Fig. 16-18). The highest effect of dual labeling of NPs with SLC ligands (N-A-GP) on brain uptake of cargo was detected in the mouse study (Fig. 22B). The cargo selected for our experiments, the large biomolecule albumin, has a negligible transport across the BBB in physiological conditions (Abbott et al., 2010). This is also reflected in the very low P_{app} value (0.1×10^{-6} cm/s) of the free EBA across the BBB model (Fig. 17), in accordance with our previous data (Deli et al., 2005; Walter et al., 2015). Free EBA cargo penetration to brain was also limited in mice (Fig. 22B), as we demonstrated it in our previous study (Veszelka et al., 2003). It should be noted, that compared to small molecule permeability, the P_{app} value of EBA increased by dual-targeted nanovesicles is still low (Fig. 22B). We should consider however, that this limited EBA transport represent 10- and 20-fold increases in the P_{app} value or in the brain fluorescence intensity, respectively, of this low penetrant cargo.

As a possible mechanism, the combination of two different SLC transporter ligands on the niosomal surface may produce stronger vesicular docking to brain endothelial cells facilitating NP fusion and/or endocytosis. There are two studies which may support this dual BBB targeting hypothesis, although with different systems. Liposomes (100 nm) were dually decorated with ligands of TfR and low density lipoprotein receptor-related protein-1 expressed at the BBB (Markoutsa et al., 2014). Dual-targeting for BBB these receptors increased BBB penetration of NPs both in cultured brain endothelial cells and in mice, indicating that targeting more than one receptors at the BBB can be more effective. A similar increase in effectiveness was observed when multiple BBB transporters were targeted. In another study 2 nm carbon dots prepared by pyrolysis from D-glucose and L-aspartic acid penetrated glioma tissue better than normal brain in mice, but not carbon dots prepared from D-glucose, L-aspartic acid, or D-glucose and L-glutamic acid (Zheng et al., 2015). In this study, however, no experiments were performed to reveal possible uptake mechanisms and whether it was an active, energy dependent process.

Dual-targeted drug delivery systems were described for other glioma models too, but in these cases multiple BBB transporters were not involved. For example, 2-deoxy-D-glucose, a hexose transporter ligand, was used as a NP ligand targeting both the BBB and glioma cells (Jiang et al., 2014). In other systems even if two different ligands were used, only one was specific for the BBB, the other ligand served different purposes, like cell penetration. Combining T7 peptide targeting TfR at the BBB with the cell-penetrating peptide TAT on liposome surfaces enhanced the efficiency of glioma targeting (Zong et al., 2014).

5.3.4. Mechanisms of targeted NP uptake

Modified physiological conditions, such as low temperature or the inhibition of ATP hydrolysis may facilitate the identification of the cellular uptake mechanisms of NPs (Fiorentino et al., 2015). In our study the uptake of the cargo decreased in the targeted NP groups in low temperature conditions and following the application of sodium azide, a metabolic inhibitor (Fig. 19). This is consistent with the hypothesis that the cellular uptake of targeted niosomes is an energy dependent active process. In agreement with our results, the uptake of GSH labeled liposomes in brain endothelial cells was also inhibited by low temperature (Maussang et al., 2016).

To shed more light on the uptake mechanisms of targeted niosomes we tested the possible involvement of endocytotic processes using inhibitors of endocytosis, namely cytochalasin D and filipin. Cytochalasin D is a drug blocking F-actin depolymerization, membrane ruffling and thereby inhibiting macropinocytosis and phagocytosis. Since actin cytoskeleton regulates several endocytotic pathways, cytochalasin D is a common inhibitor of endocytosis (Ivanov, 2008). Cytochalasin D pretreatment inhibited the uptake of GSH-PEG liposomes in hCMEC/D3 endothelial cell line (Maussang et al., 2016), as well as the uptake of platelet-derived microparticles (Faille et al., 2012), indicating that the internalization of extracellular NPs into endocytotic vesicles might be an important step in the cellular uptake mecanisms. Filipin, an antibiotic, interacts with cholesterol in biological membranes and inhibits selectively the lipid raft- and caveolae-mediated endocytosis (Ivanov, 2008). Pretreatment of brain endothelial cells with cytochalasin D or filipin decreased the uptake of the cargo in the case of dual-targeted niosomes (N-A-GSH; Fig. 20). These data indicate that endocytosis contributes to the cellular uptake of targeted niosomes.

Several specific features of the BBB limit the penetration of drugs into the CNS. Intercellular junctions and drug efflux pumps are widely investigated, but the role of the

negative surface charge of brain endothelial cells in CNS drug delivery is rather unexplored. This highly negative surface charge is composed of the negatively charged lipids in the cellular plasma membrane and the glycocalyx at the luminal surface. The glycocalyx is a 0.1-1 μm thick layer covering the entire surface of endothelial cells and composed of proteoglycans and glycoseaminoglycans (Hervé et al., 2008). The surface charge (zeta potential) of cells could be measured by dynamic light scattering and was found to be the most negative in brain endothelial cells among vascular endothelial cells (Ribeiro et al., 2012). This electrostatic barrier may influence the transport of substances and also NPs across the BBB. While NP surface charge was already investigated on BBB integrity and permeability (Fenart et al., 1999; Lockman et al., 2004), the effect of brain endothelial surface charge modification on the permeability of NPs was not measured yet. We modified the highly negative surface charge of cells with neuraminidase and cationic lipid (TMA-DPH) treatments. The neuraminidase or sialidase enzyme digests the negatively charged sialic acid residues on the luminal surface of endothelial cells and elevates the surface charge of glycocalyx (Born and Palinski, 1985). In our experiments neuraminidase treatment of brain endothelial cells significantly increased the uptake of the cargo of dual-targeted NPs compared with the untargeted and non-treated groups (Fig. 21). TMA-DPH elevates the charge of the plasma membrane because it intercalates with the hydrophilic head groups of membrane phospholipids (Ribeiro et al., 2012). Like neuraminidase, TMA-DPH also raised the cellular uptake of cargo in the dual-targeted negatively charged N-A-GSH group. Our new observations indicate that surface charge at the BBB is important in the uptake mechanism of charged NPs and can be modulated by modification of plasma membrane lipid composition or the glycocalyx.

Surfactants are well known enhancers of absorption and increase drug permeability through the cell membranes or via the modulation of intercellular junctions (Deli, 2009). Surfactants are incorporated into the lipid bilayer of cell membranes, and depending on their concentration either change the physical properties and permeability of plasma membranes or result in membrane solubilization leading to cell toxicity (Ujhelyi et al., 2012). Polysorbate surfactants, especially Solulan C24, which is one of the main components of our niosomes, concentration-dependently increased the transepithelial permeability of hydrophilic drugs as a result of solubilization of Caco-2 cell membrane components (Dimitrijevic et al., 2000). We have previously demonstrated that the non-ionic surfactant sugar esters increased the plasma membrane fluidity of epithelial cells, which could contribute to the increased transcellular passage of molecules (Kiss et al., 2014). In the present experiments both the non-targeted and

dual-targeted niosomes decreased the fluorescent anisotropy in brain endothelial cells, which indicates increased cell membrane fluidity, suggesting the fusion of the nanovesicles with the plasma membrane (Fig. 22).

5.5. Conclusion

To summarize our data, we described promising ligands of the endogenous nutrient transporters of brain endothelium to target solid and vesicular NPs for CNS delivery. We demonstrated for the first time that biotin as a targeting ligand increased the uptake and transfer of solid NPs in cultured brain endothelial cells and confirmed that glutathione increased NP permeability across the BBB model, supporting the use of these ligands for brain targeting.

Vesicular nanoparticles targeted with glutathione and SLC ligands glucopyranose and alanine either alone or in combination were prepared and characterized. The presence of targeting ligands on niosomes, especially dual labeling, increased the uptake and the permeability of the cargo molecule across the BBB. The efficacy of alanine and dual labeling with nutrient transporter and SLC ligands for BBB targeting of NPs was proved for the first time. Endocytosis, fusion of NPs with plasma membrane and brain endothelial surface charge contributed to the cellular uptake mechanisms of targeted nanocarriers. Our data indicate that dual labeling with ligands of multiple SLC transporters can potentially be exploited for BBB targeting of NPs.

6. SUMMARY

NPs for drug targeting across the BBB are promising candidates to increase the brain penetration of biopharmacons for treating CNS diseases. Effective targeting of NPs can only be achieved by exploiting the BBB specific physiological transport pathways. Despite the abundance of carrier mediated transporters at the BBB this pathway is still underresearched for drug delivery.

Solute carriers functioning as nutrient transporters are expressed at high levels in brain endothelial cells and show a specific pattern at the BBB. Our hypothesis was, that targeting SLCs expressed at the BBB can enhance nanoparticle uptake and permeability across brain endothelial cells, and using ligands for two different SLCs at the same time could further increase nanoparticle penetration. The aim of our studies was to identify and test SLC

transporter ligands and glutathione as single or dual BBB targeting molecules for solid and vesicular NPs.

In our first study we tested biotin-labeled solid NPs and compared them to glutathione-labeled NPs on an *in vitro* BBB model. Fluorescent polystyrene NPs were derivatized and investigated on human brain endothelial cells. We verified that hCMEC/D3 cells express mRNA for sodium-dependent multivitamin transporter (SMVT/SLC5A6) responsible for the BBB transport of biotin. Biotin as a ligand increased the uptake and the transfer of NPs across brain endothelial cells. Glutathione could further increase NP permeability across the BBB model, supporting its use as a brain targeting vector.

In the second series of experiments vesicular NPs were investigated. High mRNA expression levels for hexose and neutral amino acid transporting SLCs were found in isolated rat brain microvessels and a rat primary cell based co-culture BBB model. Niosomes, nanovesicles prepared from non-ionic surfactants, were decorated with glutathione and SLC ligands glucopyranose and alanine, and loaded with Evans blue-albumin complex as a large biomolecule model cargo. The presence of targeting ligands on niosomes, especially dual labeling, increased the uptake of the cargo molecule in cultured brain endothelial cells. This cellular uptake was temperature dependent and decreased following application of a metabolic inhibitor, sodium azide, and endocytosis blockers, filipin and cytochalasin D. Turning the negative surface charge of brain endothelial cells more positive with a cationic lipid or digesting the glycocalyx with neuraminidase elevated the uptake of the cargo encapsulated in targeted nanocarriers. Niosomes increased plasma membrane fluidity, suggesting the fusion of nanovesicles with the endothelial cell membranes. Targeting ligands elevated the permeability of the cargo across the BBB in the culture model and in mice, and dual-ligand decoration of niosomes was more effective than single ligand labeling. As a conclusion, our data indicate that ligands of multiple SLC transporters can be exploited for BBB targeting of NPs.

7. REFERENCES

Abbott, N.J., 2002. Astrocyte-endothelial interactions and blood-brain barrier permeability. J. Anat. 200, 629-638.

Abbott, N.J., 2013. Blood-brain barrier structure and function and the challenges for CNS drug delivery. J. Inherit. Metab. Dis. 36, 437-449.

Abbott, N.J., Patabendige, A.A., Dolman, D.E., Yusof, S.R., Begley, D.J., 2010. Structure and function of the blood-brain barrier. Neurobiol. Dis. 37, 13-25.

Abdelkader, H., Alani, A.W., Alany, R.G., 2014. Recent advances in non-ionic surfactant vesicles (niosomes): self-assembly, fabrication, characterization, drug delivery applications and limitations. Drug Deliv. 21, 87-100.

Banks, W.A., 2009. Characteristics of compounds that cross the blood-brain barrier. BMC Neurol. 9, Suppl 1:S3.

Banks, W.A., 2016. From blood-brain barrier to blood-brain interface: new opportunities for CNS drug delivery. Nat. Rev. Drug Discov. 15, 275-292.

Bartelds, R., Nematollahi, M.H., Pols, T., Stuart, M.C.A., Pardakhty, A., Asadikaram, G., Poolman, B., 2018. Niosomes, an alternative for liposomal delivery. PLoS One. 13, e0194179.

Bauer, M., Karch, R., Wulkersdorfer, B., Philippe, C., Nics, L., Klebermass, E.M., Weber, M., Poschner, S., Haslacher, H., Jäger, W., Tournier, N., Wadsak, W., Hacker, M., Zeitlinger, M., Langer, O., 2018. A proof-of-concept study to inhibit ABCG2- and ABCB1-mediated efflux transport at the human blood-brain barrier. J. Nucl. Med. 118, 216432.

Begley, D.J., 2004. Delivery of therapeutic agents to the central nervous system: the problems and the possibilities. Pharmacol. Ther. 104, 29-45.

Birngruber, T., Raml, R., Gladdines, W., Gatschelhofer, C., Gander, E., Ghosh, A., Kroath, T., Gaillard, P.J., Pieber, T.R., Sinner, F., 2014. Enhanced doxorubicin delivery to the brain administered through glutathione PEGylated liposomal doxorubicin (2B3-101) as compared with generic Caelyx,(®)/Doxil(®)-a cerebral open flow microperfusion pilot study. J. Pharm. Sci. 103, 1945-1948.

Blasi, P., Giovagnoli, S., Schoubben, A., Ricci, M., Rossi, C., 2007. Solid lipid nanoparticles for targeted brain drug delivery. Adv. Drug Deliv. Rev. 59, 454-477.

Bocsik, A., Darula, Z., Tóth, G., Deli, M.A., Wollemann, M., 2015. Transfer of opiorphin through a blood-brain barrier culture model. Arch. Med. Res. 46, 502-506.

Bocsik, A., Gróf, I., Kiss, L., Ötvös, F., Zsíros, O., Daruka, L., Fülöp, L., Vastag, M., Kittel Á, Imre, N., Martinek, T.A., Pál, C., Szabó-Révész, P., Deli, M.A., 2019. Dual action of the PN159/KLAL/MAP peptide: Increase of drug penetration across Caco-2 intestinal barrier model by modulation of tight junctions and plasma membrane permeability. Pharmaceutics. 10, 11.

Bocsik, A., Walter, F.R., Gyebrovszki, A., Fülöp, L., Blasig, I., Dabrowski, S., Ötvös, F., Tóth, A., Rákhely, G., Veszelka, S., Vastag, M., Szabó-Révész, P., Deli, M.A., 2016. Reversible opening of intercellular junctions of intestinal epithelial and brain endothelial cells with tight junction modulator peptides. J. Pharm. Sci. 105, 754-765.

Born, G.V., Palinski, W., 1985. Unusually high concentrations of sialic acids on thesurface of vascular endothelia. Br. J. Exp. Pathol. 66, 543-549.

Campos-Bedolla, P., Walter, F.R., Veszelka, S., Deli, M.A., 2014. Role of the blood-brain barrier in the nutrition of the central nervous system. Arch. Med. Res. 45, 610-638.

César-Razquin, A., Snijder, B., Frappier-Brinton, T., 2015. A call for systematic research on solute carriers. Cell. 162, 478-487.

Craparo, E.F., Bondì, M.L., Pitarresi, G., Cavallaro, G., 2011. Nanoparticulate systems for drug delivery and targeting to the central nervous system. CNS Neurosci. Ther. 6, 670-677.

Csete, M., Sipos, Á., Kőházi-Kis, A., Szalai, A., Szekeres, G., Matesz, A., Csákó, T., Osvay, K., Bor, Z., Penke, B., Deli, M.A., Veszelka, S., Schmatulla, A., Marti, O., 2007. Comparative study of sub-micrometer polymeric dot-arrays, linear and crossed gratings generated by UV laser based two-beam interference as surfaces for AFM and SPR based bio-sensing. Appl. Surf. Sci. 254, 1194-1205.

Dauchy S., Dutheil F., Weaver R.J., Chassoux F., Daumas-Duport C., Couraud P.O., Scherrmann J.M., De Waziers I., Declèves X., 2008. ABC transporters, cytochromes P450 and their main transcription factors: expression at the human blood-brain barrier. J. Neurochem. 107,1518-1528.

Deli, M.A., 2009. Potential use of tight junction modulators to reversibly open membranous barriers and improve drug delivery. Biochim. Biophys. Acta. 1788, 892-910.

Deli, M.A., 2011. Drug transport and the blood-brain barrier, in: Tihanyi, K., Vastag, M. (Eds.), Solubility, Delivery, and ADME Problems of Drugs and Drug-Candidates. Bentham Science Publishers Ltd., Washington, pp. 144-165.

Deli, M.A., Abrahám, C.S., Kataoka, Y., Niwa, M., 2005. Permeability studies on in vitro blood-brain barrier models: physiology, pathology, and pharmacology. Cell. Mol. Neurobiol. 25, 59-127.

Dimitrijevic, D., Shaw, A.J, Florence, A.T., 2000. Effects of some non-ionic surfactants on transepithelial permeability in Caco-2 cells. J. Pharm. Pharmacol. 52, 157-162.

Dufes, C., Gaillard, F., Uchegbu, I.F., Schätzlein, A.G., Olivier, J.C., Muller, J.M., 2004. Glucose-targeted niosomes deliver vasoactive intestinal peptide (VIP) to the brain. Int. J. Pharm. 285, 77-85.

Enerson, B.E., Drewes, L.R., 2006. The rat blood-brain barrier transcriptome. J. Cereb. Blood Flow. Metab. 26, 959-973.

Faille, D., El-Assaad, F., Mitchell, A.J., Alessi, M.C., Chimini, G., Fusai, T., Grau, G.E., Combes, V., 2012. Endocytosis and intracellular processing of platelet microparticles by brain endothelial cells. J. Cell. Mol. Med. 16, 1731-1738.

Fenart, L., Casanova, A., Dehouck, B., Duhem, C., Slupek, S., Cecchelli, R., Betbeder, D., 1999. Evaluation of effect of charge and lipid coating on ability of 60-nm nanoparticles to cross an in vitro model of the blood-brain barrier. J. Pharmacol. Exp. Ther. 291, 1017-1022.

Fiorentino, I., Gualtieri, R., Barbato, V., Mollo, V., Braun, S., Angrisani, A., Turano, M., Furia, M., Netti, P.A., Guarnieri, D., Fusco, S., Talevi, R., 2015. Energy independent uptake and release of polystyrene nanoparticles in primary mammalian cell cultures. Exp. Cell. Res. 330, 240-247.

Gaillard, P.J., 2016. BBB crossing assessment and BBB crossing technologies in CNS Drug Discovery. Drug Discov. Today Technol. 20, 1-3.

Gaillard, P.J., Appeldoorn, C.C., Dorland, R., van Kregten, J., Manca, F., Vugts, D.J., Windhorst, B., van Dongen, G.A, de Vries, H.E, Maussang, D., van Tellingen, O., 2014. Pharmacokinetics, brain delivery, and efficacy in brain tumor-bearing mice of glutathione pegylated liposomal doxorubicin (2B3-101). PLoS One. 1, e82331.

Gaillard, P.J., Appeldoorn, C.C., Rip, J., Dorland, R., van der Pol, S.M., Kooij, G., de Vries, H.E., Reijerkerk, A., 2012. Enhanced brain delivery of liposomal methylprednisolone improved therapeutic efficacy in a model of neuroinflammation. J. Control Release. 164, 364-369.

Gastaldi, L., Battaglia, L., Peira, E., Chirio, D., Muntoni, E., Solazzi, I., Gallarate, M., Dosio, F., 2014. Solid lipid nanoparticles as vehicles of drugs to the brain: current state of the art. Eur. J. Pharm. Biopharm. 87, 433-444.

Geldenhuys W., Wehrung D., Groshev A., Hirani A., Sutariya V., 2015. Brain-targeted delivery of doxorubicin using glutathione-coated nanoparticles for brain cancers. Pharm. Dev. Technol. 20,497-506.

Gharbavi, M., Amani, J., Kheiri-Manjili, H., Danafar, H., Sharafi, A., 2018. Niosome: A promising nanocarrier for natural drug delivery through blood-brain barrier. Adv. Pharmacol. Sci. 11, 2018:6847971.

Giugliani, R., Giugliani, L., de Oliveira Poswar, F., Donis, K.C., Corte, A.D, Schmidt, M., Boado, R.J., Nestrasil, I., Nguyen, C., Chen, S., Pardridge, W.M., 2018. Neurocognitive and somatic stabilization in pediatric patients with severe mucopolysaccharidosis type I after 52 weeks of intravenous brain-penetrating insulin receptor antibody-iduronidase fusion protein (valanafusp alpha): an open label phase 1-2 trial. Orphanet. J. Rare Dis. 13,110.

Gromnicova, R., Davies, H.A., Sreekanthreddy, P., Romero, I.A., Lund, T., Roitt, I.M., Phillips, J.B., Male, D.K., 2013. Glucose-coated gold nanoparticles transfer across human brain endothelium and enter astrocytes in vitro. PLoS One. 9, e81043.

Guarnieri, D., Muscetti, O., Netti, P.A., 2014. A method for evaluating nanoparticle transport through the blood-brain barrier in vitro. Methods Mol. Biol. 1141, 185-199.

Hanada, S., Fujioka, K., Inoue, Y., Kanaya, F., Manome, Y., Yamamoto, K., 2014. Cell-based in vitro blood-brain barrier model can rapidly evaluate nanoparticles' brain permeability in association with particle size and surface modification. Int. J. Mol. Sci. 15, 1812-1825.

Haseloff, R.F., Dithmer, S., Winkler, L., Wolburg, H., Blasig, I.E., 2015. Transmembrane proteins of the tight junctions at the blood-brain barrier: structural and functional aspects. Semin. Cell. Dev. Biol. 38, 16-25.

Helms, H.C., Abbott, N.J., Burek, M., Cecchelli, R., Couraud, P.O., Deli, M.A., Förster, C., Galla, H.J., Romero, I.A., Shusta, E.V., Stebbins, M.J., Vandenhaute, E., Weksler, B., Brodin, B., 2016. In vitro models of the blood-brain barrier: An overview of commonly used brain endothelial cell culture models and guidelines for their use. J. Cereb. Blood Flow Metab. 36, 862-890.

Hervé, F., Ghinea, N., Scherrmann, J.M., 2008. CNS delivery via adsorptive transcytosis. AAPS J. 10, 455-472.

Horvát, S., Fehér, A., Wolburg, H., Sipos, P., Veszelka, S., Tóth, A., Kiss, L., Kurunczi, A., Balogh, G., Kürti, L., Eros, I., Szabó-Révész, P., Deli, M.A., 2009. Sodium hyaluronate as a mucoadhesive component in nasal formulation enhances delivery of molecules to brain tissue. Eur. J. Pharm. Biopharm. 72, 252-259.

Hülper, P., Veszelka, S., Walter, F.R., Wolburg, H., Fallier-Becker, P., Piontek, J., Blasig, I.E., Lakomek, M., Kugler, W., Deli, M.A., 2013. Acute effects of short-chain alkylglycerols on blood-brain barrier properties of cultured brain endothelial cells. Br. J. Pharmacol. 169, 1561-1573.

Ito, A., Shinkai, M., Honda, H., Kobayashi, T., 2005. Medical application of functionalized magnetic nanoparticles. J. Biosci. Bioeng. 100, 1-11.

Ivanov, A.I., 2008. Pharmacological inhibition of endocytic pathways: is it specific enough to be useful? Methods Mol. Biol. 440, 15-33.

Jiang, X., Xin, H., Ren, Q., Gu, J., Zhu, L., Du, F., Feng, C., Xie, Y., Sha, X., Fang, X., 2014. Nanoparticles of 2-deoxy-D-glucose functionalized poly(ethylene glycol)-co-poly(trimethylene carbonate) for dual-targeted drug delivery in glioma treatment. Biomaterials. 35, 518-529.

Johnsen, K.B., Moos, T., 2016. Revisiting nanoparticle technology for blood-brain barrier transport: Unfolding at the endothelial gate improves the fate of transferrin receptor-targeted liposomes. J. Control. Release. 28, 32-46.

Kannan, R., Chakrabarti, R., Tang, D., Kim, K.J., Kaplowitz, N., 2000. GSH transport in human cerebrovascular endothelial cells and human astrocytes: evidence for luminal localization of Na^+-dependent GSH transport in HCEC. Brain Res. 852, 374-382.

Keren, S., Gheysens, O., Levin, C.S., Gambhir, S.S., 2008. A comparison between a time domain and continuous wave small animal optical imaging system. IEEE Trans. Med. Imaging. 27, 58-63.

Kevadiya, B.D., Ottemann, B.M., Thomas, M.B., Mukadam, I., Nigam, S., McMillan, J., Gorantla, S., Bronich, T.K., Edagwa, B., Gendelman, H.E., 2018. Neurotheranostics as personalized medicines. Adv. Drug Deliv. Rev. 18, 30261-30268.

Kiss, L., Hellinger, É., Pilbat, A.M., Kittel, Á., Török, Z., Füredi, A., Szakács, G., Veszelka, S., Sipos, P., Ózsvári, B., Puskás, L.G., Vastag, M., Szabó-Révész, P., Deli, M.A., 2014. Sucrose esters increase drug penetration, but do not inhibit P-glycoprotein in Caco-2 intestinal epithelial cells. J. Pharm. Sci. 103, 3107-3119.

Kiss, L., Walter, F.R., Bocsik, A., Veszelka, S., Ozsvári, B., Puskás, L.G., Szabó-Révész, P., Deli, M.A., 2013. Kinetic analysis of the toxicity of pharmaceutical excipients Cremophor EL and RH40 on endothelial and epithelial cells. J. Pharm. Sci. 102, 1173-1181.

Kolhar, P., Anselmo, A.C., Gupta, V., Pant, K., Prabhakarpandian, B., Ruoslahti, E., Mitragotri, S., 2013. Using shape effects to target antibody-coated nanoparticles to lung and brain endothelium. Proc. Natl. Acad. Sci. USA. 110, 10753-10758.

Kreuter, J., 2013. Mechanism of polymeric nanoparticle-based drug transport across the blood-brain barrier (BBB). J. Microencapsul. 30, 49-54.

Kreuter, J., 2014. Drug delivery to the central nervous system by polymeric nanoparticles: what do we know? Adv. Drug. Deliv. Rev. 71, 2-14.

Kumar, A.T.N., Raymond, S.B., Dunn, A.K., Bacskai, B.J., Boas, D.A., 2008. A time domain fluorescence tomography system for small animal imaging. IEEE Trans. Med. Imaging. 27, 1152-1163.

Lee, D.H., Rötger, C., Appeldoorn, C.C., Reijerkerk, A., Gladdines, W., Gaillard, P.J., Linker, R.A., 2014. Glutathione PEGylated liposomal methylprednisolone (2B3-201) attenuates CNS inflammation and degeneration in murine myelin oligodendrocyte glycoprotein induced experimental autoimmune encephalomyelitis. J. Neuroimmunol. 274, 96-101.

Lénárt, N., Walter, F.R., Bocsik, A., Sántha, P., Tóth, M.E., Harazin, A., Tóth, A.E., Vizler, C., Török, Z., Pilbat, A.M., Vígh, L., Puskás, L.G., Sántha, M., Deli, M.A., 2015. Cultured cells of the blood-brain barrier from apolipoprotein B-100 transgenic mice: effects of oxidized low-density lipoprotein treatment. Fluids Barriers CNS.17, 12-17.

Lesch, H.P., Kaikkonen, M.U., Pikkarainen, J.T., Ylä-Herttuala, S., 2010. Avidin-biotin technology in targeted therapy. Expert Opin. Drug. Deliv. 7, 551-564.

Libralato, G., Galdiero, E., Falanga, A., Carotenuto, R., de Alteriis, E., Guida, M., 2017. Toxicity effects of functionalized quantum dots, gold and polystyrene nanoparticles on target aquatic biological models: A review. Molecules. 31, 22

Liebner, S., Corada, M., Bangsow, T., Babbage, J., Taddei, A., Czupalla, C.J., Reis, M., Felici, A., Wolburg, H., Fruttiger, M., Taketo, M.M., von Melchner, H., Plate, K.H., Gerhardt, H., Dejana E., 2008. Wnt/beta-catenin signaling controls development of the blood-brain barrier. J. Cell Biol. 183, 409-417.

Lindqvist, A., Rip, J., van Kregten, J., Gaillard, P.J., Hammarlund-Udenaes, M., 2016. In vivo functional evaluation of increased brain delivery of the opioid peptide DAMGO by glutathione-PEGylated liposomes. Pharm. Res. 33, 177-185.

Liu, D., Li, Y., Deng, J., Yang, W., 2014. Helix-sense-selective polymerization of achiral substituted acetylene in chiral micelles for preparing optically active polymer nanoparticles: Effects of chiral emulsifiers. Polymer. 55, 840-847.

Livak, K.J., Schmittgen, T.D., 2001. Analysis of relative gene expression data using real-time quantitative PCR and the 2(-Delta Delta C(T)) Method. Methods. 25, 402-408.
Lockman, P.R., Koziara, J.M., Mumper, R.J., Allen, D.D., 2004. Nanoparticle surface charges alter blood-brain barrier integrity and permeability. J. Drug Target. 12, 635-641.
Loos, C., Syrovets, T., Musyanovych, A., Mailänder, V., Landfester, K., Nienhaus, G. U., & Simmet, T., 2014. Functionalized polystyrene nanoparticles as a platform for studying bio-nano interactions. Beilstein J. Nanotechnol. 5, 2403-2412.
Loureiro, J.A., Gomes, B., Fricker, G., Cardoso, I., Ribeiro, C.A., Gaiteiro, C., Coelho, M.A., Pereira, Mdo. C., Rocha, S., 2015. Dual ligand immunoliposomes for drug delivery to the brain. Colloids Surf. B. Biointerfaces. 134, 213-219.
Markoutsa, E., Papadia, K., Giannou, A.D., Spella, M., Cagnotto, A., Salmona, M., Stathopoulos, G.T., Antimisiaris, S.G., 2014. Mono and dually decorated nanoliposomes for brain targeting, in vitro and in vivo studies. Pharm. Res. 31, 1275-1289.
Masserini, M., 2013. Nanoparticles for brain drug delivery. ISRN. Biochem. 2013, 238428.
Maussang, D., Rip, J., van Kregten, J., van den Heuvel, A., van der Pol, S., van der Boom, B., Reijerkerk, A., Chen, L., de Boer, M., Gaillard, P., de Vries, H., 2016. Glutathione conjugation dose-dependently increases brain-specific liposomal drug delivery in vitro and in vivo. Drug Discov. Today Technol. 20, 59-69.
Mc Carthy, D.J., Malhotra, M., O'Mahony, A.M., Cryan, J.F., O'Driscoll, C.M., 2015. Nanoparticles and the blood-brain barrier: advancing from in-vitro models towards therapeutic significance. Pharm. Res. 32, 1161-1185
Merodio, M., Irache, J.M., Eclancher, F., Mirshahi, M., Villarroya, H., 2000. Distribution of albumin nanoparticles in animals induced with the experimental allergic encephalomyelitis. J. Drug Target. 8, 289-303.
Moghassemi, S., Hadjizadeh, A., 2014. Nano-niosomes as nanoscale drug delivery systems: an illustrated review. J. Control. Release. 185, 22-36.
Morris, M.E., Rodriguez-Cruz, V., Felmlee, M.A., 2017. SLC and ABC transporters: expression, localization, and species differences at the blood-brain and the blood-cerebrospinal fluid barriers. AAPS. J. 19, 1317-1331.
Müller, R.H., Gohla, S., Keck, C.M., 2011. State of the art of nanocrystals – special features, production, nanotoxicology aspects and intracellular delivery. Eur. J. Pharm. Biopharm. 78, 1-9.
Nakagawa, S., Deli, M.A., Kawaguchi, H., Shimizudani, T., Shimono, T., Kittel, A., Tanaka, K., Niwa, M., 2009. A new blood-brain barrier model using primary rat brain endothelial cells, pericytes and astrocytes. Neurochem. Int. 54, 253-263.
Neuwelt, E.A., Bauer, B., Fahlke, C., Fricker, G., Iadecola, C., Janigro, D., Leybaert, L., Molnár, Z., O'Donnell, M.E., Povlishock, J.T., Saunders, N.R., Sharp, F., Stanimirovic D., Watts, R.J, Drewes, L.R., 2011. Engaging neuroscience to advance translational research in brain barrier biology. Nat. Rev. Neurosci. 12, 169-182.
Neves, A.R., Queiroz, J.F., Weksler, B., Romero, I.A., Couraud, P.O., Reis, S., 2015. Solid lipid nanoparticles as a vehicle for brain-targeted drug delivery: two new strategies of functionalization with apolipoprotein E. Nanotechnology. 26, 495103.
Ohtsuki, S., Terasaki, T., 2007. Contribution of carrier-mediated transport systems to the blood-brain barrier as a supporting and protecting interface for the brain; importance for CNS drug discovery and development. Pharm. Res. 24, 1745-1758.
Pardridge, W.M., 2012. Drug transport across the blood-brain barrier. J. Cereb. Blood Flow. Metab. 11, 1959-1972.
Pardridge, W.M., 2015a. Blood-brain barrier endogenous transporters as therapeutic targets: a new model for small molecule CNS drug discovery. Expert Opin. Ther. Targets. 19, 1059-1072.

Pardridge, W.M., 2015b. Targeted delivery of protein and gene medicines through the blood-brain barrier. Clin. Pharmacol. Ther. 97, 347–361.
Pardridge, W.M., 2016. CSF, blood-brain barrier, and brain drug delivery. Expert. Opin. Drug. Deliv. 13, 963-975.
Pardridge, W.M., 2017. Delivery of biologics across the blood-brain barrier with molecular trojan horse technology. BioDrugs. 31, 503-519.
Patching, S.G., 2017. Glucose transporters at the blood-brain barrier: function, regulation and gateways for drug delivery. Mol. Neurobiol. 54, 1046-1077.
Patel, T.R., 2014. Nanocarrier-based therapies for CNS tumors. CNS oncology, 3, 115-122.
Perrière, N., Demeuse, P., Garcia, E., Regina, A., Debray, M., Andreux, J.P., Couvreur, P., Scherrmann, J.M., Temsamani, J., Couraud, P.O., Deli, M.A., Roux, F., 2005. Puromycin-based purification of rat brain capillary endothelial cell cultures. Effect on the expression of blood-brain barrier-specific properties. J. Neurochem. 93, 279-289.
Probst, C.E, Zrazhevskiy, P., Bagalkot, V., Gao, X., 2013. Quantum dots as a platform for nanoparticle drug delivery vehicle design. Adv. Drug Deliv. Rev. 65, 703-718.
Rask-Andersen, M., Masuram, S., Fredriksson, R., Schiöth, H.B., 2013. Solute carriers as drug targets: current use, clinical trials and prospective. Mol. Aspects Med. 34, 702-710.
Raucher, D., Dragojevic, S., Ryu, J., 2018. Macromolecular drug carriers for targeted glioblastoma therapy: preclinical studies, challenges, and future perspectives. Front. Oncol. 8, 624.
Reijerkerk, A., Appeldoorn, C.C., Rip, J., de Boer, M., Gaillard, P.J., 2014. Systemic treatment with glutathione PEGylated liposomal methylprednisolone (2B3-201) improves therapeutic efficacy in a model of ocular inflammation. Invest. Ophthalmol. Vis. Sci. 55, 2788-2794.
Reimold, I., Domke, D., Bender, J., Seyfried, C.A., Radunz, H.E., Fricker, G., 2008. Delivery of nanoparticles to the brain detected by fluorescence microscopy. Eur. J. Pharm. Biopharm. 70, 627-632.
Rempe, R., Cramer, S., Qiao, R., Galla, H.J., 2014. Strategies to overcome the barrier: use of nanoparticles as carriers and modulators of barrier properties. Cell Tissue Res. 355, 717-726.
Ribeiro, M.M., Domingues, M.M., Freire, J.M., Santos, N.C., Castanho, M.A., 2012. Translocating the blood-brain barrier using electrostatics. Front. Cell. Neurosci. 11, 6-44.
Rip, J., Chen, L., Hartman, R., van den Heuvel, A., Reijerkerk, A., van Kregten, J., van der Boom, B., Appeldoorn, C., de Boer, M., Maussang, D., de Lange, E.C., Gaillard, P.J., 2014. Glutathione PEGylated liposomes: pharmacokinetics and delivery of cargo across the blood-brain barrier in rats. J. Drug Target. 22, 460-467.
Ross, C., Taylor, M., Fullwood, N., Allsop, D., 2018. Liposome delivery systems for thetreatment of Alzheimer's disease. Int. J. Nanomedicine. 13, 8507-8522.
Rotman, M., Welling, M.M., Bunschoten, A., de Backer, M.E., Rip, J., Nabuurs, R.J., Gaillard, P.J., van Buchem, M.A., van der Maarel, S.M., van der Weerd, L., 2015. Enhanced glutathione PEGylated liposomal brain delivery of an anti-amyloid single domain antibody fragment in a mouse model for Alzheimer's disease. J. Control. Release. 203, 40-50.
Saraiva, C., Praça, C., Ferreira, R., Santos, T., Ferreira, L., Bernardino, L., 2016. Nanoparticle-mediated brain drug delivery: Overcoming blood-brain barrier to treat neurodegenerative diseases. J. Control. Release. 10, 34-47.
Sercombe, L., Veerati, T., Moheimani, F., Wu, S. Y., Sood, A. K., & Hua, S., 2015. Advances and Challenges of Liposome Assisted Drug Delivery. Frontiers in pharmacology, 6, 286.
Shawahna, R., Uchida, Y., Declèves, X., Ohtsuki, S., Yousif, S., Dauchy, S., Jacob, A., Chassoux, F., Daumas-Duport, C., Couraud, P.O., Terasaki, T., Scherrmann, J.M., 2011.

Transcriptomic and quantitative proteomic analysis of transporters and drug metabolizing enzymes in freshly isolated human brain microvessels. Mol. Pharm. 8, 1332-1341.

Shilo, M., Motiei, M., Hana, P., Popovtzer, R., 2014. Transport of nanoparticles through the blood-brain barrier for imaging and therapeutic applications. Nanoscale. 6, 2146-2152.

Singh, A., Satchell, S.C., Neal, C.R., McKenzie, E.A., Tooke, J.E., Mathieson, P.W., 2007. Glomerular endothelial glycocalyx constitutes a barrier to protein permeability. J. Am. Soc. Nephrol. 18, 2885-2893.

Sipos, E., Kurunczi, A., Fehér, A., Penke, Z., Fülöp, L., Kasza, A., Horváth, J., Horvát, S.,Veszelka, S., Balogh, G., Kürti, L., Eros, I., Szabó-Révész, P., Párducz, A., Penke, B., Deli, M.A., 2010. Intranasal delivery of human beta-amyloid peptide in rats: effective brain targeting. Cell. Mol. Neurobiol. 30. 405-413

Spector, R., Johanson, C.E., 2007. Vitamin transport and homeostasis in mammalian brain: focus on Vitamins B and E. J. Neurochem. 103, 425-438.

Spector, R., Mock, D., 1987. Biotin transport through the blood-brain barrier. J. Neurochem. 48, 400-404.

Tóth, A.E., Tóth, A., Walter, F.R., Kiss, L., Veszelka, S., Ózsvári, B., Puskás, L.G., Heimesaat, M.M., Dohgu, S., Kataoka, Y., Rákhely, G., Deli, M.A., 2014. Compounds blocking methylglyoxal-induced protein modification and brain endothelial injury. Arch. Med. Res. 45, 753-764.

Uchida, Y., Ito, K., Ohtsuki, S., Kubo, Y., Suzuki, T., Terasaki, T., 2015. Major involvement of Na(+) -dependent multivitamin transporter (SLC5A6/SMVT) in uptake of biotin and pantothenic acid by human brain capillary endothelial cells. J. Neurochem. 134, 97-112.

Uchida, Y., Ohtsuki, S., Katsukura, Y., Ikeda, C., Suzuki, T., Kamiie, J., Terasaki, T., 2011. Quantitative targeted absolute proteomics of human blood-brain barrier transporters and receptors. J Neurochem. 117, 333-345.

Ujhelyi, Z., Fenyvesi, F., Váradi, J., Fehér, P., Kiss, T., Veszelka, S., Deli, M., Vecsernyés, M., Bácskay, I., 2012. Evaluation of cytotoxicity of surfactants used in self-micro emulsifying drug delivery systems and their effects on paracellular transport in Caco-2 cell monolayer. Eur. J. Pharm. Sci. 47, 564-573.

Ulbrich, K., Hekmatara, T., Herbert, E., Kreuter, J., 2009. Transferrin- and transferrin-receptor-antibody-modified nanoparticles enable drug delivery across the blood-brain barrier (BBB). Eur. J. Pharm. Biopharm. 71, 251-256.

Ulbrich, K., Knobloch, T., Kreuter, J., 2011. Targeting the insulin receptor: nanoparticles for drug delivery across the blood-brain barrier (BBB). J. Drug Target. 19, 125-132.

Uyama, O., Okamura, N., Yanase, M., Narita, M., Kawabata, K., Sugita, M., 1988. Quantitative evaluation of vascular permeability in the gerbil brain after transient ischemia using Evans blue fluorescence. J. Cereb. Blood Flow. Metab. 8, 282-284.

Veszelka, S., Bocsik, A., Walter, F., Hantosi, D., Deli, M.A., 2015. Blood-brain-barrier co-culture models to study nanoparticle penetration: focus on co-culture systems. Acta Biol. 59,157-168.

Veszelka, S., Pásztói, M., Farkas, A.E., Krizbai, I., Ngo, T.K., Niwa, M., Ábrahám, CS., Deli, M.A., 2007. Pentosan polysulfate protects brain endothelial cells against bacterial lipopolysaccharide-induced damages. Neurochem. Int. 50, 219-228.

Veszelka, S., Urbányi, Z., Pázmány, T., Németh, L., Obál, I., Dung, N.T., Abrahám, C.S., Szabó, G., Deli, M.A., 2003. Human serum amyloid P component attenuates the bacterial lipopolysaccharide-induced increase in blood-brain barrier permeability in mice. Neurosci. Lett. 352, 57-60.

Vieira, D.B., Gamarra, L.F., 2016. Getting into the brain: liposome-based strategies for effective drug delivery across the blood-brain barrier. Int. J. Nanomedicine. 11, 5381-5414.

Vorbrodt, A.W., 1989. Ultracytochemical characterization of anionic sites in the wall of brain capillaries. J. Neurocytol. 3, 359-368.
Vyas, A., Jain, A., Hurkat, P., Jain, A., Jain, S.K., 2015. Targeting of AIDS related encephalopathy using phenylalanine anchored lipidic nanocarrier. Colloids Surf. B. Biointerfaces. 131, 155-161.
Walter, F.R., Valkai, S., Kincses, A., Petneházi, A., Czeller, T., Veszelka, S., Ormos, P., Deli, M.A., Dér, A., 2016. A versatile lab-on-a-chip tool for modeling biological barriers. Sens. Actuators B. Chem. 222, 1209-1219.
Walter, F.R., Veszelka, S., Pásztói, M., Péterfi, Z.A., Tóth, A., Rákhely, G., Cervenak, L., Ábrahám, C.S., Deli, M.A., 2015. Tesmilifene modifies brain endothelial functions and opens the blood-brain/blood-glioma barrier. J. Neurochem. 134, 1040-1054.
Weksler, B., Romero, I.A., Couraud, P.O., 2013. The hCMEC/D3 cell line as a model of the human blood brain barrier. Fluids Barriers CNS. 10,16.
Wohlfart, S., Gelperina, S., Kreuter, J., 2012. Transport of drugs across the blood-brain barrier by nanoparticles. J. Control. Release. 161, 264-273.
Yeh, Y.C., Creran, B., Rotello, V.M., 2012. Gold nanoparticles: preparation, properties, and applications in bionanotechnology. Nanoscale. 4, 1871-1880.
Zheng, M., Ruan, S., Liu, S., Sun, T., Qu, D., Zhao, H., Xie, Z., Gao, H., Jing, X., Sun, Z., 2015. Self-targeting fluorescent carbon dots for diagnosis of brain cancer cells. ACS Nano. 9, 11455-11461.
Zhou, Y., Peng, Z., Seven, E.S., Leblanc, R.M., 2018. Crossing the blood-brain barrier with nanoparticles. J. Control. Release. 28, 290-303.
Zong, T., Mei, L., Gao, H., Shi, K., Chen, J., Wang, Y., Zhang, Q., Yang, Y., He, Q., 2014. Enhanced glioma targeting and penetration by dual-targeting liposome co-modified with T7 and TAT. J. Pharm. Sci. 103, 3891-3901.

8. ACKNOWLEDGEMENTS

I am grateful to my supervisors Prof. Mária Deli and Dr. Szilvia Veszelka for their scientific guidance, encouragement and support throughout my Ph.D. studies.

I thank Prof. Pál Ormos and Prof. Ferenc Nagy, the director generals of the Biological Research Centre, Prof. László Zimányi, director of the Institute of Biophysics, and Dr. László Siklós, head of the Molecular Neurobiology Research Unit for their support.

I am indebted to our cooperating partners Dr. Zoltán Kupihár and Dr. Zsolt Bozsó for the synthesis of targeting ligands, Dr. Ana-Maria Pilbat for the membrane fluidization experiments; Dr. Zoltán Kóta for the fluorometric measurements; Dr Lóránd Kelemen for the scanning electronmicroscopy study; Dr. Lívia Fülöp and Dr. László Siklós for the transmission electronmicroscopy studies; Dr. Mária Csete and Dr. Áron Sipos for the atomic force microscopy study; Dr. Gábor Galbács and Albert Kéri for the determination of lanthanum content of niosomes and Dr. Petra Hülper for the *in vivo* imaging experiments.

I am grateful to my previous and present laboratory colleagues, Dr. Petra Sántha, Dr. Lóránd Kiss, Dr. Zsófia Hoyk, Dr. Fruzsina Walter, Dr. Alexandra Bocsik, Dr. András Harazin, Ilona Gróf, Ana Raquel Pato Santa Maria, Lilla Barna, Beáta Barabási, Judit Vigh, Adrián Klepe, Anikó Szecskó for excellent teamwork and sharing the excitement of research and discovery.

I am very thankful to Gergő Porkoláb for his kind help in my experimental work.

I also thank the members of the Institute of Biophysics for their help and friendship.

Finally, I am especially thankful to my parents, my grandparents, my brother and my friends for their love and untiring support during my studies.

The research was supported by the Hungarian Scientific Research Fund (OTKA/NKFIH 105622), by the National Research, Development and Innovation Office (GINOP-2.2.1-15-2016-00007, GINOP-2.3.2-15-2016-00060 and EFOP-3.6.1-162016-00008).

APPENDIX

PUBLICATION I.

Send Orders for Reprints to reprints@benthamscience.ae

Current Pharmaceutical Design, 2017, *23*, 1-8

RESEARCH ARTICLE

Biotin and Glutathione Targeting of Solid Nanoparticles to Cross Human Brain Endothelial Cells

Szilvia Veszelka[a], Mária Mészáros[a], Lóránd Kiss[a,#], Zoltán Kóta[a], Tibor Páli[a], Zsófia Hoyk[a], Zsolt Bozsó[b], Lívia Fülöp[b], András Tóth[a,c], Gábor Rákhely[a,c] and Mária A. Deli[a,*]

[a]*Institute of Biophysics, Biological Research Centre of the Hungarian Academy of Sciences, Temesvári krt. 62, H-6726 Szeged, Hungary;* [b]*Department of Medical Chemistry, University of Szeged, Dóm tér 8, H-6720 Szeged, Hungary;* [c]*Department of Biotechnology, Faculty of Science and Informatics, University of Szeged, Középfasor 52, H-6726 Szeged, Hungary*

ARTICLE HISTORY

Received: March 31, 2016
Accepted: July 12, 2016

DOI:
10.2174/1381612823666170727144450

Abstract: ***Background*:** The blood-brain barrier restricts drug penetration to the central nervous system. Targeted nanocarriers are new potential tools to increase the brain entry of drugs. Ligands of endogenous transporters of the blood-brain barrier can be used as targeting vectors for brain delivery of nanoparticles.

***Objective*:** We tested biotin-labeled solid nanoparticles for the first time and compared to biotinylated glutathione-labeled nanoparticles in brain endothelial cells.

***Method*:** Neutravidin coated fluorescent polystyrene nanoparticles were derivatized with biotin and biotinylated glutathione. As a human *in vitro* blood-brain barrier model hCMEC/D3 brain endothelial cells were used. Cell viability by MTT test, uptake and transfer of the nanoparticles across the endothelial monolayers were measured. The uptake of the nanoparticles was visualized by confocal microscopy.

***Results*:** The tested nanoparticles caused no change in cell viability. The uptake of biotin- and glutathione-labeled nanoparticles by brain endothelial cells was time-dependent and significantly higher compared to non-labeled nanoparticles. The penetration of the glutathione-labeled nanoparticles across the endothelial monolayer was higher than the biotin-targeted ones. Biotin- and glutathione-targeted nanoparticles were visualized in hCMEC/D3 cells. We verified that hCMEC/D3 express mRNA for sodium-dependent multivitamin transporter (SMVT/SLC5A6) responsible for the blood-brain barrier transport of biotin.

***Conclusion*:** Biotin as a ligand increased the uptake and the transfer of nanoparticles across brain endothelial cells. Biotinylated glutathione could further increase nanoparticle permeability through endothelial monolayers supporting its use as a brain targeting vector.

Keywords: Biotin, blood-brain barrier, brain endothelial cell, glutathione, solute carriers, solid nanocarriers, targeted nanoparticle.

1. INTRODUCTION

Pharmaceutical treatment of most disorders of the central nervous system (CNS), like neurodegenerative diseases, stroke or brain tumors, is far from satisfactory due to the poor penetration of therapeutic drugs to the brain [1]. The blood-brain barrier (BBB) is a major obstacle to prevent potential neuropharmaceuticals, especially new biopharmacons, nucleic acids, peptide or protein drugs, to reach their targets in the CNS [2]. The barrier is formed by brain endothelial cells lining the cerebral capillaries, and plays an important role in the homeostatic regulation of the brain microenvironment necessary for the stable and co-ordinated activity of neurons [3]. The major mechanisms at the level of the BBB to limit drug transport are the complex intercellular tight junctions (TJs) between brain endothelial cells restricting the paracellular permeability, the low level of non-specific vesicular transendothelial transport, and efflux transporters which deliver metabolites from brain to blood and prevent the entry of xenobiotics and drugs to the CNS [3, 4]. The restricted paracellular and transendothelial transport pathways result in the low CNS entry of hydrophilic drugs, while the active efflux transporters of brain endothelial cells limit the brain penetration of lipophilic drugs. There is a huge research effort to develop drug delivery systems for the CNS.

*Address correspondence to this author at the Institute of Biophysics, Biological Research Centre of the Hungarian Academy of Sciences, Temesvári krt. 62, H-6726 Szeged, Hungary; Tel: +36 62 599 602; Fax: +36 62 433 133; E-mail: deli.maria@brc.mta.hu

Present address: [#]Department of Pathophysiology, University of Szeged, Semmelweis u. 1, H-6701 Szeged, Hungary

In the last two decades the potential of nanoparticles (NPs) as drug carriers including vesicular and solid NPs is increasingly investigated for drug delivery across the BBB [5, 6]. The most successful approaches target specifically the endogenous transport systems at the BBB. While the receptor-mediated transport systems of brain endothelial cells have been investigated as a way of drug delivery across the BBB for several decades [2] other physiological pathways, especially the carrier systems of the BBB have been studied only recently for CNS delivery [7]. Carrier-mediated transport at the BBB is saturable, bi-directional and supplies the CNS with nutrients such as hexoses, amino acids, monocarboxylic acids, vitamins, nucleosides, purine and pyrimidine bases, fatty acids, ions, organic anions and organic cations [8]. About 40 members of the solute carrier (SLC) family were identified in brain microvessels by serial analysis of gene expression [9]. SLCs have been neglected in biomedical research despite their huge number and their potential as drug and drug delivery targets [10].

In contrast to NPs targeted by antibodies or peptides for CNS delivery, there are only few papers describing NPs labeled with ligands of nutrient transporters present at the BBB. Gold NPs covalently labeled with glucose, a ligand of hexose transporters was transferred better than unlabeled NPs across hCMEC/D3 human brain endothelial cell monolayers [11], a human *in vitro* BBB model [12, 13]. Although the paracellular tightness of hCMEC/D3 cell line does not make it a suitable BBB model for small drug screening [13], it is widely used to study the penetration of NPs, which is a transcellular process [12]. Glucose analog-targeted vesicular NPs were used successfully to deliver vasoactive intestinal

1381-6128/17 $58.00+.00

peptide to brain in mice [14]. Phenylalanine, a ligand of the large amino acid transporter-1 (LAT-1, SLC7A5), used as a vector to target solid lipid NPs increased the transfer of the anti-HIV agent efavirenz across a BBB model *in vitro* and the drug's penetration to the brain of rats [15]. A delivery system based on dendrigraft containing doxorubicin and targeted by a choline-derivate with high affinity to choline transporter (SLC44A1) was more cytotoxic to glioma cells both *in vitro* and *in vivo* than non-targeted NPs or doxorubicin alone [16].

Glutathione (GSH) is a promising new ligand of an endogenous BBB transporter for CNS drug delivery. This tripeptide with antioxidant properties has a central role in the detoxification of intracellular metabolites. GSH is actively transported across the BBB [17], but the molecular mechanism(s) and the BBB transporter(s) are not known. Based on these original observations Gaillard *et al.* developed a BBB delivery platform [18, 19]. Pegylated liposomes targeted with GSH enhance the delivery of doxorubicin cargo across hCMEC/D3 brain endothelial cells and to brain tumors in mice [20]. Further studies confirmed the improved CNS delivery by glutathione targeted NPs of doxorubicin [21] and the opioid peptide DAMGO [22] in animal models. GSH is the only BBB targeting ligand, that is part of a brain delivery platform successfully completing phase I/IIa clinical trial [18].

Biotin (vitamin B7) is a ligand of the Na^+-dependent multivitamin transporter (SMVT/SLC5A6) which is responsible for the CNS transport of this water soluble vitamin across the BBB [8, 23]. Biotin has long been used for ligation techniques, imaging and diagnostics because of the strong interaction between biotin and avidin. Biotin-avidin technology has a potential to be applied for targeted drug therapy of tumors [24]. However, until now biotin was not tested as a potential targeting ligand of NPs to cross brain endothelial cells.

The aim of our study was to investigate biotin as a targeting ligand for solid fluorescent NPs as a simplified test system in hCMEC/D3 brain endothelial cells, an *in vitro* BBB model. We compared the efficacy of biotin targeting to glutathione-labeled NPs as a reference ligand for CNS drug delivery via targeting endogenous BBB transporter(s). In the present work unlabeled, biotin- and GSH-targeted NPs were prepared and characterized, and tested for cell viability, uptake and permeability in cultured brain endothelial cells.

2. MATERIALS AND METHODS

2.1. Materials

All reagents were purchased from Sigma-Aldrich Kft. Hungary (part of Merck Life Science), except for those specifically mentioned.

2.2. Methods

2.2.1. Synthesis of Biotinyl-6-aminohexanoyl-lysyl-glutathione

The *N*-terminal amino group of glutathione is positively charged at physiological pH. Acylation of this amino group with biotin would diminish this positive charge. To avoid the change of the overall charge of the molecule a lysine residue was built into the peptide. A 6-aminohexanoic acid spacer was also incorporated between the lysyl-glutathione and the biotin. Biotinyl-6-Ahx-Lys-γGlu-Cys-Gly-OH peptide was synthesized on Fmoc-Gly-Wang resin in 0.25 mmolar scale. Fmoc group was removed by treating the resin with 20% piperidine in DMF first for 5 min then with a new portion of the above mentioned solution for 20 min. All Fmoc protected amino acids and biotin were coupled as follows: 1 mmole of the amino acid was activated with DCC/HOBt (1 mmole each) in DMF/DCM (1:1, v/v). The coupling time was 2 hours. The reaction was monitored with qualitative ninhydrin test. If the test was positive, the coupling was repeated using HATU/DIEA activation of the amino acid. The peptide was cleaved from the resin by treating the peptide-resin with a mixture containing TFA (90 v/v%), TIS (2 v/v%), DTT (4 m/v%) and water (4 v/v%) for 15 min at 0 ºC and for 1 hour 45 min at room temperature. The peptide was then precipitated with cold diethyl ether, filtered, washed with diethyl ether, dissolved and lyophilized. The product was analyzed and purified by HPLC. Analytical analysis was done on a Hewlett-Packard Agilent 1100 Series HPLC apparatus using a Luna C18 column (100 Å, 5 µm, 250×4.60 mm, Phenomenex). Preparative chromatography was done on a Shimadzu HPLC apparatus equipped with a Luna C18 column (100 Å, 15 µm, 250×21.2 mm, Phenomenex). As eluent A and eluent B 0.1 % TFA in d.d. water (Solvent A) and 80% ACN, 0.1% TFA in distilled water (Solvent B) was used, respectively.

2.2.2. Derivatization and Characterization of Nanoparticles

Neutravidin labeled 40 nm polystyrene red fluorescent nanoparticles (TransFluoSpheres Fluorescent Microspheres, T8860, Thermo Fisher Scientific Inc., Waltham, MA USA) were used for the study. The nanoparticle suspension contained 1% solid of 7.8 nmoles/mg bearing 8.23 mmole neutravidin functionality, the density of polystyrene was 1.055 g/cm^3 in buffer (50 mM sodium phosphate, 50 mM NaCl, pH 7.5, 0.02% Tween 20, 5 mM azide). To label the nanoparticles 100 µL of suspension was incubated with 30 µL distilled water containing 3 fold molar excess of biotinyl-6-aminohexanoyl-lysyl-glutathione or biotin for 2 hours at room temperature. The different groups of nanoparticles were prepared from different batches of TransFluoSpheres. The control, non-labeled solid nanoparticles (SNP) and the derivatized biotin-labeled (SNP-B) and biotinylated glutathione-labeled (SNP-B-GSH) nanoparticles were stored at 4 ºC until the experiments (Fig. **1**). The nanoparticles were characterized for particle size and zeta potential using dynamic light scattering (Malvern Zetasizer Nano ZS, Worcestershire, UK). Before measurements, the SNPs were diluted and the final concentrations were 0.15 mg/mL in phosphate buffered saline (PBS). The mean particle size and mean zeta potential values were calculated from three measurements per sample.

2.2.3. Scanning Electron Microscopy

The morphology of nanoparticles was visualized by scanning electron microscopy (SEM; JEOL, JSM-7100F-LV, Akishima, Tokyo, Japan). Before SEM observation, a droplet of nanoparticles was diluted to 10^5 and 1 µL of the solution was pipeted onto a clean mica surface and then air-dried. After sputtering 8 nm gold on the sample, the nanoparticles were imaged in high vacuum mode at 5 kV.

2.2.4. Cell Culture

The human brain microvascular endothelial cell line hCMEC/D3 [12] was grown in MCDB 131 medium (Pan Biotech) supplemented with FBS (5%), GlutaMAX (100×, Life Technologies, USA), Chemically Defined Lipid Concentrate (100×, Life Technologies, USA), ascorbic acid (10 µg/mL), hydrocortisone (550 nM), heparin (100 µg/mL), bovine basic fibroblast growth factor (1 ng/mL, Roche, Switzerland), insulin (2.5 µg/mL), transferrin (2.5 µg/mL), sodium selenite (2.5 ng/mL) and gentamicin (50 µg/mL). hCMEC/D3 cells (passage number ≤ 35) were cultured for 3-5 days until full confluency and received 10 mM lithium chloride (Merck, USA) 24 hours before experiments to induce BBB properties [25, 12].

2.2.5. MTT Toxicity Assay

To test the viability and metabolic activity of brain endothelial cells after treatment with SNPs cellular reduction of the yellow 3-(4,5-dimethylthiazol-2-yl)-2,5-diphenyltetrazolium bromide (MTT) dye to formazan crystals was used [26]. Confluent cultures of brain endothelial cells in 96-well plates (Orange Scientific, Braine-l'Alleud, Belgium) were treated with SNPs diluted in culture medium in the concentration range of 0.01–1 mg/mL for 24 hours. Triton X-100 detergent (1 mg/mL) was used as a reference substance to determine the 100% cellular toxicity. After treatment

MTT solution (0.5 mg/ mL) was added to the wells for 3 hours at 37°C. Formazan produced by living cells was dissolved in dimethyl sulfoxide. Absorbance was detected by a multiwell plate reader at 570 nm (Fluostar Optima, BMG Labtechnologies, Ortenberg, Germany). Cell viability and metabolic activity are reflected by the MTT dye conversion and was calculated as the percentage of dye reduction by culture medium treated (control) cells.

2.2.6. Measurement of the Uptake of SNPs in Brain Endothelial Cells

Brain endothelial cell were seeded in 24-well plates (Corning Costar) at the density of 2×10^4 cells/well. After 3 days the confluent monolayers were incubated with 150 µg/mL SNP, SNP-B or SNP-B-GSH for 4 or 8 hours at 37 ºC in a CO_2 incubator. After incubation the cells were washed three times with ice cold PBS and lysed in 500 µL/well Triton X-100 detergent (10 mg/mL). To quantify the uptake of SNPs the fluorescence of cell lysates was measured with a spectrofluorometer (Horiba Jobin Yvon Fluorolog 3, Edison New Jersey, USA) at 488 nm excitation and 605 nm emission wavelengths.

To visualize the cellular uptake of the fluorescent particles brain endothelial cells were grown on collagen coated glass cover slips (VWR, USA) and treated with 150 µg/ml SNP, SNP-B or SNP-B-GSH for 24 hours. Cells were fixed with 4% paraformaldehyde in PBS for 30 min, washed three times with PBS then cell nuclei were stained with bis-benzimide (Hoechst dye 33342) for 10 min. Samples were mounted with Fluoromount-G (Southern Biotech, Birmingham, AL, USA), and examined with a confocal laser scanning microscope (Olympus Fluoview FV1000, Olympus Life Science Europa GmbH, Hamburg, Germany).

2.2.7. Permeability Measurement

For permeability studies brain endothelial cells were seeded onto collagen coated 12-well tissue culture inserts (Transwell clear, polyester membrane, 0.4 µm pore size, Corning Costar, USA) and cultured for 5 days. Culture medium was changed and resistance checked every second day. The integrity of the monolayers was checked by Evans blue labeled bovine serum albumin (Mw: 67 kDa) marker molecule. The cells were treated with 150 µg/mL SNP, SNP-B or SNP-B-GSH diluted in culture medium in the upper compartments (0.5 mL) for 8 hours. After incubation samples were collected from the lower compartments (1.5 mL) and measured with spectrofluorometer Horiba Jobin Yvon Fluorolog 3 at 488 nm excitation and 605 nm emission wavelengths for the SNPs and with Fluostar Optima at 584 nm excitation and 680 nm emission wavelengths for Evans blue-albumin. The apparent permeability coefficients (P_{app}, cm/s) were calculated as described previously [27] by the following equation:

$$P_{app}(\text{cm/s}) = \frac{\Delta[C]_A \times V_A}{A \times [C]_D \times \Delta t}$$

Briefly, P_{app} was calculated from the concentration difference of the nanoparticles in the lower or acceptor compartment ($\Delta[C]_A$) after 4 hours and $[C]_D$ is the concentration in the donor (upper) compartments at 0 hour, and V_A is the volume of the acceptor compartment (1.5 mL), and A is the surface area available for permeability (1.1 cm^2).

2.2.8. RNA Isolation and Quality Control

Rat brain microvessels were isolated as described in our previous article [28]. Primary brain endothelial cells (isolated and cultured according to the method described in our previous studies [28, 29]) and hCMEC/D3 cells were cultured for 5 days in 10 cm dishes. After reaching confluency cells were scraped and collected by centrifugation. Microvessel and cell pellets were used for total RNA isolation using RNAqueous-4PCR Kit (Ambion, Life Technologies, Austin, TX, USA) with DNase1 (RNase-free) treatment according to the manufacturer's instructions. The concentrations and purity of the DNase-treated RNA samples was assessed by a NanoDrop ND-1000 spectrophotometer (NanoDrop Technologies, Rockland, DE). The integrity of the isolated RNA was checked by Bioanalyzer 2100 (Agilent Technologies, Santa Clara, CA). The RNA integrity number (RIN) was 9.2-10 in the case of all studied RNA samples.

2.2.9. Quantitative Real-Time Polimerase Chain Reaction and Data Analysis

Quantitative real-time PCR (RT-PCR) and data analysis were performed as described in our previous study [30]. The cDNA synthesis was performed on 1 µg total RNA samples by High Capacity cDNA Reverse Transcription Kit (Life Technologies) using random hexanucleotides primers and MultiScribe Reverse Transcriptase in the presence of RNase inhibitor according to the manufacturer's standard protocols. The expression of the SMVT/SLC5A6 vitamin transporter gene was analyzed by quantitative PCR using TaqMan Low Density Array 384-well microfluidic cards preloaded with inventoried TaqMan Gene Expression Assays (for hCMEC/D3 human brain cells: Hs00221573_m1, for rat brain cells: Rn00590633_m1; Life Technologies). RT PCRs were performed by ABI TaqMan Universal Master Mix (Life Technologies) using the ABI Prism 7900 system (Applied Biosystems, Life Technologies). RT-PCR data were analyzed using the ABI SDS 2.0 software (Applied Biosystems, Life Technologies). In all samples the expression of genes was normalized to 18S rRNA, which was used as an endogenous control (ΔCt = Ctgene - Ct18S rRNA). Expression values reflecting the activity of studied genes were determined based on the normalized expression of genes calculated with 2-ΔCt formula which were correlated to the lowest normalized expression measured by the applied RT-PCR method. For quantification of relative expression level of genes of interest the normalized expression data were analyzed using the comparative ΔΔCt method.

2.2.10. Statistical Analysis

Data are presented as means ± SEM or SD. Values were compared using one-way or two-way analysis of variance following Dunnett or Bonferroni multiple comparison posttests (GraphPad-Prism 5.0; GraphPad Software, USA). Changes were considered statistically significant at $P < 0.05$. All experiments were repeated at least two times, the number of parallel samples was 4-8.

3. RESULTS

Table **1** summarizes the main physicochemical characteristics of the untargeted and targeted SNPs (for schematic drawing see Fig. **1**).

Table 1. Characterization of the non-targeted and targeted solid nanoparticles.

Nanoparticle	Size (nm)	Polydispersity index	Zeta potential (mV)
SNP	93 ± 0.59	0.131 ± 0.02	-14 ± 0.87
SNP-B	118.1 ± 2.9	0.251 ± 0.001	-23.1 ± 0.62
SNP-B-GSH	120.5 ± 2.86	0.261 ± 0.01	-23.8 ± 1.33

Values presented are means ± SD. SNP, non-targeted solid nanoparticles; SNP-B, biotin-targeted solid nanoparticles; SNP-B-GSH, glutathione-targeted solid nanoparticles.

The commercially available solid fluorescent particles (nominal size of 40 nm) were already functionalized with neutravidin which enlarged the SNPs. These neutravidin-coated particles were labeled with biotin and glutathione which further increased their size. All SNPs had low polydispersity index, indicating a relatively narrow size distribution. The average zeta potential for both targeted particles was very similar. The charge of the non-labeled SNP was less negative. The morphology of the nanoparticles was observed by

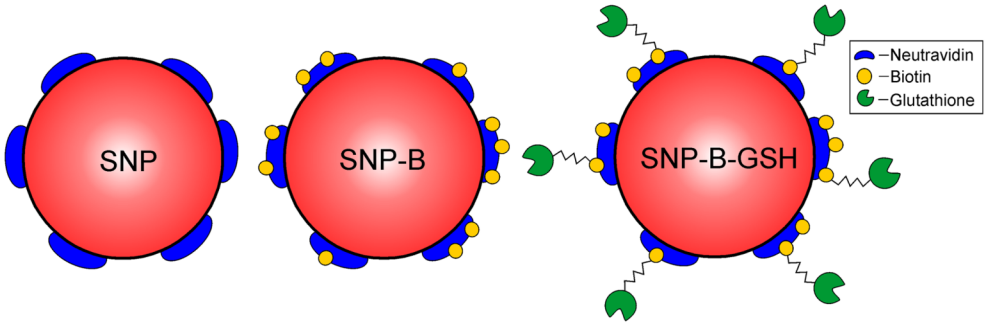

Fig. (1). Schematic drawing of non-targeted (SNP), biotin- (SNP-B) and glutathione-labeled (SNP-B-GSH) solid nanoparticles.

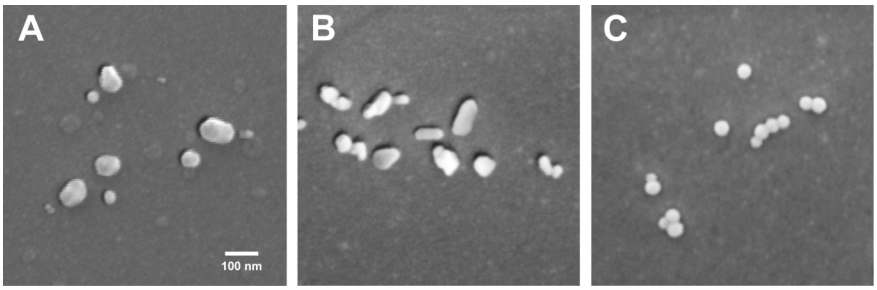

Fig. (2). Scanning electron microscopy images of non-targeted (A), biotin-targeted (B), and glutathione-targeted (C) solid nanoparticles. Bar: 100 nm.

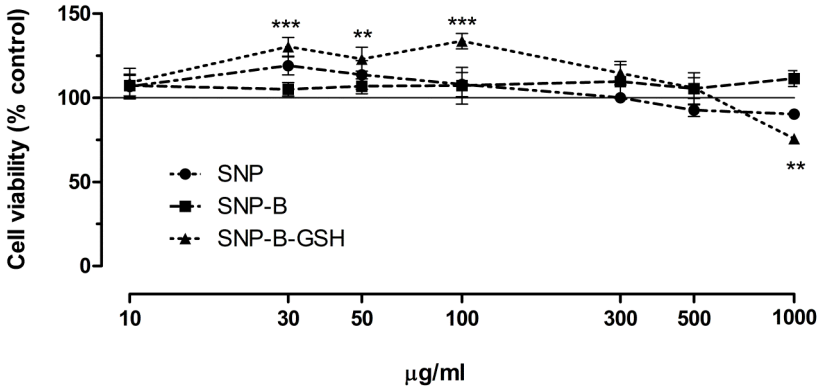

Fig. (3). The effect of non-targeted (SNP), biotin-targeted (SNP-B), and glutathione-targeted (SNP-B-GSH) solid nanoparticles on the viability of brain endothelial cells (24 hours). Values presented are means ± SEM. Statistical analysis: one-way analysis of variance followed by Dunnett's posttest, ** $P < 0.01$; *** $P < 0.001$ compared to control. n = 4-8. X-axis: log-10 scale.

SEM and shown on Fig. **2**. The particles had mostly spherical shapes, but some SNPs were elongated. The size of the SNPs were all in the same range, and corresponds well to data measured by dynamic light scattering. No aggregation was visible.

3.1. Effect of SNPs on the Cell Viability of Brain Endothelial Cells

Incubation of the brain endothelial monolayers with SNP and SNP-B in the 10-1000 µg/mL concentration range for 24 hours had no effect on cell viability assessed by MTT dye conversion (Fig. **3**). As a comparison, the reference substance Triton X-100 detergent decreased the cell viability below 10% of the control values. SNP-B-GSH (30-100 µg/mL) increased the metabolic activity of cells, while the highest concentration (1000 µg/mL) caused a reduction in viability (Fig. **3**). For further experiments we selected the 150 µg/mL concentration for all three SNPs, which can be considered as non-toxic.

3.2. Uptake of SNPs in Brain Endothelial Cells

The uptake of SNPs in endothelial cells was tested at two time points (Fig. **4**). In the design of our study we determined the time points for the uptake experiments based on the results of Gaillard *et al.* obtained on nanoparticles labeled with GSH, our reference ligand [31, 19, 20]. To be able to compare our data to these previous observations we selected 4 and 8 hours incubations. After 4 hours of incubation no significant difference between the uptakes of three SNPs in brain endothelial cells could be measured, although an increasing trend was seen in case of targeted SNPs. After 8-hour incubation the uptake of all tested nanoparticles was significantly higher compared to the 4-hour group. Importantly the uptake of the biotin- and glutathione-targeted SNPs was significantly increased; it was two times higher than the uptake of the non-targeted particle.

The uptake of the fluorescent nanoparticles could be visualized in brain endothelial cells by confocal microscopy (Fig. **5**). Red

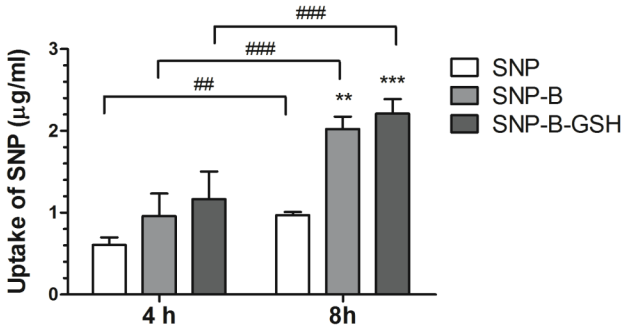

Fig. (4). The uptake of non-targeted (SNP), biotin-labeled (SNP-B) and glutathione-labeled (SNP-B-GSH) solid nanoparticles in brain endothelial cells after 4 or 8 hours incubation. The concentration of SNPs is 150 µg/mL in each group. Values presented are means ± SEM. Statistical analysis: two-way analysis of variance followed by Bonferroni posttest, where $^{**}P < 0.01$; $^{***}P < 0.001$, compared to SNP treated group, $^{\#\#}P < 0.01$; $^{\#\#\#}P < 0.001$, compared to the 4 hour-incubation group; n = 4–6.

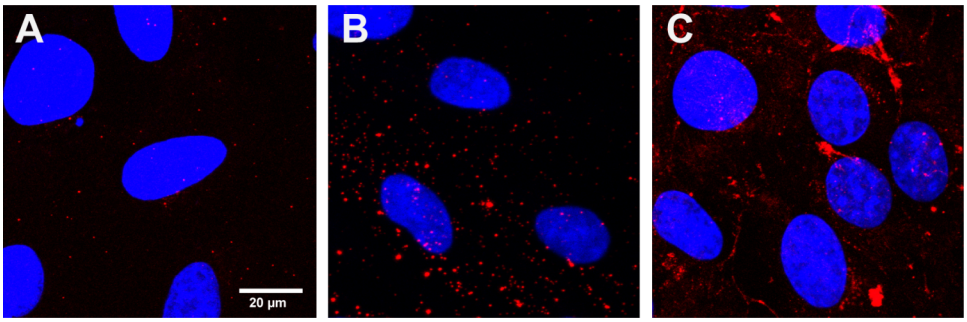

Fig. (5). Confocal microscopy images of cultured human brain endothelial cells incubated with non-labeled (A), biotin-labeled (B), and glutathione-labeled (C) solid nanoparticles (red) for 8 hours at 37 ºC. The concentration of SNPs is 150 µg/mL in each group. Cell nuclei were stained with bis-benzimide (blue). Bar: 20 µm.

fluorescent dots can be seen in the cytoplasm of the cells treated with SNPs. More fluorescent particles were seen in cells incubated with glutathione-labeled SNPs indicating better uptake of these nanoparticles as compared to the non-targeted SNPs.

3.3. Penetration of SNPs Across Brain Endothelial Monolayers

The permeability of hCMEC/D3 brain endothelial cell monolayers for Evans blue-albumin was 1.6 ± 0.3 $\times 10^{-6}$ cm/s which was in the same range as in our previous study [32] and reflects a suitable barrier for testing SNPs. All SNPs crossed the brain endothelial layers in the permeability tests but at different extent (Fig. **6**). After 8-hour incubation the P_{app} of biotin targeted SNP was 2.8 fold higher than that of the non-targeted SNP. The penetration of the GSH targeted nanoparticles was the highest, a significant, 5.8 fold increase was measured as compared to the unlabeled SNP group.

3.4. Expression of SMVT/SLC5A6 mRNA in Brain Microvessels and Cultured Brain Endothelial Cells

The expression level of SMVT/SLC5A6 vitamin transporter gene mRNA was expressed in isolated rat brain microvessels, and both in hCMEC/D3 human brain endothelial cell line and primary rat brain endothelial cells (Fig. **7**). No statistically significant change was found in the mRNA expression level between the groups (one-way ANOVA and Bonferroni posttest).

4. DISCUSSION

Although drug delivery systems to cross the BBB are an intensely researched area there are no targeted nanoparticles in the human therapy yet to deliver therapeutics to the brain in a controlled and non-invasive manner. Specific targeting can be achieved

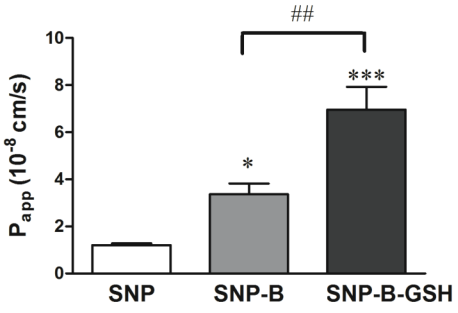

Fig. (6). Permeability changes of brain endothelial monolayers after SNP treatments (150 µg/mL, 8 h). Values presented are means ± SEM. Statistical analysis: one-way analysis of variance followed by Bonferroni posttest. $^{*}P < 0.05$, $^{***}P < 0.001$, compared to non-labeled SNP treated group; $^{\#\#}P < 0.01$, compared to biotin-labeled SNP treated group, n = 6.

through exploiting the physiological transport pathways of the BBB including the endogenous nutrient transporters of brain endothelium [2, 7]. Despite the abundance of carrier mediated transporters at the BBB this physiological pathway is still not fully exploited for drug delivery.

Biotin is a potential BBB targeting ligand, since it has a highly expressed carrier, SLC5A6, at the human BBB including hCMEC/D3 brain endothelial cells [23, 30]. We have verified the presence of SLC5A6 mRNA in hCMEC/D3 brain endothelial cells, which showed an expression level similar to isolated brain

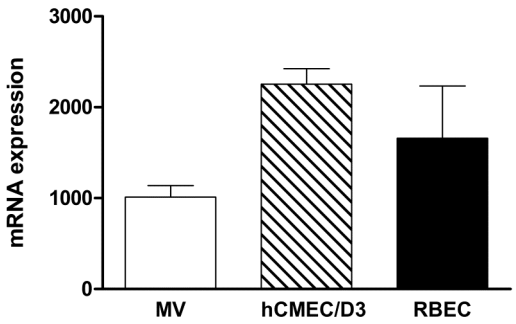

Fig. (7). The expression level of SMVT/SLC5A6 vitamin transporter gene mRNA in isolated rat brain microvessels (MV), hCMEC/D3 human brain endothelial cell line and primary rat brain endothelial cells (RBEC).

microvessels and cultured primary brain endothelial cells. Biotin is a cofactor for several carboxylase enzymes and a cell growth promoter. It cannot be synthesized endogenously in the brain therefore it is supplied from the blood across the BBB. The brain concentration of biotin is about 50-fold higher than that in the plasma [33].

Biotin technology based on the exceptionally strong binding between biotin and avidin has long been used in basic research for immunohistochemistry and molecular biology. Recently biotin-avidin technology has been applied for drug targeting to tumors [24]. In several studies nanoparticles are biotinylated to easily detect them on tissue slices with streptavidin-FITC [34]. Biotinylation of drugs is also used to bind them to avidin-functionalized particles [35]. However, none of the studies used biotin as a ligand for BBB targeting.

We prepared and characterized biotin- and glutathione-labeled SNPs from neutravidin-coated commercially available red fluorescent polystyrene particles. Labeling with biotin and biotin-glutathione increased the particle size, in accordance with literature data on biotinylated albumin NPs [34]. The average size and surface charge of the targeted SNPs were similar measured by dynamic light scattering. The heterogeneity seen by scanning electron microscopy may be related to the different batches of SNPs used for labeling. The size of NPs related to their cellular uptake and biodistribution is widely studied. In general, particles with a size below 100 nm can be taken up by all cells by endocytosis and are considered as high risk NPs from nanotoxicology point of view, especially if they are non-biodegradable [36]. These small NPs are non-specifically taken up by the liver, lungs and kidneys. This is the reason why most NPs developed for possible therapeutic use has a size in the range of 100-200 nm. The glutathione targeted NPs used by Gaillard and his colleagues were also in this range, e.g. 108 nm, [31]; 95 nm, [20]. The size of SNPs used in this study fell also in this range. NPs larger, than 200 nm do not enter brain tissue [37]. In agreement with *in vivo* findings NPs with 400 nm size did not cross a culture BBB model [38].

We are the first to demonstrate, that biotin-labeling increases the uptake and transfer of SNPs in human brain endothelial cells as compared to unlabeled particles. This finding is in agreement with active transport of biotin at the BBB *in vivo* [39] and in hCMEC/D3 brain endothelial cell cultures [23]. An experimental study indicates that biotinylated NPs can enter the brain [34] and this targeting concept may work *in vivo*, too. Intravenously administered biotinylated albumin NPs could be detected in several brain regions of rats with experimental autoimmune encephalomyelitis using *post mortem* streptavidin-FITC labeling [34]. However, this observation may provide indirect support only, because the aim of this study was the visualization of albumin NPs in the CNS, and no data are available in control rats or with unlabeled albumin NPs.

We showed a high uptake for the biotinylated glutathione-labeled SNPs in brain endothelial cells. Gaillard *et al*. proved in several studies the increased uptake of glutathione-labeled pegylated liposomes in both cultured rat and human endothelial cells [31, 20]. We found that the transfer of glutathione-labeled SNPs across the *in vitro* BBB model was the highest among the tested particles and several fold higher than that of the non-targeted ones. Our results are in concordance with the *in vivo* data on the enhanced brain penetration of drugs and biopharmacons, including cytostatic doxorubicin, antiinflammatory methylprednisolone, opioid peptide DAMGO, and an anti-amyloid antibody by glutathione-labeled vesicular NPs. Glutathione as a vector not only increased the brain delivery of doxorubicin (543 Da) in rats [21], but it also inhibited tumor growth and increased survival in a mouse model of glioblastoma multiforme [20]. Brain uptake of methylprednisolone (374 Da) was elevated by glutathione targeting [19], and improved therapeutic efficacy was described for GSH-pegylated liposomal methylprednisolone in experimental autoimmune encephalomyelitis in rats [19], in mice [40], and in ocular inflammation in rats [41]. Increased brain delivery was demonstrated for the opioid pentapeptide DAMGO (513 Da) by GSH-pegylated liposomes in rats [22]. Enhanced GSH-pegylated liposomal brain delivery of a llama single domain anti-amyloid antibody fragment (15 kDa) was demonstrated in a mouse model for Alzheimer's disease [42], indicating that the platform may also be used for CNS delivery of biopharmacons.

Targeted NPs may use several transport routes at the BBB as reviewed by Rempe *et al*. [43]. Solid NPs were described to cross brain endothelial cells by receptor- or adsorption-mediated transcytosis [36, 43]. The higher transfer of SNP-B and SNP-B-GSH particles may be related to transcytosis due to the binding of targeting ligands to the surface of the brain endothelial cells. Indeed, we have verified the presence of SMVT/SLC5A6 mRNA in hCMEC/D3 brain endothelial cells, our BBB model system. In the case of biotin targeted SNPs, we hypothesize that the targeting ligand helps the binding of the nanocarriers to the surface of brain endothelial cells, which triggers transcytosis across the brain endothelial monolayers. For the clinical-stage GSH drug delivery platform, although the BBB receptor/transporter is unknown, the suggested mechanism of BBB crossing is a secific liposomal endocytosis pathway indicative of receptor-mediated transcytosis [19]. Further experiments are needed to explore the exact mechanism.

CONCLUSION

Biotin as a ligand increased the uptake and the transfer of nanoparticles across brain endothelial cells and may have a potential to be used as a BBB targeting molecule. Biotinylated glutathione was more effective as a ligand to increase nanoparticle permeability through endothelial monolayers supporting its use as successful brain targeting vector.

LIST OF ABBREVIATIONS

ACN	=	Acetonitrile
B	=	Biotin
BBB	=	Blood-brain barrier
DCC	=	*N,N*-dicyclohexyl-carbodiimide
DCM	=	Dichloromethane
DIEA	=	*N,N*-diisopropylethylamine
DMF	=	*N.N*-dimethylformamide
DTT	=	1,4-dithiothreitol
Fmoc	=	9-flourenylmethyloxycarbonyl
GSH	=	Glutathione

HATU	=	1-[Bis(dimethylamino)methylene]-1H-1,2,3-triazolo[4,5-b]pyridinium 3-oxid hexafluorophosphate
hCMEC/D3	=	Human brain endothelial cell line
HOBt	=	1-hydroxybenzotriazole
HPLC	=	High performance liquid chromathography
MTT	=	3-(4,5-dimethylthiazol-2-yl)-2,5-diphenyltetrazolium bromide
NP	=	Nanoparticle
SLC	=	Solute carrier transporter
SNP	=	Solid nanoparticle
SNP-B	=	Biotin targeted solid nanoparticle
SNP-B-GSH	=	Biotinylated-glutathione targeted solid nanoparticle
TFA	=	Triflouroacetic acid
TIS	=	Triisopropylsilane

CONFLICT OF INTEREST

The authors declare that there is no conflict of interest in connection to the present work.

ACKNOWLEDGEMENTS

This work was supported by the Hungarian Scientific Research Fund (OTKA PD105622) and by the National Research, Development and Innovation Office (GINOP-2.2.1-15-2016-00007, GINOP-2.3.2-15-2016-00060). S.V. was supported by the János Bolyai Research Fellowship of the Hungarian Academy of Sciences (BO/00724/12).

REFERENCES

[1] Neuwelt EA, Bauer B, Fahlke C, *et al.* Engaging neuroscience to advance translational research in brain barrier biology. Nat Rev Neurosci 2011; 12(3): 169-82.

[2] Pardridge WM. Drug transport across the blood-brain barrier. J Cereb Blood Flow Metab 2012; 32(11): 1959-72.

[3] Abbott NJ, Patabendige AA, Dolman DE, *et al*. Structure and function of the blood-brain barrier. Neurobiol Dis 2010; 37(1): 13-25.

[4] Deli MA. Drug transport and the blood-brain barrier. In: Tihanyi K, Vastag M, editors. Solubility, Delivery, and ADME Problems of Drugs and Drug-Candidates. Washington: Bentham Science Publishers Ltd.; 2011. p. 144-65.

[5] Kreuter J. Drug delivery to the central nervous system by polymeric nanoparticles: what do we know? Adv Drug Deliv Rev 2014; 71: 2-14.

[6] Veszelka S, Bocsik A, Walter F, *et al*. Blood-brain-barrier coculture models to study nanoparticle penetration: focus on coculture systems. Acta Biol Szeged 2015; 59(Suppl.2): 157-68.

[7] Pardridge WM. Blood-brain barrier endogenous transporters as therapeutic targets: a new model for small molecule CNS drug discovery. Expert Opin Ther Targets 2015; 19(8): 1059-72.

[8] Campos-Bedolla P, Walter FR, Veszelka S, *et al.* Role of the blood-brain barrier in the nutrition of the central nervous system. Arch Med Res 2014; 45(8): 610-38.

[9] Enerson BE and Drewes LR. The rat blood-brain barrier transcriptome. J Cereb Blood Flow Metab 2006; 26(7): 959-73.

[10] César-Razquin A, Snijder B, Frappier-Brinton T, *et al.* A call for systematic research on solute carriers. Cell 2015; 162(3): 478-87.

[11] Gromnicova R, Davies HA, Sreekanthreddy P, *et al.* Glucose-coated gold nanoparticles transfer across human brain endothelium and enter astrocytes *in vitro*. PLoS One 2013; 8(12): e81043.

[12] Weksler B, Romero IA, Couraud PO. The hCMEC/D3 cell line as a model of the human blood brain barrier. Fluids Barriers CNS 2013; 10(1): 16.

[13] Helms HC, Abbott NJ, Burek M, *et al. In vitro* models of the blood-brain barrier: An overview of commonly used brain endothelial cell culture models and guidelines for their use. J Cereb Blood Flow Metab 2016; 36(5): 862-90.

[14] Dufes C, Gaillard F, Uchegbu IF, *et al.* Glucose-targeted niosomes deliver vasoactive intestinal peptide (VIP) to the brain. Int J Pharm 2004; 285(1-2): 77-85.

[15] Vyas A, Jain A, Hurkat P, *et al.* Targeting of AIDS related encephalopathy using phenylalanine anchored lipidic nanocarrier. Colloids Surf B Biointerfaces 2015; 131: 155-61.

[16] Li J, Guo Y, Kuang Y, *et al.* Choline transporter-targeting and co-delivery system for glioma therapy. Biomaterials 2013; 34(36): 9142-8.

[17] Kannan R, Chakrabarti R, Tang D, *et al.* GSH transport in human cerebrovascular endothelial cells and human astrocytes: evidence for luminal localization of Na+-dependent GSH transport in HCEC. Brain Res 2000; 852(2): 374-82.

[18] Gaillard PJ. BBB crossing assessment and BBB crossing technologies in CNS Drug Discovery. Drug Discov Today Technol 2016; 20: 1-3.

[19] Gaillard PJ, Appeldoorn CC, Rip J, *et al*. Enhanced brain delivery of liposomal methylprednisolone improved therapeutic efficacy in a model of neuroinflammation. J Control Release 2012; 164: 364-9.

[20] Gaillard PJ, Appeldoorn CC, Dorland R, *et al*. Pharmacokinetics, brain delivery, and efficacy in brain tumor-bearing mice of glutathione pegylated liposomal doxorubicin (2B3-101). PLoS One 2014; 9(1): e82331.

[21] Birngruber T, Raml R, Gladdines W, *et al.* Enhanced doxorubicin delivery to the brain administered through glutathione PEGylated liposomal doxorubicin (2B3-101) as compared with generic Caelyx,(®)/Doxil(®)--a cerebral open flow microperfusion pilot study. J Pharm Sci 2014; 103(7): 1945-8.

[22] Lindqvist A, Rip J, van Kregten J, *et al.* Hammarlund-Udenaes M. *In vivo* functional evaluation of increased brain delivery of the opioid peptide DAMGO by glutathione-PEGylated liposomes. Pharm Res 2016; 33(1): 177-85.

[23] Uchida Y, Ito K, Ohtsuki S, *et al*. Major involvement of Na^+-dependent multivitamin transporter (SLC5A6/SMVT) in uptake of biotin and pantothenic acid by human brain capillary endothelial cells. J Neurochem 2015; 134(1): 97-112.

[24] Lesch HP, Kaikkonen MU, Pikkarainen JT, *et al*. Avidin-biotin technology in targeted therapy. Expert Opin Drug Deliv 2010; 7(5): 551-64.

[25] Liebner S, Corada M, Bangsow T, *et al.* Wnt/beta-catenin signaling controls development of the blood-brain barrier. J Cell Biol 2008; 183(3): 409-17.

[26] Kiss L, Walter FR, Bocsik A, *et al*. Kinetic analysis of the toxicity of pharmaceutical excipients Cremophor EL and RH40 on endothelial and epithelial cells. J Pharm Sci 2013; 102(4): 1173-81.

[27] Bocsik A, Darula Z, Tóth G, *et al.* Transfer of opiorphin through a blood-brain barrier culture model. Arch Med Res 2015; 46(6): 502-6.

[28] Veszelka S, Pásztói M, Farkas AE, *et al.* Pentosan polysulfate protects brain endothelial cells against bacterial lipopolysaccharide-induced damages. Neurochem Int 2007; 50(1): 219-28.

[29] Nakagawa S, Deli MA, Kawaguchi H, *et al.* A new blood-brain barrier model using primary rat brain endothelial cells, pericytes and astrocytes. Neurochem Int 2009; 54(3-4): 253-63.

[30] Tóth AE, Tóth A, Walter FR, *et al.* Compounds blocking methylglyoxal-induced protein modification and brain endothelial injury. Arch Med Res 2014; 45(8): 753-64.

[31] Rip J, Chen L, Hartman R, *et al*. Glutathione PEGylated liposomes: pharmacokinetics and delivery of cargo across the blood-brain barrier in rats. J Drug Target 2014; 22(5): 460-7.

[32] Walter FR, Valkai S, Kincses A, *et al*. A versatile lab-on-a-chip tool for modeling biological barriers. Sens Actuators B Chem 2016; 222: 1209-19

[33] Spector R, Johanson CE. Vitamin transport and homeostasis in mammalian brain: focus on Vitamins B and E. J Neurochem 2007; 103(2): 425-38.

[34] Merodio M, Irache JM, Eclancher F, *et al.* Distribution of albumin nanoparticles in animals induced with the experimental allergic encephalomyelitis. J Drug Target 2000; 8(5): 289-303.

[35] Neves AR, Queiroz JF, Weksler B, *et al.* Solid lipid nanoparticles as a vehicle for brain-targeted drug delivery: two new strategies of functionalization with apolipoprotein E. Nanotechnology 2015; 26(49): 495103

[36] Müller RH, Gohla S, Keck CM. State of the art of nanocrystals—special features, production, nanotoxicology aspects and intracellular delivery. Eur J Pharm Biopharm 2011; 78(1): 1-9.

[37] Mc Carthy DJ, Malhotra M, O'Mahony AM, *et al.* Nanoparticles and the blood-brain barrier: advancing from in-vitro models towards therapeutic significance. Pharm Res 2015; 32(4): 1161-85.

[38] Hanada S, Fujioka K, Inoue Y, *et al.* Cell-based *in vitro* blood-brain barrier model can rapidly evaluate nanoparticles' brain permeability in association with particle size and surface modification. Int J Mol Sci 2014; 15(2): 1812-25.

[39] Spector R, Mock D. Biotin transport through the blood-brain barrier. J Neurochem 1987; 48(2): 400-4.

[40] Lee DH, Rötger C, Appeldoorn CC, *et al.* Glutathione PEGylated liposomal methylprednisolone (2B3-201) attenuates CNS inflammation and degeneration in murine myelin oligodendrocyte glycoprotein induced experimental autoimmune encephalomyelitis. J Neuroimmunol 2014; 274(1-2): 96-101.

[41] Reijerkerk A, Appeldoorn CC, Rip J, *et al.* Systemic treatment with glutathione PEGylated liposomal methylprednisolone (2B3-201) improves therapeutic efficacy in a model of ocular inflammation. Invest Ophthalmol Vis Sci 2014; 55(4): 2788-94.

[42] Rotman M, Welling MM, Bunschoten A, *et al*. Enhanced glutathione PEGylated liposomal brain delivery of an anti-amyloid single domain antibody fragment in a mouse model for Alzheimer's disease. J Control Release 2015; 203: 40-50.

[43] Rempe R, Cramer S, Qiao R, *et al.* Strategies to overcome the barrier: use of nanoparticles as carriers and modulators of barrier properties. Cell Tissue Res 2014; 355(3): 717-26.

PUBLICATION II.

frontiers in Molecular Neuroscience

ORIGINAL RESEARCH
published: 22 May 2018
doi: 10.3389/fnmol.2018.00166

Comparison of a Rat Primary Cell-Based Blood-Brain Barrier Model With Epithelial and Brain Endothelial Cell Lines: Gene Expression and Drug Transport

Szilvia Veszelka[1†], András Tóth[1,2†], Fruzsina R. Walter[1‡], Andrea E. Tóth[1‡], Ilona Gróf[1,3], Mária Mészáros[1,4], Alexandra Bocsik[1], Éva Hellinger[5], Monika Vastag[5], Gábor Rákhely[1,2†] and Mária A. Deli[1*†]*

[1]Biological Barriers Research Group, Institute of Biophysics, Biological Research Centre, Hungarian Academy of Sciences, Szeged, Hungary, [2]Department of Biotechnology, Faculty of Science and Informatics, University of Szeged, Szeged, Hungary, [3]Doctoral School in Biology, Faculty of Science and Informatics, University of Szeged, Szeged, Hungary, [4]Doctoral School in Theoretical Medicine, Faculty of Medicine, University of Szeged, Szeged, Hungary, [5]In Vitro Metabolism Research, Division of Pharmacology and Drug Safety, Gedeon Richter Plc., Budapest, Hungary

OPEN ACCESS

Edited by:
Marina Guizzetti, Oregon Health & Science University, United States

Reviewed by:
Hector Rosas-Hernandez, National Center for Toxicological Research (FDA), United States
Xiaolu Zhang, Northern Jiangsu People's Hospital, China

***Correspondence:**
Mária A. Deli
deli.maria@brc.mta.hu
Gábor Rákhely
rakhely.gabor@brc.mta.hu

[†]These authors have contributed equally to this work.

[‡]Present address:
Fruzsina R. Walter, University of Wisconsin-Madison, Madison, WI, United States
Andrea E. Tóth, Department of Biomedicine, University of Aarhus, Aarhus, Denmark

Received: *21 December 2017*
Accepted: *01 May 2018*
Published: *22 May 2018*

Citation:
Veszelka S, Tóth A, Walter FR, Tóth AE, Gróf I, Mészáros M, Bocsik A, Hellinger É, Vastag M, Rákhely G and Deli MA (2018) Comparison of a Rat Primary Cell-Based Blood-Brain Barrier Model With Epithelial and Brain Endothelial Cell Lines: Gene Expression and Drug Transport. Front. Mol. Neurosci. 11:166. doi: 10.3389/fnmol.2018.00166

Cell culture-based blood-brain barrier (BBB) models are useful tools for screening of CNS drug candidates. Cell sources for BBB models include primary brain endothelial cells or immortalized brain endothelial cell lines. Despite their well-known differences, epithelial cell lines are also used as surrogate models for testing neuropharmaceuticals. The aim of the present study was to compare the expression of selected BBB related genes including tight junction proteins, solute carriers (SLC), ABC transporters, metabolic enzymes and to describe the paracellular properties of nine different culture models. To establish a primary BBB model rat brain capillary endothelial cells were co-cultured with rat pericytes and astrocytes (EPA). As other BBB and surrogate models four brain endothelial cells lines, rat GP8 and RBE4 cells, and human hCMEC/D3 cells with or without lithium treatment (D3 and D3L), and four epithelial cell lines, native human intestinal Caco-2 and high P-glycoprotein expressing vinblastine-selected VB-Caco-2 cells, native MDCK and MDR1 transfected MDCK canine kidney cells were used. To test transporter functionality, the permeability of 12 molecules, glucopyranose, valproate, baclofen, gabapentin, probenecid, salicylate, rosuvastatin, pravastatin, atorvastatin, tacrine, donepezil, was also measured in the EPA and epithelial models. Among the junctional protein genes, the expression level of occludin was high in all models except the GP8 and RBE4 cells, and each model expressed a unique claudin pattern. Major BBB efflux (P-glycoprotein or ABCB1) and influx transporters (GLUT-1, LAT-1) were present in all models at mRNA levels. The transcript of BCRP (ABCG2) was not expressed in MDCK, GP8 and RBE4 cells. The absence of gene expression of important BBB efflux and influx transporters BCRP, MRP6, -9, MCT6, -8, PHT2, OATPs in one or both types of epithelial models suggests that Caco-2 or MDCK models are not suitable to test drug candidates which are substrates of these transporters. Brain endothelial cell lines GP8, RBE4, D3 and

D3L did not form a restrictive paracellular barrier necessary for screening small molecular weight pharmacons. Therefore, among the tested culture models, the primary cell-based EPA model is suitable for the functional analysis of the BBB.

Keywords: blood-brain barrier, brain endothelial cells, Caco-2, MDCK, RBE4, hCMEC/D3, gene expression, CNS drug permeability

INTRODUCTION

The development and introduction of novel neuropharmaceuticals lags behind other groups of medicines, which is partially due to the poor central nervous system (CNS) pharmacokinetics (Banks, 2016). One of the reasons for the low number of CNS active drugs in clinical use is the restricted penetration of most drugs across the blood-brain barrier (BBB; Pardridge, 2015). The BBB is the major barrier of the CNS and is composed of brain capillary endothelial cells surrounded by pericytes embedded in the capillary basal membrane, and astrocytic endfeet (Abbott, 2013). The four main mechanisms at the level of the BBB to limit drug transport are: (i) the restricted paracellular pathway regulated by interendothelial tight junctions (TJ); (ii) the low level of non-specific transendothelial vesicular traffic; (iii) active efflux transporters which deliver metabolites from brain to blood and prevent the entry of xenobiotics and drugs to the CNS; and (iv) enzymes which metabolize drug molecules (Deli, 2011; Banks, 2016).

There is a need for reliable methods in drug development to screen drug candidates for BBB penetration, on the one hand, and to determine if substances acting in the periphery do not cross the BBB to avoid CNS side effects, on the other hand. Models that predict brain penetration are also valuable tools to study and develop new targeted nanoparticles that cross the BBB (Veszelka et al., 2015). There are several types of models for BBB permeability from *in silico* approaches to *in vivo* studies (Vastag and Keseru, 2009; Veszelka et al., 2011; Avdeef et al., 2015).

An important novel field in BBB research is the use of microfluidic devices and organ-on-chip models. These chip devices with the possibility of fluid flow provide more realistic and physiological culture conditions. In contrast to static culture inserts, in dynamic *in vitro* BBB models the endothelial cells are exposed to shear stress, induced by fluid flow, an important regulator of barrier function (Cucullo et al., 2011). In dynamic models higher transendothelial electrical resistance (TEER) and lower permeability were reported in comparison to culture insert based *in vitro* models (Cucullo et al., 2013; Booth and Kim, 2014; Walter et al., 2016). Despite these advantages, dynamic *in vitro* models have not been widely accepted for BBB permeability screening in the pharmaceutical industry yet. None of the existing dynamic *in vitro* BBB models utilizing channel microfluidics (Griep et al., 2013; Prabhakarpandian et al., 2013; Booth and Kim, 2014; Walter et al., 2016) or hollow fiber cartridges (Cucullo et al., 2011, 2013) have been assessed for a set of CNS penetrating and non-penetrating drugs with different chemical properties to elucidate a translational standard for permeability.

Cell culture BBB models are versatile tools in both basic research and permeability testing of drugs (Deli et al., 2005; Veszelka et al., 2011; Helms et al., 2016). A large number of models were developed based on primary cultures of cerebral endothelial cells or immortalized cell lines (Deli et al., 2005; Veszelka et al., 2011; Helms et al., 2016). Among the brain endothelial cell lines, the rat GP8 (Greenwood et al., 1996) and RBE4 (Roux et al., 1994), and human hCMEC/D3 cells (Weksler et al., 2005) are the best characterized and the most widely used in BBB research. RBE4 rat brain microvessel endothelial cells were employed for drug transport studies, while no drug permeability data were published for GP8 cells (Veszelka et al., 2011). The most studied BBB cell line, hCMEC/D3, is also used in drug transport and uptake experiments (Weksler et al., 2013). While the paracellular barrier is not strong in hCMEC/D3 cells, treatment with LiCl, a Wnt/β-catenin pathway activator increases TJ protein expression and barrier function (Weksler et al., 2013). The most complex *in vitro* BBB models are based on primary cultures of brain capillary endothelial cells from bovine (Dehouck et al., 1990), rat (Szabó et al., 1997), or porcine brain (Hoheisel et al., 1998; Patabendige et al., 2013), which are used in many models in co-culture with astrocytes and/or pericytes (Nakagawa et al., 2009). A recent article gives an updated overview on culture models of the BBB with guidelines for their use in permeability studies (Helms et al., 2016). A big advantage of primary BBB models is that they are complex and retain many of the *in vivo* physiological characteristics of the BBB. However, as compared to cell line models, they are more expensive, their preparation requires more time and technical expertise (Avdeef et al., 2015).

Since cost and test capacity are important factors in industrial drug screening, models based on epithelial cell lines are still used to predict permeability of CNS drug candidates (Vastag and Keseru, 2009). The most widespread culture model of human drug absorption is the Caco-2 human intestinal epithelial cell line derived from a colon adenocarcinoma, which is used primarily as a screening tool for small intestine absorption (Artursson et al., 2001). For passive diffusion compounds, Caco-2 cells give a good correlation even when compared with BBB models (Garberg et al., 2005; Hellinger et al., 2012). Caco-2 cells treated with vinblastine (VB-Caco-2), express a higher level of P-glycoprotein and this model is a good predictor of ligands for efflux transporters (Hellinger et al., 2010). The other cell lines used in pharma industry for testing drug penetration are the Madin-Darby canine kidney (MDCK) cell line and MDCK-MDR1, a subclone transfected with the human MDR1 gene. Using passive diffusion drugs MDCK cells gave a weaker correlation as compared to BBB or Caco-2 models but in the case of efflux transporter ligands the MDCK-MDR model gave

accurate prediction (Garberg et al., 2005). Both Caco-2 and MDCK cells form a tight paracellular barrier and overexpress P-glycoprotein efflux pump, two factors participating in BBB permeability regulation, therefore these epithelial models in addition to prediction of intestinal absorption are also used as surrogate models for the prediction of brain penetration (Vastag and Keseru, 2009) despite cytoarchitectural differences and other dissimilarities from BBB models (Hellinger et al., 2012).

The paracellular tightness of the various BBB models measured by TEER and permeability (P_e/P_{app}) for marker molecules is in general well characterized (Deli et al., 2005; Helms et al., 2016). With the exception of P-glycoprotein, much less is known about the efflux transporter expression pattern and functionality in these models. Solute carriers (SLC) are present at the BBB in high number, where they participate in shuttling nutrients across brain endothelial cells (for review see Campos-Bedolla et al., 2014). Despite their importance, SLC expression and functionality in BBB models is understudied (Helms et al., 2016). Even less is known about phase I and II drug metabolizing enzymes in BBB culture models, with the exception of hCMEC/D3 cells (Dauchy et al., 2009).

In our previous study, we compared a primary cell-based BBB model in which rat brain endothelial cells were co-cultured with pericytes and astrocytes (EPA model, Nakagawa et al., 2009) with Caco-2, VB-Caco-2 and MDCK-MDR1 epithelial cell models provided and highlighted differences in cellular morphology, paracellular tightness and drug transport (Hellinger et al., 2012).

The aim of the present study was to extend these observations with comparative data on the expression of selected BBB related genes including TJ proteins, SLC and ABC transporters and metabolic enzymes in nine different culture models. In addition to EPA and epithelial models we also examined rat (GP8, RBE4) and human brain endothelial cell lines (D3 and D3L). To test SLC functionality the permeability of eleven drugs was also measured in the EPA and epithelial models.

MATERIALS AND METHODS

Animals

For primary cultures of brain endothelial cells and pericytes brains were obtained from 3-week old, for glial cell culture from 2-day old Wistar outbred rats. Organ removals were performed following the regulations of the 1998. XXVIII. Hungarian law and the EU Directive 2010/63/EU about animal protection and welfare. Approval for animal studies was obtained from the local animal health authority, the Governmental Office for Csongrád County, Directorate of Food Chain Safety and Animal Health (Permit numbers: XVI./03835/001/2006, XVI./834/2012). Animals were fed on standard rodent chow and water *ad libitum* and kept under a 12 h light/dark cycle in the conventional animal house of the Biological Research Centre, Szeged.

Cell Cultures

Isolation of primary rat brain endothelial cells, glia and pericytes and the construction of the *in vitro* BBB model were performed according to the method described in our previous studies (Nakagawa et al., 2009; Walter et al., 2015). After isolation, cells were seeded on Petri dishes coated with 100 μg/ml collagen type IV and 100 μg/ml fibronectin in sterile distilled water. Brain endothelial cells were cultured in DMEM/ HAM's F-12 (Gibco, Life Technologies, Carlsbad, CA, USA), 15% plasma-derived bovine serum (PDS, First Link, Wolverhampton, UK), 100 μg/ml heparin, 5 μg/ml insulin, 5 μg/ml transferrin, 5 ng/ml sodium selenite, 1 ng/ml basic fibroblast growth factor (bFGF, Roche, Basel, Switzerland) and 50 μg/ml gentamicin. During the first 3 days of culture the medium of brain endothelial cells contained 3 μg/ml puromycin to eliminate P-glycoprotein negative, contaminating cell types (Perrière et al., 2005). Primary rat brain pericytes were isolated using the same method as for brain endothelial cells, except that pericytes were plated onto uncoated Petri dishes (Orange Scientific, Braine-l'Alleud, Belgium). Primary cultures of rat glial cells were prepared from one-day-old Wistar rats (Perrière et al., 2005) and passaged to 10 cm Petri dishes (Corning, Costar, New York, NY, USA) coated with 100 μg/ml collagen type IV in sterile distilled water and cultured for 2 weeks before use for the triple co-culture model. Pericytes and glial cells were cultured in DMEM/HAM's F-12 supplemented with 10% fetal bovine serum (FBS, Pan-Biotech GmbH) and 50 μg/ml gentamicin. For the triple co-culture model, pericytes (P3) were passaged to the bottom side of tissue culture inserts with 75 mm diameter (Transwell 3419, polycarbonate membrane, 0.4 μm pore size, Corning Costar) at a density of 1.5×10^4 cells/cm^2. Endothelial cells were seeded to the upper side of the membranes (7.5×10^4 cells/cm^2) and placed to 10 cm Petri dish containing glial cells. Both compartments received endothelial culture medium and the three types of cells were cultured together for 4 or 5 days (Nakagawa et al., 2009; Walter et al., 2015). In transport assays the triple culture BBB model was prepared on 12 well plate Transwell inserts (polyester membrane, 0.4 μm pore size, Corning Costar). When brain endothelial cell layers became confluent 550 nM hydrocortisone was added to tighten the junctions (Deli et al., 2005).

GP8 rat brain endothelial cell line (provided by Dr. John Greenwood, University College London, UK) was cultured in DMEM/ HAM's F-12, 15% PDS, 100 μg/ml heparin, 1 ng/ml bFGF and 50 μg/ml gentamicin.

RBE4 rat brain endothelial cell line (provided by Dr. Pierre-Olivier Couraud, Institut Cochin, Paris, France) was grown in DMEM/ HAM's F-12, supplemented with 10% FBS, 1 ng/ml bFGF and 50 μg/ml gentamicin.

Cultures of human brain endothelial hCMEC/D3 cell line (≤passage number 35) were grown in MCDB 131 medium (Pan Biotech) supplemented with 5% FBS, GlutaMAX (100×, LifeTechnologies, Carlsbad, CA, USA), lipid supplement (100×, Life Technologies, Carlsbad, CA, USA), 10 μg/ml ascorbic acid, 550 nM hydrocortisone, 100 μg/ml heparin, 1 ng/ml basic fibroblast growth factor (bFGF, Roche, USA), 2.5 μg/ml insulin, 2.5 μg/ml transferrin, 2.5 ng/ml sodium selenite and 50 μg/ml gentamicin (Weksler et al., 2005). For differentiation of this cell line (D3L group), the medium was supplemented with 10 mM lithium chloride (LiCl) at the first change of medium (Paolinelli et al., 2013). For the three brain endothelial cell lines, we used

culture media with very similar or identical composition to those that were originally described for their growth and maintenance.

Human Caco-2 intestinal epithelial cell line (ATCC cat.no. HTB-37) was maintained in DMEM/HAM's F-12 culture medium supplemented with 10% FBS and 50 μg/ml gentamicin. VB-Caco-2 cultures were created from Caco-2 cultures by selecting cells with 10 nM vinblastine treatment for at least six passages (Hellinger et al., 2010). Treatment leads to a more homogeneous cell morphology and a higher expression level of efflux pumps.

Parent and MDR1 transfected Madin-Darby canine kidney epithelial cells (Evers et al., 2000) were obtained from the Netherlands Cancer Institute (Amsterdam, Netherlands). The tissue culture medium consisted of 4.5 g/l glucose containing DMEM supplemented with 10% FBS, penicillin (50 units) and streptomycin (0.05 mg/ml). For RNS isolation, all cell lines were seeded in 10 cm Petri dishes and for transport assays cells were passaged onto 12-well plate Transwell inserts coated with 0.05% rat tail collagen in sterile distilled water.

Transendothelial Electrical Resistance Measurement

Transendothelial electrical resistance (TEER), reflecting the permeability of TJ for sodium ions, was measured by an EVOM voltohmmeter (World Precision Instruments, Sarasota, FL, USA) combined with STX-2 electrodes. Recorded resistance was expressed to the surface area of the filters ($\Omega \times cm^2$, Transwell inserts, polystyrene membrane, 0.4 μm pore size, Corning Costar, USA). TEER of cell-free inserts (110 $\Omega \times cm^2$) was subtracted from the measured data.

Permeability Measurement

For permeability tests the epithelial and endothelial cell types were cultured on culture inserts (polycarbonate membrane, 0.4 μm pore size, 1.2 cm^2 surface, Transwell, Corning Costar). The inserts were transferred to 12-well plates containing 1.5 ml Ringer-Hepes buffer (EPA model) or HBSS-Hepes buffer (epithelial models) in the lower (basal/abluminal) compartments. In the upper (apical/luminal) compartments culture medium was replaced by 0.5 ml buffer containing permeability marker molecules albumin (1 mg/ml; Mw: 65 kDa) labeled with Evans blue (167.5 μg/ml) and fluorescein (10 μg/ml; Mw: 376 Da). After incubation with permeability markers for 30 min, samples were collected from both compartments and concentrations of the marker molecules were determined by a fluorescence multi-well plate reader (Fluostar Optima; excitation wavelength: 485 nm, emission wavelength: 535 nm in the case of fluorescein and excitation wavelength: 584 nm, emission wavelength: 680 nm in the case of Evans-blue labeled albumin). The apparent permeability coefficients (P_{app}) were calculated as we described previously (Kürti et al., 2012). Briefly, cleared volume was calculated from the concentration difference of the tracer in the lower/basal compartment ($\Delta[C]_B$) after 30 min (t) and upper/apical compartments at 0 h ($[C]_A$), the volume of the lower/basal compartment (V_B; 1.5 mL) and the surface area available for permeability (A; 1.1 cm^2) by the following equation:

$$P_{app}(cm/s) = \frac{[C]_B \times V_B}{A \times [C]_A \times t}$$

For the permeability study on the EPA and epithelial models, nine different SLC ligands (at 10 μM concentrations, except glucopyranose (100 μM) and valproic acid (300 μM), 60–120 min) and two anticholinergic drugs, tacrine and donepezil (0.5 μM, 30 min), approved for the treatment of Alzheimer's disease, were tested. The transport of tacrine and donepezil was also measured in the presence of choline and carnitine, two endogenous cationic metabolites to examine whether they share influx transporters. The concentrations of the test molecules in samples from the donor and acceptor compartments were determined by high-pressure liquid chromatography (HPLC) or liquid chromatography-mass spectrometry (LC/MS). P_{app} was calculated for each drug as described above. The efflux or permeability directional ratio (PDR) was given as the ratio of P_{app} values in BA to AB direction (Hellinger et al., 2012).

Immunohistochemistry

Brain endothelial and epithelial cells were cultured on rat tail collagen coated glass cover slips. Endothelial cells were stained for the integral membrane tight junction protein claudin-5 and epithelial cells were stained for claudin-4. After the removal of the culture medium cells were fixed with ethanol—acetic acid (95:5 mixture) for 5 min at −20°C, blocked with 3% bovine serum albumin diluted in phosphate buffer (PBS) and incubated overnight with primary antibodies: anti-claudin-5 (rabbit polyclonal antibody, 1:200, Sigma, AB_10753223) or anti-claudin-4 (mouse monoclonal antibody, 1:200, Thermo Fisher Scientific, AB_2533096). Incubation with secondary antibodies Cy3-labeled anti-rabbit (Sigma) or Alexa488-labeled anti-mouse immunglobulin (Invitrogen, Life Technologies, 1:500) and Hoechst dye 33342 (Sigma) for nucleus staining lasted for 1 h. Cells were washed three times with PBS between incubations. After mounting the samples (Fluoromount-G; Southern Biotech, Birmingham, AL, USA) staining was visualized by Olympus Fluoview FV1000 confocal laser scanning microscope (Olympus Life Science Europe GmbH, Hamburg, Germany).

RNA Isolation and Quality Control

The endothelial (primary brain endothelial cells, GP8, RBE4, D3, D3L) and epithelial cells (Caco-2, VB-Caco-2, MDCK and MDCK-MDR1) were cultured for 5 days in 10 cm dishes. After reaching confluency cells were scraped, collected and cell pellets were used for total RNA isolation using RNAqueous-4PCR Kit (Ambion, Life Technologies, Austin, TX, USA) with DNase1 (RNase-free) treatment according to the manufacturer's instructions. The concentrations and purity of the DNase-treated RNA samples were assessed by a NanoDrop ND-1000 spectrophotometer (NanoDrop Technologies, Rockland, DE, USA). The integrities of the isolated RNAs were characterized using Bioanalyzer 2100 (Agilent Technologies, Santa Clara, CA, USA). The RNA integrity numbers (RIN) were between 9.2 and 10 in the case of all studied RNA samples.

Quantitative Real-Time Polymerase Chain Reaction and Data Analysis

In all cases, cDNA synthesis was performed on 1 μg total RNA samples by a High Capacity cDNA Reverse Transcription Kit (Life Technologies) using random hexanucleotide primers and MultiScribe Reverse Transcriptase in the presence of RNase inhibitor according to the manufacturer's protocols. The expression of the selected BBB genes was analyzed by quantitative PCR using TaqMan Low Density Array 384-well microfluidic cards preloaded with TaqMan Gene Expression Assays (Life Technologies). The list of the studied genes and applied TaqMan Gene Expression Assays are shown in the supplementary materials (Supplementary Table S1). Quantitative real-time PCRs (qPCR) were performed by ABI TaqMan Universal Master Mix (Life Technologies) using the ABI Prism 7900 system (Applied Biosystems, Life Technologies). qPCR data were analyzed using the ABI SDS 2.0 software (Applied Biosystems, Life Technologies). In all samples the expression of genes was normalized to 18S rRNA, which was used as an endogenous control ($\Delta C_t = C_{tgene} - C_{t18S\ rRNA}$). Expression values of studied genes were determined based on the normalized expression of genes calculated with $2^{-\Delta C_t}$ formula which were correlated to the lowest normalized expression measured by the applied qPCR method. For quantification of the relative expression level of genes of interest, the normalized expression data were analyzed using the comparative $\Delta\Delta C_t$ method (Livak and Schmittgen, 2001; Tóth et al., 2014).

Statistical Analysis

Data are presented as means ± SEM or SD. Values were compared using unpaired *t*-test, one-way or two-way analyses of variances following Dunnett or Bonferroni multiple comparison posttests (GraphPadPrism 5.0; GraphPad Software, USA). Changes were considered statistically significant at $P < 0.05$. All experiments were repeated at least two times and the number of parallel samples was 4–8.

RESULTS

Comparison of the Triple Co-culture BBB Model With Caco-2, VB-Caco-2, MDCK and MDCK-MDR1 Epithelial Cell Lines: Expression of Selected Tight Junction Protein, Transporter and Metabolic Enzyme Genes

Tight Junction Proteins

Primary rat brain endothelial cells grown in co-culture with glial cells and pericytes (EPA) produced high levels of mRNA for key tight junction proteins such as claudin-5 (CLDN5), occludin and the endothelial cells specific adhesion molecule ESAM (**Figure 1**). Caco-2 epithelial cells also showed a high level of expression for occludin, while in MDCK cells it was lower as compared to both EPA and Caco-2 models (Supplementary Figure S1). The gene of endothelial cell specific ESAM was expressed at a low level in epithelial cells. High level of CLDN5 expression, comparable to occludin and ESAM, was measured in brain endothelial cells in the EPA model. In the BBB model, the cells expressed low level of CLDN1, CLDN2, CLDN3, CLDN4 transcripts and did not express CLDN7 mRNA, specific for epithelial cells. The absence of CLDN16 transcript and relatively high level of CLDN15 mRNA could be observed in the rat primary BBB model (**Figure 1**). CLDN19 mRNA was detected in the rat BBB model, but not in Caco-2 epithelial cells. The expression pattern of claudins in MDCK cells was similar to that of the Caco-2 cells with some exceptions, CLDN2, CLDN5, CLDN16 and CLDN19 gene expression levels were higher in the kidney epithelial cells as compared to the intestinal epithelial cell lines (**Figure 1**).

Solute Carrier or Other Transporters

In the BBB model, primary brain endothelial cells expressed high levels of mRNAs for glucose transporter GLUT1 (Slc2a1) and GLUT3 (Slc2a3; **Figure 2**) and the transcript level of GLUT5 (Slc2a5) was low. Caco-2 epithelial cells expressed high levels of all three GLUT transporters from which GLUT5 showed the highest and GLUT1 the lowest expression (Supplementary Figure S2). MDCK cells also expressed high levels of the GLUT1 gene, a low level of GLUT3, and did not express GLUT5. Brain endothelial cells in co-culture expressed high amount of mRNA coding monocarboxylic acid transporters MCT1 (Slc16a1), -2 (Slc16a2) and -6 (Slc16a6), which provide secondary energy sources and thyroid hormones for the CNS, respectively (**Figure 2**). Caco-2 epithelial cells expressed a high level of MCT1 only and a lower level of MCT8 and MCT6 mRNAs. MDCK cells did not produce the MCT1 transcript. In the BBB model, high mRNA expression levels were measured for all the amino acid transporters tested except for small neutral amino acid transporter SNAT5 (Slc38a5), where a moderate expression level was measured. Caco-2 and MDCK epithelial cells also expressed all these transporter genes at a high and moderate level. Among the peptide transport systems tested, cells of the primary rat brain endothelial cell-based model did not express PEPT1 (Slc15a1) but produced a significant amount of PHT2 transcript (Slc15a3; **Figure 2**). In contrast, in the Caco-2 cells the expression level of PEPT1 was relatively high, but low in the case of PHT2. MDCK cell lines produced a small amount of PEPT1 mRNA. Fatty acid transporter FATP1 (Slc27a1) was well expressed in the BBB and the epithelial models (**Figure 2**). Among the sterol transporters, the ABCA2 gene was expressed in all models, while the highest transcript level of ABCA8 was found in MDCK cells, however, in the other investigated models its transcript level was low. The gene of MFSD2A, a transporter for ω-3 fatty acids was also transcribed in all five models. Its expression level was higher in the Caco-2 and MDCK cells as compared to the EPA model (**Figure 2**). Among the genes of Slc6 family rat brain endothelial cells produced a high amount of mRNA of the gene of the carrier for creatine (CRT, Slc6a8), and moderate transcript levels were measured for glycine (GLYT1, Slc6a9) and taurine (TAUT, Slc6a6) genes (**Figure 2**). A similar expression pattern was seen for Caco-2 and MDCK epithelial cells. High levels of mRNAs

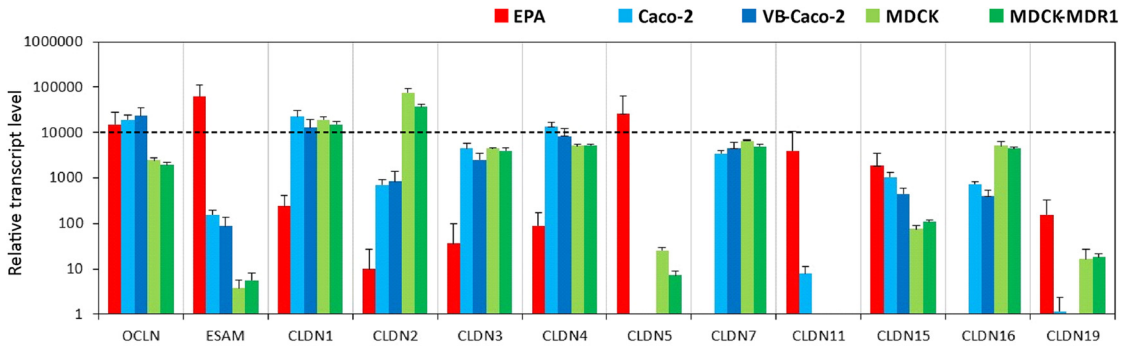

FIGURE 1 | Relative transcript levels of selected genes encoding tight junction proteins measured by inventoried TaqMan Gene Expression Assays in a primary rat brain endothelial cell-based blood-brain barrier (BBB) model (EPA) and in epithelial cell line models (Caco2, VB-Caco2, MDCK and MDCK-MDR1).

of the sodium-dependent vitamin transporter (SMVT, Slc5a6) and vitamin C transporters ASCT2 (Slc1a5) and ASCT1 (Slc1a4; Supplementary Table S2) genes were detected in rat brain endothelial cells (**Figure 2**). Epithelial cells also expressed all these carriers. Except for the absence of dopamine transporter gene transcription (DAT, Slc6a3), low transcript levels of the noradrenalin (NET, Slc6a2), serotonin (SERT, Slc6a4), and GABA (GAT1, Slc6a1; GAT2, Slc6a13; GAT3, Slc6a11) genes were seen in the BBB model (Supplementary Table S2). Epithelial cells did not produce a detectable amount of mRNAs of the genes of neurotransmitter carriers except for the high-level expression of the SERT gene in Caco-2 cells (Supplementary Table S2). The genes of organic anion-transporting polypeptides (OATP1C1, Slco1c1; OATP1A2, Slco1a2) which mediate the transport of thyroid and steroid hormones in addition to organic anions, were expressed in primary brain endothelial cells but not in epithelial models (**Figure 2** and Supplementary Table S2).

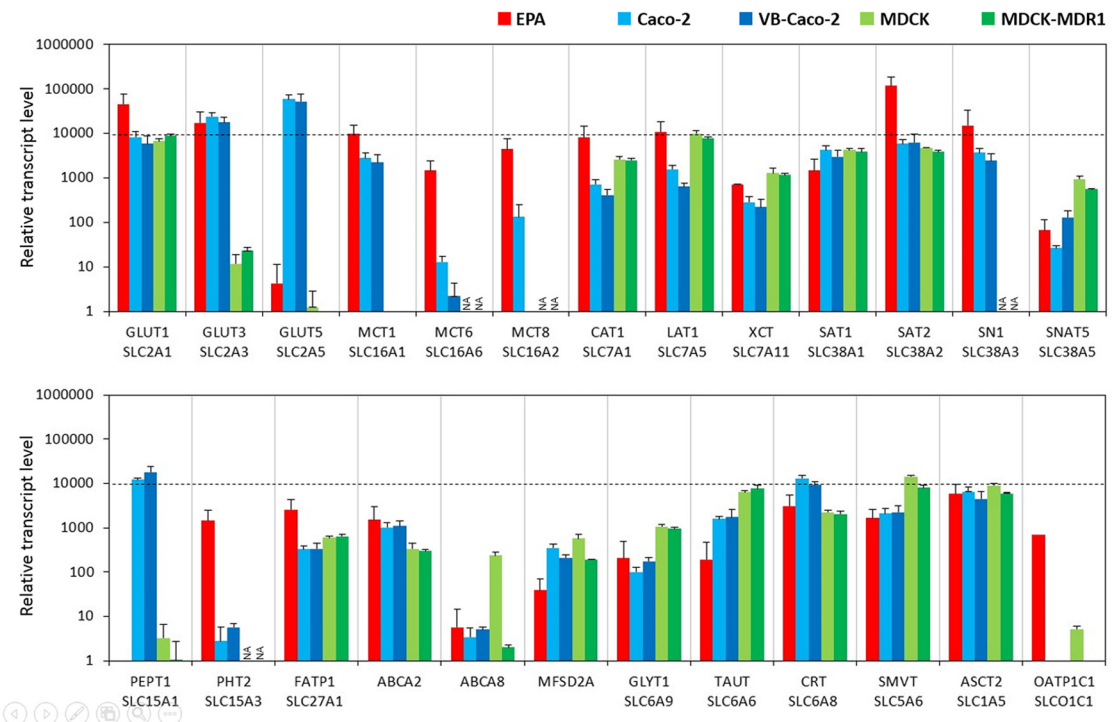

FIGURE 2 | Relative transcript levels of selected genes encoding solute carriers (SLC) and other nutrient transporters measured by inventoried TaqMan Gene Expression Assays in a primary rat brain endothelial cell-based BBB model (EPA) and in epithelial cell line models (Caco-2, VB-Caco-2, MDCK and MDCK-MDR1). NA: assay not available.

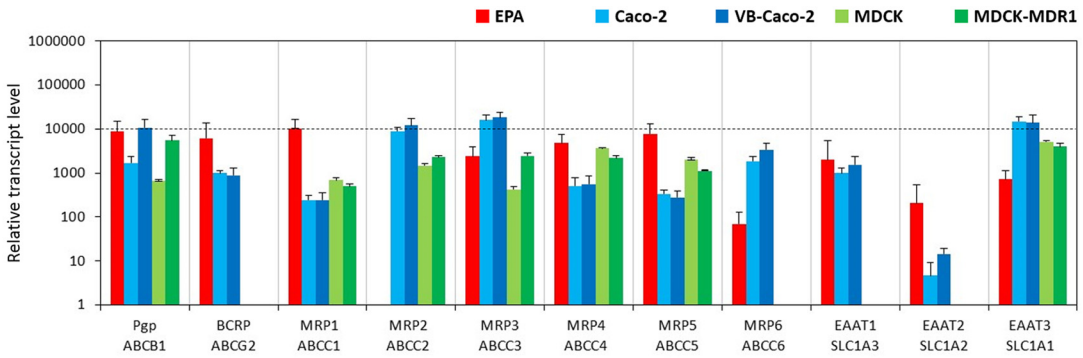

FIGURE 3 | Relative transcript levels of selected genes encoding efflux transporters measured by inventoried TaqMan Gene Expression Assays in a primary rat brain endothelial cell-based BBB model (EPA) and in epithelial cell line models (Caco-2, VB-Caco-2, MDCK and MDCK-MDR1).

Efflux Transporters

The BBB model EPA expressed a similarly high amount of mRNA for the two primary efflux transporters at the BBB, P-glycoprotein (Pgp, ABCB1) and breast cancer resistance protein (BCRP, ABCG2; **Figure 3**). Vinblastine—selected VB-Caco-2 cells showed significantly higher P-gp expression than native Caco-2 cells, while MDCK-MDR1 cells transfected with human ABCB1 gene also produced a higher level of canine ABCB1 gene transcript (**Figure 3**, Supplementary Figure S3). The expression of the BCRP gene could not be detected in the kidney epithelial cells, but Caco-2 cells do express BCRP. Among the tested multidrug resistance-associated proteins (MRP), the mRNAs of the MRP-1, -3, -4 and -5 were the four most dominant efflux transporter transcripts in brain endothelial cells, the MRP-6 genes were expressed at a lower level, while the MRP-2 gene was not expressed at all (**Figure 3**). Caco-2 cells produced high amounts of mRNAs of the MRP-2, -3 and -6, and a lower level of MRP-1, -4 and -5 genes. MDCK cells had a similar expression pattern to that of Caco-2 cells, except that they did not transcribe the MRP-6 gene. Among the excitatory amino acid transporters (EAAT, Slc1a family) which are participating in the efflux transport of glutamate across the BBB and are responsible for the low level of glutamate in the brain interstitial fluid, the EAAT1 (Slc1a3) gene was highly expressed in brain endothelial cells (**Figure 3**). The EAAT2 (Slc1a2) and EAAT3 (Slc1a1) genes were expressed at moderate levels. In Caco-2 and MDCK cells the expression level of EAAT3 gene was the highest. The gene of EAAT1 was also highly expressed in Caco-2 cells, but not expressed in MDCK cells. In contrast to the EPA model the transcript level of the EAAT2 gene was very low in epithelial cell lines.

Metabolic Enzymes

Among the tested genes of the phase-I drug metabolic enzymes, brain endothelial cells of the EPA BBB model expressed mRNA of CYP1A1, CYP2D6, CYP2R1, CYP2S1, CYP2U1 and CYP27A1 cytochrome P450 enzymes (**Figure 4**, Supplementary Figure S4), but not CYP1A2, CYP2E1 and CYP7A1. In Caco-2 cells the highest transcript level of the cytochrome P450 genes was seen for CYP2S1 and CYP27A1 genes. Only two genes, the CYP2C9 and CYP2D6 genes were transcriptionally active in MDCK cells. The other genes either could not be tested in MDCK cells due to the unavailability of appropriate gene probes or they were not expressed. Among the genes of phase-II metabolic enzymes selected, rat brain endothelial cells expressed high levels of mRNA of the glutathione S-transferase π (GSTP1 gene;

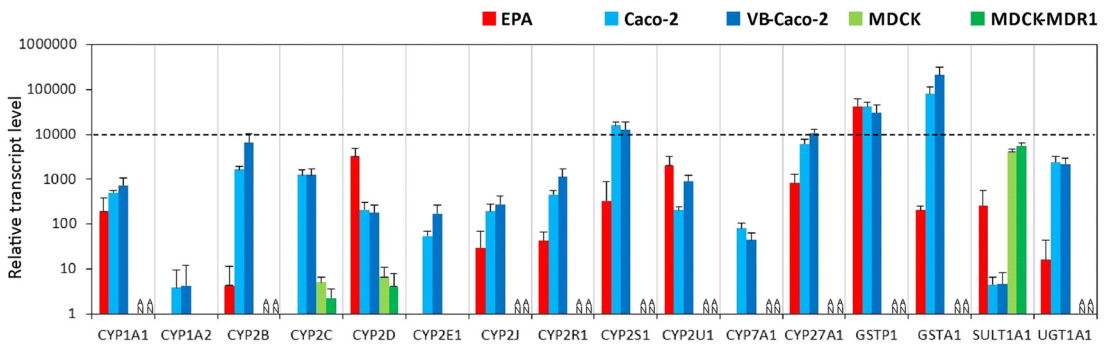

FIGURE 4 | Relative transcript levels of selected genes encoding metabolic enzymes measured by inventoried TaqMan Gene Expression Assays in a primary rat brain endothelial cell-based BBB model (EPA) and in epithelial cell line models (Caco-2, VB-Caco-2, MDCK and MDCK-MDR1). NA: assay not available.

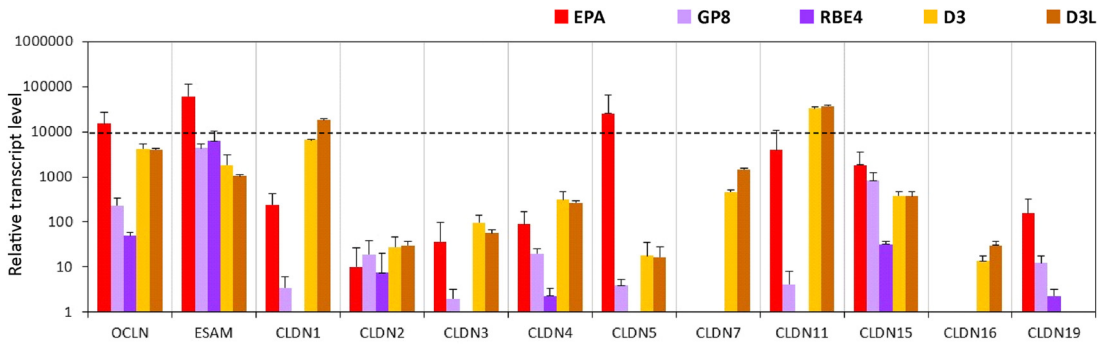

FIGURE 5 | Relative transcript levels of selected genes encoding tight junction proteins measured by inventoried TaqMan Gene Expression Assays in a primary rat brain endothelial cell-based BBB model (EPA) and in brain endothelial cell line models (GP8, RBE4, D3 and D3L).

Figure 4). Caco-2 cells expressed a high level of both GSTP1 and GSTA1 genes of the glutathione S-transferase enzyme. The expression level of the sulfotransferase 1A1 (SULT1A1) gene was low in Caco-2 cells, moderate in EPA and high in the MDCK cell lines. The expression level of the drug metabolizing enzyme UDP-glucuronosyltransferase UGT1A1 gene was moderate in the EPA model and high in Caco-2 cells (**Figure 4**). The relative expression levels of all the measured genes in the BBB and the epithelial models are shown in Supplementary Table S2.

Comparison of the Triple Co-culture BBB Model With GP8, RBE4 and D3 Brain Endothelial Cell Lines: Expression of Selected Tight Junction Protein, Transporter and Metabolic Enzyme Genes

Tight Junction Proteins

The expression level of occludin is high in the EPA and the D3 models but low in the rat GP8 and RBE4 cell lines (**Figure 5**, Supplementary Figure S5). The endothelial cell specific adhesion molecule (ESAM) was expressed at high levels in all brain endothelial cell models and was the highest in primary rat brain endothelial cells. The level of CLDN5 mRNA was significantly higher in the primary EPA model than in any of the cell lines (**Figure 5**). The expression of the CLDN5 gene in the RBE4 cell line was below the detection limit. Among the claudins, the expression of the epithelial specific CLDN2 and -4 genes, was lower in the endothelial than in the epithelial models, while CLDN7 and CLDN16 was not expressed in the rat BBB models, only in the human D3 cells (**Figure 5**). The CLDN1 and CLDN11 genes were expressed in the EPA and D3 models, their transcript levels were low in GP8 cells and absent in RBE4 cells. With the exception of ESAM, occludin and CLDN15 all of the tested TJ protein genes were not or expressed at low level in the rat GP8 and RBE4 cell lines. The lithium treatment did not change the transcript profile of the TJ protein genes in the D3L model compared to the untreated D3 cells.

Solute Carriers and Other Transporters

The expression levels of glucose transporters GLUT1 and -3 genes were the highest in the EPA model. These two carriers were also well transcribed in the other four cell lines, except for GLUT3 in GP8 cells. In the D3 and GP8 models the primary glucose transporter was GLUT1, while in RBE4 cells it was GLUT3 (**Figure 6**, Supplementary Figure S6). The mRNA level

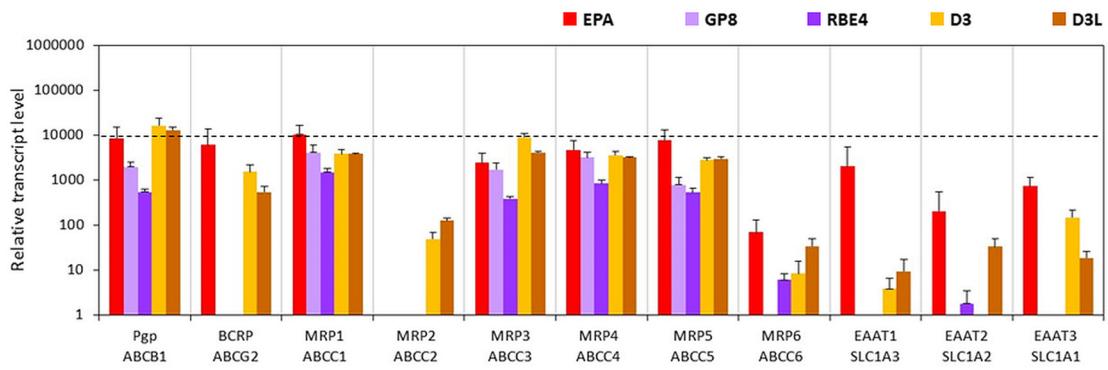

FIGURE 6 | Relative transcript levels of selected genes encoding SLC and other nutrient transporters measured by inventoried TaqMan Gene Expression Assays in a primary rat brain endothelial cell-based BBB model (EPA) and in brain endothelial cell line models (GP8, RBE4, D3 and D3L).

of the GLUT5 gene was low in all tested endothelial models, and not expressed in RBE4 cells. The monocarboxylic acid carrier MCT1 gene was also well expressed in all brain endothelial cells except for RBE4. The MCT8 expression was the highest in the EPA model. The MCT6 gene expression was at a moderate level in all cell types.

From the seven amino acid transporters examined, high expression level was measured for CAT1, LAT1 and SAT2 genes in all models. In the human D3 cells, the expression of XCT, SAT1 and SNAT5 genes was higher than in the rat BBB models. The SN1 transcript level was high in the EPA model and moderate in D3 cells. GP8 and RBE4 rat brain endothelial cell lines expressed low level of SN1 and did not express SNAT5. From the two tested peptide transporters PEPT1 was not expressed in brain endothelial models (**Figure 6**). The PHT2 gene expression level was moderate in the EPA and D3 models and low in GP8 and RBE4 cells.

The fatty acid transporter FATP1 gene was equally well expressed in all BBB models. From the lipid transporters, the ABCA2 gene was expressed in all models at a moderate level. The highest mRNA level of ABCA8 was measured in D3 and D3L cells. In the EPA model, the ABCA8 gene expression was low and in GP8 and RBE4 cell lines it was not expressed. The highest expression of the MFSD2A gene coding for the CNS transporter for docosahexaenoic acid was measured in the D3 cells. The transcription MFSD2A occurred at a moderate level in the EPA model, but not in GP8 and RBE4 cells (**Figure 6**).

From the SLC6 family, moderate expression levels were measured for the genes of creatine (CRT), glycine (GLYT1) and taurine (TAUT) carriers in all brain endothelial cells (**Figure 6**) except of the TAUT gene, which was expressed at a low level in GP8 and RBE4 cells. The genes of the vitamin transporters, SMVT and ASCT2 were well expressed in all endothelial models, only the ASCT2 mRNA level was low in GP8 cells (**Figure 6**). The gene of the organic anion-transporting polypeptide OATP1C1 was expressed only in the primary EPA model but not in the brain endothelial cell lines. Lithium treatment in D3 cells elevated the expression level in half of the tested carriers and transporter genes (GLUT3, -5, MCT8, SN1, SNAT5, PEPT1, FATP1, ABCA2, GLYT1, TAUT, CRT, ASCT2; **Figure 6**).

Efflux Transporters

The gene of one of the main efflux transporters of the BBB, Pgp was well expressed in both the EPA (Abcb1a, **Figure 7**; Abcb1b, Supplementary Table S3) and the D3 models. The BCRP gene expression was also high in the EPA but lower in the D3 models. Compared to the EPA and D3 models, the expression level of the Abcb1a gene was lower in the GP8 and RBE4 cells, while the BCRP transcript level was below the detection limit in these models (**Figure 7**, Supplementary Figure S7). The genes of the ABC transporter subfamily C members MRP1, 3, 4, 5 were well expressed in all models. The lowest expression for these genes was seen in RBE4 cells. MRP2 was only expressed in the D3 models. The MRP6 gene expression was the highest in the primary EPA model, very low in the other endothelial models and not detected in GP8 cells. The genes of the glutamate efflux transporters EAAT1, -2, -3 were expressed at high and moderate levels in the EPA model, lower levels in D3 cells and at a negligible level in the rat brain endothelial cell lines (**Figure 7**). In D3 cells a trend for elevation in gene expression was observed for MRP2, -6 and EAAT1, while an increase was seen in EAAT2 expression.

Metabolic Enzymes

We found two cytochrome P450 enzymes, CYP2U1 and CYP27A1 from the tested 12 isoforms which were expressed in all brain endothelial models (**Figure 8**, Supplementary Figure S8). No gene expression was seen for Cyp1a2, Cyp2c11, Cyp2e1 and Cyp7a1 genes in the EPA model, however these genes (CYP1A2, CYP2C9, CYP2E1, CYP7A1) were expressed in D3 cells. In the primary EPA model, the Cyp2d4, in D3 brain endothelial cells the CYP2S1 and CYP2U1 transcript levels were the highest among the genes of the selected phase I enzymes (**Figure 8**). GP8 cells did not express Cyp genes except for the Cyp2d4, Cyp2u1 and Cyp27a1 genes. In RBE4 cells only 3 Cyp enzyme genes, Cyp1a1, Cyp2u1 and Cyp27a1, were well expressed, while the others were expressed at very low or negligible levels.

The gene expression level of the GSTP1 phase II enzyme was high in all models (**Figure 8**). The GSTA1, SULT1A1 and UGT1A1 genes were expressed in the EPA and were absent or very low in the other brain endothelial models (**Figure 8**).

Evaluation of the Barrier Integrity in Brain Endothelial and Epithelial Models

Among the brain endothelial cell-based models the TEER was the highest in the primary cell-based BBB model (475 ± 48 Ω cm^2; **Table 1**). Both native Caco-2 (854 ± 24 Ω cm^2) and vinblastine selected VB-Caco-2 (1186 ± 71 Ω cm^2) models showed a tight paracellular barrier. The MDCK, MDCK-MDR1, RBE4, D3 and D3L cultures presented a TEER that was below 100 Ω cm^2. Treatment with lithium significantly elevated the TEER of D3 cells (unpaired *t*-test, $P < 0.0004$). The lowest resistance was measured in the GP8 cell line model. The EPA and the epithelial models were the least permeable for both fluorescein, a low molecular weight marker of paracellular integrity, and for Evans blue-labeled albumin, the marker of transcellular permeability (**Table 1**). All the four brain endothelial cell lines demonstrated significant, one order of magnitude higher values of P_{app} for both markers (**Table 1**).

The confluent, non-overlapping, uniform monolayer of cells in all investigated models was well visible on both the phase contrast images and the immunostainings for junctional proteins (**Figure 9**). The most striking difference in the pattern of endothelial cells compared to epithelial cells was the cell shape. Endothelial cells were elongated, fusiform, and formed a swirling pattern well observable on **Figure 9**. Primary brain endothelial cells in the EPA model gave a strong pericellular staining for claudin-5, the most abundant claudin type at the BBB. Claudin-5 staining was concentrated to the cell border at the interendothelial junctions. In the brain endothelial cell lines, the claudin-5 staining was cytoplasmic and not visible at the cell border (**Figure 9**, Supplementary Figure S9). Epithelial cells presented characteristic "cobblestone" morphology. In accordance with the gene expression data

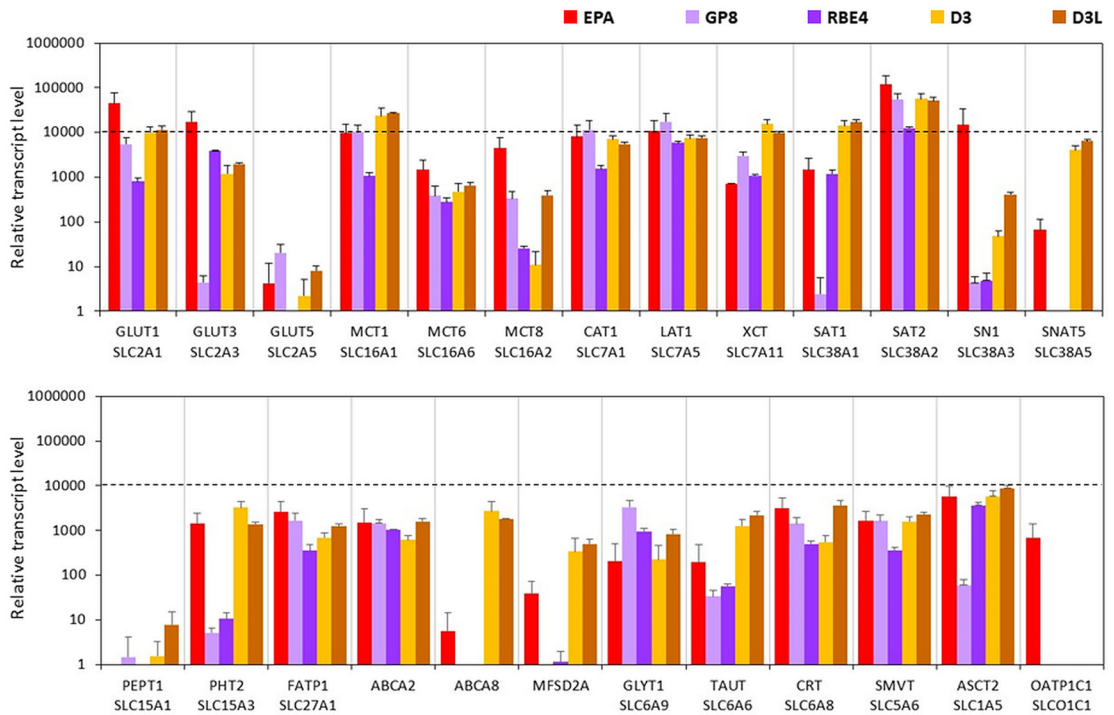

FIGURE 7 | Relative transcript levels of selected genes encoding efflux transporters measured by inventoried TaqMan Gene Expression Assays in a primary rat brain endothelial cell-based BBB model (EPA) and in brain endothelial cell line models (GP8, RBE4, D3 and D3L).

(**Figure 1**) epithelial cells stained intensely for claudin-4 (**Figure 9**), a TJ protein typical for epithelial cells.

SLC Related Drug Transport in the Culture Models

The selected nine ligands for SLCs were tested on the BBB and the four epithelial models. Drug penetration in the apical to basal (A-B) direction (P_{app}) and the PDR ratio (PDR: P_{app} B-A/P_{app} A-B) are shown in **Table 2**. The GLUT1 ligand 3-O-methyl-D-glucopyranose was transported in all models. PDR ratios indicating active influx was observed in the case of EPA and Caco-2 models. Among the clinically used drugs in the case of LAT1 substrates, the highest permeability values were measured for valproic acid on all models (**Figure 10**). Baclofen penetration was the highest in the EPA model, while it was very low across the epithelial cell layers. In this group of drugs, the lowest P_{app} was measured for gabapentin on all models. None of the LAT1 ligand drugs were identified as efflux pump ligands based on the PDR (**Table 2**). To further prove the functionality of LAT1, L-DOPA (3, 4-dihydroxy-L-phenylalanine) transport was measured in the EPA model in two

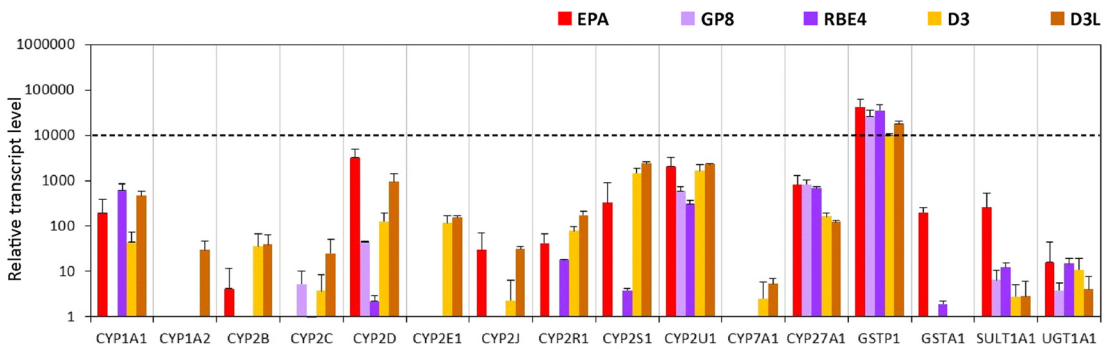

FIGURE 8 | Relative transcript levels of selected genes encoding metabolic enzymes measured by inventoried TaqMan Gene Expression Assays in a primary rat brain endothelial cell-based BBB model (EPA) and in brain endothelial cell line models (GP8, RBE4, D3 and D3L).

TABLE 1 | Paracellular tightness of different brain endothelial and epithelial cell culture models measured by transendothelial/epithelial electrical resistance (TEER) and permeability for markers fluorescein and albumin.

Models	TEER (Ω × cm^2)	Fluorescein P_{app} (10^{-6} cm/s)	Albumin P_{app} (10^{-6} cm/s)
EPA	475 ± 48	2.1 ± 0.25	0.2 ± 0.03
CaCo2	854 ± 24	1.5 ± 0.28	0.8 ± 0.09
VB-CaCo2	1186 ± 71	0.3 ± 0.06	0.2 ± 0.08
MDCK	72 ± 9	2.8 ± 0.23	0.6 ± 0.05
MDCK-MDR1	81 ± 7	2.7 ± 0.31	-
GP8	28 ± 13	39.8 ± 3.51	16.5 ± 7.51
RBE4	64 ± 5	27.4 ± 1.63	3.9 ± 0.23
D3	45 ± 2	22.2 ± 3.71	2.1 ± 0.31
D3L	86 ± 6	19.3 ± 1.22	1.7 ±0.12

P_{app}: apparent permeability coefficients. Values are presented as mean ± SD.

directions. We observed a high P_{app} in A-B direction (73 ± 4 10^{-6} cm/s) and a low PDR (0.4). The second highest P_{app} value was measured for the organic anion probenecid, especially in the Caco-2 models (**Table 2**). The other organic anion, salicylic acid had a low permeability in the BBB model as compared with the epithelial models (**Figure 10**). Among the tested three statins, rosuvastatin and pravastatin had significantly higher P_{app} in the BBB model than in the Caco-2 or MDCK cells. In the statin group the lowest P_{app} value in A–B direction and the highest PDR (1.4) was measured for atorvastatin in the EPA model, indicating that atorvastatin may be the subject of active efflux transport. Parallel to the low penetration, the PDR for

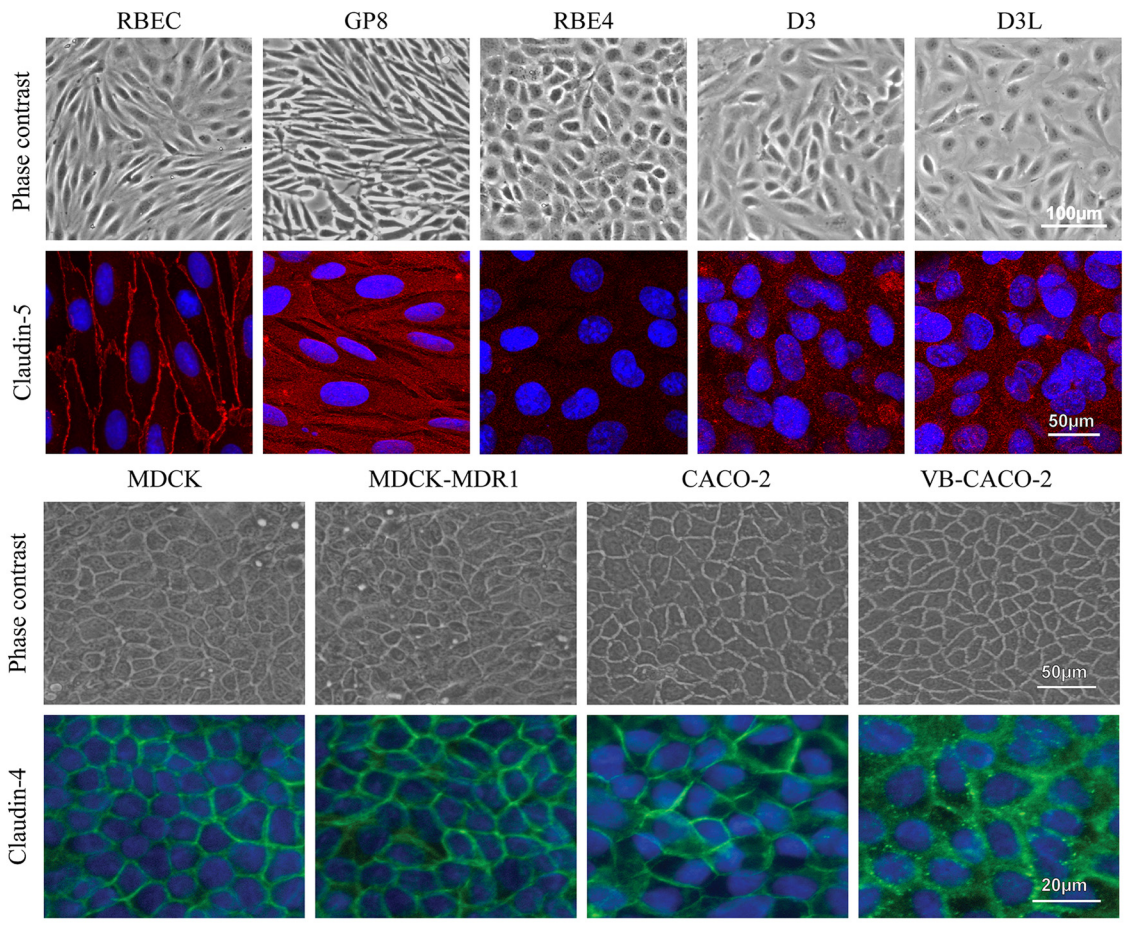

FIGURE 9 | Different types of brain endothelial and epithelial cell cultures examined by phase contrast microscopy and stained for tight junction proteins CLDN5 (red) and CLDN4 (green), and cell nucleus (blue). The CLDN5 immunostaining was well visible on the cell border of RBEC cells, while it was very weak or undetectable in the brain endothelial cell lines. MDCK and Caco-2 epithelial cells showed an intense staining for CLDN4. Bars: 50 and 100 µm (phase contrast pictures); 20 and 50 µm (immunostaining pictures).

TABLE 2 | Permeability coefficients (P_{app}) for selected drugs on the primary rat brain endothelial cell-based BBB model (EPA) and in epithelial cell line models (Caco-2, VB-Caco-2, MDCK and MDCK-MDR1) measured in the apical to basal (A-B) direction.

Ligands	SLC	EPA		Caco-2		VB-Caco-2		MDCK		MDCK-MDR1	
		P_{app} A-B	PDR	P_{app} A-B	PDR	P_{app} A-B	PDR	P_{app} A-B	PDR	P_{app} A-B	PDR
Glucopyranose	GLUT1	<65.7	>0.14	57.83	0.64	17.17	1.17	<18.5	NA	<18.5	NA
Valproic acid	LAT1, OATPs	39.37	0.98	51.91	0.82	42.22	0.87	26.62	1.22	27.49	1.26
Baclofen	LAT1	16.34	0.85	1.23	0.77	0.31	0.47	1.28	0.77	0.68	0.82
Gabapentin	LAT1, Pgp, BCRP	2.98	0.92	1.80	0.77	<0.88	>0.27	3.35	0.28	4.75	0.42
Probenecid	MCT, OATs	18.96	0.79	27.34	0.88	33.39	0.88	19.37	0.83	17.23	0.98
Salicylic acid	MCT1, OATPs, MRP4	4.78	1.88	16.63	1.11	7.60	1.19	13.01	0.86	9.31	0.85
Rosuvastatin	OATPs, Pgp, MRP2, BCRP	11.31	0.80	0.92	9.41	0.38	12.80	0,.9	0.52	0.81	1.13
Pravastatin	OATPs, MRP2	7.61	1.14	1.50	0.90	0.19	0.80	0.58	2.40	0.30	1.09
Atorvastatin	OATPs, MCT, Pgp, MRP2, BCRP	3.93	1.44	7.53	1.28	2.98	4.34	2.36	1.09	1.66	5.76

BCRP, breast cancer resistance protein; GLUT1, glucose transporters; LAT1, large neutral amino acid transporter; MCT, monocarboxylic acid transporter; MRP, multidrug resistance-associated proteins; OAT, organic anion transporter; OATP, organic anion-transporting polypeptide; PDR, permeability directional ratio; Pgp, P glycoprotein.

the statins was higher in the epithelial than in the BBB model (**Table 2**).

We tested the penetration of two additional SLC ligands, the organic cation tacrine and donepezil on the EPA and VB-Caco-2 models (**Figure 11A**). The P_{app} of these two anticholinergic CNS drugs were high among the tested SLC related drugs in the EPA model (donepezil: 63 ± 13 10^{-6} cm/s; tacrine: 102 ± 27 10^{-6} cm/s). In primary brain endothelial cells significantly higher P_{app} values were measured for both drugs compared to those of the epithelial cells. The permeability of donepezil was higher in the A-B direction (blood-to-brain) in the BBB model indicating preferential influx transport. In the epithelial model the donepezil permeability was higher in the opposite, B-A (brain-to-blood) direction as reflected in their PDR values (0.85 in EPA vs. 1.78 in VB-Caco-2). In the BBB model the penetration of both drugs could be inhibited significantly with the endogenous cationic metabolites/nutrients choline and carnitine (**Figure 11B**), indicating that the drugs and the endogenous ligands may share common transporter(s).

DISCUSSION

A large number of BBB culture models are used in basic as well as applied research and detailed characterization and comparative datasets are needed to select the appropriate model for a particular research aim. However, such studies are scarce. The present work on nine different primary cell and cell line-based models is unique, no such comparative study with gene expression data, paracellular tightness and drug transport has been published previously.

Comparison of EPA BBB Model to Epithelial and Brain Endothelial Cell Lines: TJ Pattern and Paracellular Barrier Tightness

Our results confirm that the mRNA pattern of TJ proteins in the primary culture-based EPA BBB model differs from the pattern seen in epithelial cells (**Figure 12**). In the Caco-2 and MDCK cells the highest expression was measured for CLDN1, CLDN3, CLDN4 and CLDN7 genes, which is a typical pattern for intestinal epithelium *in vivo* (Chiba et al., 2008). In contrast to Caco-2 epithelial cells and in agreement with brain capillary data CLDN19, which has a tightening potential could be detected in the rat BBB model (Ohtsuki et al., 2008). Despite the different TJ transcript patterns, the TEER of epithelial cells, except for MDCK cells, was well above the critical threshold value of 150–200 Ω cm^2, signifying a paracellular integrity necessary for permeability assays (Gaillard and de Boer, 2000; Deli et al., 2005). The reason for the low TEER value of the kidney epithelial cells is the high expression of the genes encoding the pore forming CLDN2, CLDN7 and CLDN16 which facilitate cation permeability, thereby decrease TEER (Krause et al., 2008). In spite of the low TEER values, MDCK cells form a tight paracellular barrier for small marker molecules

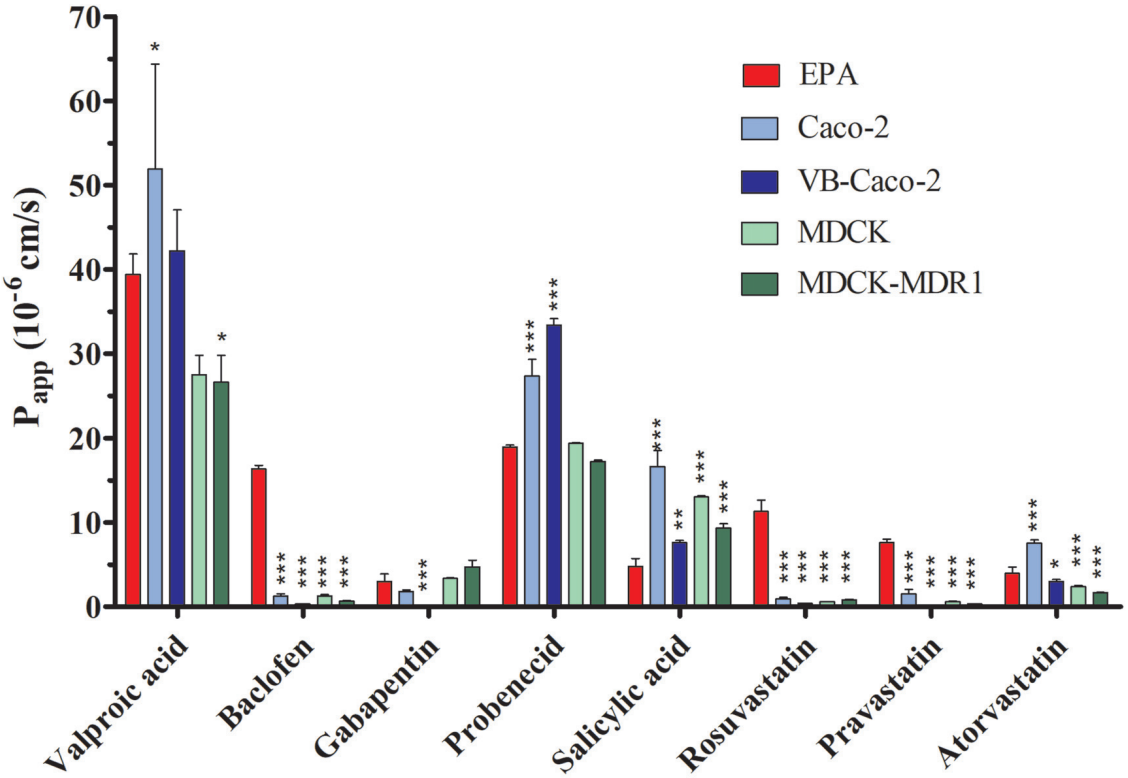

FIGURE 10 | Permeability coefficients (P_{app}) for selected drugs on primary rat brain endothelial cell-based BBB model (EPA) and in epithelial cell line models (Caco-2, VB-Caco-2, MDCK and MDCK-MDR1) measured in the apical to basal (blood-to-brain) direction. Statistics: mean ± SD, $n = 4$, ANOVA and Dunnett test; $^{*}P < 0.05$, $^{**}P < 0.01$; $^{***}P < 0.001$ compared to control.

of passive permeability (Veszelka et al., 2011; Hellinger et al., 2012).

In agreement with literature data on gene expression of rodent brain microvessels (Enerson and Drewes, 2005; Ohtsuki et al., 2008) and according to our expectations the endothelial specific ESAM and CLDN5 were measured in the EPA at the highest expression level. ESAM was described as a cell surface protein present at interendothelial cell contacts (Nasdala et al., 2002). It is expressed in all vascular endothelium. ESAM immunostaining was localized to the cell border in bEnd.3 mouse brain endothelial cell line, and co-localized with TJ proteins claudin-5 and occludin in mouse brain capillaries by electron microscopy (Nasdala et al., 2002). While claudin-5 is known to tighten BBB, no functional data are known on how ESAM contributes to brain endothelial barrier tightness.

The only transmembrane TJ protein that was unequivocally proven to contribute to the restriction of hydrophilic small molecule permeability at the BBB *in vivo* is claudin-5 (Nitta et al., 2003), this was the reason why we selected CLDN5 protein for immunostaining. CLDN5 immunostaining was well visible on the cell border of brain endothelial cells in co-culture indicating junctional tightness verified by TEER and permeability measurements. The low expression level of the CLDN5 and occludin genes measured in all the immortalized brain endothelial cell lines is responsible for the weak paracellular barrier properties, the low TEER and the high permeability values. In accordance with the gene expression data, the CLDN5 immunostaining was very weak or undetectable in these cells. Since these cell lines do not form a restrictive paracellular barrier, they are not suitable for screening small molecular drug candidates (Veszelka et al., 2011).

In the case of brain endothelial cell lines, culture media that were originally described for them were used. The culture medium of the D3 cell line contained more supplements than the medium of the primary brain endothelial cells. Despite this complex medium D3 cells still did not form a tight barrier, indicating that the cells' intrinsic properties are responsible for the weak junctions. To improve barrier properties, brain endothelial cell lines have already been examined in co-culture conditions. Co-culture data on the rat cell lines, RBE4 and GP8, were summarized in our previous review (Deli et al., 2005). In RBE4 cells the permeability of the sucrose marker molecule was in all conditions higher than the accepted level for small molecule testing (Deli et al., 2005). Co-culture of GP8 rat brain endothelial cells with C6 glioma still resulted in very low TEER and high fluorescein permeability values (Deli et al., 2005). These data indicate, that the weak barrier properties of these two rat cell lines were not significantly

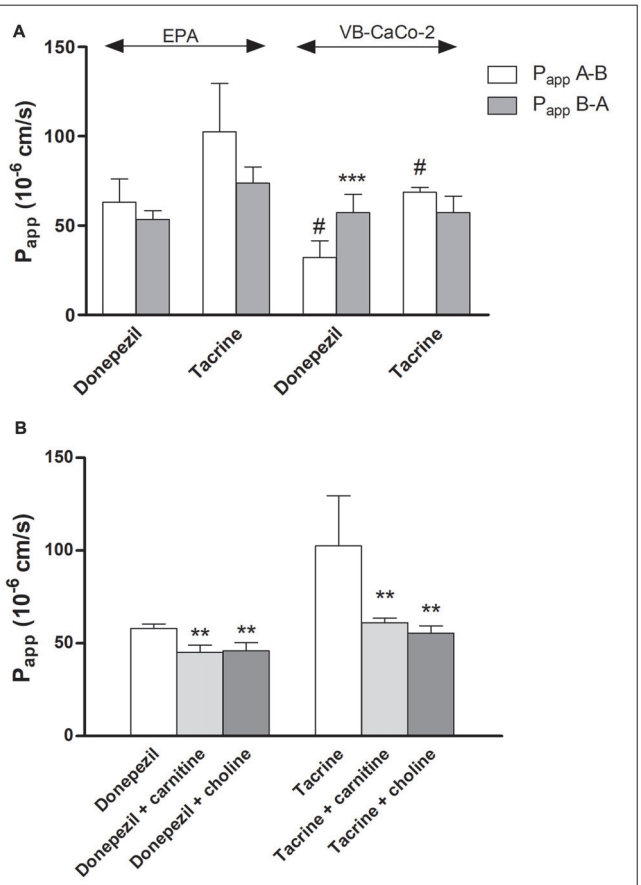

FIGURE 11 | Permeability coefficients (P_{app}) for donepezil and tacrine on primary rat brain endothelial cell-based BBB model (EPA) and epithelial cell line VB-Caco-2 **(A)**. Transport of donepezil and tacrine in the presence of choline (50 μM) and L-carnitine (50 μM) on the EPA model **(B)**. Statistics: mean ± SD, $n = 4$, two-way ANOVA and Bonferroni test; $^{**}P < 0.01$; $^{***}P < 0.001$ compared to control; $^{\#}P < 0.05$ compared to EPA.

improved by astrocytic influence. The basic permeability of D3 monolayers is about 10 times higher for small molecule tracers than in primary BBB models (Helms et al., 2016), similarly to our findings. Co-culture of D3 cells with both human astrocytes and pericytes did not elevate TEER as compared to mono-cultures (Hatherell et al., 2011; Helms et al., 2016). Taken together, these literature data indicate, that cell culture supplements and co-culture conditions do not improve the barrier tightness of the examined brain endothelial cell lines to such an extent that they would be suitable for drug penetration screening.

Comparison of EPA BBB Model to Epithelial and Brain Endothelial Cell Lines: Efflux Transporters

Pgp and BCRP were identified as the two primary efflux transporters at the BBB in both human (Shawahna et al., 2011; Uchida et al., 2011) and rat brain microvessels (Enerson and Drewes, 2005; Hoshi et al., 2013). The rat EPA BBB model expressed a similarly high amount of mRNA for Pgp and BCRP. In native Caco-2 cells the expression of Pgp and BCRP genes was lower than in the EPA model (**Figure 12**). Vinblastine treatment significantly elevated the Pgp gene expression in VB-Caco-2 cells in agreement with the literature data (Hellinger et al., 2010). MDCK-MDR1 cells also expressed a higher level of the ABCB1 gene that can contribute to the high efflux potential of this cell line in agreement with our previous results (Hellinger et al., 2012). In the MDCK and MDCK-MDR1 cell lines the mRNA levels of ABCB1 determined by RT-qPCR and protein levels of Pgp determined by Western blot correlated very well (Gartzke and Fricker, 2014), suggesting that for this important BBB efflux pump mRNA levels may reflect well protein levels. We have verified in our previous work that Pgp protein is present in the rat EPA BBB model, and in the VB-Caco-2 and MDCK-MDR1 cells (Hellinger et al., 2012). In addition to Pgp, MRP1 was demonstrated at protein level by both Western blot and immunohistochemistry in our EPA model (Nakagawa et al., 2009). The canine kidney cells did not express BCRP, as it was demonstrated in an independent study (Quan et al., 2012), which should be taken into account for drug efflux studies. In the epithelial cell lines, the most dominant efflux transporters were MRP2 and MRP3, while in the EPA model MRP1 and MRP5. The data on epithelial cells are in concordance with the findings of Hayeshi et al. (2008) and Quan et al. (2012).

In RBE4 cells the Pgp mRNA expression was the lowest among brain endothelial cell lines, the BCRP gene expression was below the detection limit, and the transcript level of other ABC transporters was also low. In GP8 cells also lower Pgp mRNA level was measured, while BCRP and MRP6 genes were not expressed. Based on these data the usage of rat RBE4 or GP8 cell lines for (efflux) drug screening is not suggested. We measured a high gene expression for Pgp in the human D3 cell line and they also expressed BCRP. In D3 cell plasma membrane fractions high protein expression for Pgp, MRP1 and MRP4 were measured by LC-MS/MS-based protein quantification analysis (Ohtsuki et al., 2013), supporting our present mRNA findings.

EAAT transporters participate in the efflux transport of glutamate across the BBB and are responsible for the low level of glutamate in the brain interstitial fluid (Helms et al., 2017). L-glutamate is taken up via EAAT1 at the abluminal membrane of brain endothelial cells and exits at the luminal membrane via a low affinity glutamate/aspartate transporter. Among EAAT transporter genes, the EAAT1 gene was expressed at the highest level in brain endothelial cells while in Caco-2 and MDCK cells the expression level of EAAT3 was the highest. The mRNA level of the EAAT2 was very low in Caco-2 cells and it was not expressed in MDCK cells. In contrast to the EPA BBB model, the expression of EAAT genes was negligible in brain endothelial cell lines except for D3 cells in which the EAAT3 gene was expressed at a low level. Our results support the findings of Helms et al. (2012). They demonstrated the presence of EAAT1, -2 and -3 mRNA in brain endothelial cells by conventional RT-PCR and the localization of EAAT1 and -3 in endothelial cells by immunostaining.

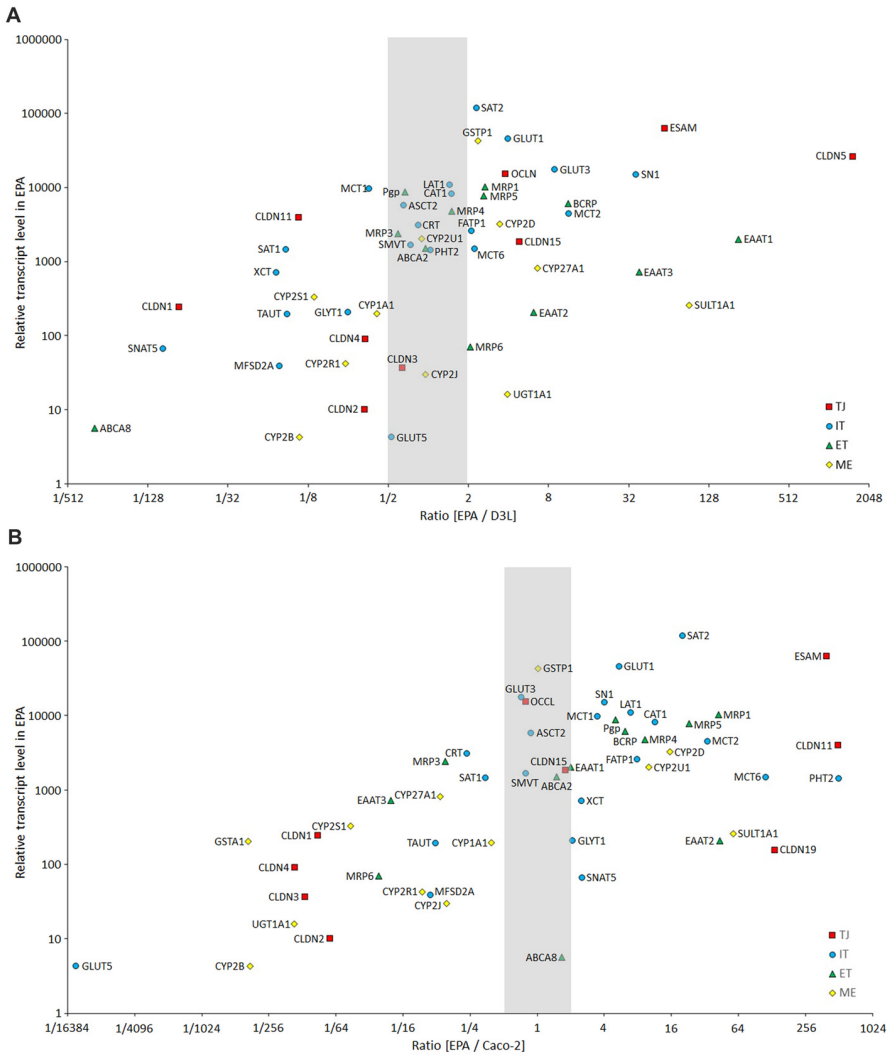

FIGURE 12 | Comparison of the expression of selected BBB genes between the primary rat brain endothelial cell-based EPA model and the human brain endothelial cell line D3 **(A)**, and the human intestinal cell line Caco-2 **(B)** measured by inventoried TaqMan Gene Expression Assays. The figure shows the ratio between the gene expression level of tight junction proteins (TJ, red square), influx transporters (IT, blue dot), efflux transporters (ET, green triangle) and selected metabolic enzymes (ME, yellow diamond) in EPA and D3 or Caco-2 cells. The graph also displays the expression values in the EPA sample on the y-axis to demonstrate the level of expression of studied genes.

Comparison of the EPA BBB Model to Epithelial and Brain Endothelial Cell Lines: Metabolic Enzymes

Endothelial cells of brain capillaries express enzymes that are capable of modifying drugs and xenobiotics that could bypass the BBB and thereby protect the CNS from the potential harmful effects of these molecules (Deli, 2011). Specific phase I and phase II enzymes participate in the formation of this metabolic barrier, with a supposed role in local drug metabolism and transport. Our data confirm that cultured brain endothelial cells express genes for phase-I and phase-II drug-metabolizing enzymes in levels comparable to epithelial cells (**Figure 12**). Among the cytochrome P450 enzymes, the CYP2D6 and the CYP2U1 mRNA levels were the highest in the EPA BBB model. CYP2D6 is involved in the hepatic metabolism of many clinically used drugs, while CYP2U1 is an extrahepatic isoform expressed in the thymus and brain, which metabolize arachidonic acid and other long chain fatty acids (Dauchy et al., 2009). In Caco-2 cells, the gene of extrahepatic CYP2S1 enzyme, which metabolizes naphthalene, was expressed at the highest level. Only two enzyme genes, CYP1A2 and CYP2E1 could be tested in MDCK canine cells, which were not expressed. Gene probes for other CYP enzymes in this species were unavailable. In D3 cells the CYP2S1 and the CYP2U1 genes were most dominantly expressed, in concordance with the data of Dauchy et al. (2009). In GP8 and RBE4 cell lines all the genes of the tested phase-I enzymes were expressed at very low or negligible levels except for the CYP1A1 gene in RBE4 cells, which encodes an enzyme metabolizing arachidonic acid and

other polyunsaturated fatty acids into signaling molecules. We found in a previous work that the arachidonic acid metabolism and the vasoactive properties of GP8 and RBE4 cell lines are altered compared to primary brain endothelial cells (Kis et al., 1999).

From the tested phase-II metabolic enzymes involved in the cellular detoxification processes, the glutathione S-transferase π (GSTP1) gene was expressed at the highest level in the EPA model. GSTP1 is expressed in brain capillaries, where it colocalizes to a large extent with MRP2 at the luminal plasma membrane of brain endothelial cells (Bauer et al., 2008). Colocalization and coordinated upregulation of MRP2 and GSTP1 by pregnane X receptor activation suggest functional coupling of this metabolizing enzyme and efflux transporter (Bauer et al., 2008). In Caco-2 cells, the genes of tested phase-II metabolic enzymes were transcribed at high levels, except SULT1A1. GSTP1 gene expression was high in brain endothelial cell lines. GSTA1, SULT1A1 and UGT1A1 genes were expressed in the EPA, but were absent or detected at very low level in brain endothelial cell lines. Summarizing these data, phase-I and phase-II metabolic enzymes are expressed in brain endothelial cells of the EPA model, suggesting a role in the regulation of local drug transport.

Comparison of the EPA BBB Model to Epithelial and Brain Endothelial Cell Lines: Influx Transporters and Drug Permeability

In the present study, we compared the expression levels of 25 influx and 11 efflux transporter genes in nine different culture models. To check the functionality of these transporters we tested nine different drugs on EPA, Caco-2 and MDCK cells, which showed the best paracellular tightness properties among the models. We excluded the brain endothelial cell lines, because they did not form a restrictive paracellular barrier to screening the permeability of small molecules.

The dominant SLC transporter for hexoses at the mammalian BBB is the GLUT1, which provides D-glucose, the primary source of energy for brain functions (Shawahna et al., 2011). The EPA model, expressed the highest level of the GLUT1 gene of all the models. We have previously verified the presence of GLUT1 protein by both Western blot and immunohistochemistry in the EPA model (Nakagawa et al., 2009). GLUT3 mRNA was also present in this BBB model, but at a lower level, in concordance with rat and human brain microvessel gene and protein data (Enerson and Drewes, 2005; Shawahna et al., 2011; Uchida et al., 2011; Hoshi et al., 2013). In contrast to BBB data, we found that in Caco-2 cells GLUT3 and GLUT5 are the dominant hexose transporters, not GLUT1. Similar mRNA data were obtained on Caco-2 cells by other groups (Hayeshi et al., 2008). SLC transporter genes, that were expressed at a high mRNA level in our study, like GLUT-1, MCT-1, LAT-1 and PEPT1 were all demonstrated in Caco-2 cells by proteomic analysis, too (Ölander et al., 2016). Moreover, a correlation was found between normalized mRNA rank and normalized protein abundance rank in Caco-2 cells for selected SLC genes (Ölander et al., 2016). The renal MDCK cell line expressed GLUT1 at high level, as it was already published (Quan et al., 2012), but not the other two GLUT transporters.

Similarly to the primary BBB model, the dominant glucose transporter in D3 cells was also GLUT1, in agreement with literature data (Carl et al., 2010; Urich et al., 2012; Ohtsuki et al., 2013). In GP8 cells the main glucose transporter was also GLUT1, while in RBE4 cells it was GLUT3. In RBE4, as well as in primary rat brain endothelial cells, both the 55 kDa GLUT1 and a 45–50 kDa band corresponding to brain GLUT3 were detected by Western blot analysis (Régina et al., 2001), in concordance with our mRNA findings. The expression level of the GLUT5 gene was low or not detectable in the endothelial cell lines. We tested GLUT1 functionality on the EPA model, and using glucopyranose as a transporter ligand (Bidder, 1968) we found a higher P_{app} value as compared to the epithelial cell lines and a very low PDR value, suggesting influx transport. These data are the first functional results on GLUT1 in a rat BBB culture model. The functionality of GLUT1 was only proved on bovine and human stem cell-based BBB culture models so far (Helms et al., 2016).

The MCT transporter family provides the CNS with the secondary energy source ketone bodies, like lactate, and also with thyroid hormones. Lactate is used by the human brain during development and the postnatal period, and in adult life during starvation, diabetes and ischemic insults to maintain energy homeostasis in the CNS (Campos-Bedolla et al., 2014). Lactate is bidirectionally transported by MCTs, among which the principal transporter at the BBB is MCT1 both in rodents and humans (Enerson and Drewes, 2005; Dahlin et al., 2009; Shawahna et al., 2011). The EPA model expressed high levels of all three tested MCT genes. Caco-2 cells expressed MCT1 at a lower level, and much less MCT8 and -6. MDCK cells did not express MCT1. In contrast, all brain endothelial cells except RBE4 expressed this transporter well. Besides monocarboxylates, MCTs participate also in the transport of drugs like salicylic acid or probenecid at the BBB (Enerson and Drewes, 2003; Bhattacharya and Boje, 2006). The functional presence of the MCT transporters at the EPA model was proved by the moderate permeability rate of probenecid, an organic anion, and a ligand for MCTs and organic anion transporter systems (OAT, SLC22; Deguchi et al., 2000). The low permeability of salicylic acid, a substrate for MCT1, OATP2 and MRP4 at the EPA model might be explained by the potential counteracting vectorial transport of SLC transporters and MRP efflux pumps. Significantly higher permeability was measured for probenecid on the Caco-2 cell lines, and for salicylic acid on the epithelial cells than on the BBB model, which might be explained by the different expression pattern for SLC and ABC transporters in the BBB model vs. epithelial cell lines.

All models expressed high levels of SLC transporters for amino acids, with significantly higher levels of large amino acid transporters CAT1, LAT1 and small amino acid transporters SAT2 and SN1 in the EPA model compared to epithelial models. The expression of LAT1 gene is the highest SLC in human brain microvessels (Shawahna et al., 2011), and is approximately 100-fold greater than in other tissues. LAT1, the most abundant amino acid carrier, is selectively expressed on both plasma membranes of brain capillaries. LAT1 supplies

leucine, tryptophan, tyrosine and phenylalanine to the brain and participates in the transport of drugs like L-DOPA, baclofen, valproic acid and gabapentin across the BBB (Ohtsuki and Terasaki, 2007). L-DOPA, a well-known example of LAT1 substrates, gave the highest P_{app} value among all tested drugs in the BBB model. For valproic acid, which is also transported by OATPs (Taogoshi et al., 2005), higher P_{app} values were measured in the Caco-2 and lower in the MDCK cell lines than in the EPA model. In the BBB model, baclofen had significantly higher P_{app} compared to the two epithelial cell lines. Similar results were obtained for baclofen on bovine brain endothelial cells vs. epithelial culture models (Hakkarainen et al., 2010). Among the LAT1 transported drugs, gabapentin, which has a significant efflux transport by ABC transporters (Nakanishi et al., 2013), had the lowest permeability on all five models. The transfer of gabapentin across the VB-Caco-2 cell line was below the detection limit, in accordance with the strong efflux properties of this cell line (Hellinger et al., 2012).

The gene expression of the tested two peptide transporters was strikingly different among the models. A high level of PEPT1 mRNA in the Caco-2 models and no expression in EPA and MDCK models, in contrast a high transcript level of PHT2 in the EPA model and no expression in Caco-2 models were measured, suggesting that peptide transport must be very different on these models. PHT2 was identified as a BBB-related SLC transporter in two independent studies (Enerson and Drewes, 2005; Dahlin et al., 2009), confirming our results. MFSD2A transports DHA in the form of lysophosphatidylcholine in a sodium-dependent manner. MFSD2A is selectively expressed in brain capillaries and mediate the brain uptake of DHA. The brain endothelial expression of MFSD2A is regulated by pericytes *in vivo* (Ben-Zvi et al., 2014). This is the first study to compare the gene expression level of this important BBB transporter in nine different models. The MFSD2A gene was expressed in all models, except in GP8 and RBE4 cell lines, and showed a higher mRNA expression in the epithelial models and D3 cells than in the EPA model. All models expressed high to moderate levels of mRNA for SLC transporters of fatty acids, glycine, taurine, creatinine and vitamin C. There was no significant difference in SLC transporter gene expression between Caco-2 and VB-Caco-2 cells, except down-regulation for MCT8. In the D3 cell line the highest expression among the SLC transporters was for SAT2, followed by GLUT1, LAT1 and MCT1 in our study, as well as in the literature (Carl et al., 2010; Urich et al., 2012). Lithium treatment of D3 cells, which increase BBB properties by the Wnt pathway (Weksler et al., 2013), upregulated the expression level in half of the tested carrier and transporter genes, such as GLUT3, -5, MCT8, SN1, SNAT5, PEPT1, FATP1, ABCA2, GLYT1, TAUT, CRT, ASCT2.

Exogenous substrates of OATPs include antibiotics, antidiabetic and anti-inflammatory drugs, antivirals, antihistamines, antihypertensives, immunosuppressants, and anticancer drugs, thus OATPs at the BBB are important regulators of CNS drug disposition (Campos-Bedolla et al., 2014). Statins were also identified as substrates of OATPs (Kalliokoski and Niemi, 2009). There is an increasing interest in statins to use them in neuronal diseases, such as stroke, Parkinson's disease, or Alzheimer's disease (Malfitano et al., 2014), but brain penetration is the key for their potential therapeutic efficacy. In the present study, the permeability of rosuvastatin, pravastatin and atorvastatin was compared on five models. The higher penetration of the tested three statins across the EPA model as compared to epithelial cells may be explained by the higher expression of Oatp-1a2 and -1c1 influx transporters in brain endothelial cells, and the stronger efflux mechanisms, especially MRP2 in epithelial cells. In agreement with our observation, very low apical to basal P_{app} values were measured for rosuvastatin and atorvastatin in Caco-2 cells (Li et al., 2011). In this article, the role of Pgp, BCRP, and MRP2 in the efflux transport of these statin was also proven.

Tacrine and donepezil are two anticholinergic drugs with good brain penetration, approved for the treatment of Alzheimer's disease. Using an immortalized brain endothelial cell line, the organic cation transporter-2 (OCT2, SLC22A2), the organic cation/carnitine transporter OCTN2 (SLC22A5), and the choline transporter CHT1 (SLC5A7) were identified as influx transporters of these drugs (Kang et al., 2005; Lee et al., 2012). We also found a high permeability for both drugs on the EPA BBB model. The endogenous cationic metabolites choline and carnitine could significantly inhibit the penetration of tacrine and donepezil, indicating that the drugs and the endogenous ligands may share common transporters. Lower permeability was measured for these two drugs on VB-Caco-2 cells, and for donepezil the basal to apical permeability was higher, in contrast to the EPA model.

In conclusion, our study reveals major differences in the gene expression patterns between the primary cell-based BBB model and epithelial or brain endothelial cell lines for several key BBB related genes. Epithelial cell line models showed appropriate paracellular tightness, even if the pattern for TJ protein genes were distinct between epithelial cell lines and the BBB model. Disparity in the gene expression of transporters between BBB and epithelial models were also reflected in the permeability of selected drugs. These findings emphasize the growing importance of SLC-mediated drug targeting to brain and the use of appropriate culture models. Among the tested culture models, the primary cell-based EPA model is suitable for the functional analysis of the BBB.

AUTHOR CONTRIBUTIONS

MD, SV, MV and GR: conceived and designed the experiments. SV, AT, FW, AT, IG, MM, AB and ÉH: performed the experiments. SV, AT, MV and MD: analyzed the data. MD, MV and GR: contributed reagents/materials/analysis tools. SV, AT, FW, AT, MV, GR and MD: wrote and edited the article.

FUNDING

This work was supported by the Hungarian Scientific Research Fund (OTKA/NKFIH 105622), the National Research,

Development and Innovation Office (GINOP-2.2.1-15-2016-00007, GINOP-2.3.2-15-2016-00060) and by EFOP-3.6.1-16-2016-00008. SV was supported by the János Bolyai Research Fellowship of the Hungarian Academy of Sciences (BO/00724/12).

REFERENCES

Abbott, N. J. (2013). Blood-brain barrier structure and function and the challenges for CNS drug delivery. *J. Inherit. Metab. Dis.* 36, 437–449. doi: 10.1007/s10545-013-9608-0

Artursson, P., Palm, K., and Luthman, K. (2001). Caco-2 monolayers in experimental and theoretical predictions of drug transport. *Adv. Drug Deliv. Rev.* 46, 27–43. doi: 10.1016/S0169-409X(00)00128-9

Avdeef, A., Deli, M. A., and Neuhaus, W. (2015). "*In vitro* assays for assessing BBB permeability: artificial membrane and cell culture models," in *Blood-Brain Barrier in Drug Discovery: Optimizing Brain Exposure of CNS Drugs and Minimizing Brain Side Effects for Peripheral Drugs*, eds L. Di and E. H. Kerns (New Jersey, NJ: John Wiley & Sons), 188–237.

Banks, W. A. (2016). From blood-brain barrier to blood-brain interface: new opportunities for CNS drug delivery. *Nat. Rev. Drug Discov.* 15, 275–292. doi: 10.1038/nrd.2015.21

Bauer, B., Hartz, A. M., Lucking, J. R., Yang, X., Pollack, G. M., and Miller, D. S. (2008). Coordinated nuclear receptor regulation of the efflux transporter, Mrp2, and the phase-II metabolizing enzyme, GSTpi, at the blood-brain barrier. *J. Cereb. Blood Flow Metab.* 28, 1222–1234. doi: 10.1038/jcbfm.2008.16

Ben-Zvi, A., Lacoste, B., Kur, E., Andreone, B. J., Mayshar, Y., Yan, H., et al. (2014). Mfsd2a is critical for the formation of the blood-brain barrier. *Nature* 509, 507–511. doi: 10.1038/nature13324

Bhattacharya, I., and Boje, K. M. (2006). Potential gamma-hydroxybutyric acid (GHB) drug interactions through blood-brain barrier transport inhibition: a pharmacokinetic simulation-based evaluation. *J. Pharmacokinet. Pharmacodyn.* 33, 657–681. doi: 10.1007/s10928-006-9029-x

Bidder, T. G. (1968). Hexose translocation across the blood-brain interface: configurational aspects. *J. Neurochem.* 15, 867–874. doi: 10.1111/j.1471-4159.1968.tb10333.x

Booth, R., and Kim, H. (2014). Permeability analysis of neuroactive drugs through adynamic microfluidic *in vitro* blood-brain barrier model. *Ann. Biomed. Eng.* 42, 2379–2391. doi: 10.1007/s10439-014-1086-5

Campos-Bedolla, P., Walter, F. R., Veszelka, S., and Deli, M. A. (2014). Role of the blood-brain barrier in the nutrition of the central nervous system. *Arch. Med. Res.* 45, 610–638. doi: 10.1016/j.arcmed.2014.11.018

Carl, S. M., Lindley, D. J., Das, D., Couraud, P. O., Weksler, B. B., Romero, I., et al. (2010). ABC and SLC transporter expression and proton oligopeptide transporter (POT) mediated permeation across the human blood—brain barrier cell line, hCMEC/D3. *Mol. Pharm.* 7, 1057–1068. doi: 10.1021/mp900178j

Chiba, H., Osanai, M., Murata, M., Kojima, T., and Sawada, N. (2008). Transmembrane proteins of tight junctions. *Biochim. Biophys. Acta* 1778, 588–600. doi: 10.1016/j.bbamem.2007.08.017

Cucullo, L., Hossain, M., Puvenna, V., Marchi, N., and Janigro, D. (2011). The role of shear stress in blood-brain barrier endothelial physiology. *BMC Neurosci.* 12:40. doi: 10.1186/1471-2202-12-40

Cucullo, L., Hossain, M., Tierney, W., and Janigro, D. (2013). A new dynamic *in vitro* modularcapillaries-venules modular system: cerebrovascular physiology in a box. *BMC Neurosci.* 14:18. doi: 10.1186/1471-2202-14-18

Dahlin, A., Royall, J., Hohmann, J. G., and Wang, J. (2009). Expression profiling of the solute carrier gene family in the mouse brain. *J. Pharmacol. Exp. Ther.* 329, 558–570. doi: 10.1124/jpet.108.149831

Dauchy, S., Miller, F., Couraud, P. O., Weaver, R. J., Weksler, B., Romero, I. A., et al. (2009). Expression and transcriptional regulation of ABC transporters and cytochromes P450 in hCMEC/D3 human cerebral microvascular endothelial cells. *Biochem. Pharmacol.* 77, 897–909. doi: 10.1016/j.bcp.2008.11.001

Deguchi, Y., Yokoyama, Y., Sakamoto, T., Hayashi, H., Naito, T., Yamada, S., et al. (2000). Brain distribution of 6-mercaptopurine is regulated by the efflux transport system in the blood-brain barrier. *Life Sci.* 66, 649–662. doi: 10.1016/s0024-3205(99)00637-2

Dehouck, M. P., Méresse, S., Delorme, P., Fruchart, J. C., and Cecchelli, R. (1990). An easier, reproducible and mass-production method to study the blood-brain barrier *in vitro*. *J. Neurochem.* 54, 1798–1801. doi: 10.1111/j.1471-4159.1990.tb01236.x

Deli, M. A. (2011). "Drug transport and the blood-brain barrier," in *Solubility, Delivery, and ADME Problems of Drugs and Drug-Candidates*, eds K. Tihanyi and M. Vastag (Washington, DC: Bentham Science Publ. Ltd.), 144–165.

Deli, M. A., Abrahám, C. S., Kataoka, Y., and Niwa, M. (2005). Permeability studies on *in vitro* blood-brain barrier models: physiology, pathology, and pharmacology. *Cell. Mol. Neurobiol.* 25, 59–127. doi: 10.1007/s10571-004-1377-8

Enerson, B. E., and Drewes, L. R. (2003). Molecular features, regulation, and function of monocarboxylate transporters: implications for drug delivery. *J. Pharm. Sci.* 92, 1531–1544. doi: 10.1002/jps.10389

Enerson, B. E., and Drewes, L. R. (2005). The rat blood—brain barrier transcriptome. *J. Cereb. Blood Flow Metab.* 26, 959–973. doi: 10.1038/sj.jcbfm.9600249

Evers, R., Kool, M., Smith, A. J., van Deemter, L., de Haas, M., and Borst, P. (2000). Inhibitory effect of the reversal agents V-104, GF120918 and Pluronic L61 on MDR1 Pgp-, MRP1- and MRP2-mediated transport. *Br. J. Cancer* 83, 366–374. doi: 10.1054/bjoc.2000.1260

Gaillard, P. J., and de Boer, A. G. (2000). Relationship between permeability status of the blood-brain barrier and *in vitro* permeability coefficient of a drug. *Eur. J. Pharm. Sci.* 12, 95–102. doi: 10.1016/s0928-0987(00)00152-4

Garberg, P., Bal, L. M., Borg, N., Cecchelli, R., Fenart, L., Hurst, R. D., et al. (2005). *In vitro* models of the blood-brain barrier. *Toxicol. in vitro* 19, 299–334. doi: 10.1016/j.tiv.2004.06.011

Gartzke, D., and Fricker, G. (2014). Establishment of optimized MDCK cell lines for reliable efflux transport studies. *J. Pharm. Sci.* 103, 1298–1304. doi: 10.1002/jps.23901

Greenwood, J., Pryce, G., Devine, L., Male, D. K., dos Santos, W. L., Calder, V. L., et al. (1996). SV40 large T immortalised cell lines of the rat blood-brain and blood-retinal barriers retain their phenotypic and immunological characteristics. *J. Neuroimmunol.* 71, 51–63. doi: 10.1016/s0165-5728(96)00130-0

Griep, L., Wolbers, F., de Wagenaar, B., ter Braak, P., Weksler, B., Romero, I. A., et al. (2013). BBB on chip: microfluidic platform to mechanically and biochemically modulate blood-brain barrier function. *Biomed. Microdevices* 15, 145–150. doi: 10.1007/s10544-012-9699-7

Hakkarainen, J. J., Jalkanen, A. J., Kääriäinen, T. M., Keski-Rahkonen, P., Venäläinen, T., Hokkanen, J., et al. (2010). Comparison of *in vitro* cell models in predicting *in vivo* brain entry of drugs. *Int. J. Pharm.* 402, 27–36. doi: 10.1016/j.ijpharm.2010.09.016

Hatherell, K., Couraud, P. O., Romero, I. A., Weksler, B., and Pilkington, G. J. (2011). Development of a three-dimensional, all-human *in vitro* model of the blood-brain barrier using mono-, co-, and tri-cultivation Transwell models. *J. Neurosci. Methods* 199, 223–229. doi: 10.1016/j.jneumeth.2011.05.012

Hayeshi, R., Hilgendorf, C., Artursson, P., Augustijns, P., Brodin, B., Dehertogh, P., et al. (2008). Comparison of drug transporter gene expression and functionality in Caco-2 cells from 10 different laboratories. *Eur. J. Pharm. Sci.* 35, 383–396. doi: 10.1016/j.ejps.2008.08.004

Hellinger, É, Bakk, M. L., Pócza, P., Tihanyi, K., and Vastag, M. (2010). Drug penetration model of vinblastine-treated Caco-2 cultures. *Eur. J. Pharm. Sci.* 41, 96–106. doi: 10.1016/j.ejps.2010.05.015

Hellinger, É, Veszelka, S., Tóth, A. E., Walter, F., Kittel, A., Bakk, M. L., et al. (2012). Comparison of brain capillary endothelial cell-based and epithelial (MDCK-MDR1, Caco-2, and VB-Caco-2) cell-based surrogate

SUPPLEMENTARY MATERIAL

The Supplementary Material for this article can be found online at: https://www.frontiersin.org/articles/10.3389/fnmol.2018.00166/full#supplementary-material

blood-brain barrier penetration models. *Eur. J. Pharm. Biopharm.* 82, 340–351. doi: 10.1016/j.ejpb.2012.07.020

Helms, H. C., Abbott, N. J., Burek, M., Cecchelli, R., Couraud, P. O., Deli, M. A., et al. (2016). *In vitro* models of the blood-brain barrier: an overview of commonly used brain endothelial cell culture models and guidelines for their use. *J. Cereb. Blood Flow Metab.* 36, 862–890. doi: 10.1177/0271678x16630991

Helms, H. C., Madelung, R., Waagepetersen, H. S., Nielsen, C. U., and Brodin, B. (2012). *In vitro* evidence for the brain glutamate efflux hypothesis: brain endothelial cells cocultured with astrocytes display a polarized brain-to-blood transport of glutamate. *Glia* 60, 882–893. doi: 10.1002/glia.22321

Helms, H. C. C., Nielsen, C. U., Waagepetersen, H. S., and Brodin, B. (2017). Glutamate transporters in the blood-brain barrier. *Adv. Neurobiol.* 16, 297–314. doi: 10.1007/978-3-319-55769-4_15

Hoheisel, D., Nitz, T., Franke, H., Wegener, J., Hakvoort, A., Tilling, T., et al. (1998). Hydrocortisone reinforces the blood-brain barrier properties in a serum free cell culture system. *Biochem. Biophys. Res. Commun.* 247, 312–315. doi: 10.1006/bbrc.1997.8051

Hoshi, Y., Uchida, Y., Tachikawa, M., Inoue, T., Ohtsuki, S., and Terasaki, T. (2013). Quantitative atlas of blood-brain barrier transporters, receptors, and tight junction proteins in rats and common marmoset. *J. Pharm. Sci.* 102, 3343–3355. doi: 10.1002/jps.23575

Kalliokoski, A., and Niemi, M. (2009). Impact of OATP transporters on pharmacokinetics. *Br. J. Pharmacol.* 158, 693–705. doi: 10.1111/j.1476-5381.2009.00430.x

Kang, Y. S., Lee, K. E., Lee, N. Y., and Terasaki, T. (2005). Donepezil, tacrine and a-phenyl-ntert- butyl nitrone (PBN) inhibit choline transport by conditionally immortalized rat brain capillary endothelial cell lines (TR-BBB). *Arch. Pharm. Res.* 28, 443–450. doi: 10.1007/bf02977674

Kis, B., Szabó, C. A., Pataricza, J., Krizbai, I. A., Mezei, Z., Gecse, A., et al. (1999). Vasoactive substances produced by cultured rat brain endothelial cells. *Eur. J. Pharmacol.* 368, 35–42. doi: 10.1016/s0014-2999(99)00024-2

Krause, G., Winkler, L., Mueller, S. L., Haseloff, R. F., Piontek, J., and Blasig, I. E. (2008). Structure and function of claudins. *Biochim. Biophys. Acta* 1778, 631–645. doi: 10.1016/j.bbamem.2007.10.018

Kürti, L., Veszelka, S., Bocsik, A., Dung, N. T., Ozsvári, B., Puskás, L. G., et al. (2012). The effect of sucrose esters on a culture model of the nasal barrier. *Toxicol. in vitro* 26, 445–454. doi: 10.1016/j.tiv.2012.01.015

Lee, N. Y., Choi, H. O., and Kang, Y. S. (2012). The acetylcholinesterase inhibitors competitively inhibited an acetyl L-carnitine transport through the blood-brain barrier. *Neurochem. Res.* 37, 1499–1507. doi: 10.1007/s11064-012-0723-3

Li, J., Volpe, D. A., Wang, Y., Zhang, W., Bode, C., Owen, A., et al. (2011). Use of transporter knockdown Caco-2 cells to investigate the *in vitro* efflux of statin drugs. *Drug Metab. Dispos.* 39, 1196–1202. doi: 10.1124/dmd.111.038075

Livak, K. J., and Schmittgen, T. D. (2001). Analysis of relative gene expression data using real-time quantitative PCR and the $2^{-\Delta\Delta C_T}$ method. *Methods* 25, 402–408. doi: 10.1006/meth.2001.1262

Malfitano, A. M., Marasco, G., Proto, M. C., Laezza, C., Gazzerro, P., and Bifulco, M. (2014). Statins in neurological disorders: an overview and update. *Pharmacol. Res.* 88, 74–83. doi: 10.1016/j.phrs.2014.06.007

Nakagawa, S., Deli, M. A., Kawaguchi, H., Shimizudani, T., Shimono, T., Kittel, A., et al. (2009). A new blood-brain barrier model using primary rat brain endothelial cells, pericytes and astrocytes. *Neurochem. Int.* 54, 253–263. doi: 10.1016/j.neuint.2008.12.002

Nakanishi, H., Yonezawa, A., Matsubara, K., and Yano, I. (2013). Impact of P-glycoprotein and breast cancer resistance protein on the brain distribution of antiepileptic drugs in knockout mouse models. *Eur. J. Pharmacol.* 710, 20–28. doi: 10.1016/j.ejphar.2013.03.049

Nasdala, I., Wolburg-Buchholz, K., Wolburg, H., Kuhn, A., Ebnet, K., Brachtendorf, G., et al. (2002). A transmembrane tight junction protein selectively expressed on endothelial cells and platelets. *J. Biol. Chem.* 277, 16294–16303. doi: 10.1074/jbc.M111999200

Nitta, T., Hata, M., Gotoh, S., Seo, Y., Sasaki, H., Hashimoto, N., et al. (2003). Size-selective loosening of the bloodbrain barrier in claudin-5-deficient mice. *J. Cell Biol.* 161, 653–660. doi: 10.1083/jcb.200302070

Ohtsuki, S., Ikeda, C., Uchida, Y., Sakamoto, Y., Miller, F., Glacial, F., et al. (2013). Quantitative targeted absolute proteomic analysis of transporters, receptors and junction proteins for validation of human cerebral microvascular endothelial cell line hCMEC/D3 as a human blood-brain barrier model. *Mol. Pharm.* 10, 289–296. doi: 10.1021/mp3004308

Ohtsuki, S., and Terasaki, T. (2007). Contribution of carrier-mediated transport systems to the blood-brain barrier as a supporting and protecting interface for the brain; importance for CNS drug discovery and development. *Pharm. Res.* 24, 1745–1758. doi: 10.1007/s11095-007-9374-5

Ohtsuki, S., Yamaguchi, H., Katsukura, Y., Asashima, T., and Terasaki, T. (2008). mRNA expression levels of tight junction protein genes in mouse brain capillary endothelial cells highly purified by magnetic cell sorting. *J. Neurochem.* 104, 147–154. doi: 10.1111/j.1471-4159.2007.05008.x

Ölander, M., Wiśniewski, J. R., Matsson, P., Lundquist, P., and Artursson, P. (2016). The proteome of filter-grown Caco-2 cells with a focus on proteins involved in drug disposition. *J. Pharm. Sci.* 105, 817–827. doi: 10.1016/j.xphs.2015.10.030

Paolinelli, R., Corada, M., Ferrarini, L., Devraj, K., Artus, C., Czupalla, C. J., et al. (2013). Wnt activation of immortalized brain endothelial cells as a tool for generating a standardized model of the blood brain barrier *in vitro*. *PLoS One* 8:e70233. doi: 10.1371/journal.pone.0070233

Pardridge, W. M. (2015). Blood-brain barrier endogenous transporters as therapeutic targets: a new model for small molecule CNS drug discovery. *Expert Opin. Ther. Targets.* 19, 1059–1072. doi: 10.1517/14728222.2015.1042364

Patabendige, A., Skinner, R. A., and Abbott, N. J. (2013). Establishment of a simplified *in vitro* porcine blood-brain barrier model with high transendothelial electrical resistance. *Brain Res.* 1521, 1–15. doi: 10.1016/j.brainres.2012.06.057

Perrière, N., Demeuse, P., Garcia, E., Regina, A., Debray, M., Andreux, J. P., et al. (2005). Puromycin-based purification of rat brain capillary endothelial cell cultures. Effect on the expression of blood-brain barrier-specific properties. *J. Neurochem.* 93, 279–289. doi: 10.1111/j.1471-4159.2004.03020.x

Prabhakarpandian, B., Shen, M.-C., Nichols, J. B., Mills, I. R., Sidoryk-Wegrzynowicz, M., Aschner, M., et al. (2013). SyM-BBB: a microfluidic blood brain barrier model. *Lab Chip* 13, 1093–1101. doi: 10.1039/c2lc41208j

Quan, Y., Jin, Y., Faria, T. N., Tilford, C. A., He, A., Wall, D. A., et al. (2012). Expression profile of drug and nutrient absorption related genes in Madin-Darby canine kidney (MDCK) cells grown under differentiation conditions. *Pharmaceutics* 4, 314–333. doi: 10.3390/pharmaceutics4020314

Régina, A., Morchoisne, S., Borson, N. D., McCall, A. L., Drewes, L. R., and Roux, F. (2001). Factor(s) released by glucose-deprived astrocytes enhance glucose transporter expression and activity in rat brain endothelial cells. *Biochim. Biophys. Acta* 1540, 233–242. doi: 10.1016/s0167-4889(01)00133-1

Roux, F., Durieu-Trautmann, O., Chaverot, N., Claire, M., Mailly, P., Bourre, J. M., et al. (1994). Regulation of gamma-glutamyl transpeptidase and alkaline phosphatase activities in immortalized rat brain microvessel endothelial cells. *J. Cell. Physiol.* 159, 101–113. doi: 10.1002/jcp.1041590114

Shawahna, R., Uchida, Y., Declèves, X., Ohtsuki, S., Yousif, S., Dauchy, S., et al. (2011). Transcriptomic and quantitative proteomic analysis of transporters and drug metabolizing enzymes in freshly isolated human brain microvessels. *Mol. Pharm.* 8, 1332–1341. doi: 10.1021/mp200129p

Szabó, C. A., Deli, M. A., Ngo, T. K., and Joó, F. (1997). Production of pure primary rat cerebral endothelial cell culture: a comparison of different methods. *Neurobiology* 5, 1–16.

Taogoshi, T., Nomura, A., Murakami, T., Nagai, J., and Takano, M. (2005). Transport of prostaglandin E1 across the blood-brain barrier in rats. *J. Pharm. Pharmacol.* 57, 61–66. doi: 10.1211/0022357055173

Tóth, A. E., Tóth, A., Walter, F. R., Kiss, L., Veszelka, S., Ózsvári, B., et al. (2014). Compounds blocking methylglyoxal-induced protein modification and brain endothelial injury. *Arch. Med. Res.* 45, 753–764. doi: 10.1016/j.arcmed.2014.10.009

Uchida, Y., Ohtsuki, S., Katsukura, Y., Ikeda, C., Suzuki, T., Kamiie, J., et al. (2011). Quantitative targeted absolute proteomics of human blood-brain barrier transporters and receptors. *J. Neurochem.* 117, 333–345. doi: 10.1111/j.1471-4159.2011.07208.x

Urich, E., Lazic, S. E., Molnos, J., Wells, I., and Freskgård, P. O. (2012). Transcriptional profiling of human brain endothelial cells reveals key properties crucial for predictive *in vitro* blood-brain barrier models. *PLoS One* 7:e38149. doi: 10.1371/journal.pone.0038149

Vastag, M., and Keseru, G. M. (2009). Current *in vitro* and *in silico* models of blood-brain barrier penetration: a practical view. *Curr. Opin. Drug Discov. Devel.* 12, 115–124.

Veszelka, S., Kittel, Á. and Deli, M. A. (2011). "Tools of modelling blood-brain barrier penetrability," in *Solubility, Delivery and ADME Problems of Drugs and Drug-Candidates*, eds K. Tihanyi and M. Vastag (Washington, DC: Bentham Science Publ. Ltd.), 166–188.

Veszelka, S., Bocsik, A., Walter, F., Hantosi, D., and Deli, M. A. (2015). Blood-brain-barrier coculture models to study nanoparticle penetration: focus on coculture systems. *Acta Biol. Szeged.* 59, 157–168.

Walter, F. R., Valkai, S., Kincses, A., Petneházi, A., Czeller, T., Veszelka, S., et al. (2016). A versatile lab-on-a-chip tool for modeling biological barriers. *Sens. Act. B Chem.* 222, 1209–1219. doi: 10.1016/j.snb.2015.07.110

Walter, F. R., Veszelka, S., Pásztói, M., Péterfi, Z. A., Tóth, A., and Rákhely, G. (2015). Tesmilifene modifies brain endothelial functions and opens the blood-brain/blood-glioma barrier. *J. Neurochem.* 134, 1040–1054. doi: 10.1111/jnc.13207

Weksler, B., Romero, I. A., and Couraud, P. O. (2013). The hCMEC/D3 cell line as a model of the human blood brain barrier. *Fluids Barriers CNS* 10:16. doi: 10.1186/2045-8118-10-16

Weksler, B. B., Subileau, E. A., Perrière, N., Charneau, P., Holloway, K., Leveque, M., et al. (2005). Blood-brain barrier-specific properties of a human adult brain endothelial cell line. *FASEB J.* 19, 1872–1874. doi: 10.1096/fj.04-3458fje

Conflict of Interest Statement: The authors ÉH and MV are employed by the company Gedeon Richter Plc.

The other authors declare that the research was conducted in the absence of any commercial or financial relationships that could be construed as a potential conflict of interest.

PUBLICATION III.

European Journal of Pharmaceutical Sciences 123 (2018) 228–240

Contents lists available at ScienceDirect

European Journal of Pharmaceutical Sciences

journal homepage: www.elsevier.com/locate/ejps

Niosomes decorated with dual ligands targeting brain endothelial transporters increase cargo penetration across the blood-brain barrier

Mária Mészáros[a,b], Gergő Porkoláb[a,c], Lóránd Kiss[a,1], Ana-Maria Pilbat[d], Zoltán Kóta[a], Zoltán Kupihár[e], Albert Kéri[f], Gábor Galbács[f], László Siklós[a], András Tóth[a,g], Lívia Fülöp[e], Mária Csete[h], Áron Sipos[a], Petra Hülper[i,2], Péter Sipos[j], Tibor Páli[a], Gábor Rákhely[a,g], Piroska Szabó-Révész[j], Mária A. Deli[a,*], Szilvia Veszelka[a,*]

[a] Institute of Biophysics, Biological Research Centre of the Hungarian Academy of Sciences, Temesvári krt. 62, H-6726 Szeged, Hungary
[b] Doctoral School in Theoretical Medicine, Faculty of Medicine, University of Szeged, H-6720 Szeged, Hungary
[c] Foundation for the Future of Biomedical Sciences in Szeged, Pálfy u. 52/d, H-6725 Szeged, Hungary
[d] Institute of Biochemistry, Biological Research Centre of the Hungarian Academy of Sciences, Temesvári krt. 62, H-6726 Szeged, Hungary
[e] Department of Medical Chemistry, Faculty of Medicine, University of Szeged, Dóm tér 8, H-6720 Szeged, Hungary
[f] Department of Inorganic and Analytical Chemistry, Faculty of Science and Informatics, University of Szeged, Dóm tér 7, H-6720 Szeged, Hungary
[g] Department of Biotechnology, Faculty of Science and Informatics, University of Szeged, Szeged, Hungary, Közép fasor 52, H-6726 Szeged, Hungary
[h] Department of Optics and Quantum Electronics, Faculty of Science and Informatics, University of Szeged, Dóm tér 9, H-6720 Szeged, Hungary
[i] Department of Pediatrics I, University Medical Center Göttingen, Robert-Koch-Straße 40, 37075 Göttingen, Germany
[j] Institute of Pharmaceutical Technology and Regulatory Affairs, Faculty of Pharmacy, University of Szeged, Eötvös u. 6, H-6720 Szeged, Hungary

ARTICLE INFO

Keywords:
Blood-brain barrier
Brain endothelial cell
Drug targeting
Dual-ligand
Nanoparticle
Niosome
Solute carriers

ABSTRACT

Nanoparticles targeting transporters of the blood-brain barrier (BBB) are promising candidates to increase the brain penetration of biopharmacons. Solute carriers (SLC) are expressed at high levels in brain endothelial cells and show a specific pattern at the BBB. The aim of our study was to test glutathione and ligands of SLC transporters as single or dual BBB targeting molecules for nanovesicles. High mRNA expression levels for hexose and neutral amino acid transporting SLCs were found in isolated rat brain microvessels and our rat primary cell based co-culture BBB model. Niosomes were derivatized with glutathione and SLC ligands glucopyranose and alanine. Serum albumin complexed with Evans blue (67 kDa), which has a very low BBB penetration, was selected as a cargo. The presence of targeting ligands on niosomes, especially dual labeling, increased the uptake of the cargo molecule in cultured brain endothelial cells. This cellular uptake was temperature dependent and could be decreased with a metabolic inhibitor and endocytosis blockers filipin and cytochalasin D. Making the negative surface charge of brain endothelial cells more positive with a cationic lipid or digesting the glycocalyx with neuraminidase elevated the uptake of the cargo after treatment with targeted nanocarriers. Treatment with niosomes increased plasma membrane fluidity, suggesting the fusion of nanovesicles with endothelial cell membranes. Targeting ligands elevated the permeability of the cargo across the BBB in the culture model and in mice, and dual-ligand decoration of niosomes was more effective than single ligand labeling. Our data indicate that dual labeling with ligands of multiple SLC transporters can potentially be exploited for BBB targeting of nanoparticles.

1. Introduction

The blood-brain barrier (BBB) restricts the entry of the potential neuropharmaceuticals, especially biopharmacons, like nucleic acids, peptide or protein drugs into the central nervous system (CNS). Although it is generally assumed that small molecule drugs can cross the BBB, actually, only about a small fraction of them is able to enter the brain parenchyma (Pardridge, 2015). Several clinical trials ended with failure because of the low penetration of the biologic drugs across the BBB (Pardridge, 2016). Strategies to solve this problem can be

* Corresponding authors.
E-mail addresses: deli.maria@brc.mta.hu (M.A. Deli), veszelka.szilvia@brc.mta.hu (S. Veszelka).
[1] Present affiliation: Department of Pathophysiology, University of Szeged, Semmelweis u. 1, H-6701 Szeged, Hungary.
[2] Present affiliation: Department of Neuroscience, Carl von Ossietzky University, 26,111, Oldenburg, Germany.

https://doi.org/10.1016/j.ejps.2018.07.042
Received 20 March 2018; Received in revised form 13 July 2018; Accepted 19 July 2018
Available online 20 July 2018
0928-0987/

classified into three major groups, namely (i) circumvention of the BBB, (ii) modification of the BBB functions, (iii) modification of the molecules (Deli, 2011). Invasive drug delivery strategies, like intraventricular or intrathecal drug administration are successful in circumventing the BBB, however limitations, such as potential infectious risks must be considered. The non-invasive alternative nasal pathway is also being investigated for transport of molecules to the brain (Horvát et al., 2009; Sipos et al., 2010) but the major drawbacks of this method are the very low amount of molecules transported to the brain and limited distribution. Modification of BBB functions with transient increase of brain endothelial permeability pathways (Hülper et al., 2013; Walter et al., 2015) could potentially increase CNS drug delivery if problems with safety, reversibility, systemic and CNS side-effects will be solved in the future. Medicinal chemistry uses several methods to enhance brain delivery of molecules by changing their physico-chemical properties, including techniques to increase the lipid solubility or cationic charge of molecules. While high lipid solubility can augment the transport of a given drug across the BBB it can also enhance its uptake by peripheral tissues and also sequestration in the capillary bed resulting in decreased concentration in blood and in the CNS (Banks, 2009). Therefore new approaches are needed to improve the brain delivery of drugs.

Nanosized drug carriers, or nanoparticles (NP) are in the focus of research efforts to develop successful drug delivery systems for the CNS (Masserini, 2013; Saraiva et al., 2016; Zhou et al., 2018). Vesicular NPs are especially versatile, because they can accomodate drug cargo with different properties. The non-ionic surfactant based vesicular nanocarriers, niosomes, have several favorable properties such as good biocompatibility and biodegradability, non-immunogenicity, and physical stability. Niosomes are also able to accumulate both water and lipid soluble drugs and control their release (Abdelkader et al., 2014). Another advantage of nanovesicles is that they increase the penetration of drugs across biological barriers and reduce their toxic side effects due to the encapsulation process (Masserini, 2013). However, the encapsulation of drugs in NPs alone is not enough for the successful delivery of drugs to the CNS, specific targeting is needed to elevate the BBB specific uptake and permeability of drugs (Kreuter, 2014). Various essential influx transport systems are expressed on the cerebral endothelium, which have physiological role in the delivery of nutrients and can be potentially exploited to shuttle nanocarriers to the brain, including receptor mediated endocytosis, adsorptive mediated endocytosis and carrier mediated transport systems (Abbott, 2013; Campos-Bedolla et al., 2014). The receptor mediated transport pathway and the ligands of BBB receptors are widely investigated to deliver fusion peptides or NPs to the brain (Pardridge, 2012; Johnsen and Moos, 2016).

Solute carriers (SLC) compose a large family of transporters at the BBB delivering nutrients (Enerson and Drewes, 2006; Campos-Bedolla et al., 2014). Several clinically used drugs cross the endothelial cells of brain capillaries *via* SLCs. The most well known drug to treat Parkinson's disease, L-DOPA, enters the brain *via* the LAT1/SLC7A5 transporter (Pardridge, 2015). SLC transporters are actively investigated as drug targets and the number of drug candidates developed for SLCs and reaching clinical trials increases (Rask-Andersen et al., 2013). However this pathway is not fully exploited for drug delivery (César-Razquin et al., 2015), especially for targeted NPs.

Among the SLC transporters, the expression level of glucose transporter GLUT1 (SLC2A1) is the highest at the BBB, but other members of the SLC2A family are also present (Campos-Bedolla et al., 2014; Enerson and Drewes, 2006). Glucose analogs have a potential to be efficient and selective targeting ligands for both vesicular and gold nanocarriers to cross the BBB (Dufes et al., 2004; Gromnicova et al., 2013). The number and expression level of SLCs transporting amino acids across the BBB are also high (Enerson and Drewes, 2006; Shawahna et al., 2011). Neutral amino acids, like alanine, serine and cysteine, are transported by carriers belonging to the SLC38A sodium coupled amino acid transporter family (SLC38A1, SLC38A2, SLC38A5) and the SLC1A neutral amino acid transporters (ASCT1/SLC1A4, ASCT2/SLC1A5) (Campos-Bedolla et al., 2014). These neutral amino acids could be also considered as targeting molecules, but have not been used for decorating nanocarriers yet. SLCs also transport vitamins to brain (Campos-Bedolla et al., 2014). The Na^+-dependent multivitamin transporter SLC5A6 mediates the uptake of biotin in brain endothelial cells (Uchida et al., 2015). We were the first to demonstrate that biotin as a targeting ligand significantly elevated the uptake and permeability of solid NPs in cultured human brain endothelial cells as compared to non-targeted NPs (Veszelka et al., 2017). Since the expression pattern of SLCs is specific for the BBB, our hypothesis was that labeling vesicular NPs with two different SLC ligands (dual targeting) will increase the brain endothelial uptake of the cargo and its permeability across the BBB as compared to a single ligand.

One of the most successful targeting ligands of NPs to cross the BBB is the tripeptide glutathione. There is an active glutathione transport across the BBB, but the transporter(s) were not yet identified (Gaillard, 2016). Nevertheless glutathione, as a targeting ligand, increased drug delivery to brain by NPs in several studies (Birngruber et al., 2014; Lindqvist et al., 2016). The group of Gaillard established the efficacy of glutathione targeted liposomal doxorubicin in a mouse glioma model (Gaillard et al., 2014) and these NPs were also investigated in clinical trials (Gaillard, 2016).

The aim of our study was to test glucopyranose and alanine, ligands of SLC transporters, as single or dual BBB targeting molecules for nanovesicles loaded with a large biomolecule, serum albumin, as cargo. Glutathione was used as a reference BBB targeting ligand. We characterized the properties of the different niosomes and investigated their effects on viability, cellular uptake and permeability of the cargo using a BBB culture model. The mechanism of the cellular uptake process and the role of the brain endothelial surface charge were also studied. Single and dual-targeted niosomes were also examined in mice using optical imaging.

2. Materials and methods

2.1. Animals

Animal studies were performed following the regulations of the 1998. XXVIII. Hungarian law and the EU Directive 2010/63/EU about animal protection and welfare. Approval for animal studies was obtained from the local animal health authority, the Governmental Office for Csongrád County, Directorate of Food Chain Safety and Animal Health (Permit numbers: XVI./03835/001/2006, XVI./834/2012). For the *in vivo* experiments ten week old male CD1-Foxn1nu nude mice (Charles River Laboratories, Wilmington, MA, USA) were used. For the *in vitro* primary cell isolations, brain tissues were obtained from 3-week-old and newborn outbred Wistar rats (Harlan Laboratories, United Kingdom) of both sexes. Animals were fed on standard rodent chow and water *ad libitum* and kept under a 12 h light/dark cycle in the conventional animal house of the Biological Research Centre. During the experiments, all efforts were made to minimize animal suffering and pain.

2.2. Materials

All reagents were purchased from Sigma-Aldrich Kft., Hungary (part of Merck Life Science), except for those specifically mentioned.

2.3. Synthesis of targeted ligands for niosomes

For the synthesis of DSPE-PEG-glutathione, 13.5 mg glutathione (0.044 mM) was reacted with 100 mg DSPE-PEG-maleimide (0.035 mM) (N-[(3-Maleimide-1-oxopropyl) aminopropyl polyethyleneglycol-carbamyl] distearoylphosphatidyl-ethanolamine,

SUNBRIGHT® DSPE-020MA (DSPE-PEG-MAL) obtained from NOF Europe, Belgium) in 0.1 M ammonium acetate for a day under nitrogen. The product was lyophilized three times to remove ammonium acetate.

Dodecanoyl alanine was prepared according to the literature method (Liu et al., 2014). Briefly, 100 ml NaOH (1 M) and 1.34 g (0.015 mol) L-alanine were added into a one-neck flask. After the system was cooled to 0 °C, 3.31 ml (0.014 mol) dodecanoyl chloride was added dropwise to the mixture and maintained for 5 h at 0 °C. Then 16 ml hydrochloric acid (12 M) was added to the reaction and the white precipitate was filtrated. Finally the product was washed three times with deionized water and dried at 45 °C for 24 h.

2.4. Preparation of targeted niosomes loaded with albumin

Non-ionic surfactants, Span 60 (sorbitane-monostearate) and Solulan C24 (cholesteryl-poly-24-oyxyethylene-ether, Chemron Co. USA) were dissolved with cholesterol in hot 1:2 mixtures of chloroform and ethanol in a round-bottom flask. N-dodecyl-β-D-glucopyranose (GP, 9% (*w*/w) of total lipid), dodecanoyl-alanine (A, 5% (w/w) of total lipids) or pegylated-GSH (GSH, 5% (w/w) of total lipids) were added to prepare targeted niosomes (N-GP, N-A, N-GSH) (Dufes et al., 2004; Gaillard et al., 2014). For dual-targeted NPs (N-A-GP, N-A-GSH, N-GP-GSH) the content of ligands was 4–4% (w/w) of the total lipids. The removal of organic solvents by vacuum pump yielded a thin lipid film layer. The dry lipid film was hydrated with phosphate buffer (PBS; KCl 2.7 mM, KH_2PO_4 1.5 mM, NaCl 136 mM, $Na_2HPO_4 \times 2\ H_2O$ 6.5 mM, pH 7.4) containing Evans blue-labeled bovine serum albumin (EBA, 67 kDa; 0.167 mg/ml EB, 10 mg/ml BSA). For transmission electron microscopy niosomes with the electron dense lanthanum nitrate (433 Da), as a cargo, were prepared. The mixture was heated at 40 °C in a water bath and sonicated for 25 min. The suspension was forced through a polycarbonate filter (Whatman filter, 13 mm, 100 nm pore size) by lipid extrusion technique (high pressure thermobarrel extruder, Lipex Biomembranes Inc. USA) to yield vesicles. The non entrapped cargo was removed by ultracentrifugation (123,249 *g*, 6 h, 4 °C), the pelleted niosomes were resuspended in PBS or DMEM medium and stored at 4 °C.

2.5. Preparation of targeted niosomes loaded with lanthanum and lanthanum measurement

For transmission electron microscopy experiments niosomes with the electron dense lanthanum nitrate hexahydrate (433 Da), as a cargo were prepared by hydrating the lipid film with PBS containing 5 mg/ml lanthanum. The lanthanum content of the particles was determined by a quadrupole Agilent 7700× inductively coupled plasma mass spectrometer (ICP-MS), was used for trace element analysis. The sample introduction system consisted of an Agilent I-AS auto sampler and a Micro Mist pneumatic nebulizer in a Peltier-cooled Scott-type spray chamber. The sample uptake rate was 400 µL/min. The ICP plasma and interface parameters were set up as follows: RF forward power: 1550 W, plasma gas flow rate: 15.0 L/min, carrier gas flow rate: 1.05 L/min, sampling depth: 10.0 mm. Ultra trace quality HNO_3 acid was also used for the acid dissolution of the samples at 180 °C. The digestion time was one hour. Signal tuning was performed by Agilent (No. G1820-60410) solutions, whereas calibration was done using solutions prepared from an Inorganic Ventures (Christiansburg, Virginia, USA) IV-ICPMS-71A multielement stock standard. The 99.996% purity argon gas used was purchased from Messer Hungarogáz (Hungary). Data processing was performed within the Agilent Mass Hunter (Santa Clara, California, USA) software.

2.6. Characterization of niosomes: Size, charge and encapsulation efficiency

The NPs were characterized for particle size and zeta potential using dynamic light scattering (Malvern Zetasizer Nano ZS, Worcestershire, UK). Before measurements the niosome samples were diluted in PBS to a final concentration of 200 µg/mL. The means of particle size and zeta potential data were calculated from the average of three measurements per sample. To determine the amount of encapsulated dye in the NPs, EBA was released from the niosomes with 50% v/v ethanol and measured by spectrofluorometer (Fluorolog 3, Horiba Jobin Yvon) at 584 nm excitation and 663 nm emission wavelengths. The concentrations were determined from a standard fluorescence calibration curve ($r^2 = 0.9985$). The encapsulation efficiency % (EE%) was calculated by the following equation:

$$EE\% = \frac{\text{Amount of EBA in the NP sample}}{\text{Amount of EBA in the hydrating buffer}} \times 100$$

2.7. Characterization of niosomes: Transmission electron microscopy

Aliquots of the niosome samples (10 µL) were placed on formvar carbon 400-mesh copper grids (Electron Microscopy Sciences, Washington, PA, USA). Images were taken on a JEOL JEM-1400 transmission electron microscope (JEOL Ltd., Japan) operating at 120 kV. Images were captured routinely at magnifications of 20,000×, 25,000× and 30,000×, and analyzed with a SightX Viewer Software (EM-15300SXV Image Edit Software, JEOL Ltd., Tokyo, Japan).

2.8. Characterization of niosomes: Atomic force microscopy

A two-beam interference lithography arrangement was applied to generate sub-micrometer periodic intensity modulation in the laser beam irradiating the samples (Csete et al., 2007). The fourth harmonic of a Nd:YAG laser (λ_{FH} = 266 nm, t = 10 ns, f = 10 Hz) was diffracted impinged on a reflective grating (PUV 1200, Spectrogon), and the first order diffracted beams were recombined at the sample surface. The samples were NBK7 substrates evaporated by gold-silver bimetallic layers, and spin-coated by polycarbonate.

The samples were silicone wafer substrates spin-coated by polycarbonate, which were treated by s-polarized beams, to produce linear gratings as described earlier (Csete et al., 2007). The laser treated surfaces were scanned by atomic force microscopy (AFM) operating in digital pulsed force mode (DPFM, Witec GmbH, Germany). The advantage of this scanning mode is the possibility to map the micromechanical properties of the surface with high resolution. We applied standard PFM tips (NSC 18/NoA1, 2.5 N/m) and collected pictures about the topography and adhesion, which revealed that the adhesion is stronger in the valleys of the linear grating, thus facilitating the deposition of particles.

To examine niosomes the samples with laser-grated surfaces were completely immersed in fresh PBS solutions containing niosomes. Incubation of the samples in the solutions lasted for 1 h at 37 °C, then all samples were washed three times in sterile distilled water on a horizontal shaker and finally allowed to dry overnight at room temperature. An AFM (XE-100, PSIA Corp.) operating in tapping-mode was applied to detect the attached biomolecules using tapping-mode NT-MDT tips (NSG11, 5.5 N/m, 150 kHz, NT-MDT).

2.9. RNA isolation and quality control

Rat brain microvessels were isolated as described in our previous article (Veszelka et al., 2007). Primary rat brain endothelial cells (RBEC; isolated according to the method described in section *2.11.* and in our previous studies (Veszelka et al., 2007; Nakagawa et al., 2009; Walter et al., 2015) were cultured for 5 days in 10 cm dishes. After reaching confluency the cells were scraped, collected and cell pellets were used for total RNA isolation using RNAqueous-4PCR Kit (Ambion, Life Technologies, Austin, TX, USA) with DNase1 (RNase-free) treatment according to the manufacturer's instructions. The concentrations

and purity of the DNase-treated RNA samples were assessed by a NanoDrop ND-1000 spectrophotometer (NanoDrop Technologies, Rockland, DE). The integrities of the isolated RNAs were characterized using Bioanalyzer 2100 (Agilent Technologies, Santa Clara, CA). The RNA integrity numbers (RIN) were between 9.2 and 10 in the case of all studied RNA samples.

2.10. Quantitative real-time polimerase chain reaction and data analysis

In all cases, cDNA synthesis was performed on 1 µg total RNA samples by High Capacity cDNA Reverse Transcription Kit (Life Technologies) using random hexanucleotide primers and MultiScribe Reverse Transcriptase in the presence of RNase inhibitor according to the manufacturer's protocols. The expression of the genes of transporters for alanine (sodium-coupled neutral amino acid transporters, *Snat1/Slc38a1*, *Snat2/Slc38a2*, *Snat5/Slc38a5*; neutral amino acid transporters, *Asct1/Slc1a4*, *Asct2/Slc1a5*) and the genes of transporters for glucose (*Glut1/Slc2a1*, *Glut3/Slc2a3*, *Glut5/Slc2a5*) were analyzed by quantitative PCR using TaqMan Low Density Array 384-well microfluidic cards preloaded with TaqMan Gene Expression Assays (Life Technologies). Quantitative real-time PCRs (qPCR) were performed by ABI TaqMan Universal Master Mix (Life Technologies) using the ABI Prism 7900 system (Applied Biosystems, Life Technologies). qPCR data were analyzed using the ABI SDS 2.0 software (Applied Biosystems, Life Technologies). In all samples the expression of genes was normalized to 18S rRNA, which was used as an endogenous control ($\Delta C_t = C_{tgene} - C_{t18S\ rRNA}$). Expression values of studied genes were determined based on the normalized expression of genes calculated with $2^{-\Delta Ct}$ formula which were correlated to the lowest normalized expression measured by the applied qPCR method. For quantification of relative expression level of genes of interest, the normalized expression data were analyzed using the comparative $\Delta\Delta C_t$ method (Livak and Schmittgen, 2001; Tóth et al., 2014).

2.11. Primary cell cultures and BBB model for permeability studies

Isolation of RBEC cells, glia and pericytes, and the construction of the *in vitro* BBB model were performed according to the method described in our previous studies (Nakagawa et al., 2009; Walter et al., 2015). After isolation cells were seeded on culture dishes (Corning, Costar, New York, NY, USA) coated with 100 µg/mL collagen type IV and 100 µg/mL fibronectin in sterile distilled water. RBEC cells were cultured in DMEM/HAM's F-12 (Gibco, Life Technologies, Carlsbad, CA, USA), 15% plasma-derived bovine serum (PDS, First Link, Wolverhampton, UK), 100 µg/mL heparin, medium supplement with 5 µg/mL insulin, 5 µg/mL transferrin, 5 ng/mL sodium selenite (ITS, Pan-Biotech Gmbh., Germany), 1 ng/mL basic fibroblast growth factor (bFGF, Roche, Basel, Switzerland) and 50 µg/mL gentamycin. During the first three days of culture the medium of RBEC cells contained 3 µg/mL puromycin to eliminate P-glycoprotein negative, contaminating cell types (Perrière et al., 2005).

For the permeability studies a triple co-culture BBB model was used (Nakagawa et al., 2009). For this model, in addition to brain endothelial cells, primary rat brain pericytes were isolated using the same method as for brain endothelial cells, except that pericytes were plated onto uncoated culture dishes and did not receive puromycin. Primary cultures of rat glial cells were prepared from one-day-old Wistar rats and passaged (8.5×10^4 cells/cm^2) to 12 well plates (Corning, Costar, New York, NY, USA) coated with collagen type IV (100 µg/ml in sterile distilled water). Rat glial cells were cultured for two weeks before using them for the co-culture model (Veszelka et al., 2007). Pericytes and glial cells were cultured in DMEM/HAM's F-12 supplemented with 10% fetal bovine serum (FBS, Pan-Biotech GmbH) and 50 µg/mL gentamycin. To prepare the co-culture model, pericytes at P2 were passaged (1.5×10^4 cells/cm^2) to the collagen coated bottom side of tissue culture inserts (Transwell, polycarbonate membrane, 3 µm pore size,

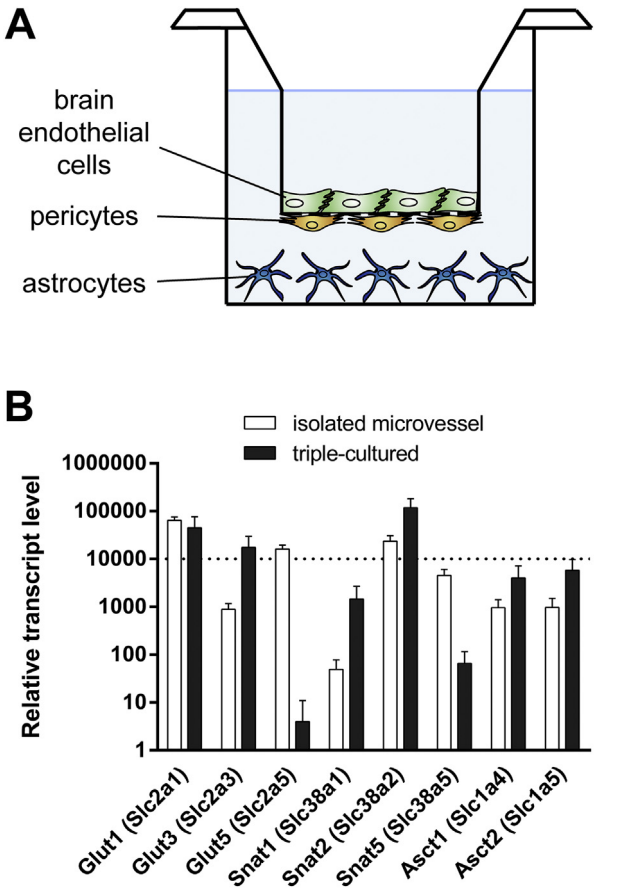

Fig. 1. (A) Schematic drawing of the BBB co-culture model. (B) Expression of genes encoding solute carriers for glucose and alanine in isolated rat brain microvessels and in primary rat brain endothelial cells in co-culture with rat pericytes and astrocytes.

Corning Costar) and brain endothelial cells were seeded (7.5×10^4 cells/cm^2) to the upper side of the Matrigel (growth factors reduced, Corning Costar, USA) coated membranes. Then the inserts containing brain endothelial cells and pericytes on the two sides of the membrane were placed to 12 well plates in which glial cells were grown at the bottom (Fig. 1A). Both the upper and lower fluid compartments of this system received endothelial culture medium supplemented with 550 nM hydrocortisone and the three types of cells were cultured together for four days before permeability experiments (Nakagawa et al., 2009; Walter et al., 2015).

2.12. Cell viability assay

Kinetics of RBEC cell reaction to niosome treatment were monitored by impedance measurement (RTCA-SP instrument; ACEA Biosciences, San Diego, CA). Impedance measurement is label-free, real time, non-invasive, and correlates linearly with adherence and growth of cells. After background measurements, cells were seeded at a density of 6×10^3 cells/well in collagen coated 96-well plates with integrated gold electrodes (*E*-plate 96, ACEA Biosciences). Cells were cultured for 5–7 days in CO_2 incubator at 37 °C and monitored for 4 h. Triton X-100 detergent (10 mg/mL) was used as a reference compound inducing cell toxicity. Cell index was defined as $R_n - R_b$ at each time point of measurement, where R_n is the cell-electrode impedance of the well when it contains cells and R_b is the background impedance of the well with the medium alone. Cell index values reflect cell number and viability (Kiss et al., 2013; Bocsik et al., 2016).

2.13. Measurement of the uptake of niosomes in RBEC cells

The RBEC cells were cultured in 24 well plates (Corning Costar, USA) at the density of 3×10^4 cells/well. The confluent monlayers were incubated with 10 mg/mL niosome solutions (N, N-GP, N-A, N-GSH, N-A-GP, N-GP-GSH, N-A-GSH) in culture medium for 4 h. The uptake of single or dual-targeted niosomes in RBEC cells was tested at 4 °C and 37 °C. To elucidate the uptake mechanisms of targeted niosomes cells were co-treated with metabolic inhibitor sodium azide (1 mg/ml) or pretreated with endocytosis inhibitors, filipin (15 min, 6 μM) and cytochalasin D (1 h, 20 μM) in culture medium. To study the role of the surface charge in cellular uptake of NPs we digested the surface glycocalyx of RBECs with neuraminidase (1 U/ml, 1-hour pretreatment), or treated the cells with 54 μM cationic lipid 1-(4-trimethylammoniumphenyl)-6-phenyl-1,3,5-hexatriene (TMA-DPH; Molecular Probes, Life Technologies) for 30 min before the uptake. After incubation with niosomes RBECs were washed three times with ice cold PBS supplemented with 1% BSA and once with acid stripping buffer (glycine 50 mM, NaCl 100 mM, pH 3) to remove cell surface associated niosomes. Finally cells were lysed in PBS with Triton X-100 detergent (10 mg/mL) and the fluorescent signal was detected with a spectrofluorometer (Horiba Jobin Yvon Fluorolog 3, Edison New Jersey, USA) at 584 nm excitation and 663 nm emission wavelengths.

2.14. Visualization of the uptake of niosomes in RBEC cells

To visualize the cellular uptake of the fluorescent particles RBECs were grown on glass bottom Petri dishes coated with Matrigel and treated with 10 mg/mL niosomes for 4 h. The stain cell nuclei H33342 dye (1 μg/mL; 10 min) was used. After incubation living cells were washed three times with Ringer-Hepes buffer (118 mM NaCl, 4.8 mM KCl, 2.5 mM $CaCl_2$, 1.2 mM $MgSO_4$, 5.5 mM D-glucose, 20 mM Hepes, pH 7.4) supplemented with 1% PDS and examined with a confocal laser scanning microscope (Olympus Fluoview FV1000, Olympus Life Science Europa GmbH, Hamburg, Germany).

The cellular uptake of targeted NPs was also examined by transmission electron microscopy. RBECs were grown on culture inserts and treated untargeted (N) or dual-targeted (N-A-GSH) niosomes (10 mg/ml) with lanthanum cargo for 4 h at 37 °C. Control cells were treated 0.2 μg/mL lanthanum, the same concentration entrapped in the niosomes. After incubation, RBECs were briefly rinsed in 0.1 M phosphate buffer (PB), then fixed in 4% paraformaldehyde + 2.5% glutaraldehyde dissolved in 0.1 M PB at 4 °C for 30 min. After rinsing in 0.1 M PB the inserts were removed from the tissue culture plates and transferred into 50 ml centrifuge tubes containing 0.1 M PB and kept at 4 °C overnight. Cells on the membranes were postfixed in 1% aqueous OsO_4 for 1 h at room temperature, washed in tri-distilled water for 10 min and processed in a graded series of ethanol (50%, 70%, 90%, 96%, 100%, 100%) for 10 min in each solution. Then, 4–5 mm small pieces of the membranes with cells were embedded in Durcupan. Semithin (0.5 μm) sections were cut from the blocks on a Reichert OM-U2 ultramicrotome, which were stained to localize the cell layers on the membranes. Next, ultrathin section (60 nm) were cut on a Leica Ultracut S ultramicrotome, mounted either on formvar coated single slot or uncoated 300 mesh copper grids, and stained with 2% uranyl acetate for 15 min. Sections were examined in a JEOL JEM 1400 Plus electron microscope operated at 100 kV accelerating voltage. Digital images were taken with a Matataki 8 MPix CCD camera at 16-bit gray scale color depth and saved in uncompressed TIFF format.

2.15. Permeabilty of niosomes across the BBB co-culture model

The tightness of the BBB co-culture model was verified by measurement of transendothelial electric resistance (TEER) by EVOM voltohmmeter (World Precision Instruments, Sarasota, 45 FL, USA) combined with STX-2 electrodes. When high TEER values ($539 \pm 71\ \Omega \times cm^2$) were obtained, the model was used for experiments. Cells were treated in the upper, donor compartment (0.5 mL) with single or dual-targeted niosomes (10 mg/mL) diluted in phenol red free DMEM F12 supplemented with 1% PDS and 1% ITS for 4 h. After incubation samples were collected from the lower, acceptor compartments (1.5 mL) and measured with spectrofluorometer (Horiba Jobin Yvon Fluorolog 3) at 584 nm excitation and 663 nm emission wavelengths. The apparent permeability coefficients (P_{app}) were calculated as described previously (Bocsik et al., 2016) by the following equation:

$$P_{app}(\mathrm{cm/s}) = \frac{\Delta[C]_A \times V_A}{A \times [C]_D \times \Delta t}$$

Briefly, P_{app} (cm/s) was calculated from the concentration difference of the NPs in the acceptor compartment ($\Delta[C]_A$) after 4 h. $[C]_D$ is the concentration in the donor compartments at 0 h, V_A is the volume of the acceptor compartment (1.5 mL), and A is the surface area available for permeability (1.1 cm^2).

2.16. Measurement of plasma membrane fluidity

RBECs grown in culture dishes were treated with N and N-A-GSH (10 mg/ml) diluted in culture medium for 4 h at 37 °C in a CO_2 incubator. The cells were washed twice with PBS, collected by trypsinization, and resuspended in Ringer-Hepes buffer. The density of cells was set by absorbance measurement to $OD_{360} = 0.1$ (Hewlett Packard 8452A Diode Array Spectrophotometer). Cells were labeled with 0.2 μM TMA-DPH for 5 min. Fluorescence anisotropy was measured on a T-format fluorescence spectrometer (Quanta Master QM-1, Photon Technology International, Princeton, NJ, USA). Excitation and emission wavelengths were 360 and 430 nm, respectively (5 nm and 6 nm slits). Cells were kept at 37 °C under stirring conditions. Anisotropy data were acquired in every second for 5 min, then benzyl alcohol (50 mM; Merck, Darmstadt, Germany), a strong membrane fluidizer, was added and data were acquired for another 5 min. The average of 50 anisotropy measurements in the last 1 min of each treatments was calculated and compared (Kiss et al., 2014; Lénárt et al., 2015).

2.17. In vivo imaging of targeted niosomes

Ten-week old male CD1-Foxn1nu nude mice (Winkelmann, Borchen, Germany) were used for *in vivo* imaging. Animals were kept under conventional controlled conditions (22 °C, 55% humidity, day-night rhythm) and had free access to a standard diet (ssniff Spezialdiäten GmbH, Soest, Germany) and tap water. A time domain *in vivo* small animal fluorescence imager Optix™ (ART, Montreal, Canada; Keren et al., 2008; Kumar et al., 2008) was used to monitor the brain penetration of the EBA cargo of niosomes in real-time and over several time points in the same animal. Animals were placed in prone position on the table of the imager. Anesthesia was maintained during the fluorescence detection by offering an oxygen-isoflurane gas mix *via* a small mask. EBA encapsulated in different niosomes (N, N-A, N-GP, N-A-GP) were injected intravenously (100 μL, tail vein). Fluorescence measurement to visualize the EBA was performed repeatedly after niosome injection at defined time points up to 24 h (0, 10 and 30 min, 3, 6 and 24 h). The animals were returned to their cage and provided access to food and water between the longer measurement points. Head-detector distance was equal in all measurements. The red fluorescent signal of EBA was detected over the whole body of living anesthetized mice in 0.5 mm steps. For fluorescence detection, a time-correlated single-photon counting system (TCSPC-130) was used. Intensity units were normalized for the same excitation power and excitation time per raster point (integration time).

2.18. Statistical analysis

Data are presented as means ± SEM or SD. Values were compared

using one-way or two-way analyses of variances following Dunnett or Bonferroni multiple comparison posttests (GraphPadPrism 5.0; GraphPad Software, USA). Changes were considered statistically significant at $P < 0.05$. All experiments were repeated at least two times and the number of parallel samples was 4–10.

3. Results

3.1. Expression of selected Slc genes coding nutrient transporters

We verified the expression of genes for Slc transporters carrying glucose and alanine in the BBB co-culture model and in freshly isolated rat brain microvessels (Fig. 1B). Among the carriers of glucose the expression level of the gene *Glut1*, coding the predominant glucose transporter at the BBB, was the highest, followed by *Glut5* and *Glut3* in brain microvessels. In RBECs the relative transcript levels for *Glut1* and *Glut3* were also high, while that of *Glut5* was very low. All the tested neutral amino acid transporter genes were detectable in both brain microvessels and RBECs. The mRNA of *Snat2* was expressed at the highest level in both models. From the tested eight genes only in two cases, for *Glut5* and *Snat5,* were transcript levels much lower in RBECs than in brain microvessels **(**Fig.1B**).**

3.2. Characterization of niosomes

Table 1 summarizes the main physicochemical properties of the untargeted (N), single ligand targeted (N-GP, N-A, N-GSH), and dual-ligand targeted (N-A-GSH, N-A-GP, N-GP-GSH) niosomes (for schematic drawing see Fig. 2). The average diameter of the niosomes varied between 92 and 107 nm. All groups had low polydispersity index, indicating a relatively narrow size distribution. The zeta potentials of niosomes were between −3 and −4 mV, except those decorated with GSH ligand (N-GSH, N-A-GSH, N-GP-GSH), which had a more negative surface charge, around −7 mV. The encapsulation efficiency of the cargo EBA was in the range of 4.6–10.4%. The amount of the encapsulated large hydrophilic biomolecule EBA was between 0.5 and 1.1 mg/100 mg nanoparticle total weight (Table 1). The morphology of the NPs was spherical as observed by transmission electron microscopy (Fig. 3A) and atomic force microscopy (Fig. 3B). No aggregation was visible.

The stability of untargeted niosome loaded with EBA was followed for six months. The size of niosomes changed from 92.8 ± 1.8 nm to 119.5 ± 1.9 nm during this period. At 6 months the polydispersity index was 0.30 ± 0.003 indicating monodispersity, and the zeta potential (−4.03 ± 0.49 mV *vs.* −3.67 ± 0.09 mV) and the encapsulation efficiency (11.5% *vs.* 9.21%) have changed minimally. Based on these data the niosome preparation can be considered as stable regarding size, encapsulated cargo and aggregation for at least 6 months.

3.3. Effect of niosomes on cell viability of RBECs

Incubation of RBECs with non-targeted or targeted niosomes in the 0.3–10 mg/mL concentration range for 4 h did not decrease the impedance of cell layers reflecting good cell viability (Fig. 4). For further experiments we selected the 10 mg/mL concentration, which can be considered as a safe concentration for all niosome groups.

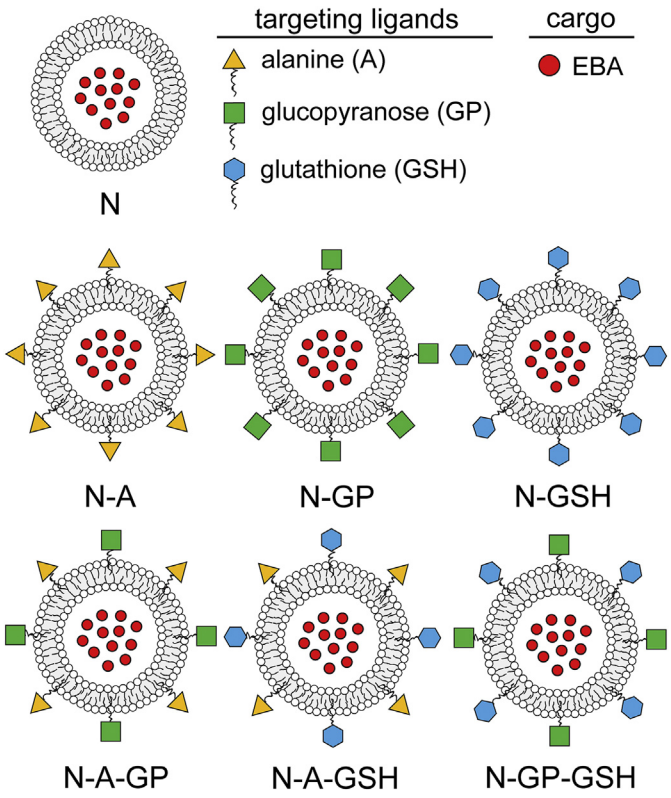

Fig. 2. Schematic drawing of non-targeted (N), single ligand targeted (N-A: alanine-, N-GP: glucopyranose-, N-GSH: glutathione-targeted) and dual-targeted niosomes (N-A-GP: glucose-alanine-, N-A-GSH: alanine-glutathione-, N-GP-GSH: glucose-glutathione-targeted).

3.4. Uptake of the cargo of single and dual-targeted niosomes in RBEC

The uptake of the large hydrophilic free EBA was very low in brain endothelial cells, only 1.5% of the EBA uptake in cells treated with non-targeted niosome containing the cargo (N) (Fig. 5). As compared to non-targeted niosomes, the uptake of EBA in RBECs treated with nanovesicles decorated with alanine, glucopyranose or glutathione was higher (N-A: 131%, N-GP: 130%, N-GSH: 191%). The presence of dual-ligands statistically significantly increased the cellular concentration of EBA in brain endothelial cells in the case of N-A-GP (293%) and N-A-GSH groups (249%), but not in the N-GP-GSH group.

Table 1
Characterization of the non-targeted and targeted niosomes.

Niosomes	Size (nm)	Polydispersity index	Zeta potential (mV)	Encapsulation efficiency (%)	Encapsulated BSA (mg/100 mg NP)
N	106 ± 10	0.18 ± 0.04	−3.41 ± 0.50	8.47 ± 3.24	0.85 ± 0.33
N-A	92 ± 40	0.18 ± 0.01	−4.36 ± 0.60	7.54 ± 3.57	0.75 ± 0.36
N-GP	98 ± 14	0.20 ± 0.04	−4.19 ± 0.29	4.90 ± 0.52	0.49 ± 0.05
N-GSH	107 ± 11	0.17 ± 0.02	−7.39 ± 0.77	10.43 ± 6.17	1.04 ± 0.62
N-A-GSH	103 ± 50	0.18 ± 0.01	−7.14 ± 1.15	6.14 ± 2.60	0.61 ± 0.26
N-A-GP	94 ± 10	0.17 ± 0.01	−3.83 ± 1.03	10.87 ± 0.53	1.09 ± 0.05
N-GP-GSH	101 ± 80	0.17 ± 0.01	−6.40 ± 1.27	4.66 ± 2.53	0.47 ± 0.25

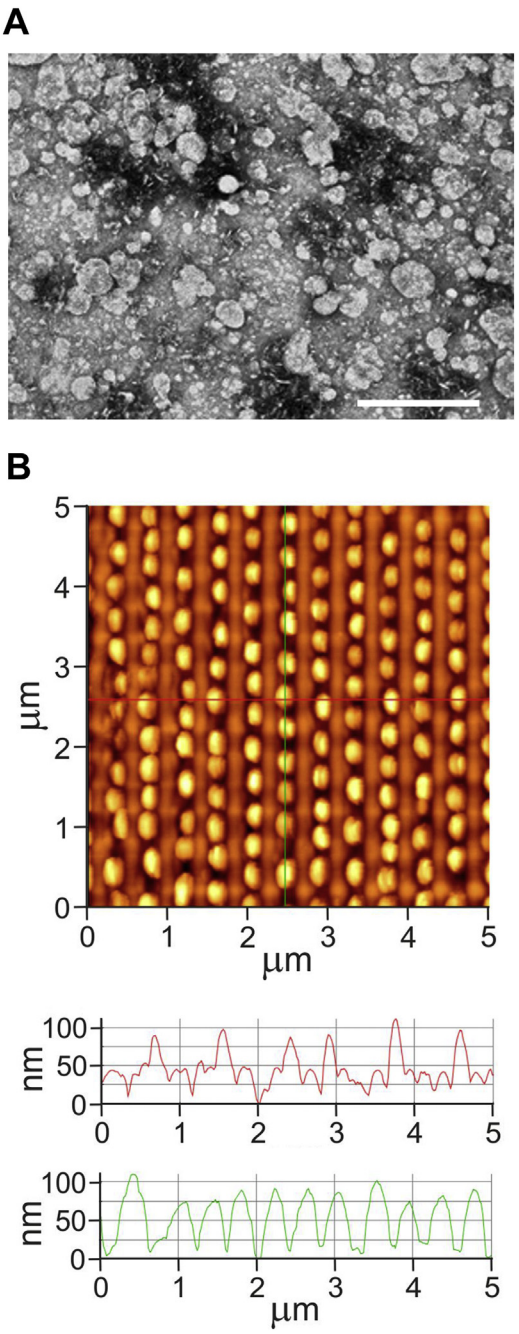

Fig. 3. (A) Transmission electron microscopy image of niosomes, bar: 500 nm. (B) Atomic force microscopy image of niosomes.

3.5. Penetration of the cargo by targeted niosomes across a BBB co-culture model

The permeability of the BBB model for EBA was also very low (0.13×10^{-6} cm/s) reflecting a tight barrier (Fig. 6). This P_{app} value for EBA, a transendothelial marker molecule, is in accordance with our previous results (Walter et al., 2015). The encapsulation of EBA in non-targeted niosomes (N) increased the permeability of the cargo through brain endothelial cells (0.28×10^{-6} cm/s). Labeling the particles with single ligands resulted in further increase in the penetration of EBA across the BBB model (N-A: 1.18×10^{-6} cm/s; N-GP: 1.01×10^{-6} cm/s; N-GSH: 1.29×10^{-6} cm/s). The amount of EBA cargo that crossed brain endothelial cells was increased 17-fold in case of the N-A-GSH group (2.26×10^{-6} cm/s) and 14-fold in the N-A-GP group (1.83×10^{-6} cm/s) as compared to the EBA group (Fig. 6). The combination of GP-GSH ligands was not efficient to elevate EBA penetration across the BBB model. Based on the results, the N-A, N-GSH and N-A-GSH groups were selected for further *in vitro* experiments.

3.6. Cellular uptake: Visualization

Since EBA, our model cargo gives a red fluorescent signal (Uyama et al., 1988), the uptake of free EBA and EBA encapsulated in nanovesicles (N, N-A-GSH) was visualized in RBECs by confocal microscopy (Fig. 7A). Red fluorescence was detected in cells treated with dual-targeted N-A-GSH niosomes indicating uptake of the cargo. Less fluorescent signal was seen in the non-targeted vesicle (N) group, while the cellular entry of free dye (EBA) was barely detectable.

For transmission electron microscopy the cells were treated with free lanthanum (LA), lanthanum entrapped non-targeted niosomes (N) and vesicles labeled with dual-ligands containing lanthanum (N-A-GSH) (Fig. 7B). The particles were non toxic (data not shown) and their physicochemical properties (N: 110 nm, −2.25 mV; N-A-GSH: 115 nm, −5.08 mV) were similar to the niosomes filled with EBA. The concentration of lanthanum was equal in each groups. More dark precipitates and structures can be seen in cells treated with N-A-GSH compared to the untargeted nanoparticle (N) and lanthanum groups.

3.7. Cellular uptake: Temperature dependence and metabolic inhibition

To test the temperature dependence of the cellular uptake of nanovesicle encapsulated EBA, cells were treated with selected niosomes (N, N-A, N-GSH, N-A-GSH) at both 4 °C and 37 °C (Fig. 8). At 37 °C the EBA uptake was significantly higher in all targeted nanovesicle groups (N-A: 119%, N-GSH: 150%, N-A-GSH: 308%) compared to the non-targeted group (N: 100%). Decreased EBA uptake was seen in RBECs at 4 °C (N-A: 36%, N-GSH: 55%, N-A-GSH: 17%) as compared to the non-targeted group at 37 °C. Treatment of the cells with metabolic inhibitor sodium azide resulted in lower uptake of the cargo (N-A: 88%, N-GSH: 113%, N-A-GSH: 81%) compared to data measured at 37 °C in the same treatment groups (Fig. 8).

3.8. Cellular uptake: Inhibition of endocytosis

Two inhibitors of endocytosis (Ivanov, 2008) were used to further elucidate the mechanism of cellular uptake of EBA after treating the cells with dual-targeted N-A-GSH particles (Fig. 9A). Filipin, which inhibits lipid raft/caveolae-mediated endocytosis, slightly, but statistically significantly decreased the uptake of cargo in RBECs (94% of the control group). Cytochalasin-D, a common inhibitor of endocytosis by blocking F-actin depolymerization, also induced a partial, but significant inhibition of EBA uptake (80% as compared to the control group).

3.9. Cellular uptake: Modification of cell surface charge

We modified the surface charge of cultured brain endothelial cells by digestion of the surface glycocalyx with neuraminidase enzime (Singh et al., 2007) and treatment with a cationic lipid, TMA-DPH (Ribeiro et al., 2012). Surface charge alterations in RBECs did not affect the cellular uptake of EBA after treatment with non-targeted NPs as compared to the control, untreated group (Fig. 9B). In contrast, both modifications increased significantly the uptake of EBA in brain endothelial cells after incubation with N-A-GSH niosomes (Fig. 9B). The uptake of EBA was increased by 16%, after treatment of RBECs with neuraminidase and by 19% after incubation with TMA-DPH, as compared to untreated cells in the N-A-GSH nanoparticle group.

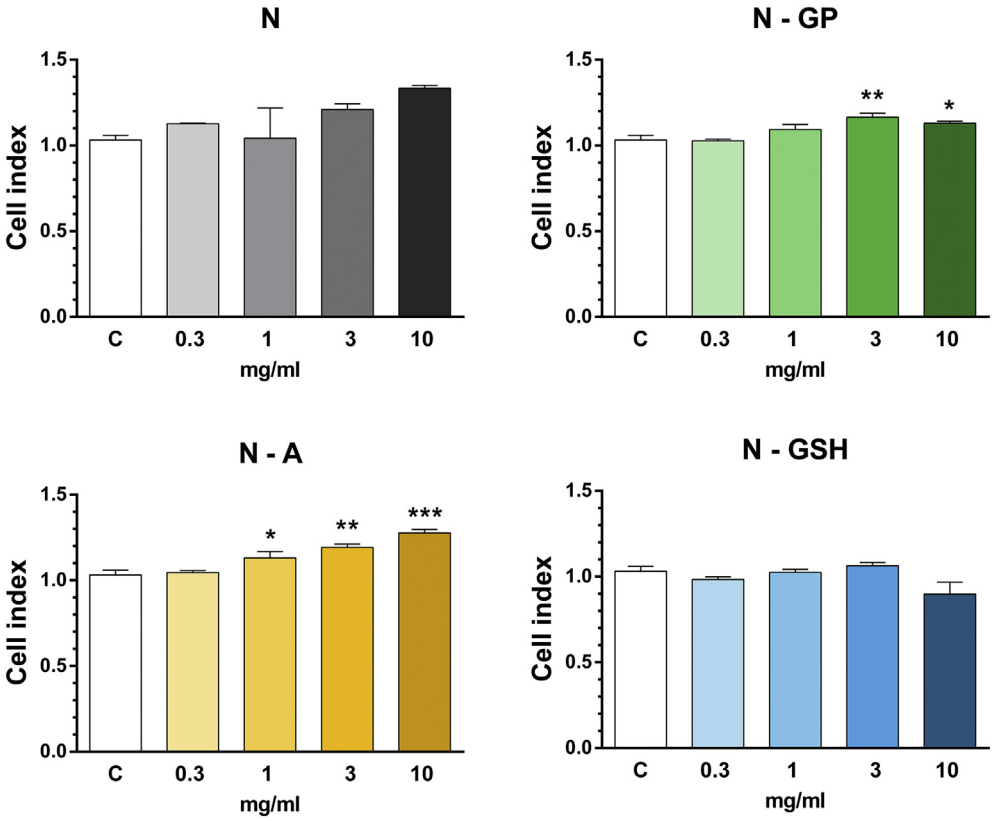

Fig. 4. The effect of non-targeted (N), alanine-targeted (N-A), glucopyranose-targeted (N-GP) and glutathione-targeted (N-GSH) niosomes on the viability of brain endothelial cells after 4-hour incubation. Values presented are means ± SEM. Statistical analysis: ANOVA followed by Dunnett's posttest, $^{*}P < 0.05$, $^{**}P < 0.01$, $^{***}P < 0.001$, compared to control group, $n = 8$. C: medium treated control group.

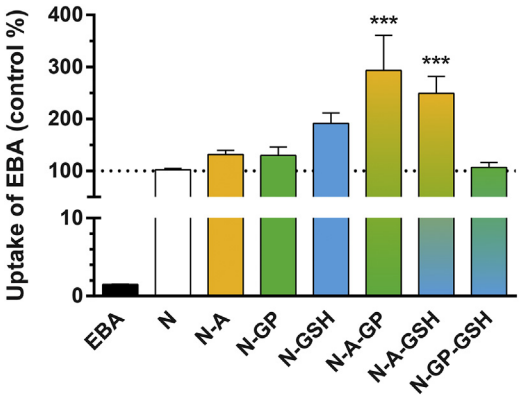

Fig. 5. The uptake of non-targeted (N), single- (N-A, N-GP, N-GSH) and dual-targeted (N-A-GP, N-A-GSH, N-GP-GSH) niosomes in brain endothelial cells after 4-hour incubation. Values presented are means ± SEM. Statistical analysis: ANOVA followed by Dunnett's posttest, where $^{***}P < 0.001$, compared to non-targeted N group; $n = 10$.

3.10. Interaction of nanovesicles with RBECs: Plasma membrane fluidity

The membrane fluidity of brain endothelial cells, determined by fluorescence anisotropy (Kiss et al., 2014), was significantly decreased after 4 h treatment with N and N-A-GSH nanovesicles (Fig. 10) indicating increased cell membrane fluidity and a fusion process. The membrane fluidizer benzyl alcohol (30 mM) quickly and greatly reduced the TMA-DPH fluorescence anisotropy after 3 min compared to the control and niosome treated groups indicating maximal plasma membrane fluidity.

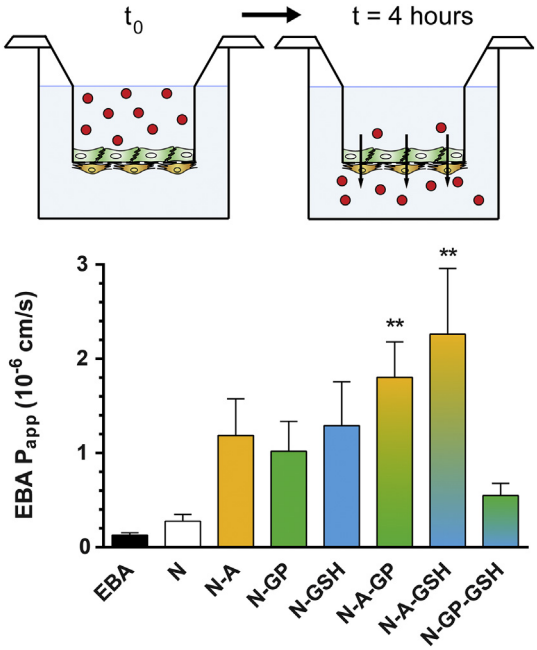

Fig. 6. Permeability of albumin cargo across the culture BBB model after treatment with different niosomes (10 mg/mL, 4 h). Values presented are means ± SEM. Statistical analysis: ANOVA, Dunnett's posttest. $^{**}P < 0.01$, compared to non-targeted N group; n = 10.

3.11. Imaging of EBA in mice after intravenous injection of targeted niosomes

Brain penetration of the red fluorescent EBA was measured by imaging in nude mice. Free EBA and EBA encapsulated in targeted and non-targeted niosomes were injected intravenously. There was no

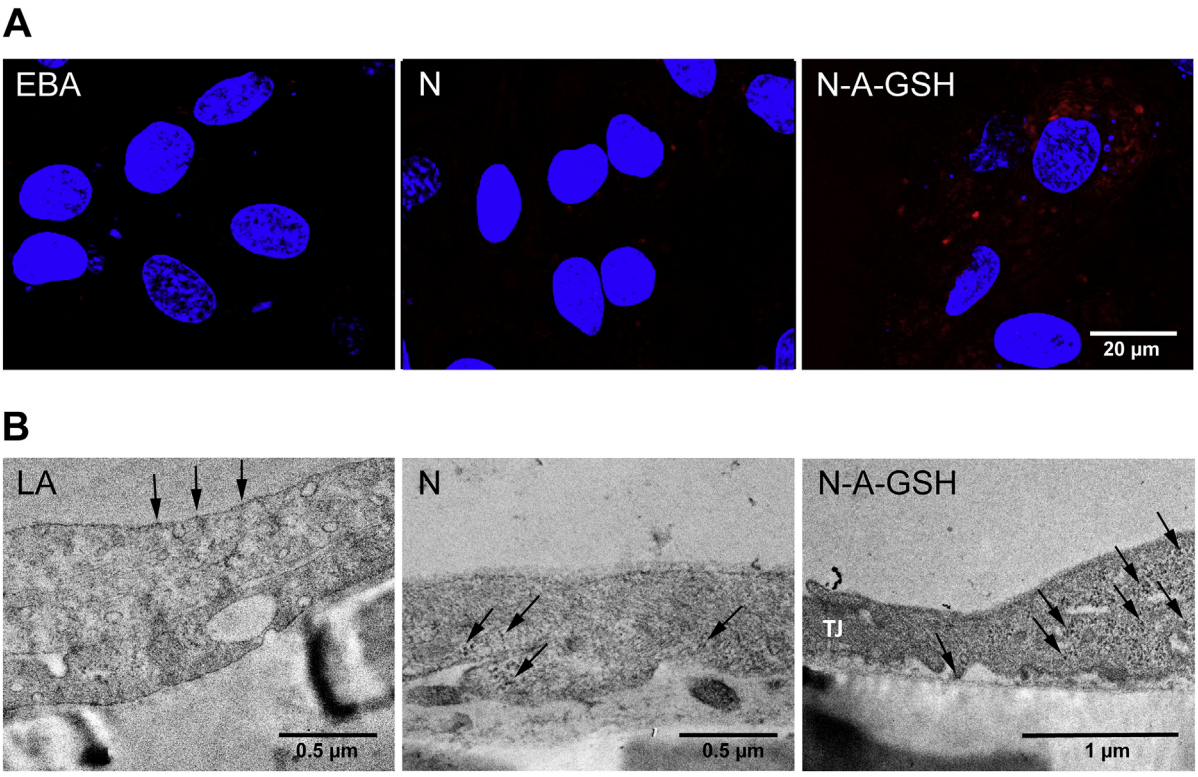

Fig. 7. (A) Confocal microscopy images of cultured brain endothelial cells incubated with unencapsulated cargo (EBA, showing red fluorescence), non-targeted (N) or alanine-glutathione-targeted (N-A-GSH) niosomes for 4 h at 37 °C. Cell nuclei were stained with bis-benzimide (blue). Bar: 20 µm. (B) Transmission electron microscopy images of the uptake of free lanthanum (LA) and lanthanum (black arrows) encapsulated in non-targeted (N) or alanine-glutathione-targeted (N-A-GSH) niosomes in brain endothelial cells after 4 h incubation. Bar: 0.5 and 1 µm. TJ: tight junction. (For interpretation of the references to color in this figure legend, the reader is referred to the web version of this article.)

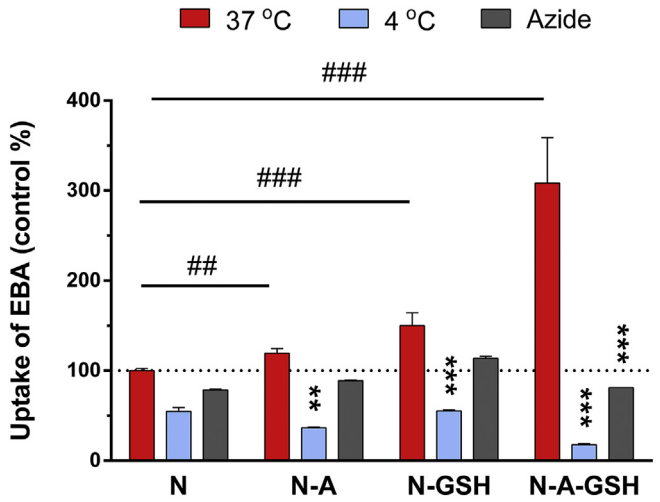

Fig. 8. The effect of temperature and metabolic inhibitor sodium azide (0.1%) on the uptake of EBA cargo in brain endothelial cells after 4 h incubation with non-targeted (N), alanine-targeted (N-A), glutathione-targeted (N-GSH) and alanine-glutathione-targeted (N-A-GSH) niosomes. Values presented are means ± SEM. Statistical analysis: two-way ANOVA, Bonferroni posttest. $^{*}P < 0.5$; $^{**}P < 0.01$; $^{***}P < 0.001$, compared to first column of each groups, $^{\#\#\#}P < 0.001$, compared to N treated group; $n = 4–6$.

significant accumulation of fluorescent signal in the brain area in the case of free EBA (Fig. 11). Encapsulation of EBA in non-targeted niosomes resulted in enhanced brain fluorescent intensity. The fluorescent signal in the brain area was further increased in the single ligand targeted N-A and N-GP groups. Fluorescent signal from EBA cargo in the dual-ligand targeted N-A-GP group was the highest as compared to all groups at all time points (Fig. 11). The differences between targeted, dual-ligand targeted and non-targeted niosomes were still visible at 24 h.

4. Discussion

4.1. Functionalization of NPs for BBB targeting by SLC ligands

Nanocarriers are intensively investigated as novel therapeutic tools to prevent or to treat CNS disorders (Masserini, 2013; Loureiro et al., 2015; Saraiva et al., 2016). The key problem for the effective targeting of NPs to brain is the proper functionalization of these carriers to cross the BBB (Wohlfart et al., 2012; Masserini, 2013; Kreuter, 2014). NPs accumulate in several organs, including liver, spleen, and kidney, and only specific BBB targeting can increase the ratio of nanocarriers penetrating the CNS (Saraiva et al., 2016). To ensure this relative brain specificity it is important to functionalize the NPs with targeting molecules which are substrates of physiological transporters of the BBB and able to trigger active and specific transport mechanisms to cross the BBB.

As compared to BBB receptors, SCLs are underresearched as molecular targets of CNS drug delivery systems (Rask-Andersen et al., 2013). The glucose consumption of the brain is the highest among the organs, and hexose transporters, especially GLUT-1 (SLC2A1), are highly expressed at the BBB (Campos-Bedolla et al., 2014). We confirmed that several glucose transporters were expressed in isolated rat brain microvessels and in brain endothelial cells of the BBB co-culture model with the *Glut1* gene showing the highest mRNA expression. N-dodecyl-β-D-glucopyranose was selected as a non-degraded glucose analog to decorate the niosomes. Using culture models of the BBB we found about 30% increase in the uptake and three-fold elevation in the permeability of the EBA cargo with N-GP, as compared to non-targeted niosomes, but

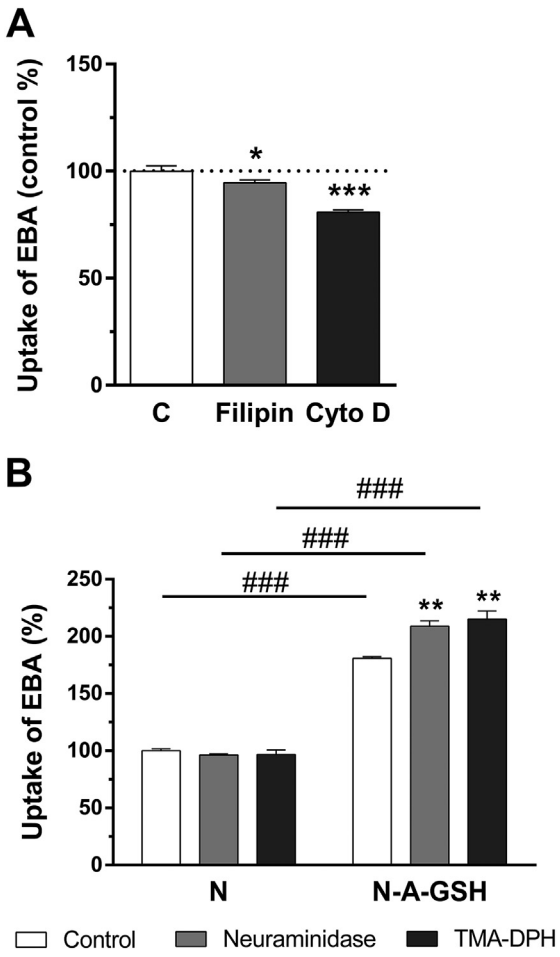

Fig. 9. (A) Inhibition of the uptake of EBA cargo with filipin (6 μM) or cytochalasin D (20 μM) in rat brain endothelial cells after 4 hours incubation with alanine-glutathione duale-targeted niosomes (N-A-GSH). Values presented are means ± SEM. Statistical analysis: ANOVA followed by Dunnett's posttest where $^{*}P < 0.5$; $^{***}P < 0.001$, compared to the control group; $n = 6$. (B) The effect of neuraminidase (1 U/ml) and TMA-DPH (30 mM) on the uptake of EBA cargo in brain endothelial cells incubated with non-targeted (N) and alanine-glutathione dual-targeted niosomes (N-A-GSH). Statistical analysis: two-way ANOVA, Bonferroni posttest. $^{**}P < 0.01$ compared to first column of each groups; $^{###}P < 0.001$, compared to N treated groups; $n = 6$.

these changes were statistically not significant. In mice the brain fluorescence of EBA significantly increased at 10 min and several fold elevation was observed until 24 h after tail vein injection of N-GP. Our *in vivo* results are in agreement with the findings of Dufes et al., who described that niosomes targeted with N-palmitoylglucosamine ligand enhanced the brain entry of the cargo vasoctive intestinal peptide in mice (Dufes et al., 2004). Small gold NPs covalently coated with β2-mercaptoethoxy-glucose entered and crossed cultured human brain endothelial cells better than non-brain endothelial cells (Gromnicova et al., 2013). Nanoparticles, including liposomes, micelles and solid polymeric NPs derivatized with different glucose analogs improve the delivery of encapsulated drugs or fluorescent dyes to the brain by targeting GLUTs as reviewed by Patching (2017) indicating the potential applicability of these SLCs.

The small neutral amino acid alanine, which is transported by several SLCs at the BBB (Campos-Bedolla et al., 2014), was selected as the other targeting ligand of the tested niosomes. The mRNAs of both the sodium coupled and neutral amino acid carriers were highly represented in brain microvessels and the BBB culture model. To our best knowledge, this is the first report indicating that NPs decorated with alanine as a targeting ligand elevated the uptake of the cargo in

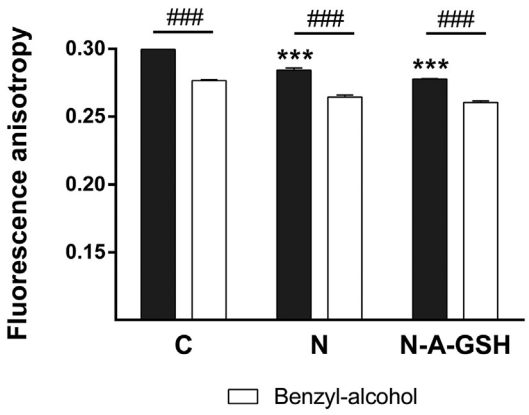

Fig. 10. The effect of non-targeted (N) and alanine-glutathione dual-targeted niosomes (N-A-GSH) and benzyl alcohol (30 mM) on plasma membrane fluidity measured by fluorescence anisotropy on living brain endothelial cell suspensions. Values presented are means ± SEM. Statistical analysis: two-way ANOVA, Bonferroni posttest. $^{***}P < 0.001$, all groups were compared to non-treated control (C); $^{###}P < 0.001$, compared to first column of each groups, $n = 3$.

cultured brain endothelial cells (Fig. 8) and its brain entry in mice (Fig. 11).

As a reference targeting ligand niosomes were also functionalized with glutathione. Labeling of niosomes with GSH-PEG significantly increased the uptake of EBA in primary RBECs (Fig. 8) and elevated four-fold the EBA permeability across the BBB culture model as compared to untargeted NPs (Fig. 6). These findings are supported by data showing that GSH targeting of liposomes elevated the uptake of carboxifluorescein in RBE4 rat brain endothelial cell line (Rip et al., 2014) and that of doxorubicin in hCMEC/D3 human brain endothelial cell line (Gaillard et al., 2014). GSH labeling also elevated the permeability of solid NPs across BBB culture models (Grover et al., 2014; Veszelka et al., 2017). The GSH-PEGylated liposomal drug delivery system was effective in rodent models for brain delivery of different drug cargos, like doxorubicin (Gaillard et al., 2014) or ribavirin (Maussang et al., 2016), indicating the *in vivo* applicability of GSH and the predictive value of *in vitro* BBB models.

4.2. Dual targeting of BBB transporters

In concordance with our hypothesis, dual labeling of niosomes with ligands of BBB transporters (N-A-GP and N-A-GSH) elevated the cargo uptake in RBECs and penetration across the BBB model as compared to both single ligand targeted or untargeted NPs. The effect of dual labeling of NPs with SLC substrates (N-A-GP) on brain uptake of cargo was the highest in the mouse study (Fig. 11). The cargo selected for our study, the large biomolecule albumin, has a negligible transport across the BBB in physiological conditions (Abbott et al., 2010). This is also reflected in the very low P_{app} value (0.1×10^{-6} cm/s) of the free EBA across the BBB model (Fig. 6), in accordance with our previous data (Deli et al., 2005; Walter et al., 2015; Veszelka et al., 2018). Free EBA cargo penetration to brain was also limited in mice (Fig. 11), as we demonstrated it in our previous study (Veszelka et al., 2003). It should be noted, that compared to small molecule permeability, the P_{app} value of EBA increased by dual targeted nanovesicles is still low (Fig. 11). We should consider however, that this limited EBA transport represent 10- and 20-fold increases in the P_{app} value or in the brain fluorescence intensity, respectively, of this low penetrant cargo.

As a possible mechanism, the combination of two different SLC transporter ligands on the niosomal surface may produce stronger vesicular docking to brain endothelial cells facilitating NP fusion and/or endocytosis. There are two studies which may support this dual BBB targeting hypothesis, although with different systems. Liposomes

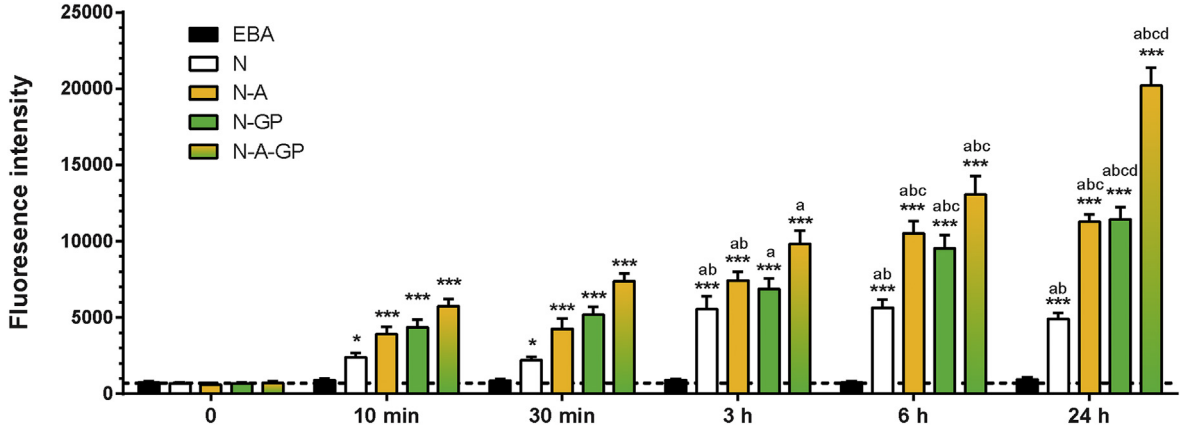

Fig. 11. Fluorescent intensity of EBA in the brain regions of mice after injection of free EBA or EBA encapsulated in non-targeted (N), single- (N-A, N-GP) or dual-targeted (N-A-GP) niosomes measured by optical imaging. Values presented are means ± SD. Statistical analysis: two-way ANOVA, Bonferroni posttest. $*P < 0.5$; $**P < 0.01$; $***P < 0.001$, as compared to the EBA-treated group within each time point; a: as compared to the 10 min, b: as compared to the 30 min, c: as compared to the 3 h, d: as compared to the 6 h time points within each group, $n = 3–4$.

(100 nm) were dually decorated with ligands of the transferrin and LRP receptors expressed at the BBB (Markoutsa et al., 2014). Dual-targeting for BBB receptors increased BBB penetration of NPs both in cultured brain endothelial cells and in mice, indicating that targeting more than one receptors at the BBB can be more effective, similarly to targeting multiple BBB transporters. In another study 2 nm carbon dots prepared by pyrolysis from D-glucose and L-aspartic acid penetrated glioma tissue better than normal brain in mice, but not carbon dots prepared from D-glucose, L-aspartic acid, or D-glucose and L-glutamic acid (Zheng et al., 2015). In this study, however, no experiments were done to reveal the uptake mechanism(s) and whether this was an active, energy dependent process.

Dual-targeted drug delivery systems are also described for other glioma preclinical models, but in these cases not multiple BBB transporters are involved. For example, the ligand of hexose transporters, 2-deoxy-D-glucose, was used as a NP ligand targeting both the BBB and the glioma cells (Jiang et al., 2014). In other systems even if two different ligands are used, only one is specific for the BBB, the other ligand serves for different purposes, like cell penetration. The combination of T7 peptide targeting TfR at the BBB and the cell-penetrating peptide TAT enhanced the efficiency of glioma targeting of liposomes (Zong et al., 2014).

4.3. Mechanism of targeted NP uptake

Modified physiological conditions, such as low temperature or the inhibition of ATP hydrolysis can help to identify the cellular uptake mechanisms of NPs (Fiorentino et al., 2015). In our study the uptake of cargo was decreased in the targeted NP groups by both low temperature and the metabolic inhibitor sodium azide, which is consistent with the hypothesis that the cellular uptake of targeted niosomes was an energy-dependent active process. In agreement with our experiments the uptake of GSH labeled liposomes in brain endothelial cells was also inhibited by low temperature (Maussang et al., 2016).

We also supposed that endocytotic processes might participate in the uptake of targeted niosomes, therefore we used inhibitors of endocytosis, cytochalasin D and filipin. Cytochalasin D is a drug blocking F-actin depolymerization, membrane ruffling and thereby inhibiting macropinocytosis and phagocytosis. Since actin cytoskeleton regulates several endocytotic pathways cytochalasin D is a common inhibitor of endocytosis (Ivanov, 2008). Cytochalasin D pretreatment inhibited the uptake of GSH-PEG liposomes in hCMEC/D3 endothelial cell line (Maussang et al., 2016) as well as the uptake of platelet-derived microparticles (Faille et al., 2012) indicating that the internalization of extracellular NPs into endocytotic vesicles might be an important step in the cellular uptake mecanisms. The antibiotic filipin interacts with cholesterol in the biological membranes and inhibits selectively the lipid raft and caveolae-mediated endocytosis (Ivanov, 2008). Pretreatment of brain endothelial cells with cytochalasin D or filipin significantly decreased the uptake of the cargo in the case of dual-targeted niosomes (N-A-GSH). These data indicate that endocytosis contributes to the cellular uptake of targeted niosomes.

Several specific features of the BBB limit the penetration of drugs to CNS. Intercellular junctions and drug efflux pumps are widely investigated, but the role of the negative surface charge of brain endothelial cells in CNS drug delivery is rather unexplored. This highly negative surface charge is composed of the negatively charged lipids in the cellular plasma membrane and the glycocalyx at the luminal surface. The glycocalyx is a 0.1–1 μm thin layer covering the entire surface of endothelial cells and composed of proteoglycans and glycosaminoglycans (Hervé et al., 2008). The surface charge of cells can be measured by dynamic light scattering (zeta-sizer) and was found to be the most negative in brain endothelial cells among vascular endothelial cells (Ribeiro et al., 2012). This electrostatic barrier may influence the transport of substances and also NPs across the BBB. While NP surface charge was already investigated on BBB integrity and permeability (Fenart et al., 1999; Lockman et al., 2004), the effect of brain endothelial surface charge modification on the permeability of NPs was not measured yet. We modified the highly negative surface charge with neuraminidase and the TMA-DPH cationic lipid. The neuraminidase or sialidase digests the negatively charged sialic acid residues on the luminal surface of vascular endothelial cells and elevates the surface charge of glycocalyx (Born and Palinski, 1985). In our experiments neuraminidase treatment of brain endothelial cells significantly increased the uptake of the cargo of dual-targeted NPs compared with the untargeted and non-treated groups. TMA-DPH elevates the charge of the plasma membrane because it intercalates with the hydrophilic head groups of membrane phospholipids (Ribeiro et al., 2012). TMA-DPH also raised the cellular uptake of cargo in the dual-targeted NP group, similarly to neuraminidase. Our new observations indicate that surface charge at the BBB is important in the uptake mechanism of charged NPs and can be modulated by modification of plasma membrane lipid composition or the glycocalyx.

Surfactants are well known enhancers of absorption and increase drug permeability through the cell membranes or *via* the modulation of intercellular junctions (Deli, 2009). Surfactants are incorporated into the lipid bilayer of cell membranes, and depending on their concentration either change the physical properties and permeability of plasma membranes or result in membrane solubilization leading to cell toxicity (Ujhelyi et al., 2012). Polysorbate surfactants, especially

Solulan C24 which is one of the main components of our niosomes concentration-dependently increased the transepithelial permeability of hidrophilic drug as a result of solubilization of membrane components of Caco-2 cells (Dimitrijevic et al., 2000). We have previously demonstrated that the non-ionic surfactant sugar esters increased the plasma membrane fluidity of epithelial cells which could contribute to the increased transcellular passage of molecules (Kiss et al., 2014). In the present experiments both the non-targeted and dual-targeted niosomes decreased the fluorescent anisotropy in brain endothelial cells, which indicates increased cell membrane fluidity, suggesting the fusion of the nanovesicles with the plasma membrane.

4.4. Possible advantages and limitations of niosomes targeting BBB as a delivery system

Niosomes in terms of stability and permeability for drug-size molecules are comparable to liposomes (Abdelkader et al., 2014; Bartelds et al., 2018). In addition, the components of niosomes are cheap, not sensitive for oxidation, and can be easily stored and handled. Similarly to liposomes, they are suitable for the encapsulation of both water and lipid soluble molecules (Abdelkader et al., 2014). Before our study, the 3.3 kDa hormone, vasoctive intestinal peptide, was the largest cargo encapsulated in niosomes and targeted successfully to brain in mice (Dufes et al., 2004). The molecular mass of our cargo, serum albumin is 20 times bigger, suggesting that niosomes are able to deliver large biomolecules. Due to their non-ionic components and good biodegradability niosomes show low toxicity (Abdelkader et al., 2014). It should be noted, that non-ionic surfactants may increase in a concentration dependent way the plasma membrane fluidity of mammalian cells, as we demonstrated in our previous study with sucrose esters (Kiss et al., 2014), and in our present study with niosomes. This effect may help in the delivery of molecules, but can also contribute to cellular toxicity. While liposomes are already used in pharmacotherapy, only preclinical data, but no clinical studies were reported for niosomes. To assess the efficacy of BBB targeted niosomes as a delivery system, comparative studies including other nanoparticles, like liposomes, and other targeting ligands are needed.

4.5. Conclusion

Ligands targeting brain endothelial transporters elevated the permeability of the albumin cargo across the BBB in the culture model and in mice, and dual-ligand decoration of niosomes was more effective than single ligand labeling. Our data indicate that dual labeling with ligands of multiple SLC transporters can potentially be exploited for BBB targeting of NPs.

Acknowledgements

This work was supported by the Hungarian Scientific Research Fund (OTKA/NKFIH 105622), the National Research, Development and Innovation Office (GINOP-2.2.1-15-2016-00007, GINOP-2.3.2-15-2016-00060) and by the EU-funded Hungarian grant EFOP-3.6.1-16-2016-00008. S.V. was supported by the János Bolyai Research Scholarship of the Hungarian Academy of Sciences (BO/00724/12, BO/00793/18/8). G.P. is a Szent-Györgyi student in the Szeged Scientists Academy Program of the Foundation for the Future of Biomedical Sciences in Szeged implemented with the support of the Ministry of Human Resources (TSZ:34232-3/2016/INTFIN).

References

Abbott, N.J., 2013. Blood-brain barrier structure and function and the challenges for CNS drug delivery. J. Inherit. Metab. Dis. 36, 437–449.
Abbott, N.J., Patabendige, A.A., Dolman, D.E., Yusof, S.R., Begley, D.J., 2010. Structure and function of the blood-brain barrier. Neurobiol. Dis. 37, 13–25.
Abdelkader, H., Alani, A.W., Alany, R.G., 2014. Recent advances in non-ionic surfactant vesicles (niosomes): self-assembly, fabrication, characterization, drug delivery applications and limitations. Drug Deliv. 21, 87–100.
Banks, W.A., 2009. Characteristics of compounds that cross the blood-brain barrier. BMC Neurol. 9 (Suppl. 1), S3.
Bartelds, R., Nematollahi, M.H., Pols, T., Stuart, M.C.A., Pardakhty, A., Asadikaram, G., Poolman, B., 2018. Niosomes, an alternative for liposomal delivery. PLoS One 13, e0194179.
Birngruber, T., Raml, R., Gladdines, W., Gatschelhofer, C., Gander, E., Ghosh, A., Kroath, T., Gaillard, P.J., Pieber, T.R., Sinner, F., 2014. Enhanced doxorubicin delivery to the brain administered through glutathione PEGylated liposomal doxorubicin (2B3-101) as compared with generic Caelyx,(®)/Doxil(®)-a cerebral open flow microperfusion pilot study. J. Pharm. Sci. 103, 1945–1948.
Bocsik, A., Walter, F.R., Gyebrovszki, A., Fülöp, L., Blasig, I., Dabrowski, S., Ötvös, F., Tóth, A., Rákhely, G., Veszelka, S., Vastag, M., Szabó-Révész, P., Deli, M.A., 2016. Reversible opening of intercellular junctions of intestinal epithelial and brain endothelial cells with tight junction modulator peptides. J. Pharm. Sci. 105, 754–765.
Born, G.V., Palinski, W., 1985. Unusually high concentrations of sialic acids on thesurface of vascular endothelia. Br. J. Exp. Pathol. 66, 543–549.
Campos-Bedolla, P., Walter, F.R., Veszelka, S., Deli, M.A., 2014. Role of the blood-brain barrier in the nutrition of the central nervous system. Arch. Med. Res. 45, 610–638.
César-Razquin, A., Snijder, B., Frappier-Brinton, T., 2015. A call for systematic research on solute carriers. Cell 162, 478–487.
Csete, M., Sipos, Á., Kőházi-Kis, A., Szalai, A., Szekeres, G., Matesz, A., Csákó, T., Osvay, K., Bor, Z., Penke, B., Deli, M.A., Veszelka, S., Schmatulla, A., Marti, O., 2007. Comparative study of sub-micrometer polymeric dot-arrays, linear and crossed gratings generated by UV laser based two-beam interference as surfaces for AFM and SPR based bio-sensing. Appl. Surf. Sci. 254, 1194–1205.
Deli, M.A., 2009. Potential use of tight junction modulators to reversibly open membranous barriers and improve drug delivery. Biochim. Biophys. Acta 1788, 892–910.
Deli, M.A., 2011. Drug transport and the blood-brain barrier. In: Tihanyi, K., Vastag, M. (Eds.), Solubility, Delivery, and ADME Problems of Drugs and Drug-Candidates. Bentham Science Publishers Ltd., Washington, pp. 144–165.
Deli, M.A., Abrahám, C.S., Kataoka, Y., Niwa, M., 2005. Permeability studies on in vitro blood-brain barrier models: physiology, pathology, and pharmacology. Cell. Mol. Neurobiol. 25, 59–127.
Dimitrijevic, D., Shaw, A.J., Florence, A.T., 2000. Effects of some non-ionic surfactants on transepithelial permeability in Caco-2 cells. J. Pharm. Pharmacol. 52, 157–162.
Dufes, C., Gaillard, F., Uchegbu, I.F., Schätzlein, A.G., Olivier, J.C., Muller, J.M., 2004. Glucose-targeted niosomes deliver vasoactive intestinal peptide (VIP) to the brain. Int. J. Pharm. 285, 77–85.
Enerson, B.E., Drewes, L.R., 2006. The rat blood-brain barrier transcriptome. J. Cereb. Blood Flow Metab. 26, 959–973.
Faille, D., El-Assaad, F., Mitchell, A.J., Alessi, M.C., Chimini, G., Fusai, T., Grau, G.E., Combes, V., 2012. Endocytosis and intracellular processing of platelet microparticles by brain endothelial cells. J. Cell. Mol. Med. 16, 1731–1738.
Fenart, L., Casanova, A., Dehouck, B., Duhem, C., Slupek, S., Cecchelli, R., Betbeder, D., 1999. Evaluation of effect of charge and lipid coating on ability of 60-nm nanoparticles to cross an in vitro model of the blood-brain barrier. J. Pharmacol. Exp. Ther. 291, 1017–1022.
Fiorentino, I., Gualtieri, R., Barbato, V., Mollo, V., Braun, S., Angrisani, A., Turano, M., Furia, M., Netti, P.A., Guarnieri, D., Fusco, S., Talevi, R., 2015. Energy independent uptake and release of polystyrene nanoparticles in primary mammalian cell cultures. Exp. Cell Res. 330, 240–247.
Gaillard, P.J., 2016. BBB crossing assessment and BBB crossing technologies in CNS drug discovery. Drug Discov. Today Technol. 20, 1–3.
Gaillard, P.J., Appeldoorn, C.C., Dorland, R., van Kregten, J., Manca, F., Vugts, D.J., Windhorst, B., van Dongen, G.A., de Vries, H.E., Maussang, D., van Tellingen, O., 2014. Pharmacokinetics, brain delivery, and efficacy in brain tumor-bearing mice of glutathione pegylated liposomal doxorubicin (2B3-101). PLoS One 1, e82331.
Gromnicova, R., Davies, H.A., Sreekanthreddy, P., Romero, I.A., Lund, T., Roitt, I.M., Phillips, J.B., Male, D.K., 2013. Glucose-coated gold nanoparticles transfer across human brain endothelium and enter astrocytes in vitro. PLoS One 9, e81043.
Grover, A., Hirani, A., Pathak, Y., Sutariya, V., 2014. Brain-targeted delivery of docetaxel by glutathione-coated nanoparticles for brain cancer. AAPS PharmSciTech 15, 1562–1568.
Hervé, F., Ghinea, N., Scherrmann, J.M., 2008. CNS delivery via adsorptive transcytosis. AAPS J. 10, 455–472.
Horvát, S., Fehér, A., Wolburg, H., Sipos, P., Veszelka, S., Tóth, A., Kiss, L., Kurunczi, A., Balogh, G., Kürti, L., Eros, I., Szabó-Révész, P., Deli, M.A., 2009. Sodium hyaluronate as a mucoadhesive component in nasal formulation enhances delivery of molecules to brain tissue. Eur. J. Pharm. Biopharm. 72, 252–259.
Hülper, P., Veszelka, S., Walter, F.R., Wolburg, H., Fallier-Becker, P., Piontek, J., Blasig, I.E., Lakomek, M., Kugler, W., Deli, M.A., 2013. Acute effects of short-chain alkylglycerols on blood-brain barrier properties of cultured brain endothelial cells. Br. J. Pharmacol. 169, 1561–1573.
Ivanov, A.I., 2008. Pharmacological inhibition of endocytic pathways: is it specific enough to be useful? Methods Mol. Biol. 440, 15–33.
Jiang, X., Xin, H., Ren, Q., Gu, J., Zhu, L., Du, F., Feng, C., Xie, Y., Sha, X., Fang, X., 2014. Nanoparticles of 2-deoxy-D-glucose functionalized poly(ethylene glycol)-co-poly (trimethylene carbonate) for dual-targeted drug delivery in glioma treatment. Biomaterials 35, 518–529.
Johnsen, K.B., Moos, T., 2016. Revisiting nanoparticle technology for blood-brain barrier transport: unfolding at the endothelial gate improves the fate of transferrin receptor-targeted liposomes. J. Control. Release 28, 32–46.
Keren, S., Gheysens, O., Levin, C.S., Gambhir, S.S., 2008. A comparison between a time

domain and continuous wave small animal optical imaging system. IEEE Trans. Med. Imaging 27, 58–63.
Kiss, L., Walter, F.R., Bocsik, A., Veszelka, S., Ozsvári, B., Puskás, L.G., Szabó-Révész, P., Deli, M.A., 2013. Kinetic analysis of the toxicity of pharmaceutical excipients Cremophor EL and RH40 on endothelial and epithelial cells. J. Pharm. Sci. 102, 1173–1181.
Kiss, L., Hellinger, É., Pilbat, A.M., Kittel, Á., Török, Z., Füredi, A., Szakács, G., Veszelka, S., Sipos, P., Ózsvári, B., Puskás, L.G., Vastag, M., Szabó-Révész, P., Deli, M.A., 2014. Sucrose esters increase drug penetration, but do not inhibit P-glycoprotein in Caco-2 intestinal epithelial cells. J. Pharm. Sci. 103, 3107–3119.
Kreuter, J., 2014. Drug delivery to the central nervous system by polymeric nanoparticles: what do we know? Adv. Drug Deliv. Rev. 71, 2–14.
Kumar, A.T.N., Raymond, S.B., Dunn, A.K., Bacskai, B.J., Boas, D.A., 2008. A time domain fluorescence tomography system for small animal imaging. IEEE Trans. Med. Imaging 27, 1152–1163.
Lénárt, N., Walter, F.R., Bocsik, A., Sántha, P., Tóth, M.E., Harazin, A., Tóth, A.E., Vizler, C., Török, Z., Pilbat, A.M., Vígh, L., Puskás, L.G., Sántha, M., Deli, M.A., 2015. Cultured Cells of the Blood-Brain Barrier From Apolipoprotein B-100 Transgenic Mice: Effects of Oxidized Low-Density Lipoprotein Treatment. Fluids Barriers CNS.17. pp. 12–17.
Lindqvist, A., Rip, J., van Kregten, J., Gaillard, P.J., Hammarlund-Udenaes, M., 2016. In vivo functional evaluation of increased brain delivery of the opioid peptide DAMGO by glutathione-PEGylated liposomes. Pharm. Res. 33, 177–185.
Liu, D., Li, Y., Deng, J., Yang, W., 2014. Helix-sense-selective polymerization of achiral substituted acetylene in chiral micelles for preparing optically active polymer nanoparticles: effects of chiral emulsifiers. Polymer 55, 840–847.
Livak, K.J., Schmittgen, T.D., 2001. Analysis of relative gene expression data using real-time quantitative PCR and the 2(−Delta Delta C(T)) method. Methods 25, 402–408.
Lockman, P.R., Koziara, J.M., Mumper, R.J., Allen, D.D., 2004. Nanoparticle surface charges alter blood-brain barrier integrity and permeability. J. Drug Target. 12, 635–641.
Loureiro, J.A., Gomes, B., Fricker, G., Cardoso, I., Ribeiro, C.A., Gaiteiro, C., Coelho, M.A., Pereira, Mdo C., Rocha, S., 2015. Dual ligand immunoliposomes for drug delivery to the brain. Colloids Surf. B. Biointerfaces. 134, 213–219.
Markoutsa, E., Papadia, K., Giannou, A.D., Spella, M., Cagnotto, A., Salmona, M., Stathopoulos, G.T., Antimisiaris, S.G., 2014. Mono and dually decorated nanoliposomes for brain targeting, in vitro and in vivo studies. Pharm. Res. 31, 1275–1289.
Masserini, M., 2013. Nanoparticles for brain drug delivery. ISRN. Biochem. 2013, 238428.
Maussang, D., Rip, J., van Kregten, J., van den Heuvel, A., van der Pol, S., van der Boom, B., Reijerkerk, A., Chen, L., de Boer, M., Gaillard, P., de Vries, H., 2016. Glutathione conjugation dose-dependently increases brain-specific liposomal drug delivery in vitro and in vivo. Drug Discov. Today Technol. 20, 59–69.
Nakagawa, S., Deli, M.A., Kawaguchi, H., Shimizudani, T., Shimono, T., Kittel, A., Tanaka, K., Niwa, M., 2009. A new blood-brain barrier model using primary rat brain endothelial cells, pericytes and astrocytes. Neurochem. Int. 54, 253–263.
Pardridge, W.M., 2012. Drug transport across the blood-brain barrier. J. Cereb. Blood Flow Metab. 11, 1959–1972.
Pardridge, W.M., 2015. Targeted delivery of protein and gene medicines through the blood-brain barrier. Clin. Pharmacol. Ther. 97, 347–361.
Pardridge, W.M., 2016. CSF, blood-brain barrier, and brain drug delivery. Expert. Opin. Drug. Deliv. 13, 963–975.
Patching, S.G., 2017. Glucose transporters at the blood-brain barrier: function, regulation and gateways for drug delivery. Mol. Neurobiol. 54, 1046–1077.
Perrière, N., Demeuse, P., Garcia, E., Regina, A., Debray, M., Andreux, J.P., Couvreur, P., Scherrmann, J.M., Temsamani, J., Couraud, P.O., Deli, M.A., Roux, F., 2005. Puromycin-based purification of rat brain capillary endothelial cell cultures. Effect on the expression of blood-brain barrier-specific properties. J. Neurochem. 93, 279–289.
Rask-Andersen, M., Masuram, S., Fredriksson, R., Schiöth, H.B., 2013. Solute carriers as drug targets: current use, clinical trials and prospective. Mol. Asp. Med. 34, 702–710.
Ribeiro, M.M., Domingues, M.M., Freire, J.M., Santos, N.C., Castanho, M.A., 2012. Translocating the blood-brain barrier using electrostatics. Front. Cell. Neurosci. 11, 6–44.
Rip, J., Chen, L., Hartman, R., van den Heuvel, A., Reijerkerk, A., van Kregten, J., van der Boom, B., Appeldoorn, C., de Boer, M., Maussang, D., de Lange, E.C., Gaillard, P.J., 2014. Glutathione PEGylated liposomes: pharmacokinetics and delivery of cargo across the blood-brain barrier in rats. J. Drug Target. 22, 460–467.
Saraiva, C., Praça, C., Ferreira, R., Santos, T., Ferreira, L., Bernardino, L., 2016. Nanoparticle-mediated brain drug delivery: overcoming blood-brain barrier to treat neurodegenerative diseases. J. Control. Release 10, 34–47.
Shawahna, R., Uchida, Y., Declèves, X., Ohtsuki, S., Yousif, S., Dauchy, S., Jacob, A., Chassoux, F., Daumas-Duport, C., Couraud, P.O., Terasaki, T., Scherrmann, J.M., 2011. Transcriptomic and quantitative proteomic analysis of transporters and drug metabolizing enzymes in freshly isolated human brain microvessels. Mol. Pharm. 8, 1332–1341.
Singh, A., Satchell, S.C., Neal, C.R., McKenzie, E.A., Tooke, J.E., Mathieson, P.W., 2007. Glomerular endothelial glycocalyx constitutes a barrier to protein permeability. J. Am. Soc. Nephrol. 18, 2885–2893.
Sipos, E., Kurunczi, A., Fehér, A., Penke, Z., Fülöp, L., Kasza, A., Horváth, J., Horvát, S., Veszelka, S., Balogh, G., Kürti, L., Eros, I., Szabó-Révész, P., Párducz, A., Penke, B., Deli, M.A., 2010. Intranasal delivery of human beta-amyloid peptide in rats: effective brain targeting. Cell. Mol. Neurobiol. 30, 405–413.
Tóth, A.E., Tóth, A., Walter, F.R., Kiss, L., Veszelka, S., Ózsvári, B., Puskás, L.G., Heimesaat, M.M., Dohgu, S., Kataoka, Y., Rákhely, G., Deli, M.A., 2014. Compounds blocking methylglyoxal-induced protein modification and brain endothelial injury. Arch. Med. Res. 45, 753–764.
Uchida, Y., Ito, K., Ohtsuki, S., Kubo, Y., Suzuki, T., Terasaki, T., 2015. Major involvement of Na(+) -dependent multivitamin transporter (SLC5A6/SMVT) in uptake of biotin and pantothenic acid by human brain capillary endothelial cells. J. Neurochem. 134, 97–112.
Ujhelyi, Z., Fenyvesi, F., Váradi, J., Fehér, P., Kiss, T., Veszelka, S., Deli, M., Vecsernyés, M., Bácskay, I., 2012. Evaluation of cytotoxicity of surfactants used in self-micro emulsifying drug delivery systems and their effects on paracellular transport in Caco-2 cell monolayer. Eur. J. Pharm. Sci. 47, 564–573.
Uyama, O., Okamura, N., Yanase, M., Narita, M., Kawabata, K., Sugita, M., 1988. Quantitative evaluation of vascular permeability in the gerbil brain after transient ischemia using Evans blue fluorescence. J. Cereb. Blood Flow Metab. 8, 282–284.
Veszelka, S., Urbányi, Z., Pázmány, T., Németh, L., Obál, I., Dung, N.T., Abrahám, C.S., Szabó, G., Deli, M.A., 2003. Human serum amyloid P component attenuates the bacterial lipopolysaccharide-induced increase in blood-brain barrier permeability in mice. Neurosci. Lett. 352, 57–60.
Veszelka, S., Pásztói, M., Farkas, A.E., Krizbai, I., Ngo, T.K., Niwa, M., Ábrahám, C.S., Deli, M.A., 2007. Pentosan polysulfate protects brain endothelial cells against bacterial lipopolysaccharide-induced damages. Neurochem. Int. 50, 219–228.
Veszelka, S., Meszaros, M., Kiss, L., Kota, Z., Pali, T., Hoyk, Z., Bozso, Z., Fulop, L., Toth, A., Rakhely, G., Deli, M.A., 2017. Biotin and glutathione targeting of solid nanoparticles to cross human brain endothelial cells. Curr. Pharm. Des. 23, 4198–4205.
Veszelka, S., Tóth, A., Walter, F.R., Tóth, A.E., Gróf, I., Mészáros, M., Bocsik, A., Hellinger, É., Vastag, M., Rákhely, G., Deli, M.A., 2018. Comparison of a rat primary cell-based blood-brain barrier model with epithelial and brain endothelial cell lines: gene expression and drug transport. Front. Mol. Neurosci. 11, 166.
Walter, F.R., Veszelka, S., Pásztói, M., Péterfi, Z.A., Tóth, A., Rákhely, G., Cervenak, L., Ábrahám, C.S., Deli, M.A., 2015. Tesmilifene modifies brain endothelial functions and opens the blood-brain/blood-glioma barrier. J. Neurochem. 134, 1040–1054.
Wohlfart, S., Gelperina, S., Kreuter, J., 2012. Transport of drugs across the blood-brain barrier by nanoparticles. J. Control. Release 161, 264–273.
Zheng, M., Ruan, S., Liu, S., Sun, T., Qu, D., Zhao, H., Xie, Z., Gao, H., Jing, X., Sun, Z., 2015. Self-targeting fluorescent carbon dots for diagnosis of brain cancer cells. ACS Nano 9, 11455–11461.
Zhou, Y., Peng, Z., Seven, E.S., Leblanc, R.M., 2018. Crossing the blood-brain barrier with nanoparticles. J. Control. Release 28, 290–303.
Zong, T., Mei, L., Gao, H., Shi, K., Chen, J., Wang, Y., Zhang, Q., Yang, Y., He, Q., 2014. Enhanced glioma targeting and penetration by dual-targeting liposome co-modified with T7 and TAT. J. Pharm. Sci. 103, 3891–3901.